

Studies on the Combustion and Gasification of Concentrated Distillery Effluent

A Thesis

Submitted for the Degree of

Doctor of Philosophy

in the Faculty of Engineering

by

Nikhil Patel



Department of Aerospace Engineering

INDIAN INSTITUTE OF SCIENCE

BANGALORE-560 012, (INDIA)

October 2000

To my parents and my sister

my wife

and

my sweet little son

who has brought laughter and happiness when life was at its hardest

Acknowledgements

Through the ages, the power of fire has been well recognised, not the least for its immense capacity to regenerate life from the seemingly dead, but also for its cleansing capabilities. From the ancient texts of humankind- the Puranas, the Gospel, and various other texts of philosophy and religion, one can see the fascination man has held for fire, thereby imbuing it with anthropomorphic and spiritual qualities. Fire and therefore combustion, have thus always fascinated me and induced in me, a desire to find means to burn, the difficult-to-burn, environmentally hazardous wastes.

In this endeavour of mine, my guides, Prof. H. S. Mukunda and Prof. P. J Paul are to be thanked for having introduced me to the field of combustion and gasification and helped me to fulfill this desire.

They have been a constant source of inspiration and have always motivated me to give of my best with erudite suggestions during the course of the research.

I thank the chairman of the Aerospace Engineering Department and Combustion Gasification and Propulsion Laboratory for allowing me to use the infrastructure and necessary support.

The immense support, both professional and personal rendered by Dr. Jayamurthy as an esteemed friend and colleague, cannot be quantified. I thank him for being there for me during the good times and especially during the rough times.

The friendly interactions with the staff of CGPL, have also served to lighten my load, especially Dr. Dasappa. I would also like to thank Dr. N. K. S. Rajan for his words of wisdom and support.

V. Gayathri, H. V. Sridhar, G. Sridhar, Subbukrishna, Hegde, Nisha, Annsuya, Shankarlingam, Chowthri, have been of great help and timely support as well.

This work would have been doubly gruelling without the technical, professional and emotional input by way of brainstorming, ideation, and debate, that I could do with my friends. I am indebted to Ramakrishna, Anil Kumar, Basani, Bhasker Dixit, Sudarshan, Murli Dey, Venkatesh, Sriram A. T., Shridhar, Dr. Debashis Chakravorty, Dr. Mishra, Dr. Ramesh R., Dr. Ramesh O. N., Dr. Oomen, Dr. Sridhara S., Dr. Shivkumar, Keyur, for all the unstinting help they have given me.

Without the technical support staff on the shop floor, especially Ramesh Acharya and Anilkumar, Sridhar T. C., Thirupathaiah, Shankara, Anantha, Venu, Mallaiah, the experiments would not have been as successful.

I also thank the office staff of Aerospace Engineering Department for providing support, especially Mrs. Gayathri.

The IISc, with its long and rich tradition of inspiring and motivating research scholars and scientists, has become a very special place for me. I could interact with inter-departmental colleagues faculties in a free and frank manner, simply because of this umbrella of knowledge sharing.

I thank Prof. Prabhu Nott of Chemical Engineering Department and his students Anugrah Singh and K. Suneel for support extended to conduct rheology study of concentrated effluents. I also thank Prof. S. Subramanian of Metallurgy department for having helped me in the determination of effluent char surface area.

The financial support offered by CSIR, during the tail end of this work, has been of immense help to me.

I thank Mr. Ponshe of M/s Khoday Distilleries for providing 20 T of effluent during the course of experimentation.

Here, I would like to particularly mention the service that Prof. Atul Choksi and his learned wife, Dr. Arti Choksi have performed. They have inspired me to aim for the best, by virtue of their mental strength and fortitude. Our discussions have meant a lot to me, on a personal note as well.

In each life, a person is always known by the company he keeps. In my case, I have been very lucky to have known Mr. Venkatesh, Mr. Gurjar, Mr Balaji, Prof. Sood and their families, for having given my wife and me, all the emotional and mental support, during our stay in the IISc campus. I thank them for going out of their way in helping us.

I also thank all my dear friends of Gujarati Group for all the affectionate support rendered.

Bangalore has given me a sense of belonging. In this regard, I would like to mention Mrs. and Brig Rangachari, Mrs. and Mr. Sarangan for giving me love, familial support and encouragement. Bindi, Nitin, their parents and Gita Vasudevan have been a great source of support and affection.

My friends from other walks of life, Anand, Ramdas and Heeru have also contributed by taking me out for endless cups of coffee, while I was in the midst of my work! I don't know whether to acknowledge them for this unselfish deed!

The most support that I have ever received, over and above all others, are from the loved members of my family.

My parents, Parul and Manubhai Patel cannot be thanked enough- not only for giving me life, but for a lifetime of unconditional love and unstinting devotion. I cannot express my regard and gratitude for them enough.

My sister, Dr. Ankita Patel, for her love and support, all my life.

My father-in-law, Mr. B Munshi and my sister-in-law Nirali, for welcoming me into their family and being there for me as much as they have.

My most wanted and beloved son, Devarishi, for making me laugh, keeping me on my toes and brightening my darkest times with his innocence.

Last, but actually foremost, both in terms of my love and regard and unending gratitude on this difficult journey, my most beloved wife, Neha. She has uncomplainingly stood by me through my worst moments and I have had many of them! Without regard for her own personal feelings, my wife has boosted me on her shoulders. Mere words are feeble to express my feelings to have such a wonderful wife and the best friend.

Abstract

The need for effective disposal of huge volumes of industrial waste is becoming more challenging due to expected imposition of stringent pollution control regulations in the near future. Thermochemical conversion, particularly gasification of organics in the waste is considered the best route from the perspective of volume reduction and prevalent eco-friendly concept of waste-to-energy transformation. It is considered imperative to have adequate understanding of basic combustion features as a part of the thermochemical conversion process, leading to gasification. The aim of this thesis is to understand the fundamental combustion processes associated with one of the top listed hazardous wastes from distilleries (Biochemical Oxygen Demand (BOD) \sim 40,000 – 50,000 mg/L), commonly known as vinasse, stillage or spent wash, through experiments and modeling efforts. Specially designed experiments on distillery effluent combustion and gasification are conducted in laboratory scale reactors.

As an essential starting point of the studies on ignition and combustion of distillery effluent containing solids consisting of 62 ± 2 % organics and 38 ± 2 % inorganics (primarily sugarcane derivatives), the roles of solids concentration, drop size and ambient temperature were investigated through experiments on (1) liquid droplets of 65 % and 77 % solids (remaining water) and (2) spheres of dried effluent (100 % solids) of size 0.5 mm to 20 mm diameter combusted at ambient temperatures of 773 to 1273 K. The investigation reveals that the droplets burn with two distinct regimes of combustion, flaming and char glowing. The ignition delay ' t_i ' of the droplets increased with size as is in the case of non-volatile droplets, while that of bone-dry spheres was found to be independent of size. The ' t_i ' decreased with increase in solids concentration. The ignition delay has showed an Arrhenius dependence on temperature. The initial ignition of the droplets and the dry spheres led to either homogeneous (flaming) or heterogeneous (flameless) combustion, depending on the ambient temperature in the case of sphere and on solid concentration and the ambient temperature, in the case of liquid droplets. The weight loss during the flaming combustion was found to be 50 – 80 % while during the char glowing it was 10 – 20 % depending on the ambient temperature. The flaming time ' t_f ' is observed as $t_f \sim d_o^2$, as in the case of liquid fuel droplets and wood spheres. The char glowing time ' t_c ' is observed as $t_c \sim d_c^2$ as in the case of wood char, though the inert content of effluent char is as large as 50 % compared to

2 – 3 % in wood char. In the case of initial flameless combustion, the char combustion rate is observed to be lower. The heterogeneous char combustion in quiescent air in controlled temperature conditions has been studied and modeled using one-dimensional, spherically-symmetric conservation equations and the model predicts most of the features of char combustion satisfactorily. The measured surface and core temperatures during char glowing typically are in the range of 200 to 400 K and are higher than the controlled temperature of the furnace.

Based on the results of single droplet combustion studies, combustion experiments were conducted in a laboratory scale vertical reactor (throughput ranging from 4 to 10 g/s) with the primary aim of obtaining sustained combustion. Spray of effluents with 50 % and 60 % solids (calorific value 6.8 – 8.2 MJ/kg), achieved by an air blast atomizer, was injected into a hot oxidizing environment to determine the parameters (ambient temperature and air-fuel ratio) at which auto-ignition could occur and subsequently studies were continued to investigate pre-ignition, ignition and combustion processes. Effluent with lower solids concentration was considered first from the point of view of the less expensive evaporator required in the field conditions for concentration and a spin-off in terms of better atomization consequently. Three classes of experiments were conducted: 1) Effluent injection from the wall with no auxiliary heat input, 2) Effluent injection with auxiliary heat input and 3) effluent injection within kerosene enveloping flame. Though individual particles in the spray periphery were found to combust, sustained spray combustion was not achieved in any of the three sets of experiments even with fine atomization. While conducting the third class of experiments in an inclined metallic reactor, sustained combustion of the pool resulting of accumulated spray seemed to result in large conversion of carbon. This led to the adoption of a new concept for effluent combustion in which the residence time is controlled by varying reactor inclination and the regenerative heat transfer from the product gases supplies heat for endothermic pre-ignition process occurring on the bed.

Combustion and gasification experiments were conducted in an inclined plate reactor with rectangular cross section (80 mm x 160 mm) and 3000 mm long. A support flame was found necessary in the injection zone in addition to the regenerative heat transfer. Effluent with 60% solids was injected as film on the reactor bed. This film disintegrated into fine particles due to induced aerodynamic stretching and shear stripping. Combustion of individual particles provided exothermic heat profile and resulted into high carbon

Abstract

conversion. However, effluent clogging in the cold injection zone hindered system from attaining steady state. Effluent injected directly on the hot zone caused it to remain mobile due to the spheroidal evaporation and thus assuaging this problem. Improved mass distribution was achieved by displacing nozzle laterally in a cycle, actuated by a mechanism. Consistent injection led to sustained effluent combustion with resulting carbon conversion in excess of 98 %. The typical gas fractions obtained during gasification condition (air ratio = 0.3) were $\text{CO}_2 = 14.0 \%$, $\text{CO} = 7.0 \%$, $\text{H}_2 = 12.9 \%$, $\text{CH}_4 = 1 \%$, $\text{H}_2\text{S} = 0.6 - 0.8 \%$ and about 2 % of saturated moisture. This composition varied due to variation in temperature ($\pm 30 \text{ K}$) and is attributed to combined effect of local flow variations, shifting zones of endothermic processes due to flowing of evaporating effluent over a large area. In order to minimize this problem, experiments were conducted by injecting effluent at higher solids (73 % solids is found injectable). The effluent was found to combust close to the injection location-due to the reduced ignition delay and lower endothermic evaporation load helped raising the local temperature. This caused the pyrolysis to occur in this hottest zone of the reactor with higher heating rates resulting in larger yield of devolatilized products and improved char conversion. Effluent combustion was found to sustain temperature in the reactor under sub-stoichiometric conditions without support of auxiliary heat input and achieved high carbon conversion. These results inspired the use of higher concentration effluent, which is also known in the case of wood to have improved gasification efficiency due to reduction in moisture fraction. In addition, the recent studies on the sulfur emission in the case of black liquor combustion in recovery boilers have revealed that with increase in solids concentration, release of sulfur in gas phase is reduced. The required concentration can be carried out using low-grade waste heat from the reactor itself. It was found through experiments that, even though spray ignition occurred at this concentration, the confined reactor space prevented the spray from attaining sustained combustion. This led to the conduct of experiments in a new vertical reactor with adequate thermal inertia, essential to prevent variations in local temperature to reach a steady state gasification and required space to accommodate the spray.

The results of the experiments conducted in the vertical reactor in which effluents with 73 % solids, heated close to the boiling point and injected as fine spray in a top-down firing mode are consolidated and reported in the thesis in detail. Single particle combustion with enveloping faint flame was seen unlike stable flame found in coal water slurry spray combustion. Sustained gasification of gas-entrained particles occurred at reactor

temperature in the range of 950 K – 1000 K and sub-stoichiometric air ratio 0.3 – 0.35 without the support of auxiliary fuel. The typical gas fractions obtained during gasification condition (air ratio = 0.3) were $\text{CO}_2 = 10.0 - 11.5 \%$, $\text{CO} = 10.0 - 12.0 \%$, $\text{H}_2 = 6.7 - 8.0 \%$, $\text{CH}_4 = 1.75 \%$ $\text{H}_2\text{S} = 0.2 - 0.4 \%$ and about 2 % of saturated moisture. The carbon conversion obtained was in the range of 95 – 96 %. These experiments have provided the conditions for gasification. The extraction of potassium salts (mostly sulfates, carbonate and chloride) from the ash, using a simple water leaching process, was found to recover these chemicals to as high an extent as 70 – 75 % of total ash.

In summary it is concluded that increasing the solid concentrations to as high levels as acceptable to the system (~ 75 %) and introducing as a fine spray of heated material (~ 363 K) into furnace with air at sub-stoichiometric conditions in a counter current combustion reactor will provide the frame work for the design of a gasification system for vinasse and similar effluent material.

The thesis consists of seven chapters. Chapter 1 introduces the problem and motivation of the work presented in the thesis. Literature review is presented in Chapter 2. The Chapter 3 deals with the single particle combustion studies. The results of effluent spray combustion experiments conducted in a laboratory scale vertical reactor are presented in Chapter 4. The results of combustion and gasification experiments conducted in another variant of a reactor, namely, inclined flat plate rectangular reactor is consolidated in Chapter 5. The results of gas-entrained spray gasification experiment of higher concentration effluent injected as spray in the vertical reactor are presented in Chapter 6. The general conclusions and scope for the future work are presented in the concluding chapter 7.

List of Publications

1. Patel, N. M., Paul, P. J., Mukunda, H. S., and Dasappa, S., Combustion studies on concentrated distillery effluents, *Twenty-Sixth Symposium (International) on Combustion*, The Combustion Institute, Pittsburgh, pp. 1401 – 1407, (1996)
2. Patel, N. M., Paul, P. J., and Mukunda, H. S., Droplet combustion studies on dried concentrated distillery effluents, XIV National conference on IC engines and Combustion, Pune, pp. 389 – 394, (1995)

Content

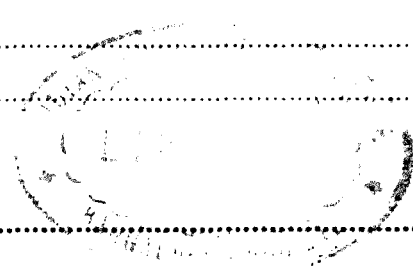
Acknowledgement	i
Abstract	iii
List of Publications	vii
List of Figures	xv
List of Tables	xxi

Chapter 1

Introduction	1
1.1. Background.....	2
1.2. The chemical composition of effluent	3
1.3. Classical routes of distillery effluent treatment	6
1.3.1. Ferti-irrigation.....	6
1.3.2. Anaerobic lagooning.....	6
1.3.3. Bio-methanation.....	7
1.3.4. Incineration	7
1.3.5. Wet Air Oxidation.....	9
1.4. Alternate Route	10
1.5. Comparison of energy recovery from bio-methanation and gasification process	12
1.5.1. Energy recovery from bio-methanation	12
1.5.2. Energy recovery from gasification of concentrated effluent	12
1.6. The Gasification Process.....	14
1.7. Comparison of gasification of black liquor and wood with distillery effluent	16
1.7.1. Black liquor gasification	17
1.7.2. Wood gasification	18
1.7.3. Distillery effluent vs. black liquor	18
1.8. Overview and objective of the present work	20

Chapter 2

Literature Survey	23
2.1. Introduction.....	23
2.2. Physico-chemical properties	23
2.3. Method of injection and combustion in furnace environment	25



2.3.1. Distillery Effluent	25
2.3.2. Black Liquor combustion.....	26
2.3.3. Slurry Fuels.....	27
2.4. Combustion process in high temperature environment	27
2.4.1. Single Particle combustion studies	28
2.4.1.1. Pre-ignition Processes.....	29
2.4.1.2. Swelling behavior	30
2.4.1.3. Pyrolysis or devolatilization	31
2.4.1.4. Ignition and Ignition Delay.....	32
2.4.1.5. Flaming.....	34
2.4.1.6. Char Combustion	35
2.5. Gasification of liquid effluents or black liquor.....	36
2.6. Conclusion	37
Chapter 3	
Single Particle Combustion	39
3.1 Introduction.....	39
3.2 Experimental Techniques	41
3.3 Experimental Setup.....	42
3.4 Sample Preparation	45
3.5 Physical Observations.....	46
3.5.1. Flaming	47
3.5.2. Char Glowing.....	48
3.5.3. Ignition.....	49
3.5.4. Heating, swelling and devolatilization.....	50
3.5.5. Structure of fresh sample, char and ash	52
3.5.6. Fumes During Combustion.....	54
3.6 Scanning electron micrograph	54
3.7 DTA/TGA	58
3.8 Mathematical Model.....	58
3.8.1. Char combustion process	58
3.8.2. The Governing Equation.....	59
3.8.3. Initial, interface and boundary conditions	60
3.8.4. Method of Solution	61
3.8.5. Choice of Parameters	61

3.9 Results and Discussion	62
3.9.1 Ignition Delay	62
3.9.1.1 Ignition delay of dry effluent spheres	66
3.9.1.2 Ignition delay of liquid droplets.....	67
3.9.2 Pre-ignition heating phase.....	68
3.9.2.1 Dry Effluent Sphere	68
3.9.3 Weight Loss	71
3.9.3.1 Weight vs. time profile of combusting effluents at various T_a	73
3.9.3.2 Weight vs. time profile of sphere combusted with and without flaming.....	74
3.9.4 Chemical Transformation	76
3.9.4.1 Reduction of sulfate	77
3.9.4.2 Release of chlorine.....	79
3.9.4.3 Release of alkali metal	80
3.9.5 Flaming of effluent droplet and dry spheres	85
3.9.6 Char Glowing: experimental and computational results.....	86
3.9.6.1 Weight – time profile of char: experimental and computed results.....	88
3.9.7 Flaming and char glowing time as a function of ambient temperature.....	89
3.9.8 Core and surface temperature vs. time history.....	91
3.9.8.1 Dry spheres: experimental and computed results	92
3.9.8.2 Droplet Combustion.....	92
3.10 Conclusions.....	106

Chapter 4

Combustion Experiments in a Vertical Cylindrical Reactor	109
4.1. Introduction.....	109
4.2. Objective of the experiments	110
4.3. The design of experimental set-up.....	112
4.4. The Experimental Setup.....	114
4.4.1. Instrumentation	115
4.4.1.1. Pressure Measurement	115
4.4.1.2. Flow Measurement.....	116
4.4.1.3. Temperature Measurement	116
4.4.1.4. Gas Composition Measurement.....	117
4.5. Experimental Procedure.....	117

4.6. Observations, Results and Discussions.....	119
4.6.1. Experiment set I: With zero auxiliary heat input.....	119
4.6.2. Experiment Set II: With auxiliary heat input.....	122
4.6.3. Experiment Set III: Injection in turbulent flame.....	123
4.6.3.1. Combined injection in the reactor.....	123
4.6.3.2. Combined injection outside the reactor	124
4.6.4. Injection in confined hot cylinder.....	125
4.7. Conclusions.....	127

Chapter 5

Inclined plain sheet reactor: Experiments and Results	129
5.1. Introduction.....	129
5.2. Experiment Setup.....	131
5.3. Observations and Results.....	132
5.3.1. Phase II : Effluent Injection.....	135
5.3.1.1. Experiment set 1: Injection as film on flat plate.....	135
5.3.1.2. Experiment set 2: Splash Injection in hot zone.....	145
5.3.1.3. Experiment Set 3: Spray injection	149
5.4. Conclusions.....	155

Chapter 6

Experiments in Modified Vertical Reactor.....	157
6.1. Introduction.....	157
6.2. The Design of experimental set-up.....	158
6.3. Experiment Setup.....	159
6.4. Experimental Procedure.....	160
6.5. Observations and Results and Discussion	161
6.5.1. Post-Experiment observations	163
6.6. Conclusions.....	164

Chapter 7

Overview and concluding remarks.....	167
---	------------

Appendix A4

Vertical Reactor: The Experimental Setup and Procedure	171
A4.1. The Experimental Setup – 1.....	171

A4.1.1.	The Reactor.....	171
A4.1.2.	Reactor Heating System.....	173
A4.1.3.	Kerosene Feed System.....	175
A4.1.4.	Effluent Feed System.....	175
A4.1.5.	Steam jacketed storage tank and supply lines.....	176
A4.1.6.	Effluent Atomizer	178
A4.1.7.	Air Feed System.....	179
A4.2.	Experimental Procedure.....	180
A4.2.1.	Initial setup procedure.....	180
A4.2.1.1.	Effluent Feed System.....	181
A4.2.1.2.	Kerosene Feed System.....	181
A4.2.1.3.	Air Feed system	182
A4.2.1.4.	Reactor	182
A4.2.1.5.	Instrumentation	182
A4.2.2.	Start-up procedure.....	183
A4.2.2.1.	Phase I: Reactor heat up phase.....	183
A4.2.2.2.	Phase II: Spray injection	183

Appendix A5

Inclined Reactor: The experimental setup and procedure.....	185
A5.1. The Experimental Setup – 1.....	185
A5.1.1. The Reactor.....	185
A5.1.1.1. Section I.....	185
A5.1.1.2. Section II.....	186
A5.1.1.3. Section III.....	187
A5.1.2. Gas Scrubber.....	189
A5.1.3. Ejector and Gas Flare.....	190
A5.1.4. Effluent Injectors	190
A5.1.4.1. Film Injector.....	191
A5.1.4.2. Splash Injector	192
A5.1.4.3. Effluent Atomizer	193
A5.1.5. Effluent Feed system.....	193
A5.1.6. Air Feed System.....	194
A5.1.7. Instrumentation	196
A5.2. Experimental Procedure.....	196

A5.2.1.	Initial setup procedure	196
A5.2.1.1.	Effluent preparation	196
A5.2.1.2.	Kerosene Feed System.....	197
A5.2.1.3.	Air Feed system	197
A5.2.1.4.	Reactor	197
A5.2.1.5.	Instrumentation	197
A5.2.2.	Experimental startup	198
A5.2.2.1.	Phase I: Reactor heat up phase	198
A5.2.2.2.	Phase II: Effluent injection	198

Appendix A6

Gasification in Vertical Reactor: The Experimental Setup and Procedure 201

A6.1.	The Experimental Setup.....	201
A6.1.1.	The Reactor.....	201
A6.1.2.	Gas Scrubber, Ejector and Gas Flare	201
A6.1.3.	Effluent Feed system	201
A6.1.4.	Air Feed System.....	203
A6.1.5.	Effluent Atomizer	203
A6.1.6.	Instrumentations.....	206
A6.2.	Experimental Procedure.....	206
A6.2.1.	Initial setup procedure	206
A6.2.2.	Experimental startup.....	206
A6.2.2.1.	Phase I: Reactor heat up phase	206
A6.2.2.2.	Phase II: Effluent injection	206
References	209

List Of Figures

Figure 1.1: Schematic of distillery effluent incinerator.....	8
Figure 1.2: Gasification process	10
Figure 1.3: Schematic of gasification of distillery effluent	11
Figure 1.4: Flow chart of energy and mass balance of effluent gasification.....	13
Figure 3.1a: Schematic view of the experimental setup.....	43
Figure 3.1b: Schematic view of the experimental setup for gravimetric study.....	44
Figure 3.2: Stages of effluent combustion in hot quiescent air at $T_a = 973$ K.....	47
Figure 3.3: Flaming combustion of dry effluent sphere and formation of char.....	47
Figure 3.4: Comparison of flaming combustion of dry effluent and wood at 973 K.....	48
Figure 3.5: Heterogeneous char glowing.....	49
Figure 3.6: Swelling of suspended droplet and internal porous structure of swelled effluent droplet (80 % solids)	51
Figure 3.7: Initial effluent droplet and coherent ash of the same droplet suspended on quartz fiber.....	52
Figure 3.8: Fume releasing during char glowing at $T_o = 973$ K of effluent droplet.....	53
Figure 3.9: Fumes releasing from combusting effluent droplet ($d_o=2.0$ mm, 65 % solids) suspended on quartz fiber at 1173 K.....	53
Figure 3.10a: SEM of fresh sample (SEM No. 1), partly devolatilized sample (SEM No. 2 & 3) and of char (SEM No. 4) of dry effluent sphere obtained at $T_a = 973$ K.....	55
Figure 3.10b: SEM of char (SEM No. 5, 6), partly converted char (SEM No. 7 & 8) and of ash (SEM No. 9, 10) of dry effluent sphere obtained at $T_a = 973$ K.....	56
Figure 3.11: TG and DTA of distillery effluent and wood.....	57
Figure 3.12: Dependence of primary ignition as flaming or glowing on the effluent initial diameter and ambient temperature.....	63
Figure 3.13: Ignition feature of sphere and liquid droplet with 65 % solids at various T_a	64
Figure 3.14: Ignition delay of liquid effluent droplets with 65 % solid concentration and dry spheres vs. diameter.....	65
Figure 3.15: Dependence of ignition delay of dry effluent spheres of various diameters on ambient temperature.....	66
Figure 3.16: Variation of ignition delay with droplet initial diameter of effluent (77 % solid).....	68
Figure 3.17: Experimentally obtained profile of surface temperature and percent weight loss vs. time of 8.5 mm dry effluent spheres at $T_a = 973$ K and 1073 K.....	69
Figure 3.18: Measured pre-ignition core temperature profile of 65 % effluent droplets of 1.1 mm diameter at different ambient temperature.....	70

Figure 3.19: Measured pre-ignition core temperature profile of 65 % effluent droplet of different diameter at 873K ambient temperatures.....	71
Figure 3.20: Weight losses vs. ambient temperature of dry effluent spheres obtained at the end of flaming and char glowing	72
Figure 3.21: The plot shows weight loss–time history of an 8.5 mm diameter combusting sphere vs. time at 873, 973 and 1073 K ambient temperature in quiescent air... ..	73
Figure 3.22: Percent weight vs. time history of two effluent spheres of 8.2 mm diameter, combusting at 873 K, one having primary homogeneous ignition and other having heterogeneous ignition.	74
Figure 3.23: Thermogravimetric analysis with respect to the reduction reaction of K_2SO_4 . Temperature rate, 10 C/min; flow rate of each gas 1 ml/s. A): K_2SO_4 in H_2 ; B) K_2SO_4 in CO; C) 1:1 graphite– K_2SO_4 mixture in He; D) K_2SO_4 in He. (<i>Kikuchi et al., 1983</i>)	78
Figure 3.24: Surface temperature and weight loss vs. time profile obtained up to end of devolatilization of dry effluent sphere of $d_0 = 8.5$ mm, combusted in quiescent air at $T_a = 973$ K.....	81
Figure 3.25: Surface temperature and weight loss vs. time profile obtained for char glowing of dry effluent sphere of $d_0 = 8.5$ mm, combusted in quiescent air at $T_a = 973$ K.....	84
Figure 3.26: Normalized flaming time vs. diameter for effluent spheres (100 % solids) and droplets (77 % solids). Results of n-heptane and wood are also shown.	85
Figure 3.27: Char glowing time vs diameter for concentrated liquid droplets and dried effluent material at different temperatures. Results for wood char and pure carbon are also shown. Comparison with model prediction is shown as continuous lines in the figure.....	87
Figure 3.28: Experimental and computed weight–time profile of 9.6 mm diameter char combusted at ambient 973 K.....	88
Figure 3.29: Experimental and computed weight–time profile of 8.2 and 8.5 mm diameter char combusted at ambient 873 K.....	89
Figure 3.30: Flaming and char glowing time as a function of ambient temperature for dried effluent sphere of diameter 6.5 mm.....	90
Figure 3.31: Surface temperature–time history of combusting dry effluent sphere of 8.15 mm diameter at 973, 1073 and 1173 K ambient temperature. Computed results of char glowing are also shown.	91
Figure 3.32: Core temperature profile of droplets of effluent with 65 % solids of different diameter combusted at 873 K ambient temperature.....	93
Figure 3.33: Core temperature history of 1.1 mm initial diameter of effluent with 65 % solids combusted at various ambient temperatures in quiescent air.	94
Figure 3.34: Temperature-time history of combusting effluent (77 % solids) droplet of initial diameter $d_0 = 0.65, 0.85$ and 1.14 mm at 823 K ambient temperature. ...	96
Figure 3.35: Core temperature–time history of effluent droplet with 77 % solids combusting at 863 K ambient temperature.	97

Figure 5.11: (a) Fine ash in the dump (b) View port glass coated with fumes and accumulation of fine ash behind glass.	143
Figure 5.12 Observations of process occurring after injecting from splash injector in inclined reactor.....	146
Figure 5.13: Bed temperature, gas composition and air mass flow rate vs. time history obtained at various locations in the reactor during effluent injection phase (Phase II) (Expt. No. I – 9)	147
Figure 5.14: Mass distribution of effluent injected as spray on reactor walls	150
Figure 5.15: Bed temperature vs. time profile of effluent (73 % solid) combustion injected as fine spray.....	151
Figure 5.16: Concentrated effluent spray combustion in a heated reactor.....	154
Figure 6.1: Schematic view of the experiment setup.....	159
Figure 6.2: (a) Typical plot of reactor cooling history vs. time obtained during trial experiment, (b) Thermocouple locations in the reactor	160
Figure 6.3: Bed temperature, gas composition and air mass flow rate vs. time history obtained at various locations in the reactor during Phase II (Expt. No. V –2) .	162
Figure 6.4: Direct pictures obtained during gasification phase	163
Figure A4.1 Dimensional view of the conical and the cylindrical shells used in the reactor	171
Figure A4.2: Direct pictures of vertical reactor assembled upright on support structure with and without thermal insulation. It also shows kerosene burner and effluent injection ports, viewing ports located on the shells. Picture on the right shows rack of thermocouple fixtures.....	173
Figure A4.3: Sectional view of burner drawn to the scale depicting atomizers fixed to a flange.....	174
Figure A4.4: Kerosene feed system	176
Figure A4.5: direct pictures of (a) effluent feed tank and steam generator (b) effluent injection port location and (c) atomization of effluent (with 60 % solid) into fine spray.	177
Figure A4.6: Compressed air feed system.	179
Figure A5.1: Scaled side view of Section I indicating location of effluent injector, kerosene burner and gas and wall thermocouple.	186
Figure A5.2: Direct picture of section I of inclined plate reactor	186
Figure A5.3: View of section II as seen from (a) section III end, (b) section I end and (c) View of lower duct and bed stiffeners.	187
Figure A5.4: Section of the underside of the bedplate with thermocouple junction.	188

Figure 3.36: Temperature–time profiles of 77% effluent droplets of different size combusting at 963 K ambient temperature.	99
Figure 3.37: Temperature–time history of effluent droplet of different sizes combusting at 1063 K ambient temperature. Magnified view of pre–ignition temperature profile depicting dips in it is also shown.	101
Figure 3.38: Temperature–time history of effluent droplet of different sizes combusting at 1123 K ambient temperature. Magnified view of pre–ignition temperature profile depicting a dip is also shown.....	102
Figure 3.39: Temperature–time history of effluent droplets of different sizes combusting at 1248 K.....	103
Figure 3.40: Effect of solid concentration on temperature–time profile of 1.1 mm diameter effluent combusting at 873 K.....	104
Figure 3.41: Comparison core temperature vs. time profiles of droplet of effluent with 77 % and 65 % solids.....	105
Figure 4.1: Conceptual view of the reactor and location of effluent injector and burner.....	113
Figure 4.2: Schematic view of the experimental set-up.....	114
Figure 4.3: Type K thermocouple.....	117
Figure 4.4: (a) Typical plot of temperature history vs. time obtained during reactor cooling, (b) Thermocouple location in the reactor.....	118
Figure 4.5: Spray of effluent and combustion processes as was observed from the view port.	121
Figure 4.6: Effluent injection in kerosene flame in a confined cylindrical reactor.	126
Figure 5.1: The conceptual rectangular cross section reactor.....	130
Figure 5.2: Scaled front view of the experimental setup.	132
Figure 5.3: Schematic view of the reactor depicting the location of thermocouple used to measure gas and wall temperature.	133
Figure 5.4: Top view of the reactor depicting the location of the view ports.....	134
Figure 5.5: Reactor cooling profile.....	135
Figure 5.6: Schematic of the effluent film flowing over hot bed and subsequent disintegration into particles due to stretching and shear stripping.....	137
Figure 5.7: Observations of sequence of processes occurring after injecting effluent as film in the inclined reactor.....	138
Figure 5.8: Direct photographs of effluent combustion during phase II as viewed from view port # 2.	139
Figure 5.9: Temperature vs. time history obtained at various locations in the reactor during Phase II obtained during effluent film injection experiment.....	141
Figure 5.10: Wall and gas temperature vs. time history obtained at a plane perpendicular to the reactor, located at 1235 mm from injector during the Phase II of effluent film injection experiment.	142

Figure A5.5: (a) Underside view of the reactor, the flange joint between section I & II and telescopic reactor support, (b) Top side view of the reactor.	188
Figure A5.6: Scaled two views and direct picture of section III section II	189
Figure A5.7: Location of different types of injectors in hot and cold zones of the reactor ...	190
Figure A5.8: Sectional side view and three photographic views of film injector.....	191
Figure A5.9: Schematic view of Splash Injector	192
Figure A5.10: Effluent Atomizer.....	194
Figure A5.11: Effluent feed system.	195
Figure A5.12: Reactor pressure vs. kerosene burner power level operated at equivalence ratio = 1, or air mass flow rate if burner is off.....	199
Figure A6.1: Modified vertical reactor	202
Figure A6.2: Effluent Atomizer.....	204
Figure A6.3: Average mass distribution of effluent spray vs radial distance ($R = 0$ at center)	205

List of Tables

Table 1.1: Typical distillery effluent composition.....	4
Table 1.2: Elemental analysis of distillery effluent, black liquor, wood and kerosene (% weight basis).	16
Table 1.3: Equilibrium gas composition and that obtained from black liquor gasifier (72 % solid) on dry basis (Consonni. et al, 1997)	17
Table 1.4: Gas composition obtained B&W black liquor gasifier (55 % solids feed rate 1kg/h).....	17
Table 1.5: Equilibrium gas composition and that obtained from wood gasifier (28 % moisture), * ~0 means non-zero small value.	18
Table 2.1: Burn time and size correlations for different fuels found by various authors	36
Table 3.1: Composition of effluent with 65 % solids	46
Table 3.2 Observations made on the occurrence of primary ignition as heterogeneous or homogeneous and its dependence on initial diameter (d_o) and ambient temperature (T_a)	49
Table 3.3: Details of samples prepared for SEM and magnification of micrograph	54
Table 3.4 Organic and inorganic composition of dry effluent and its char produced at various temperatures.	76
Table 3.5: Compositions of dry effluent and its char and ash obtained by combusting dry effluent spheres at 973 K ambient temperature.	77
Table 3.6: Non-dimensional burn time for effluent, wood and n-heptane.....	86
Table 4.1: Shell temperature at the end of heat up phase.	118
Table 4.2: Details of experiments conducted.....	120
Table 5.1: Bed and gas temperatures prior to effluent injection.....	134
Table 5.2: Details of the experiments conducted.....	136
Table 5.3: Experimental observations of effluent injected on hot stainless steel bed	140
Table 5.4: Equilibrium and measured gas composition for combined fuel injected in the reactor at $\phi = 1.85$	148
Table 6.1: Shell temperature prior to effluent injection.....	161
Table 6.2: Details of the experiments conducted.....	161

Introduction

Twentieth century has seen quantum growth in path breaking technology and industrialization. This growth, while beneficial to humanity, has had its impact on the environment. Most developed nations have achieved a high rate of industrial growth, with inadequate respect for environmental issues, a policy decision that is now undergoing a rethinking of priorities. Developing countries on the other hand, are faced with a fast exploding population growth; in the race for rapid industrialization, environmental issues and concerns go on a low priority: a dangerous precedent to follow and one with a serious impact on the quality of life.

Therefore, there is an urgent need for evolving clean, safe, environmentally meaningful strategies to effectively dispose huge volumes of industrial and municipal wastes generated each day. The routes of waste disposal are required to be aimed at 1) recovering energy and useful byproducts, with high efficiency and 2) the complete destruction of organic pollutants and inertisation of the inorganic ingredients with little demand on the available land space. These routes will need to be ecologically superior in order to satisfy the stringent emission control regulations, expected to be imposed in the near future. Thermochemical conversion, particularly gasification; a sub-stoichiometric combustion process, is considered one of the most suitable routes for disposal that can satisfy the concept of waste-to-energy. The waste characteristics that decide the process feasibility and economy are the energy content, composition, physical state, total moisture content, and toxicity. Since the success of thermochemical conversion process depends primarily on the capability to achieve control over the combustion process, it is imperative to have adequate understanding of basic combustion features associated with waste combustion.

One such waste that needs attention for its disposal is the distillery effluent commonly known as vinasse, spent wash, mosto, rum slop, dunder and bottom stillage in various parts of the world. The present work constitutes the study of the fundamental combustion features

of concentrated distillery effluent, through both experimental and modeling efforts. The model is subsequently applied to carry out combustion and gasification experiments in a laboratory scale reactors while studying critical aspects related to effluent combustion and gasification.

1.1. Background

The enormous organic pollution load generated by distillery effluent amounts to several times more (estimates been seven times more, *Joshi, 1999*) than that generated by entire Indian population. This makes it imperative to devise an effective disposal technique while applying the concept of waste-to-energy. India is one of the world's largest producers of sugar from cane. As a by-product of sugar manufacturing process, a large quantity of molasses is generated. Molasses is the raw material for the fermentation process carried out in a distillery, for the production of ethanol. The amount of effluent generated is about 12 to 15 times that of ethanol produced. The solid concentration ranges between 7 to 12 % (depending on the molasses' dilution factor) as the material emerges from the distillery. There are 285 distilleries in India producing 2.7 billion litres of alcohol and generating 40.7 billion litres of effluent annually. Thus, distillery produces the largest quantity of effluent containing 2.8-4.0 billion kg of solids. The fuel value of the effluent generated is approximated to be 5.8×10^{10} MJ (14.5 MJ/kg dry solids, HHV)

The effluent solid consists of 62-60 % organics, primarily sugar derivatives and 38-40 % inorganic material (see Table 1.1). It has BOD (Biological Oxygen Demand) in the range of 40,000 to 50,000 mg/L and COD (Chemical Oxygen Demand) 100,000 mg/L. This qualifies its entry into the category of highly hazardous effluent and distilleries as a highly polluting industry. To make the effluent capable of disposal into inland surface waters, irrigation or into public sewers, the BOD should be 30 mg/L, 100 mg/L or 350 mg/L, respectively. If discharged untreated, the effluent would lower the dissolved oxygen level in the receiving waters and result in anoxic conditions that would kill aquatic life and harm local human habitat.

The effluent is distinct and has characteristics very different from municipal sewage, thereby making handling techniques different. Unlike municipal sewage, the organic matter is completely soluble in water, which makes it impossible to separate by sedimentation or decantation. The quantity of putrescible matter is 20 to 100 times higher than that found in sewage depending on dilution of molasses in distillery, and has a strong pungent odor that

Chapter 1: Introduction

becomes more acrid with time due to progressive oxidation and the formation of hydrogen and organic sulfides by bacterial action. Besides its high BOD and COD, chloride ion concentration in effluent is extremely high (10,000 to 12,500 mg/L). Effluent, as it is discharged, has intense dark colour and is acidic with pH ranging between 3.5 and 4.2. High acidity would inhibit the soil nitrifying bacteria and therefore its direct disposal into land or farm with soil with pH lower than 6.5 becomes impossible. Lime treatment to neutralize acidic effluent leads to imbalance of the ionic balance of the soil. Hence, cane cultivators are reluctant to irrigate soil with effluent. Effluent analysis published in Rum Report by the EPA (U.S. Environmental Protection Agency) found other toxic pollutants like Phenol, Bis (2ethylhexyl) phthalate, r-BHC-Gamma, Toulene, Carbon tetrachloride, Benzene, Cyanide, as well as traces of other inorganics (*Lee, 1996*). Since the proportions of toxic compounds are low, the prohibition to land disposal is only due to high BOD and not due to toxic compounds.

1.2. The chemical composition of effluent

Even though the occurrence of organic and inorganic material in the effluent is very complex, it is important to have an approximate estimate in order to understand their influence on combustion and their fate at high temperature. Large-scale production of ethyl alcohol in India uses the technology of yeast fermentation of molasses, of which effluent is the by-product. Essentially, the process involves dilution of molasses, inoculation with yeast, fermentation and distillation. After the fermentable sugar from the molasses has been biotechnologically used and compounds produced have been isolated, the metabolic side products and those non-sugar substances that are not assimilated remain as effluent. Therefore, understanding the composition of molasses will be essential in estimating effluent composition since it contains high portions of original raw materials left out in molasses.

Molasses is obtained after the sucrose has been crystallized and centrifuged from defecated, evaporated cane juice. The process of evaporation and crystallization is usually repeated three times until the invert sugar, non-sugar organic constituents, and high viscosity of the molasses will permit no further crystallization of the sucrose. The unfermentable reducing substance that passes directly to effluent may be as high as 17 %. Sattler and Zerban (1949) reported that about 10 % of reducing power of the unfermentable substances in cane molasses, is due to volatile ingredients such as hydroxymethylfural, acetain, formic acid and

levulinic acid which were decomposition products of the sugar. These substances are formed from fructose. Another reaction is between glucose, fructose, and amino acids in cane juice that would result in fermentable products. All these reactions are accelerated by the high temperature experienced during the processing of cane juice and the storage of molasses under hot sun. Molasses is therefore, a rather crude, complex mixture containing sucrose; unfermentable substances (glucose), invert sugar and salts leached out from cane and all of the alkali soluble non-sugar ingredients. Molasses with water content of 17–25 % has a total sugar content (sucrose, glucose, fructose) of 45–50 %. The content of polysaccharides (dextrans, pentosans, polyuronic acids) is 2–5 % and that of peptides and free amino acids is 2.5–4.5 %. The content of nitrogen free acids (aconitin, fumaric and tartaric acids) is 1.5–6 %. The content of cations, determined as carbonate ash varies between 7 and 15 %.

The carbonate ash has following composition: 30–50 % K_2O , 7–15 % CaO , 2–14 % MgO , 0.3–9 % Na_2O , 0.4–2.7 % Fe_2O_3 , 1–7 % SiO_2 and insoluble substances, 7–27 % SO_4^{2-} , 12–20 % Cl^- , and 0.5–2.5% P_2O_5 (Elvers et al., 1990).

Total solids (Dry effluent)	100 %	<u>Organic Elemental Analysis</u>	
Total inorganic solids	39.72%	C = 35.19 %	
Total organic solids	60.27%	H = 5.02 %	
Sulfates (as SO_4^{-2})	4.46%	N = 1.91 %	
Chloride (as Cl^-)	12.58%	O by difference = 16.09	
Calcium (as Ca)	2.36%	<u>Organic Composition</u>	
Magnesium (as Mg)	3.19%	Sugar	9.0*
Sodium (as Na)	2.31%	Proteins	7.4*
Potassium (as K)	14.80%	Volatile Acids	1.2*
Phosphates (as PO_4)	0.00%	Gums (Polysaccharides)	17.2*
Carbonate (CO_3)	0.00%	Combined Lactic Acid	3.7*
Group III A ppt (mostly iron)+	0.35%	Other combined organic acids	1.2*
Sulfur	1.07%	Wax, Phenolic bodies lignin, etc	13.9*
Ph	4.2 – 4.8	Glycerol	4.5*

* Underkofler et al. (1954)

Table 1.1: Typical distillery effluent composition

Chapter 1: Introduction

Effluent composition is therefore affected by process parameters involved in sugar manufacturing, fermentation of molasses and most importantly the primary composition of cane juice; its non-sugar components and various parameters affecting its composition like the quality of cane, the type and condition of soil on which it is grown etc. Representative composition is given in Table 1.1.

The complex mixture of organics present in distillery effluent, given by Underkofler et al. (1954), is also depicted in Table 1.1.

Inorganic material plays an important role in effluent combustion as is with biomass combustion. Therefore, determining its occurrence in the effluent may be useful in explaining certain chemical transformations taking place during its combustion. It is well known that the alkali and alkaline earth materials play essential roles in plant metabolism and occur in organic structures of very mobile organic forms.

Potassium

Over 90 % of the potassium in a plant occurs as either water-soluble or ion exchangeable material. It is an essential nutrient and acts as a facilitator of osmotic process. Osmotic potentials across membranes and ionic potentials in the cytoplasm are regulated to a large degree by potassium. Potassium plays important roles in enzyme activation, membrane transport and stomatal regulation and hence its concentration is large where plant growth is most vigorous, therefore, cane juice is high in potassium and thus, high in the effluent as well.

Sodium

It is a minor component of most biomass, substituting for potassium in small quantities. Excess sodium is toxic.

Calcium

It is a common constituent of cell walls and other organic components of cell structures and is largely ion exchangeable and acid soluble.

Magnesium

It occurs in trace quantities in most biomass material.

Chlorine

Chlorine in most biomass, in general, appears to occur dominantly in the form of chloride ion and serves the primary role of balancing charge. Its concentration is closely related to nutrient composition of soils. The chlorine level required for cane growth is far less than the levels available in the soil nutrients. Ivin and Doyle (1987) measured chloride concentration in the cane juice, concentrated syrup and final molasses to be 1100, 5500 and 32500 mg/L. These levels were highest for mills located in low rainfall zone and farms receiving irrigation water. In India, most cane farms receive irrigation water because of less rainfall and *cause increase in chloride ion concentration.*

Since most of the inorganic elements are soluble in water or mild acid, almost all of them are extracted in the cane juice during sugar cane crushing, gets concentrated to high levels in molasses, and subsequently find their way into the effluent. It is clear that the presence of *inorganic material will be in a highly dispersed manner at cellular levels and would be linked to organic compounds in a very complex manner.*

1.3. Classical routes of distillery effluent treatment

Effluent needs treatment prior to disposal; the classical route for its disposal is described in brief.

1.3.1. Ferti-irrigation

It is the most commonly used disposal technique employed by small and medium scale distilleries. In this technique, effluent is directly used for irrigating farmland with a view of enriching soil with inorganics present in effluent. A large quantity of dilution water is required in order to bring down BOD to acceptable values and is one of the major limiting factors. In addition to this, there is a risk of contamination of irrigation channels and ground water besides the pungent odour. Distribution of diluted effluent over large land space is therefore required and this involves unaffordable transportation cost (*Cortez et al., 1998*).

1.3.2. Anaerobic lagooning

It is the route in which effluent is allowed to flow into large open ponds for anaerobic degradation and thereby reduce the BOD content (from about 40000 to 3000 mg/L). This process requires large open spaces since its holding period is long (up to 100 days) and has never been known to attain the desired biodegradation. A large quantity of dilution water

Chapter 1: Introduction

(about six to seven times of its volume) is required to bring down the BOD further. Percolation is severe and pollutes sub-soil water.

1.3.3. Bio-methanation

An anaerobic digestion technique is perhaps the most preferred classical route of effluent treatment. The reduction in BOD using this process is about 85-90 % and in COD about 60–65 %. This is a refermentation process during which several groups of facultative organisms simultaneously assimilate and break down organic matter into substrate of volatile organic acid. Methanogenic bacteria will convert the volatile acids into Methane (CH_4), carbon dioxide (CO_2) and hydrogen sulfide (H_2S). Methanogenic bacteria propagate at a relatively slow rate and have generation times ranging between two and twenty-two days. Aerobic treatment is invariably followed after anaerobic digestion to further bring down BOD (from about 5000) to acceptable levels. The overall conversion time is therefore long and a large workspace is essential for the treatment. Complications in the process are due to uncertainties involved in influencing factors like ambient temperature, residence time, acclimatization, re-circulation, and difference in impurities. The dark color of the effluent becomes more intense and continues to be of concern even after biological treatment.

1.3.4. Incineration

This was the most favoured route (*Davis, 1946*) during the first half of the 20th century in order to extract potash from ash, perhaps because of its capability to achieve zero effluent discharge. Jackson (1956) had emphatically stressed upon incineration as the only practical means of complete treatment and anaerobic digestion can be carried out for partial purification. It was evident from a large number of patents on furnaces burning either effluent or molasses for potash recovery that there was a popular drive for the technology though there did not exist any scientific understanding of effluent combustion. The most commonly used patented furnace was called “Porion” furnace.

A schematic of a typical distillery effluent incinerator, constructed from whatever brief description available in the literature is as shown in the Fig. 1.1. Major impediments noted at the time were unbalanced heat economy resulting in consumption of extra fuel and large capital investments. The cost in concentrating effluent was offset with the recovered value from potash or from its value as fertilizer. However, inorganic fumes released during combustion carried away part of the salt into the atmosphere or to scrubbing water body and

Concentration and Incineration of Distillery Effluent

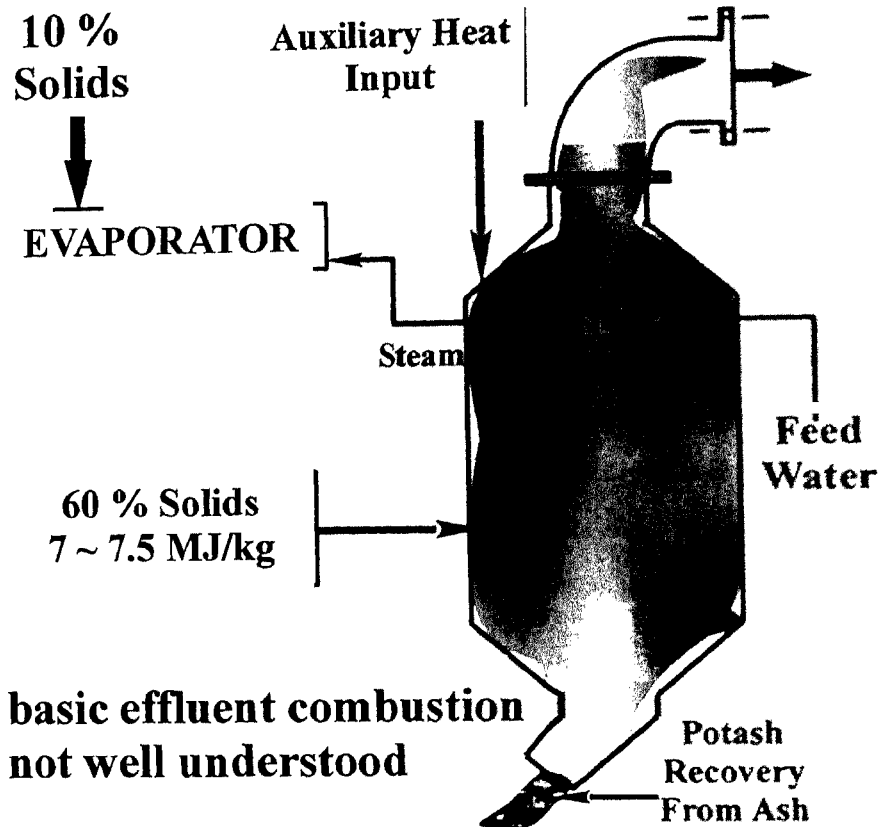


Figure 1.1: Schematic of distillery effluent incinerator

reduced the quantity of salt recovered and resulted in increased working cost. Pellet (1909) had reported to have had found incrustations composed of K_2SO_4 , KCl and $NaCl$ on walls of furnaces burning molasses and boiler tubing that caused corrosion, reduced heat transfer efficiency and potash yield. In order to improve upon steam economy, a method was devised by Reich (1929) in which fermented wash, instead of being dealcoholized in a still was sent straight to a quadruple evaporator. All the alcohol was stripped off in the first three effects, such that the fourth effect condensate would be left with concentrated effluent and no alcohol. The concentrated effluent thus obtained could be burnt in Porion furnace. The use of Porion furnace became less popular with time and one of the Brazilian distilleries was reported to have discontinued effluent combustion in Porion furnace and co-fired with bagasse in a different furnace. Reich (1945) also attempted industrial scale low temperature

Chapter 1: Introduction

(700 – 723 K) carbonization in a steel retort, in order to recover alkali salt and activated charcoal.

Since then, many researchers have tried out similar concepts from time to time. Reports that are more recent were from Swedish Alfa-Laval and a Dutch company named Hollandse Construction Group (HCG) B. V. (Spruytenburg, 1982). There are brief reports on NEM-boilers built by HCG, installed at Banghikhan distillery, Thailand, for burning concentrated effluent in furnaces. The features of the NEM boiler are similar to the schematic shown in Fig. 1.1. Cortez and Perez (1997) conducted experiments on the combustion of the emulsion of effluent (50 % solids) and # 6 fuel oil, that was fired horizontally into a preheated furnace, and found better combustion only at oil to effluent volume ratio of 3 (emulsion lower heating value of 32.7 MJ/kg). An examination of the earlier literature indicates inadequate understanding of the basic effluent combustion process. In addition, there are no published reports known to the author on any present-day operational incinerators.

1.3.5. Wet Air Oxidation

It is an alternate process to incineration that has been proposed for effluent disposal. It refers to the aqueous phase oxidation of organic and inorganic materials at elevated temperature and pressures using dissolved oxygen. The oxidation reactions occur at moderate temperatures 423–588 K and at pressures from 10 to 210 bar. The process can convert organics to CO₂, H₂O, and biodegradable short chain organic acids. Experiments were performed on distillery effluent in a 1 L capacity titanium autoclave (Lele *et al.*, 1990). The two-step experiment consisted of a) thermal pre-treatment and b) wet oxidation. In the first step, effluent was treated at 503 K under self-pressure of 5.6 MPa for two hours and coal-like charred residue was obtained. No carbon was oxidized during pretreatment and COD of filtrate reduced by 50 %. In the second step the filtrate was oxidized at 523 K and 2 MPa oxygen partial pressure for 5 five hours to obtain COD reduction of 75 %. Thus, the total reduction of COD of 87.5 % was obtained in 8 hours. It was estimated that the energy recovery obtained from this process is about 80 % and that obtained from single step direct wet oxidation and incineration of concentrated effluent is 65 %. The experiments performed were on 1-litre autoclave and hence scale-up process performance levels are not easy to estimate.

The advantage of wet oxidation comes from its capacity to handle low solid concentration aqueous waste and compactness of the system as compared to biological systems. However,

The Gasification

Process Philosophy

Sub – stoichiometric Combustion

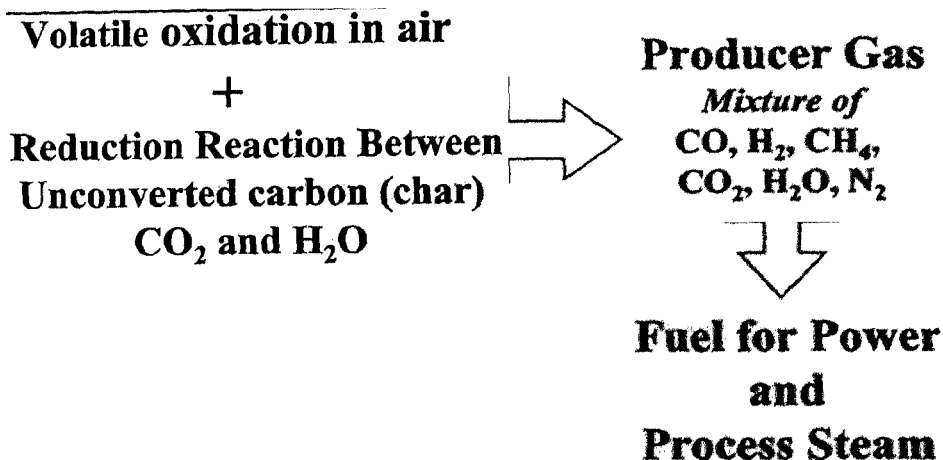


Figure 1.2: Gasification process

since the operational pressure and temperature are high, the capital and operational cost to handle large volumes may perhaps be uneconomical. This is also true because effluent is high in chlorine (~ 1000 ppm, see Table 1) and only titanium based alloy (Gr2, Ti-Gr9 and Ti-Gr12) or cladding of titanium alloys or nickel-based alloy C-276 can sustain such adverse operational ambient conditions (*Kane, 1999*). The cost of the treatment proposed by Conor Pacific Environmental Technologies Inc, who have the global rights to a patented wet oxidation technology for the existing system is US \$0.02–0.25/litre of effluent to discharge into municipal waste stream. Assessment of the critical engineering and economic aspects related to this process have not been reported.

1.4. Alternate Route

It is with this perception of existing inadequate solutions and persistent challenge of effluent disposal; a method with primary aim of disposal and energy recovery while complying with present and future environment norms is urgently required to be devised. Gasification, commonly called 'sub-stoichiometric combustion' has better prospective from the energy and environment point of view. In fact, wood and coal have been gasified and used much before the advent of natural gas, in the quest for achieving clean heat. During the Second World War, gasifiers directly fueled thousands of vehicles. Figure 1.2 depicts the process

Combustion and Gasification: A Concept

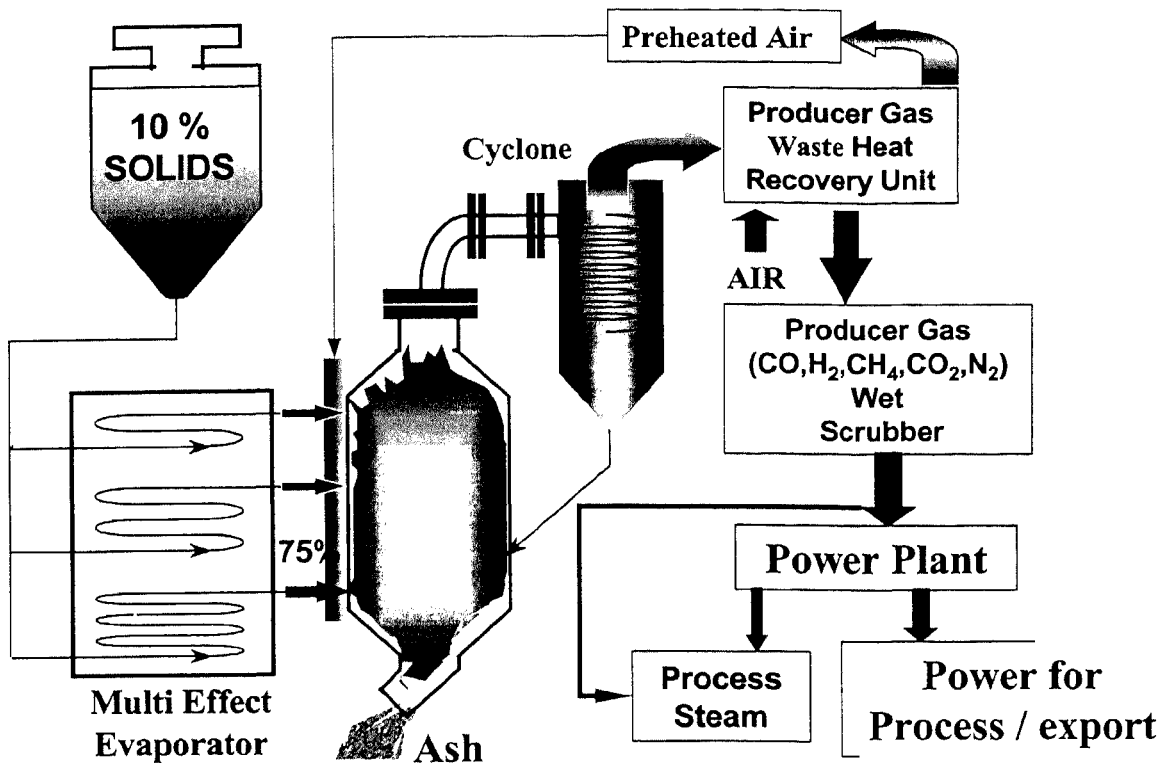


Figure 1.3: Schematic of gasification of distillery effluent

philosophy of gasification process.

Gasification is a modular and controllable combustion process where fuel is consumed in two steps. In the first step the inherently complex organic combustibles are converted to a mixture of simple combustible gases (H₂, CO, CH₄, and/or N₂, CO₂) commonly known as producer gas through a series of thermochemical reactions (pyrolysis, oxidation and reduction). In the second step the producer gas is conveniently combusted in a thermal system capable of producing work (using internal combustion engine or gas turbine to generate electricity) and/or heat (process steam), resulting in combustion products (CO₂ and H₂O, no thermal NO_x since low temperature). The advantage of stepwise conversion is its high-energy efficiency, better control of overall process and effective control over emissions. It is possible that gasification can be applied in the case of waste containing chlorinated organics where high temperature incineration is used for the destruction of dioxins, that the waste generates at lower gasification temperatures.

The Fig. 1.3 depicts a simplified schematic of the concept of effluent gasification.

Effluent with high (75 %) solid concentration is injected with a view of obtaining self-sustained exothermic heat profile and support gasification reactions. Carry-overs and dust from producer gas *are* removed in the cyclone prior to wet scrubbing. Gas can be subsequently fed to boiler furnace or an IC engine/gas turbine for electricity generation. The ash could be utilized directly as fertilizer or potassium salts can be leached out.

Therefore, the most appropriate method proposed to dispose of distillery effluent is gasification. This has the facility of generating electricity directly from producer gas, helps in reducing green house emissions and leads to a higher recovery of chemicals from residue due to reduced fuming or alkali vapors. In the case of incineration where the temperatures are comparatively higher than gasification, fuming is severe. Fumes form deposits on the heat transfer surfaces of boiler causing reduced heat transfer rate. These are known to reduce boiler efficiency subsequently over a period of time.

1.5. Comparison of energy recovery from bio-methanation and gasification process

1.5.1. Energy recovery from bio-methanation

The effluent solid concentration varies from 7–11 % on day-to-day basis and from distillery to distillery. Therefore, the calculation is based on the following primary assumptions derived from the Indian distilleries:

- ★ The out put gas composition: 60 % CH₄, 38 % CO₂, 2 % H₂S.
- ★ Volume of gas generated is 30 times that of effluent input.
- ★ 10 % solid concentration in effluent.

Considering these assumptions, CH₄ generated is 18 m³ per 1000 L of effluent. This is equivalent to 717.4 MJ/1000 L effluent (Higher Calorific Value, HCV) of CH₄ is 39.8 MJ/m³). The total energy content of 1000 litre of effluent is 1450 MJ (HCV of effluent with 10 % solids is 1.45 MJ/kg). Therefore, energy recovery is 49 %, this value is based on the above assumptions, although in practice the efficiency can be as low as 25 %.

1.5.2. Energy recovery from gasification of concentrated effluent

The most important requirement for effluent gasification is the minimum energy content of the effluent. Effluent with solid concentration higher than 60 % is favorable for gasification and above 70 % is the best due to increased energy content. Therefore, part of the heat generated during overall conversion process is utilized in concentrating effluent from 10 %

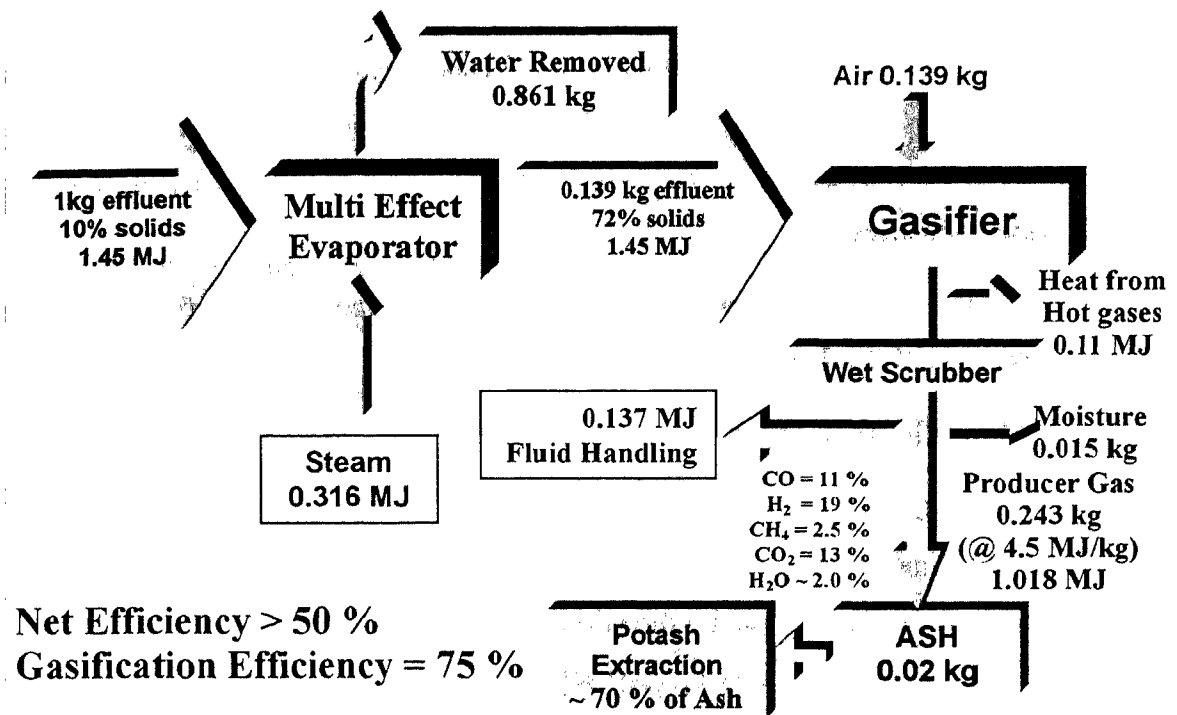


Figure 1.4: Flow chart of energy and mass balance of effluent gasification.

to 72 % solids (feed concentration used in the calculation). This energy required is about 22 % of the total energy content of the concentrated effluent (in this case concentration of 72 %). This value represents the heat content of steam used in a multiple-effect evaporator (two quadruple-effect, forced circulation or 6 or 8 effect evaporator) capable of evaporating 6 times water using one part of steam. The flow chart in Fig. 1.4 depicts energy and mass flow in the context of effluent gasification.

On gasifying concentrated effluent (72 % solids, HCV 10.5 MJ/kg) the producer gas generated will have equilibrium composition (on wet basis) 2.5 % CH₄, 11 % CO, 19 % H₂, 13 % CO₂, with HCV of 4.5 MJ/kg gas. The total gas quantity will be 1.75 times effluent (input air + effluent organics). Hence, the energy recovery efficiency (ratio of energy content of the producer gas to that of concentrated effluent) or gasification efficiency calculated based on given equilibrium composition will be 75 %. The net thermal efficiency therefore will be greater than 50 %.

Reducing heat input to evaporator can increase the net efficiency. One way to do this is to increase output solid concentration of the effluent and this is possible by the use of a process called BIOSTIL where effluent is used to dilute molasses prior to fermentation. The

use of this process will allow effluent output with solids concentration as high as 25–30 %. In this case, this route is the best possible option for its capability to achieve zero effluent discharge and added advantages of recovering chemical from the residue (ash). These evaporators can be considered as ‘water factories’ as in the case of concentrating black liquor in paper industries.

After treating and polishing evaporated water adequately, these can fulfill most process water requirements of the distillery.

1.6. The Gasification Process

Gasification is fundamentally based upon the chemical reactions between carbon and one or more of the three gases, oxygen, steam or carbon dioxide (see Fig. 1.2). Carbon can be converted exothermically into gas by direct oxidation or endothermically by the reduction of steam or carbon dioxide. It is the control of these reactions with a given fuel that determines the effectiveness of conversion.

The design of the gasification system has been largely empirical due to the complex combustion behavior of the fuel. Distillery effluent is a complex mixture of organic and inorganic material; feed containing 75 % solids is composed of about 30 % inorganic and 45 % organic material. Organics participate in combustion while inorganic materials partially catalyze the reactions and/ or act as heat sink in the gasification environment. Thus, design in this case is strictly based on the chemical and physical characteristics of the feed. For designing a fluidized bed incinerator for waste, Mullen (1992), based on assumptions pertaining to large thermal system and heat balance, derived a relationship known as the specific feed characteristic (SFC) of fuel defined as the gross (or higher) heating value (HHV) per unit mass of moisture and combustor system design. Based on this definition, effluent with 40 % solids is autogeneous (SFC value being 9.7 MJ/ kg of water) and requires no auxiliary fuel for self-sustained combustion (cold wind box operation). However, it is sub-autogeneous at 30 % solids and needs auxiliary fuel (hot wind box operation) for self-sustained combustion. In the case of gasification the required solids would be even higher than the prescribed value of 40 % solids, since exothermic oxidative processes in the gasifier should be ideally required to support the endothermic reactions under reduced air conditions. The amount of heat input suggested by Mullen to bring effluent (30 % solids) to autogeneous level is about the same as that required to concentrating effluent from 10 % solids to 73 % solids (using multi-effect evaporator). This

can help in selecting the feed solids concentration for gasification from the viewpoint of thermal efficiency.

The principal reactions taking place in a typical gasifier above 750 K with steam generated from the water present in the feed effluent are:

(1) Oxidation



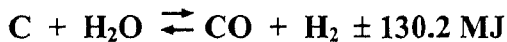
(2) Reduction



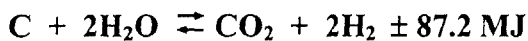
The overall effect of 1 and 2 reactions is



(3) Primary water-gas reaction



(4) Secondary water-gas reaction



(5) Water-gas shift reaction



Reactions (1)–(5) take place in well-defined regions in the fuel bed. The Boudouard (2) and water-gas (3) reactions are highly endothermic and control the upper limit of temperature in the reduction zone. In practice, higher CO and H₂ are favored in order to achieve high calorific value gas. Since the forward reactions are endothermic, high temperatures favor CO and H₂ formation. Primary water-gas reaction is known to be significant at temperatures above 1173 K. The secondary water gas reaction is known to dominate at low temperatures - between 773 and 873 K, while the water-gas shift reaction is a gaseous reaction that takes place in the presence of undecomposed steam and thus, the bed temperature must not fall below about 1373 K or gasification rate will decelerate and cease (*Littlewood, 1977*). Blackwood and McGrory (1958) found that the ash present in carbon (0.26 %) catalyzes this reaction at atmospheric pressure and temperature in excess of 1100 K and has profound influence on the increase in carbon dioxide concentration. The presence of undecomposed steam causes a high additional heat loss partly because of sensible heat and the latent heat removed from the system. This dictates the maximum limit of water that can be injected

Element		Distillery Effluent ¹	Black Liquor ²	Wood ³	Kerosene ³
Carbon	C	35.19	37.2	52.2	85.8
Hydrogen	H	5.02	3.6	4.3	14.1
Oxygen	O	16.09	34.4	41.7	0.0
Nitrogen	N	1.91	0.11		0.0
Sulfur	S	1.07	3.7		0.1
Potassium	K	14.8	2.5		
Sodium	Na	2.31	18.6		
Magnesium	Mg	12.58	0.67		
Calcium	Ca	3.19			
Chlorine	Cl	2.36			
Sulfate as	SO ₄ ⁻²	4.46			
Heating Value on dry basis MJ/kg		14.0	14.36	20.9	44.0

Table 1.2: Elemental analysis of distillery effluent, black liquor, wood and kerosene (% weight basis).

- 1) *Chemical analysis done at Laboratory Services Division, Madras*
C, H, N analysis carried out at Raman Research Institute, Bangalore
'S' analysis done at Cosmic Industrial Lab. Ltd. Bangalore
- 2) *Larson et al. (1996)*
- 3) *Gaur and Reed, 'An Atlas of Thermal Data for Biomass and other Fuels' June 1995,*
NREL/TP-433-7965

into the system along with the solids in the effluent. One of the main objectives of this work is to determine the minimum solid concentration at which effluent can be injected into the system under gasification condition and obtain a steady state operation with as high gasification efficiency as possible.

1.7. Comparison of gasification of black liquor and wood with distillery effluent

Table 1.2 presents element analysis of distillery effluent and black liquor, wood and kerosene. Black liquor, the liquid by-product of the Kraft process used for production of pulp, has features similar to distillery effluent (described later). It is one of the most important industrial fuels since its combustion in traditional recovery boilers (Tomlinson boiler) generate energy estimated to 1 % of total energy production in the US (from 60 million tons solids with total heating value amounting to 9×10^{11} MJ) (*Macek, 1999*). As an alternative to combustion in the conventional recovery furnace, gasification is recently being addressed seriously in the quest for a better option. This is due to the motivation that arises from the prospective improvements in energy, environmental safety and capital investment features that are superior compared to the existing Tomlinson recovery boilers.

1.7.1. Black liquor gasification

The gasification of black liquor can be classified according to operating temperature or the physical state of the inorganic content, the ash leaving the reactor. High-temperature gasifier operates at 1223 K or higher and produces molten smelt of inorganic chemicals in ash. Low temperature gasifier operates at 973 K or lower and inorganics leave as dry solids. Kvaerner and Noell are two companies developing high pressure, high temperature gasifiers for gas turbine technology. ABB, McDermott Inc. and Stonechem are stated to be developing low-temperature gasifiers.

The composition of black liquor used for gasification is same as in the table 1.2.

Table 1.3 depicts equilibrium gas composition and that obtained by research and development gasifier of ABB operated at the following condition (*Larson et al, 1996*).

Liquor with 72 % solid; liquor feed temperature = 388 K; Reactor pressure = 1 bar; air feed temperature = 673 K; reactor temperature = 973 K carbon conversion 99 %; heat loss = 1.065 % of HHV.

Gas Species	Ar	CH ₄	CO	CO ₂	H ₂	H ₂ O	H ₂ S	N ₂
Equilibrium (mol %)	0.47	0.06	13.12	15.21	23.82	0.0	0.87	46.92
ABB (mol %)	----	2.93	12.3	15.81	22.7	0.0	1.64	44.61

Table 1.3: Equilibrium gas composition and that obtained from black liquor gasifier (72 % solid) on dry basis (Consonni. et al, 1997)

The high content of sodium and potassium in black liquor helps catalyze gasification reactions, so that even at relatively low temperature, the composition of product gas is close to equilibrium, except for methane (CH₄) and hydrogen sulfide (H₂S). This is an interesting feature and needs investigation in the case of distillery effluent through experiments and modeling studies.

Gas Species	CH ₄	CO	CO ₂	H ₂	H ₂ S	N ₂	C ₂ H ₄	Total
Gas composition (mol %)	1.2	3.1	20.0	14.1	0.4	61	0.1	100

Table 1.4: Gas composition obtained B&W black liquor gasifier (55 % solids feed rate 1kg/h)

Table 1.4 shows the gas composition obtained by Verril and Dickinson (1998), from a bench-scale low temperature fluidized bed reactor. The average gas analysis obtained is

corrected to commercial conditions by subtracting the excess nitrogen required for fluidization and purge flows in the reactor. The fluidizing mixture (air, N₂ and steam) was preheated to 773 K and average bed temperatures of 755–866 K were maintained by partial combustion of black liquor and electric guard heater.

1.7.2. Wood gasification

Table 1.5 shows calculated equilibrium gas composition and that obtained by gasifying

Gas Species	Ar	CH ₄	CO	CO ₂	H ₂	H ₂ O	H ₂ S	N ₂
Equilibrium (mol %) $\phi=0.42$	0.49	~0*	19.1	11.0	17.0	2.0	----	50.5
Wood Gasifier (O/F = 4.46)	----	1.41	14.35	13.6	15.46	2.0	----	48.4

Table 1.5: Equilibrium gas composition and that obtained from wood gasifier (28 % moisture), * ~0 means non-zero small value.

wood containing 28 % moisture (same as in the case of black liquor feed) in a down draft wood gasifier (*Test no. 14b, performed at Chatel-St-Denis, Jan.-Apr., 1996; Sharan et al., 1996*). As is experienced in the wood gasifiers (updraft, downdraft or open top configurations), the output gas composition in the present case seems to depart from equilibrium significantly.

1.7.3. Distillery effluent vs. black liquor

There are similarities between distillery effluent and black liquor as was mentioned earlier. They are liquid; their output concentrations is about 10 % and have high viscosity at high solid concentration ($\ll 50$ %). Both originate from biomass though the inorganic content in the case of distillery effluent is leached out plant nutrients, while in the case of black liquor, inorganics appear because of the pulping process. Both are charring materials (leaving behind char after initial devolatilization) and have similar heating value and yet their combustion behavior is expected to be different due to their overall composition that results, because of the difference in their origin. Table 1.2 presents elemental analysis of distillery effluent and black liquor on dry basis. Wood and kerosene analysis are also presented in the same table for the sake of comparison. The inorganic content in black liquor is dominated by sodium, while the inorganic contents of distillery effluent are potassium, chlorine, sulfur and their elements.

The organic content of black liquor is lignin, which is the principal non-carbohydrate fraction of wood. Wood constitutes about 15–35 % of lignin. Its decomposition extends

over a range of temperature from 373 K with midpoint between 573 K and 673 K and leaves much more char. It is three-dimensional polymer of sinapyl, and coumaryl alcohols based primarily on the phenylpropane structure. The distillery effluent organic is shown in the Table 1.1. It has very small amount of lignin. Besides gum or polysaccharides, other organic compounds are relatively easy to degrade thermally. Thus, distillery effluent should be relatively simple to combust compared to black liquor. However, since the chlorine content in distillery effluent is high, the path and release mechanism of inorganics may be different.

The chars of both effluent and black liquor consist of sulfate, sulfide and carbonate of potassium and sodium along with carbonaceous organics. It is generally agreed that presence of alkali metal carbonate leads to a reactivity increase over un-catalyzed CO₂ gasification by a factor of 10-100, and that the rate normally increases with increase in atom number, i.e., Li < Na < K < Rb < Cs (*Kapteijn et al, 1984; Spiro et al., 1983*). This is indicative of the effectiveness of alkali metal for gasification increases in the depicted order along with a decrease in activation energy in the same order.

Gasification rate of black liquor char (BLC) in CO₂, obtained from black liquor solids was found to be an order of magnitude higher than of a high surface area, activated carbon, impregnated with either potassium or sodium carbonate (*Li and van Heiningen, 1990; Frederick et al, 1994*). This is so despite BET surface area of BLC (160 m²/g) being almost an order of magnitude lower than that of alkali-impregnated carbon or IAC (1000 m²/g). In addition, the types of kinetics and activation energy of gasification are the same for BLC and alkali metal impregnated chars, suggesting a similar reaction mechanism. The possible reason for high reactivity in the case of BLC was attributed to the extremely fine and uniform distribution of the alkali (sodium in the case of BLC) in the carbon matrix that catalyzed the reaction. This distribution was confirmed from SEM-EDS of both the chars (*Li and van Heiningen, 1990*). Black liquor, the by-product of Kraft process, is a solution in which sodium is mixed and chemically bound with degraded lignin and carbohydrates on a molecular scale. Therefore, the distribution of the catalyst in the solids, and subsequently in the carbon matrix of the char is expected to be extremely fine through the bulk of the char. *Similar distribution is expected in the case of distillery effluent since the complex organic and inorganic material; largely potassium coexists in solution where water is solvent.*

1.8. Overview and objective of the present work

The motivation for the present work comes from the necessity of devising a thermochemical conversion technique that can contribute to adequately disposing distillery effluent, since it poses a threat to environment. This need was realized even during the early part of this century; however, seriousness has enhanced only recently, when environment regulations have become stricter and the control of effluent discharge is inevitable. The greatest impediment found in carrying out the present work is inadequate experience in effluent combustion and on basic data like thermophysical and thermochemical properties of effluent. Moreover, earlier literature on the combustion studies of effluent material is scanty. Therefore, considerable groundwork was needed while carrying out the experiments on effluent combustion and gasification. In the case of black liquor, though its combustion in boilers has been in practice for over half a century, the fundamental combustion studies to improve the efficiency with an abatement of environmental emissions are more recent. Therefore, the present work aims at studying the fundamental combustion aspects of concentrated effluent in air, including gasification experiments in laboratory scale reactor.

The thesis consists of seven chapters. The present chapter (chapter 1) has provided the background to the issues related to dealing with distillery effluent handling, and the motivation to thermochemically treat the effluent in the light of presently available routes of disposal.

Chapter 2 presents review of the literature relevant to the present work.

Chapter 3 deals with the basic study of combustion of effluent droplet of different concentrations and dry spheres in hot quiescent air. The effects of size, ambient temperature and solids concentrations on combustion features like ignition delay, ignition time, flaming time and char glowing time are brought out. Model predictions of char combustion are presented and compared with experimental results. Continuous weight loss profile by effluent sphere during complete burn out was determined in order to understand the effect of ambient temperature on weight loss during flaming and char glowing. The chemical analysis performed on char and ash of effluent spheres obtained at different temperatures to understand the relationship between their release and ambient temperature including the transformation of sulfate – sulfite – sulfate during the course of combustion are significant parts of this chapter. The outcome of the single particle combustion experiments were utilized in devising a practical combustion system in which effluent spray experiments were

Literature Survey

2.1. Introduction

Large-scale incineration of distillery effluent was attempted since the early part of this century as is discussed in Chapter 1 (section 1.3.4). However, there appears to be no work related to the fundamental combustion process earlier to that published by Patel et al. (1996) and Patel et al. (1995). This makes it imperative to review the literature of those fuels, which have a resemblance to the distillery effluent in terms of physico-chemical properties and combustion. The single particle combustion behavior (drying, devolatilization and char glowing) of distillery effluent in high temperature environment, has some resemblance to several multi-component fuel droplet systems like black liquor, coal water slurry, coal oil slurry, oil water emulsion, high moisture biomass and a mixture of volatile and non-volatile fuels. Black liquor is the most resembling to distillery effluent, primarily due to presence of water and high inorganic content; primarily alkali (discussed in section 1.7.3) and the heating value. The resemblance to slurries and emulsion is largely due to the presence of large water content. Water is generally a solvent in all these fuels and has an impact on their rheological properties as well as combustion. Unlike distillery effluent, combustion studies of most multi-component fuels, such as single particle and spray have been extensively researched and reported in the literature. These studies are reviewed in the first part of the literature survey to relate the experimental findings obtained by combusting distillery effluent. The second part reviews fundamental studies on char combustion in air at elevated or furnace temperature. Finally, the experimental work carried out in the applied field of gasification is reviewed briefly.

2.2. Physico-chemical properties

The heat of combustion is a function of pulping condition like cooking temperature, cooking time, white liquor composition (effective alkali, sulfidity) and yield of pulp. The heat of combustion varies considerably (11.82 – 16.55 MJ/kg) with the pulping conditions.

Empirical models (non-linear product model) have been developed by Zaman and Frickle (1995) to relate heat of combustion to pulping condition. It was also found that the heat of combustion is a linear function of solid concentration and the slope remains almost similar for most liquors experimented. The heat of combustion of distillery effluent dry solids reported by Kujala et al. (1976) is 14.4 MJ/kg, by Spruytenburg (1982), 7.6 MJ/kg for 60 % solids (12.7 MJ/kg for 100 % solids), by Chakrabarty (1964), 14 MJ/kg (LHV) and Polack et al. (1981), 12.5–15.1 MJ/kg. *Thus, the heating value of distillery effluent is in the same range of that of black liquor.*

In the case of coal water slurry, the heating value is based on the type of coal selected for making slurry and coal loading. The typical heating value of coal water slurry containing 65 % coal is 23.3 MJ/kg (Michale et al., 1982) and bitumen-water emulsion containing 70 % water is 28 MJ/kg (Marcano et al., 1991). *These values are about 2.5 times higher than of 70 % solid distillery effluent or black liquor.*

Like distillery effluent, black liquor consists of heterogeneous polymers, organic and inorganic salts, caustic and water. Their rheological behavior is equally complex. The fluid character changes from a Newtonian to non-Newtonian to a viscoelastic fluid with increase in solid concentration. The rheological properties of black liquor significantly affect heat transfer and evaporation rate in evaporators, droplet size and distribution in the typical chemical recovery furnace, loads and constraints in the transport of black liquor, flow patterns, stability of combustion and emissions (SO_x). Zaman and Fricke (1995) have presented results of their study on rheological properties of slash pine Kraft black liquors for concentrations up to 80 % solids and temperatures up to 140 C. They showed that black liquor at low solid content (< 50 %) behaves as polymer solution and at high solids (> 50 %), exhibits non-Newtonian behavior depending upon temperature and solid concentration, solid composition and shear rate. It also exhibits shear-thinning (pseudoplastic) behavior.

The boiling point of black liquor is estimated by a correlation ($T=100+50 \times S^{2.74}$, where, T_{bp} in C and S is solids fraction (for $S = 0.65$, $T = 115.3$ C)) obtained by Adams and Fredrick (1988). The density of black liquor decreases with temperature and increases with solids fraction (over a range of % solids, the decrease in density is from 1380 to 1310 kg/m^3). Surface tension at elevated temperature is not well known, however, the estimated values are 50 mN/m for 65 % solids and at $T = 373$ K (Macek, 1999). This value sharply increases with solids loading. Thermal conductivity of liquors is also not well known. However, it is

certain that it increases with temperature and decreases with increase in solid concentration. *In the case of distillery effluent properties, boiling point, surface tension and thermal conductivities could not be found in the literature.*

From an abstract of a paper authored by Popov et al. (1960) reported in International Sugar Journal, it seems that the author had prepared table of specific gravity and viscosity of distillery effluent. An empirical formula was derived for determining the value of specific gravity for a given fluid temperature and % solids ($\gamma = 1020 \times \exp(0.00447 \times (DS) - 0.8t)$), 'γ' is density in kg/m³, 'DS' is dry solids and 't' is temperature in C). This relation indicates specific gravity behavior same as in the case of black liquor with respect to solid concentration and temperature. Detailed study on viscosity of distillery effluent and effects of temperature and solid concentration could not be found.

2.3. Method of injection and combustion in furnace environment

There is a vast difference in the methodologies employed in combusting black liquor and other multi-component fuels like coal-water, coal-oil slurries or oil-water emulsion in furnace environment. The primary aim of combusting black liquor is to recover spent chemicals from the residue obtained after combustion and this is done by traditionally injecting black liquor as a coarse spray with an average stream diameter in the range of 2 to 10 mm (on the other hand, stable flame with high combustion efficiency, high heat release rate and reduced emissions are the primary aim of combusting slurry fuels and emulsions to replace premium fuel use in boilers and IC engines). Fine atomization of the fuel is essentially used for the applications (droplet size < 200 μm). Besides, disruptive burning is much preferred for secondary atomization.

2.3.1. Distillery Effluent

Spruytenburg (1982) is reported to have atomized and injected distillery effluent with 60 % solid in swirl combustion chamber of NEM-boilers. There are no details on the effluent combustion process; its atomization or critical features related to system performance; however, there is a mention of the economic advantages associated with the use of incineration as effective disposal technique. Polack et al. (1981) also had injected pre-heated effluent (to 323 K) with concentration varying from 63.9 to 73° BRIX (BRIX is generally defined as total solid matter as determined after removal of water) into a furnace maintained at temperature ranging from 1033 to 1200 K using air blast atomizer. They

failed to obtain sustained combustion of effluent and concluded that distillery effluent (Louisiana vinasse) was a difficult fuel to burn. Considering this failure, Cortez and Perez (1997) injected emulsion of effluent # 6 fuel oil (heating value 43.3 MJ/kg) – effluent (heating value 7.8 MJ/kg) using same burner earlier used by Polack et al. (1981). They obtained the best combustion when the oil-effluent ratio (by volume) was greater than 3 and the emulsion lower heating value was 32.4 MJ/kg, which is even more than coal water slurry value. In addition they observed insensitivity of CO concentration measured in the stack, to the increase of excess air, unlike that found in the case of neat # 6 fuel oil. This, they interpreted as an effect of water fraction present in the droplet. Though it is known that emulsions of # 6 oil and water lead to droplet disruption, no such observations were made with distillery effluent. Authors have also not commented on the combustion residue, carbon conversion or the combustion efficiency.

2.3.2. Black Liquor combustion

Black liquor is burned as particles resulting from a coarse spray in recovery boiler furnace, with a mean particle diameter of 2-3 mm and distribution ranging from 0.5 to 5 mm (Adams and Frederick, 1988). Macek Andrej (1999) has reviewed research on combustion of black liquor droplets carried out during 1980s and 1990s. Fine droplets are not preferred to avoid carryover, responsible for plugging. Therefore, stable flame is not expected and most combustion processes occur after partly devolatilized droplets fall on the bed of typical recovery boilers. In fact, care is taken to avoid even the formation of satellite droplet along with main droplet by maintaining the Ohnesorge number ($\mu/\sqrt{(\rho \cdot \sigma \cdot d)}$, where μ is the viscosity, ρ is the density, σ is the surface tension and d is the droplet diameter) greater than 1.6 (Bousfield et al., 1990). This has restricted the work on the study of fine spray atomization of black liquor. The commonly used injectors are splash-plate, the V-jet and the swirl cone. Empie et al. (1997) have evaluated these injectors for distribution of mass flows in black liquor spray. Bousfield et al. (1990) performed extensive fundamental studies on the breakup of liquid jets over a wide range of viscosities, densities and surface tension, as well as jet diameters and velocities with an emphasis on high-viscosity liquids relevant to black liquor. The sprays are injected horizontally and owing to their large size, most drops and resulting particles at various stages of reaction fall by gravity against the boiler gas flow on the char bed. The temperature above the bed is typically 1373 K and 100–200 K lower than bed at higher elevation. The present trend is to inject black liquor with as high solids as

possible (> 70 % and < 80 %) mainly due to reduced energy losses used for evaporation of water and reduced sulfur emission (McKeough et al., 1995)

2.3.3. Slurry Fuels

In the case of coal-water-slurry, fine atomization is preferred to reduce the water evaporation time and ignition delay to attain stable flame. Liu et al. (1983) have proposed preheating of the slurry, increase of coal loading and creating fine atomization. Walsh et al. (1984) estimated the characteristic time for heating, vaporization, ignition and combustion of 10 to 100 μm coal-water slurry droplets under conditions measured in 1 MW turbulent diffusion flames with high swirl. They used single port internal mixers, air blast atomizer and found that both water and particle size increase due to agglomeration occurring after drying and heating were detrimental to flame stability. The total time required to ignite slurry with 64–68 % coal loading was approximately twice that for pulverized coal particle of the same size in air at 1400 to 1500 K. The ignition distance for coal water slurry was 50 % greater than those for equivalent combustion. Michale et al. (1982) burned CWS with 65 % coal using an external mixing air blast atomizer with high swirl number (2-3) primary air and preheated secondary air and obtained stable flame. The high degree of secondary swirl helped in significant amount of carbon burnout (78–89 %) with burn rate similar to that of pulverized coal. However, the combustion residue (bottom ash) having large particle size and considerable macroporosity was found to have contained relatively high percentage (~ 13 % of initial volatile matter obtained on dry and ash free basis) of unburned *volatile matter and this was not attributed to the presence of water*. In order to improve flame stability and intensify combustion for higher carbon burnout, opposing jet configuration was suggested. This configuration is intended to eliminate the problem of large particles escaping the recirculation zone usually found in the case of slurry fuels. Zhao (1988) experimented with a similar configuration and obtained stable combustion of CWS using non-preheated combustion air in an industrial boiler.

2.4. Combustion process in high temperature environment

After injection into the boiler-gas stream, a black liquor or CWS drop progresses through a series of processes in its flight to the char bed - heat-up to the boiling point, drying (vaporization), devolatilization, ignition, combustion of volatiles, combustion of char, and in the case of black liquor, smelt coalescence. These processes are concurrent except for the small droplets. Unlike CWS, most combustion processes of the black liquor droplets are

expected to take place on the bed (Macek, 1999) essentially to avoid carryovers. This is one reason for restricting the size of black liquor droplet to 2 to 3 mm and distribution ranging from 0.5 to 5 mm.

There are no reports on the details of the combustion processes of distillery effluent droplets, although spray combustion has been attempted (Polack et al., 1981) and employed for effective disposal and potash recovery from ash (Spruytenburg, 1982).

2.4.1. Single Particle combustion studies

Earlier laboratory studies on black liquor droplet combustion carried out by Hupa et al. (1987) (suspended droplet in stagnant hot air) and Clay et al. (1987) (suspended droplet in a gas flowing downwards) led to the definition of three-time periods, drying time, t_d from the initial contact with the gas to ignition: devolatilization time, t_v , from the appearance of flame to maximum expansion, and char burning time, t_c . Empirical correlations were established for all the three: $t_d \sim d_o$, and both t_v and $t_c \sim d_o^{1.67}$. The drying stage is mostly dependent on the water content of the black liquor, the drying time being smaller for high solids liquor. The pyrolysis time is about the same, the largest dependence being on the combustion temperature. The char burning times are the largest of the four combustion stages, being dependent on the residual carbon in the char after devolatilization, the combustion temperature and oxygen content in the quiescent atmosphere.

Burgess and Ghaffari (1988) observed, three combustion stages viz. pre-ignition, flaming and char glowing in the case of coal water slurry droplet suspended on a 50 μm thermocouple wire as was in the case of black liquor. The ignition delay ' t_i ' was found to be proportional to initial diameter, while flaming or devolatilization time ' t_f ' or ' t_v ', char burn time ' t_c ' and overall burn time are all proportional to square of diameter. Takeno et al. (1996) observed the same three combustion stages in suspended CWS droplet. The terminal period of the water vaporization stage overlapped by the flaming for short period, during which the droplet center temperature was still at the boiling point of the water. No micro-explosions were observed regardless of intensity of external heat flux. Yavuz et al. (1998) experimented on the droplet suspended on 100 μm thermocouple junction. They found the variation in all segments of process times noted above including the overall burn time, as linearly increasing with droplet diameter. Murdoch et al. (1984) found the over all burn time for a freely falling droplet following the d^2 -law with the parameters depending on the coal type. For low-swelling (swelling number = 1) coal, d^2 -law held good but for highly swelling

coal (swelling number = 7) the relationship was poor. The ignition delay for low-swelling coal also obeyed d^2 -law since it was largely controlled by water evaporation. Outassourrt et al. (1984) heated schlamm's droplet (by-product of coal processing containing 38 % water) suspended on the thermocouple junction using laser beam. On heating, droplet underwent four step transformation including water evaporation, devolatilization, volatile combustion (flaming) and heterogeneous char combustion (char glowing). They assumed water evaporation and char combustion as diffusion-controlled processes.

2.4.1.1. Pre-ignition Processes

The slurry fuel droplet, concentrated black liquor droplet (water is solvent), or coal or wood spheres containing inherent moisture undergo rapid physical and chemical changes prior to either homogeneous or heterogeneous ignition, when exposed to high temperature ambient. These pre-ignition changes are heating, inert drying (or water evaporation), swelling in the case of black liquor and CWS of swelling coals and devolatilization. Swelling may or may not necessarily occur. These processes are concurrent or successive depending on the size and heating rate. In the case of large droplets, though evaporation and devolatilization processes overlap, at any given location they are successive. For example, in the case of black liquor, the surface of a droplet can dry and can even ignite while its interior still retains liquid water (Macek, 1999). However, for small droplets, drying and pyrolysis are successive ($d_0 \sim 0.5$ mm). Saastamoinen and Richard (1996) suggested that the internal circulation is prominent up to 85 % solids in the case of black liquor and CWS. This allows for the possibility of bringing water to the droplet surface where vaporization occurs. The proposed vaporization steps are 1) evaporation of water taking place on the surface with strong internal mixing and 2) vaporization in a narrow region inside the particle approximated by shrinking core.

The suspended droplet experiment conducted by Liu and Law (1986) observed an inert stage (with no pyrolysis) during which most water was vaporized for droplet of CWS, with initial diameters ranging between 0.95 and 1.6 mm. Murdoch et al. (1984) in their combustion experiments on CWS of initial droplet size ranging between 0.5 and 1.3 mm, divided processes occurring during ignition delay into two. During the first process, droplet is heated to boiling point (of water) and surface water evaporates without any reaction and much change in its size. In the second process, swelling occurs once the outer surface gets dry and coal agglomeration on the outer surface forms a crust that prevents volatiles and

steam escaping partially or completely, building up internal pressure. Once maximum swelling occurs, the escaping volatile from the porous surface ignites. Volatile escape can also be violent and can change the droplet heating rate.

Yavuz et al. (1998) have studied the change in evaporation time as a function of droplets diameter of non-swelling coal (lignite) water slurry and ambient temperature. They found linear relationship between evaporation times with droplet diameter and determined the slope of the line decreasing with increasing ambient temperature. Marcano et al. (1991) experimented on suspended single droplet of bitumen-in-water (Orimulsion). Since this is the emulsion of two immiscible liquids, water remains on the droplet surface during early stage of combustion and receives heat. During ignition delay, water is evaporated until particles are exposed on the droplet surface, pyrolise and ignite. They found that the addition of water caused increase in the ignition delay especially when the water levels were greater than 24 % by volume. This is because water acted as a thermal sink and increased the preheating period (until the water boiling point) of the droplet. However, at higher furnace temperature (> 1123 K), ignition delay was only slightly affected by water content. They also found ignition delay time of similar sized droplets ($d_0 = 800 \mu\text{m}$) showed Arrhenius dependence with temperature.

Yao and Liu (1983) performed a study on the heating process of suspended droplet of CWS with slurries made of two types of coal 1) caking bituminous (36 % volatile) and 2) non-caking lignite (40 % volatile). Core temperature profiles of both the coals showed different characteristics. A flat step at 373 K was seen in the case of first type of coal due to water evaporation. In the case of second type, the step at 373 K was missing. The absence of step was attributed to easy removal of the generated steam that enabled the *evaporation front to march closely with the thermal front to the interior of the droplet*. It was concluded that these differences in heating processes are possibly less due to their volatile content than due to their different *agglomeration properties*. In the second type the temperature profiles showed a step at 473 K and was found due to violently occurring devolatilization process.

2.4.1.2. Swelling behavior

The swelling behavior of fuel during initial combustion phase results in the increase of surface area including the pores and thus enhances the oxidation rate (Michale et al., 1982). The products (steam and volatiles) formed during heating of fuel droplet (with higher specific volume than condensed phase) if not allowed to escape freely would lead to

swelling. The swelling can be caused by the bubble formation in the pyrolysis zone and by the pressure increase due to steam generation in the case of large droplet. The swelling is possibly reduced by the transport of bubbles to the droplet surface where gases are released (Saastamoinen and Richard, 1996). Frederick and Hupa (1994) considered the black liquor droplet swelling to start mainly after drying. However, in the case of large droplets, drying and devolatilization overlap. They found relation for the dependence of maximum swelling of black liquor with ambient temperature and uncovered a decreasing trend in swelling with increasing ambient temperature. They proposed that this is due to resolidification of the surface once it reaches temperature more than 973 K. Solidification of surface layer prevents further swelling and the increased pressure in the interior is forced out through the blow holes.

Swelling factor (d/d_0) is defined as ratio of swelled diameter (d) to initial diameter (d_0). Sakai and Saito (1983) and Liu and Law (1986) reported swelling factors of CWS between 1.1 and 1.15 over an extensive range of initial diameter and ambient temperature. This leads to semi-porous hollow structure with high total surface area for oxidation. Droplets of heavy fuel, biomass pyrolysis oil, and oak oil all swell. In the case of black liquor the swelling factor observed was 1.3–1.8 (average 1.5) noted immediately upon contact with hot gases and remaining constant during drying period (Macek, 1999). Rapid and drastic expansion ensued during devolatilization leading to swelling factor exceeding 3 at the end of the stage and diameter decreased during char combustion. Yavuz et al. (1998) concluded that the non-swelling nature of lignite in the LWS combustion is responsible for relatively long burn time in contrast to that of swelling coal (bituminous caking).

2.4.1.3. Pyrolysis or devolatilization

Complex polymeric substances like coal, wood or biomass, plastic, black liquor, and distillery effluent decompose or depolymerize when heated at high temperature and release pyrolysis products largely in the form of gases. Temperature and heating rates are important factors in determining the amount of char formed. Kobayashi et al. (1976) found that the volatile yield increased from 30 % at 1250 K to 63 % at 2100 K for the same coal. Bituminous coal pyrolyzes at about 700 K for heating rate of 100 C/s as in the case of most plastics. At higher heating rate ($> 10,000$ C/s) pyrolysis may start at as high as 1500 K. As the volatiles evolve from the particles, they escape through the pores. If the rate of release of volatiles through the pores controls the liberation rate, then the volatile evolution time

can be estimated using shrinking core model of Essenhigh and Howard (1966). According to this model the volatiles are contained in the core of the particle like a liquid, which shrinks in size as the volatiles escape from pores. The pyrolysis time is given as $t_p \sim k_v \cdot d_o^2$, $d_o = 0.3$ to 4.0 mm where $k_v = 90$ s/cm² for bituminous and 40 for anthracite.

The typical pyrolysis products for coal and most biomass derived fuels can range from higher volatiles CH₄, C₂H₄, C₂H₆, CO, CO₂, H₂, H₂O etc to heavier tar. Based on the composition of pyrolysis gas, stoichiometric requirement of oxygen is obtained. This also decides the ignition temperature for gas phase ignition. As reviewed by Annamalai and Ryan (1993), the typical composition determined by Smoot and Pratt (1979) at 1300 K are as follows: for bituminous coals the % of CH₄, H₂, CO + CO₂ are as follows: 50 %, 13 % and 27 % (in vacuum) and 8 %, 59 % and 27 % respectively in air at T = 1300 K. Lignite in He produces only about 3 % CH₄ but 38 % CO and CO₂. This clearly indicates CH₄ to be the dominating species in the case of coal devolatilization. In the case of pyrolysis of concentrated olive mill waste waters, high in inorganics, Petarca et al. (1997) determined product composition for two similar samples introduced at 673 K and 773 K in inert atmosphere are as follows: CO, CO₂, CH₄, H₂, and C₂H₆ 14.94 %, 88 %, 0.1 %, 0.75 %, at 673 K and 9.87 %, 58.59 %, 6.47 %, 22.05 % and 2.56 % at 773 K respectively and C₂H₄ was also found to be 0.46 at this temperature. This showed the effect of temperature on pyrolysis products, as temperature increases the release of hydrogen, methane and olefins significantly increases, and was attributed to second stage pyrolytic process typically occurring at high temperature.

2.4.1.4. Ignition and Ignition Delay

The spontaneous ignition of the volatile matter evolved during the heating of droplet or particle in flame is called homogeneous ignition (GI). If the volatile matter concentration in the gas phase is low, homogeneous ignition may not occur and towards the end of devolatilization, ambient oxygen will reach the solid surface of the particle and react with it, with a bright glow. The ignition in this case is called heterogeneous ignition (HI). The ignition delay is the time period between the exposure of the droplet at high ambient temperature, T_a and appearance of flame as seen as flash of light around the particle or bright glow over the particle surface. Essenhigh and Thring (1958) conducted experiments on 10 types of coal with particle diameter between 0.3 mm and 4.0 mm and found that coal particle of diameters smaller than 0.65 mm could not ignite homogeneously (flaming

ignition) but after pyrolysis had occurred, the char ignited heterogeneously. This was attributed to the low volatile matter concentration created in the gas phase incapable of reaching ignition limit of the mixture, at the ambient gas temperature involved. Burgess and Ghaffari (1988) also determined critical diameter of CWS droplet ($d_o \sim 0.9$ mm) above which flaming ignition occurred and below which heterogeneous ignition took place. As reviewed by Annamalai and Ryan (1993), typically, homogenous ignition is favored for high volatile coal and large particle diameters ($d_o > 1$ mm) since flammable mixture can be readily formed in the gas phase surrounding the particle. The diffusion time of volatiles scales with r^2/D (where, ' r ' is particle radius and ' D ' is diffusion coefficient) while the gas phase reaction time scales like $\sim 1/A \exp(-E/RT)$. While the reaction time is relatively fixed the diffusion or residence time for smaller particle is too small to balance with reaction time. Hence, small particle will never ignite homogeneously a feature consistent with the findings of Takei et al. (1993) for pure n-heptane droplet of $d_o \leq 0.65$ mm. In this case droplet evaporates without ignition since Damkohler number, defined as ratio of mass transfer time to reaction time, would be low due to higher vapor mass flux (mass flux is inversely proportional to the diameter).

Annamalai and Durbetaki (1977) analyzed the ignition of coal particles assuming (i) solely homogeneous reaction and (ii) solely heterogeneous reaction. For case (i), reactions were assumed to occur at a surface (reaction zone) where the volatile concentration is in stoichiometric proportion to oxygen. They determined near ambient temperature ($T_{r,i}$) such that reaction zone supplies the endothermic heat required for pyrolysis and to raise the temperature of volatiles to reaction zone temperature while the heat transferred to ambience is zero. They called this criterion of determining $T_{r,i}$ at which $dT/dr = 0$ near ambience as adiabatic ignition criterion. They plotted $T_{r,i}$ vs. d_o (initial diameter of the particle) for homogenous and heterogeneous ignition and found that for homogeneous ignition, decreasing particle size increases $T_{r,i}$ and same is in the case of heterogeneous ignition.

Takei et al. (1993) obtained ignition delay of a suspended fuel droplet of pure and blended hydrocarbon fuel in the furnace at high temperature for different diameters experimentally. For pure hexadecane droplets, ignition delay increased with initial diameter (d_o range from 0.4 to 1.4 mm) and for n-heptane, it decreased at $T_a = 950$ K but remained constant at $T_a = 1023$ K. They proposed that the large fuel droplets or droplets of less volatile fuel, ignition delay is predominantly due to time taken for fuel to vaporize and therefore the ignition

occurs in vaporization-control region. In the case of volatile droplets or small droplets, since mass flux is inversely proportional to the diameter, the mass transfer rate becomes large at smaller diameters resulting in increased mixing and reaction time. In such cases ignition delay is largely due to reaction process and therefore, ignition is said to occur in reaction control region. In such cases, the ignition delay of blended fuel, therefore, is decided based on initial diameter, the mixture ratio of volatility of the fuel and the region in which the region of the ignition scheme falls as an overall effect. Though, Sakai and Saito (1983) experimentally determined that the ignition delay of coal oil slurry to be independent of initial diameter unlike that of coal water slurry. The ignition delay dependence on coal particle diameter was also determined by Ragland and Weiss (1979).

Ignition delay in the case of CWS results from two processes. The first process is the droplet heating to the boiling point of the water and evaporation of surface water; while the second process is of devolatilization of dried surface till the flammable volatile mixture ignites. Murdoch et al. (1984) found the ignition delay for low-swelling coal to obey d^2 -law since it is largely controlled by water evaporation. Burgess et al. (1988) and Yavuz et al. (1998) found it to be proportional to initial diameter. In the case of black liquor, Hupa et al. (1987) determined linear relationship of ignition delay with initial droplet diameter. Yavuz et al. (1998) also determined linear reciprocal relationship between ignition delay and volatile matter content of the slurry droplets with $d_0 = 1.15$ mm at same ambient temperature.

2.4.1.5. Flaming

The volatiles form an inflammable mixture surrounding droplet or sphere of charring material, which get ignited and burn in enveloping flame. The pyrolysis front, is the source of volatile, is assumed to be a thin reaction zone because of high pyrolysis rate activation energy and regresses towards the center. Kuwata et al. (1969) investigated the combustion of paper spheres (cellulose) with d_0 ranging from 8 – 45 mm suspended on steel wire at room temperature and ignited in air at velocity ranging from 0 – 160 m/s and oxygen varying from 21 % to 70 %. They observed d^2 – law with different constants in volatile and char combustion. However, since they found char combustion occurring over the whole range of total burning time and pyrolysis termination was not clear, overall burn time was considered and was found to obey approximately the d^2 – law with the value of burn rate constant comparable to those of for oil droplets, volatiles and polymer. In the case of large

size wood spheres burnt in quiescent air, Mukunda et al. (1984) found it to be combusting with two distinct zones, flaming and char glowing, and observed d^2 – law with same burn rate constant throughout the combustion.

The d^2 and weight reduction during flaming were found to be 20 – 25 % and 75 – 80 %. A mathematical framework has been developed by Mukunda et al. (1984) for treating the flaming combustion involving the movement of an exothermic pyrolysis front into the sphere and other aspect similar to droplet combustion.

In the case of CWS droplet, the volatiles that are released during the pyrolysis phase with simultaneous agglomerate swelling usually burn homogeneously in an envelope flame around the droplet in the same manner as found in the case of pulverized coal particles. Flaming time is reported to be following d^2 – law by Liu and Law (1986) and Murdoch et al. (1984).

Hupa et al. (1987) and Clay et al. (1987) established empirical correlations between volatile combustion time and initial droplet diameter for coal particles as $t_v \sim d_o^{1.67}$. Murdoch et al. (1984) had also found that the d^2 – law does not hold good for slurry prepared from highly swelling coal as is also in the case of black liquor with swelling ratio of about 3 during devolatilization.

2.4.1.6. Char Combustion

The heterogeneous char combustion of CWS (slurry of Bituminous coal) carried out at furnace conditions ($T_a \sim 973$ K and above) was found to be diffusion-limited by Liu and Law (1986), Burgess and Ghaffari (1982), Murdoch et al. (1984) and found the char burn time ' t_c ' was found to be proportional to d_o^n , where $n = 2$. Sakai and Saito (1983) also found similar observations in the case of coal-oil-water slurry. The char combustion of ignite-water-slurry char, carried out at $T_a \sim 1073 - 1123$ K was found to have stronger influence of rate kinetic and burn time was found linearly proportional to diameter. This was attributed to the non-swelling nature of Lignite in contrast to high swelling coal. Black liquor is highly swelling material although the char burn time is proportional to $d_o^{5/3}$ indicating influence of rate kinetics. Dasappa et al. (1994) performed combustion experiments on dried wood char of diameter ranging between 2 and 15 mm in O_2 - N_2 mixture with varying O_2 concentration at 300 K and 1000 K. The char burn time given by $t_c \sim d_o^n$ with $n = 2$ and 1.87 when combusted at 1000 K and 300 K respectively indicating

combustion as diffusion controlled. The difference in exponent value is attributed to difference in mass transfer caused by free convection at 300 K, which gets minimized when char is combusted at higher temperature.

	Ignition Delay $t_i \sim d_o^n$ 'n'	Flaming $t_f^n \sim d_o^n$ 'n'	Char glowing $t_c \sim d_o^n$ 'n'
<u>Black Liquor</u>			
<i>Hupa et. al. (1987)</i> (60 % solids, $T_a \sim 1073$ K)	1	1.67	1.67
<u>Coal Water Slurry</u>			
<i>Burgess and Ghaffari (1982)</i> (70 % Bituminous Coal, $T_a \sim 1073 - 1173$)	1	2	2
<i>Murdoch et. al. (1984)</i> (60 % - 70 % Bituminous, $T_a \sim 1173 - 1223$ K)	2	2	2
<i>Yavuz et. al (1998)</i> (60 % - 70 % Lignite, $T_a \sim 1073 - 1113$ K)	1	1	1
<u>Coal-Oil-Water Slurry</u>			
<i>Sakai and Saito (1983)</i> (30 % - 50 % - 20 %, $T_a \sim 1073 - 1353$ K)	~	2	2
<u>Wood</u>			
<i>Mukunda et al. (1984)</i> ($T_a - 300$ K)	~	2	2
<i>Dasappa et al. (1994)</i>	~	~	2 (~ 973 K) 1.87(300 K)

Table 2.1: Burn time and size correlations obtained for various fuels

The variation of burn times with the size of droplets found in the literature is depicted in the table 2.1

2.5. Gasification of liquid effluents or black liquor

Gasification commonly called 'sub-stoichiometric combustion' has a better prospective from energy and environment point of view. In fact, coal has been gasified and used before the advent of natural gas in the quest for achieving clean heat. During the Second World War, gasifiers directly fueled thousands of vehicles. Gasification of solid biomass for electric and heat generation is extensively studied and reported in the literature. The study on gasification of liquid fuels with low heat content like black liquor is recent and not adequately reported in the literature, while distillery effluent or other liquid industrial waste streams have not been considered serious candidates for gasification yet. Verrill and Dickinson (1998) conducted experiments to gasify black liquor (50 – 55 % solids, at 1 – 1.2

kg/h flow rate) at low-temperature (755 K – 866 K) and obtain gas composition data (depicted in table 1.4) for a fluidized bed gasifier design. They found the temperatures insufficient to gasify the char carbon, and the accumulating agglomerates cause partial loss of fluidization and channeling in the bed.

Table 1.3a depicts equilibrium gas composition and that obtained by research and development gasifier of ABB operated at the following condition (Larson et al. (1996).

Liquor with 72 % solid; liquor feed temperature = 388 K; Reactor pressure = 1 bar; air feed temperature = 673 K; reactor temperature = 973 K carbon conversion 99 %. The gas composition seemed satisfactory and large-scale experiments are reported to have been conducted, however, the experimental details are part of internal reports that are not easily available. A large amount of financial assistance (\$ 100 million) has been approved for the year 2000 by the Department of Energy, US, for research and development on black liquor gasification as a *program intended to boost efficiency and reduce greenhouse gases from Pulp and Paper Mills (NETL 2000)*. This is an indication of serious efforts undertaken for the gasification studies in the US.

2.6. Conclusion

Unlike black liquor, the large-scale combustion experience in the case of distillery effluent is inadequately reported in the literature. It is found on the basis of composition, thermochemical and thermophysical properties that black liquor is the most resembling fuel as compared to other multi-component fuels; however, it is injected as coarse spray in recovery boilers such that its complete combustion occurs on the bed. The literature on distillery effluent droplet combustion is meagre. The basic studies to improve the combustion efficiency and cause abatement of environmental emissions are more recent.

Single particle combustion studies related to pre-ignition processes, ignition delay, ignition, flaming and char combustion of various fuels are reviewed.

Published literature on the gasification of liquid wastes is scanty. The study on gasification of black liquor is much more recent while distillery effluent or other liquid industrial waste streams, seem not to have been seriously considered fuels for gasification.

Single Particle Combustion

3.1 Introduction

Difficulties in the combustion of distillery effluent are attributable to their inherently high ash content, low energy density (due to large amount of water) and complex chemical composition. This makes the combustion study difficult but interesting.

The objectives of the present work, therefore, are:

1. To obtain adequate basic experimental data on the principal features of effluent combustion in air.
2. Construct an analysis with adequate validation with experiments to enable extension to the design of a reactor, capable of incineration and gasification.

The sequences of processes taking place in effluent combustion chamber or effluent gasifier would be:

- 1) Injection of concentrated and viscous effluent stream through atomizer as fine spray into an atmosphere of hot oxidizer and product gases.
- 2) Combustion of droplets consisting of evaporation of water, pyrolysis, combustion of volatiles in the gas phase and finally heterogeneous char combustion in gas entrained mode on a char bed.

Therefore, fundamental combustion process involved can be best understood by performing experiments on either single (particle) liquid droplets of various solids and dry effluent sphere as an essential starting point of the study. Since the combustible organic material is in dissolved state, it is extremely important to determine the effect of water concentration on combustion behavior. Effluent is highly viscous and non-volatile. This may allow a significant fraction of single-droplet burning zones in hot environment. Hence study of individual droplet burning can also be extended to spray combustion possibly without much

difficulty. This is true in case of heavy oil spray combustion and can be true even in the case of distillery effluent.

The choice of spherical geometry, besides its importance in spray combustion, has other advantages such as: (a) Well-defined symmetry (b) Existence of a large collection of experimental data on droplets or sphere combustion for comparison on wide range of materials including light and heavy oils, blended fuel, wood, paper, coals, coal-water-slurries, carbon, polymers and (c) Well-documented information on the heat and mass transfer to and from spheres and theory of both diffusion and kinetic dominated reactions of a sphere.

The present work

The experiment in the present study is carried out on the single particle of effluent with 65 %, 77 % and 100 % solids such that effect of water in the combustion process could be determined. Effluent with 65 % solid is in the range of relatively higher water content. It was determined earlier that the viscosity of effluent increases with solid concentration and therefore the limit of maximum solids in the effluent, that could be injected as spray into a combustion zone, is in the range of 75–80 %. Therefore, the experiments were carried out on effluent with 77 % solids so that it represents low water content range.

The experimental technique used for conducting experiment is discussed in Section 3.2. Section 3.3 describes the experimental setup. The effluent used in preparing samples for experiment was obtained directly from a local distillery and the sample preparation procedure is discussed in section 3.4. The physical observations made during and after effluent particle combustion pertaining to its features namely ignition, flaming, char glowing, fume release swelling during heating and devolatilization and structure of sample, are discussed in section 3.5. The scanning electron micrographs used to reveal the microstructure of samples obtained at various conversion stages are depicted and discussed in section 3.6. The DTA / TGA of the dry sample carried out in inert atmosphere to determine exothermicity of devolatilization process is presented in section 3.7. The mathematical formulation of a one-dimensional model used to validate porous effluent char combustion in air is discussed in section 3.8. Results and discussions of all the experiments are discussed in subsections of sections 3.9. Section 3.9.1 discusses results of ignition delay of dry spheres and concentrated droplets. Weight loss and surface temperature of effluent sphere and core temperature of droplet obtained during pre- ignition phase is discussed in

section 3.9.2. The weight loss found during the combustion processes and the various chemical transformations occurring including the release of alkali during flaming and char glowing is presented in section 3.9.3. Flaming phase of effluent droplets and dry spheres combustion and the comparison of their burn time with the flaming of wood and n-heptane at higher ambient temperature, are discussed in section 3.9.4. Section 3.9.5 presents experimental and computed results of the effluent char combustion. The results are also compared with those of wood and carbon combustion. In this section, experimental and computed results of char weight loss vs. time are presented. Section 3.9.6 presents the flaming and char glowing time obtained as a function of temperature. The behavior of core and surface temperature obtained during all combustion phases of effluent spheres and droplets of various sizes at different ambient temperature are discussed in section 3.9.7. Also presented in the same section is the effect of solid concentrations on the combustion features at different ambient temperatures using the core temperature profiles. Lastly, the conclusions drawn from the study are presented in section 3.10.

3.2 Experimental Techniques

Amongst the several techniques namely, porous sphere, freely falling droplet and droplet in freely falling chamber and wire/tube suspended droplet, the simplest of the techniques, namely, suspended droplet technique is used in the present study such that continuous observation of droplet burnout starting with ignition can be recorded. The concentrated liquid droplet and dry effluent spheres were combusted in hot quiescent atmosphere using this technique. In this technique, a liquid droplet is suspended at the tip of a quartz fiber or on a thermocouple junction and introduced in a hot furnace. Dry sphere is fixed between three nichrome prongs with point contact on sphere surface and the holding mechanism is slid into the hot furnace. The subsequent combustion events and characteristics such as droplet ignition delay or heat-up phase, flaming time, char burning time, flame structure, center and surface temperature profile of the droplet and burning rate are recorded. A limitation of this technique is the heat loss or gain in the droplet condensed phase through supporting fiber or holder; this can cause asymmetric effects on the combustion process. It was experimentally determined, however, that the heat gain or loss is negligible and therefore the perturbations caused are also small.

The techniques that can be used to determine mass loss histories of combusting sphere are:

- a) Spheres with same physical characteristics are combusted for a known time and weighed, thus creating continuous mass loss history. This is possible in the case of wood spheres or molded polystyrene spheres; however, in the case of effluent spheres it is difficult to obtain large number of spheres with same characteristics owing to the sphere making process.
- b) Quench – weigh – reignite method, which is suitable for volatile fuel droplets; however is not suitable for effluent sphere since re-ignition takes long time leading to erroneous results.
- c) Effluent droplet or sphere suspended directly from the single pan balance and combusted in furnace with fixed temperature. The weight loss could be continuously measured. This technique is most appropriate for determining continuous mass history and hence is used in this study.

3.3 Experimental Setup

Dry effluent with 100 % solid contains about 38 % inorganics owing to which it does not burn freely at room temperature unlike wood or polymeric solids. This is true even with liquid effluent drops. Hence, all the droplet combustion experiments on effluent with 65 % and 77 % and dry sphere were carried out in high temperature ambience with air at atmospheric pressure.

The schematic view of the experimental setup is depicted in Fig. 3.1a. It shows a 4 kW electric furnace with a fine temperature controller. The furnace temperature was measured by a chromel-alumel (K-type) thermocouple. The inside dimensions of the furnace are 250 mm height, 300 mm width, and 500 mm depth. The 150 mm thick ceramic walls and insulation made furnace almost adiabatic. The center of furnace front door has an opening of 75 mm diameter used for viewing and recording combustion events using a video camera. Video recordings were obtained at a speed of 25 frames per second. Therefore, there is a 0.04 seconds interval between two successive images.

The same view port was used to slide in and out the assembly on which sphere or droplets were suspended on Silica fiber, or thermocouple junction or, in the case of dry spheres, Nichrome holder, as shown in the figure. The whole operation was performed with jerk free motion of the assembly and this was achieved by fixing a roller guide to the inlet of the furnace. A thermocouple was fixed to the assembly, in the vicinity of the sample holder to determine local temperature. A temperature difference of 10–15 K was observed between

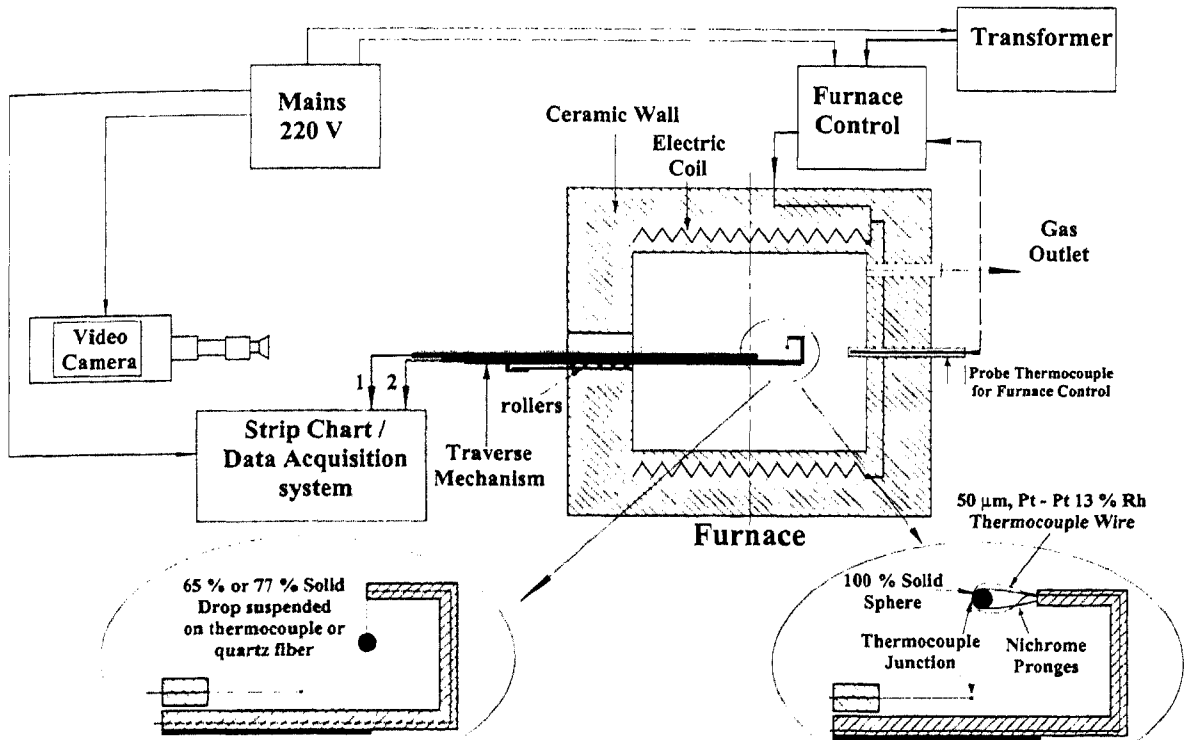


Figure 3.1a: Schematic view of the experimental setup.

the location of the sample where it would be held and the rear wall of the furnace. The effluent particle core and surface temperature were measured using a 50 μm coated thermocouple wire (Pt – 13 % Pt-Rh) connected to a strip chart recorder and high-speed data logging system.

Specially cut glass was used to cover the remaining part of the view port in the early stages of the study. However, its use was discontinued owing to the deposition of fume released from combusting sphere onto the view port, severely obstructing the viewing and recording of combustion events. The rear of the furnace has exhaust ports connected to a chimney, which also provided small-induced natural draft that helped in maintaining ambient oxygen without interfering with the flow field around the burning droplet. Since the experiments were performed in air, the front view port and rear exhaust ports were found adequate to avert the depletion of oxygen concentration in the surrounding medium during combustion. The droplet is surrounded by hot air environment within hot walls of the furnace; therefore, the thermal stimuli responsible for pyrolysis and subsequent ignition are radiation from the wall and heat conduction through hot air.

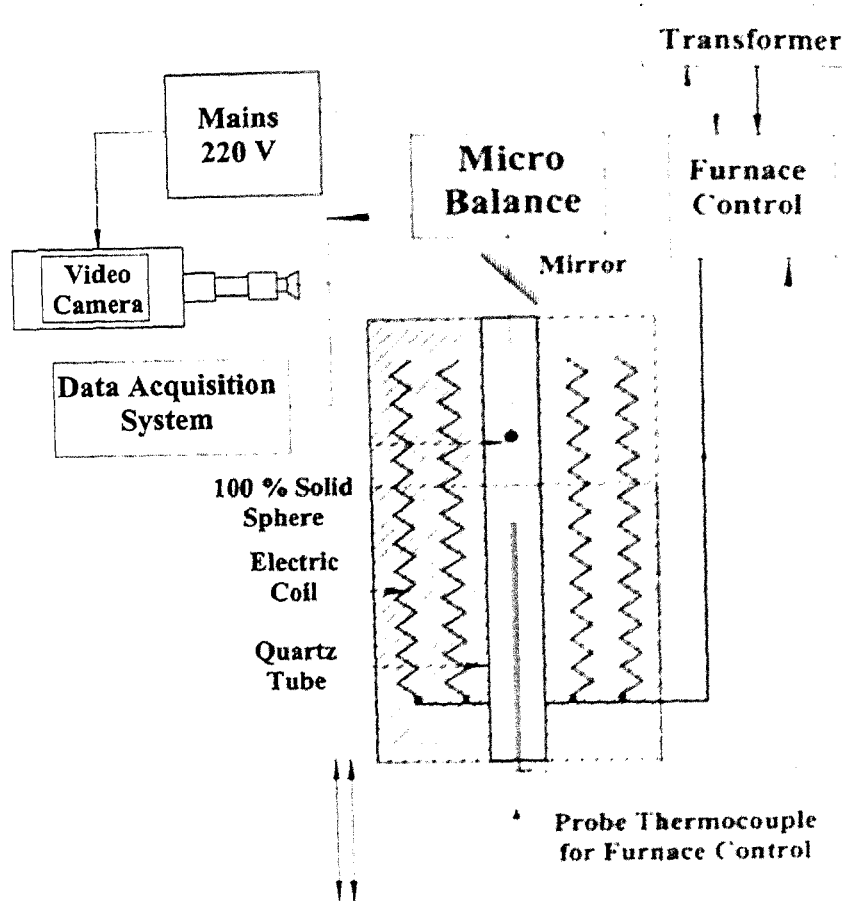


Figure 3.1b: Schematic view of the experimental setup for gravimetric study.

The experiments to determine continuous mass loss of effluent spheres ($d_p = 7 - 10$ mm) with same furnace temperature were performed in a well-insulated, vertical, cylindrical quartz furnace 350 mm long and 50 mm internal diameter with a separate electrical supply and temperature control system. Fig. 3.1b depicts the schematic view of the experimental setup. The thermocouple was kept protruding from the bottom of the quartz tube located at 20–25 mm below the suspended particle in the centerline of the furnace. The top end of the furnace was left entirely open while the bottom end was closed with ceramic wool, except a 10 mm hole so as to have air circulation under small buoyancy effect. The combustion events were observed with the help of a mirror kept inclined to 45° above and below the furnace. The sample, fixed in a holder made of nichrome wire, was hung in the furnace with the help of a thin stainless steel wire, one end of which was fixed to a single pan microbalance. The decrease in weight of the combusting sphere was recorded on videotape and was replayed to determine the weight loss corresponding to time. Temperature data were recorded by the data logging system. Care was taken to avoid electrical field interference

during weight measurement by providing nichrome wire winding on the alumina tube, such that it nullified induced electromotive force. The drag forces on the burning effluent sphere are estimated to be 0.05 – 0.07 % of the weight of the sphere.

3.4 Sample Preparation

The effluent from the downstream of the distillation column of a local distillery was procured for the experiment. The effluent contained 8 ~ 9 % solids and was concentrated to 50 % solids by slow evaporation in an open pan and preserved in a closed container. Experiments were performed on a) dry spheres (100 % solids) with diameter ranging between 2 mm to 20 mm b) liquid droplets containing 65 % and 77 % solids (mass concentration) with diameter ranging between 0.5 mm to 3.5 mm. Experiments were also conducted on 95 % solids and compared with those of 65 % solids. The density of dry spheres varies between 650 and 800 kg/m³. However, most spheres were of density between 700 and 750 kg/m³. Liquid droplets were of uniform density and depended on solid concentration (1275 kg/m³ for 65 % solids - 1345 kg/m³ for 75 % solids).

The starting material for dry sphere experiments was the concentrated effluent 70 % solids having an appearance of black viscous bitumen, thick heavy oil or grease. Since it is difficult to make a sphere with this, effluent was further concentrated to 95 % by convective heating at temperatures between 50–110 C and then was allowed to cool in air for 5-6 hours before rolling it into spheres of required sizes. Initially spheres were dried in a vacuum dessicator containing silica gel and/or phosphorus pentoxide for 24 hours. Remaining moisture was gradually removed in hot air oven at a slow rate during which each sphere swelled by 20 % to 25 % of initial diameter and sphericity was corrected subsequently. Finally, the spheres were heated at 110 C for 24 hours before being stored in a cooled condition in a vacuum dessicator.

Prior to each experiment, the samples were characterized for weight and average diameter measured across three perpendicular axes. The density of the samples varied from 650 to 800 kg/m³. Dry sample spheres when dissected into halves, showed pores formed due to moisture evaporated from the spherical mass (typical dimensions were 0.01 to 0.2 mm). The samples mounted on three adjustable nichrome prongs were inserted into the furnace maintained at a fixed temperature. The combustion process was clocked from the moment the sample was introduced into the furnace. In another set of experiments, separately conducted, the data of surface temperature with time was obtained. For this purpose, the

sample was held taut between nichrome prongs, with the prongs in a horizontal position along with thermocouple junction of 50 μm diameter (Pt—Pt 13 % Rh, coated with cerium oxide of 0.2 μm thickness to eliminate catalytic effect, if any) touching the surface under small tension so as to be firmly in position. In the case of liquid effluent with 65 % solids, the droplets of 0.5 to 2.2 mm diameter were suspended around the 50 μm , thermocouple junction, introduced into the furnace. Droplets larger than 2.5 mm were suspended on quartz fibre in order to avoid their slipping off during initial heating stage. Apart from the temperature history with time data, the combustion process was captured on a video camera for subsequent analysis.

The initial droplet diameter was measured using traveling microscope and further change in diameter in the hot ambient was measured using video recording of the event in which the drop size was compared with predetermined length of wire fixed on holder located in the same plane of suspended droplet. Change in diameter during pre-flaming, flaming and char glowing phases of combustion was obtained from direct measurement of quenched sample. The composition of 65 % solid effluent is shown in Table 3.1

H ₂ O	35.0%
Total organic solids C ₁₂ H _{20.54} O _{4.11} N _{0.56}	37.8%
total inorganic solids	27.2%
S	0.7%
K	7.0%
Na	1.5%
Mg	2.0%
Ca	0.6%
Cl	7.9%
K ₂ SO ₄	5.1%
CaCO ₃	2.2%
insolubles	0.2%

Table 3.1: Composition of effluent with 65 % solids

3.5 Physical Observations

It has been brought out earlier that the effluent is a charring material and when exposed to high temperature ambient, concentrated effluent droplet and dry sphere burn in two phases, the homogeneous or flaming and heterogeneous or char glowing. Depending on size of the droplet and ambient temperature, it can ignite homogeneously or heterogeneously. The

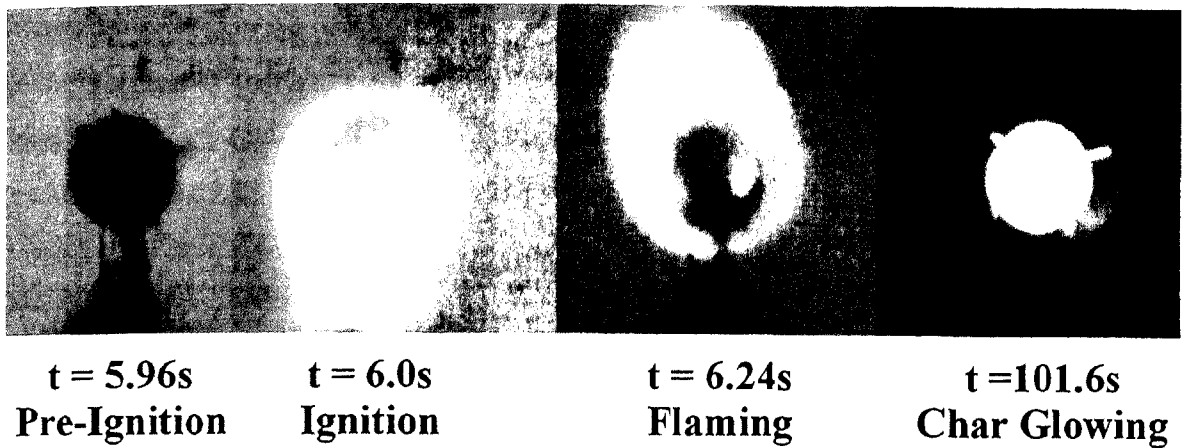


Figure 3.2: Stages of effluent combustion in hot quiescent air at $T_a = 973$ K

frames shown in the Fig. 3.2 depict pre-ignition, ignition, flaming and char glowing of the same effluent sphere (dry, $d_o = 8.25$ mm) combusted in quiescent air at $T_a = 973$ K. The first frame is taken 40 ms prior to the ignition, the second frame at $t = 6.0$ s. The third frame is taken 240 ms after ignition and the fourth frame shows char glowing with a very faint bluish flame enveloping it. The sphere is held taut between nichrome prongs.

3.5.1. Flaming

The homogeneous ignition as shown in the Fig. 3.3 involves pyrolysis and subsequent combustion of derived volatiles in flaming combustion. The gaseous flame envelops the sphere

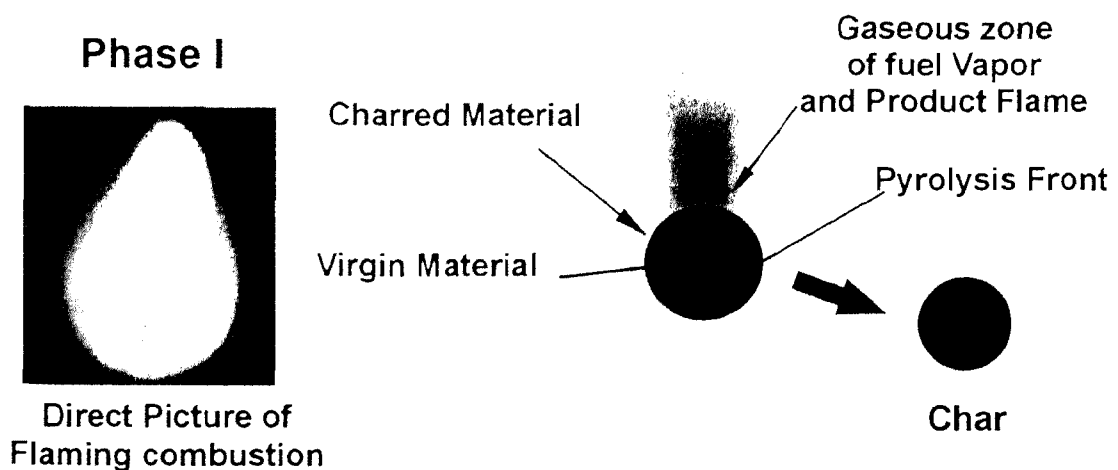
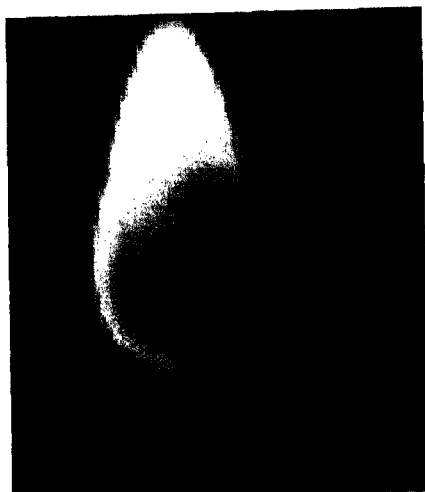
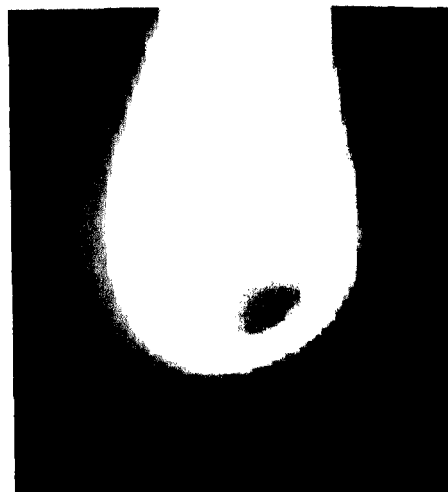


Figure 3.3: Flaming combustion of dry effluent sphere and formation of char.



**Flaming of
Dry Effluent Sphere $d_0 = 8$ mm**



**Flaming of
Dry Wood Sphere $d_0 = 8$ mm**

Figure 3.4: Comparison of flaming combustion of dry effluent and wood at 973 K.

as in the case of the liquid fuel droplet combustion. The circumambient flame is presumed to prevent char reaction by screening the sphere from access to oxygen. Sphere surface could be seen during flaming and was found to have no surface reaction. The end of flaming visually seen as the collapse of gas-phase flame surrounding the sphere, signifies the end of volatile release.

The direct pictures of dry effluent and wood flaming at ambient 973 K are shown in Fig. 3.4. The effluent flaming is largely sootless, while wood sphere flaming is accompanied by heavy soot formation. Soot is composed of particles nucleated and grown in the gas phase from the thermally cracked tar vapor in fuel rich region. This indicates that the wood contains much heavier tars as compared to effluent. Therefore, flame size is large and radiative intensity is higher in the case of wood sphere.

3.5.2. Char Glowing

The second phase has no gaseous flame and oxygen reacts with the hot surface char causing heterogeneous oxidation or smoldering combustion with gradual growth of ash layer while depleting porous char. This may also be called as char glowing. With the progress of glowing, a faint but visible bluish flame enveloping the char sphere was seen in almost all sized spheres (Kanuary, 1982). This was inferred to be due to the gas phase combustion of carbon monoxide in ambient air. This is shown in the fourth frame of Fig. 3.2. Figure 3.5 depicts a direct picture and the model of char glowing indicating the locations of ash that is

Phase II Char Glowing

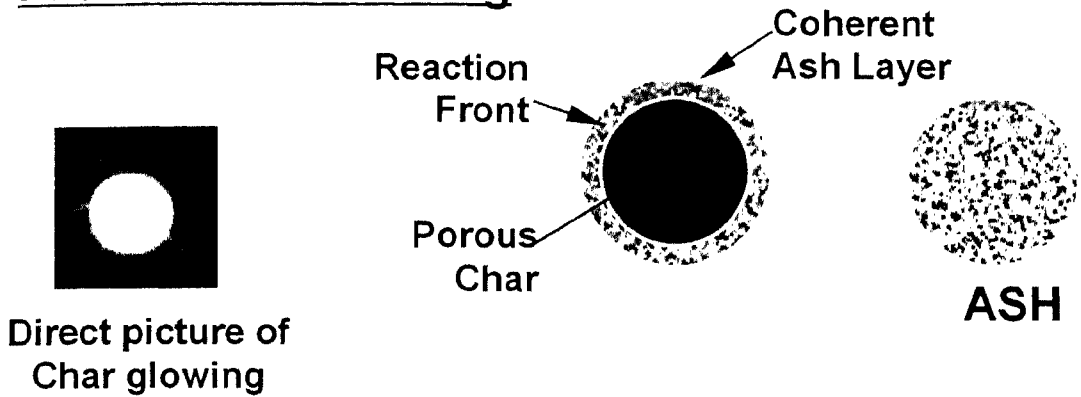


Figure 3.5: Heterogeneous char glowing

coherent and porous, the reaction front, and the porous char as is physically seen during actual glowing.

3.5.3. Ignition

The primary ignition can be homogeneous (flaming) or heterogeneous (glowing) leading to flameless combustion. The ignition features depended on the ambient temperature (T_a) and particle initial diameter (d_o). In a particular narrow range of low T_a , ignition can occur in either mode and is marked as zone of uncertain homogeneous ignition. Table 3.2 depicts the observations made with regards to the mode of primary ignition (homogeneous or heterogeneous) occurring in the case of effluent with 100 % (dry), 77 % and 65 % effluent as an effect of d_o and T_a .

Obs. No.	Material	Size	Condition	Ignition
1	100 % solids	$d_o > 15$ mm	$T_a = 800$ K	Homogeneous uncertain
2	100 % solids	$d_o < 15$ mm	$T_a < 800$ K	Heterogeneous
3	100 % solids	$d_o \geq 5$ mm	$T_a \geq 900$ K	Homogeneous
4	77 % solids	$d_o = 0.5 \sim 2$ mm	$T_a \leq 963$ K	Heterogeneous
5	77 % solids	$d_o \geq 0.7$ mm	$T_a \geq 973$ K	Homogeneous
6	65 % solids	$d_o \geq 2.0$ mm	$T_a \geq 1123$ K	Homogeneous
7	65 % solids	$d_o = 0.6 \sim 3.0$ mm	$T_a < 1123$	Heterogeneous

Table 3.2 Observations made on the occurrence of primary ignition as heterogeneous or homogeneous and its dependence on initial diameter (d_o) and ambient temperature (T_a)

Homogeneous ignition in the case of spheres with $d_o > 15$ mm and $T_a = 800$ K may or may not occur (Obs. No. 1) and this uncertainty remains until $T_a \sim 873$ K. However, homogeneous ignition will occur for all $d_o \geq 5$ mm for $T_a \geq 900$ K (Obs. No. 3). In the case of suspended liquid droplets with 65 % and 77 % solids, d_o ranged from 0. – 3.0 mm and 0.6 – 2 mm respectively.

For homogeneous ignition to occur in the case of 77 % solids, the minimum T_a was 973 K and d_o was 0.7 mm (Obs. No. 6) while in the case of 65 % solids $T_a = 1123$ K and $d_o \geq 2.0$ mm (Obs. No.7). Heterogeneous ignition occurred at lower T_a (Obs. No. 4 & 7).

In the case of primary ignition being homogeneous, two combustion stages were involved, the flaming followed by char glowing. If the primary ignition were heterogeneous, the combustion process was only single staged. In the case of single staged combustion, it was observed that only after the end of pyrolysis, was glowing initiated, indicating char combustion (mostly fixed carbon) and not effluent combustion (volatile matter plus fixed carbon). In the case of homogeneous ignition, combustion proceeds in both the phases as discussed earlier. Heterogeneous ignition led to single stage combustion and flaming did not occur in the experiments performed. At temperature lower than 723 K, no ignition occurs although up to $T_a = 640$ K, carbon conversion was found to have occurred after a long period (5 hours). This phenomenon is seen in dry as well as liquid effluent.

Essenhig and Thring (1958) observed similar ignition features in the case of 10 different types of coal.

3.5.4. Heating, swelling and devolatilization

Immediately after exposing droplet to high temperature ambient, suspended effluent droplets swelled with swelling factor (d/d_o) in the range of 1.45 – 1.5. Same amount of increase in diameter was also seen in the case of effluent with 77 % and 90 % solids droplets. Fig. 3.6 shows direct photographs of 80 % concentrated droplet suspended on a quartz fiber of 200 μm .

The initial droplet diameter was 3.6 mm. The droplet was exposed to ambient temperature of 1173 K and was pulled out just prior to ignition (ignition time was determined earlier for similar droplet with same diameter). The diameter of swelled droplet was found to be 5.3 mm ($d/d_o = 1.47$). Three large hollow spaces were seen underneath porous surface and the interior was found to be dry and stiff (or solidified) found to be 5.3 mm ($d/d_o = 1.47$).

Surface contained microscopic holes through which water vapor and volatiles escaped during heat up. In comparison to 60 % solid droplets, the outer shell of dried droplet with 80 % solids was relatively stiffer. In addition it was observed that the porous body formed at lower T_a (< 773 K) was stiffer, as compared to that formed at higher T_a (~ 973 K). However, the swelling factor variation with temperature was not distinct as was observed by Frederick and Hupa (1989), though solidification of surface layer may have prevented further swelling and the increased

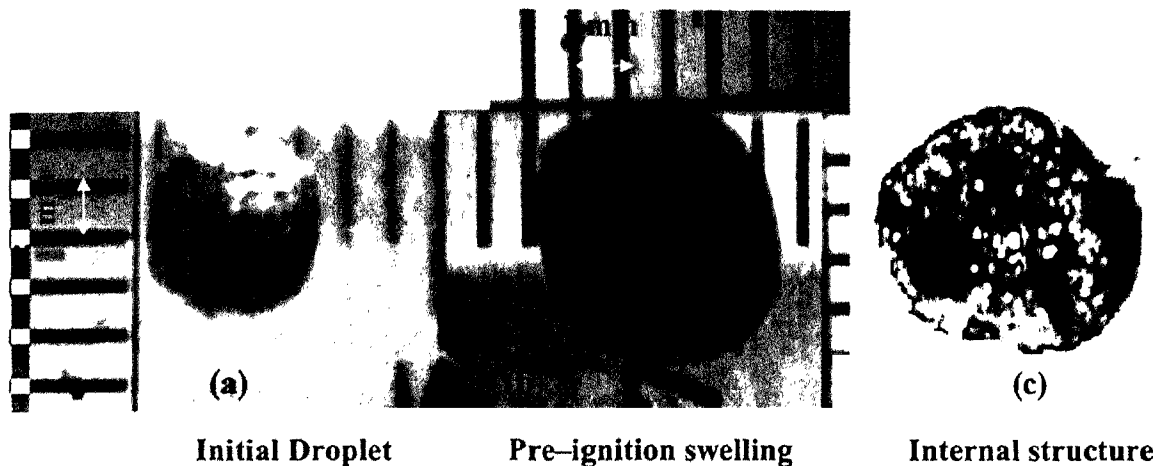
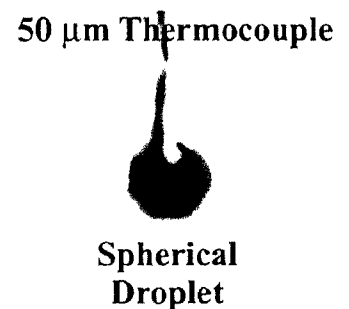


Figure 3.6: Swelling of suspended droplet and internal porous structure of swelled effluent droplet (80 % solids)

pressure in the interior would have forced the volatile gases out through the pores.

The liquid effluent droplet would become perfectly spherical once suspended on either thermocouple junction or quartz fibre due to surface tension. The figure depicts direct picture of the suspended droplet (77 % solids) on a thermocouple junction of diameter $70 \mu\text{m}$. The swelling factor is in the range of 1.4 –1.5 for droplet diameter ranging from 0.55 and 3.5 mm at different solids. Swelling occurs even in the case of dry spheres with 100 % solids; however, the swelling factor is less than 1.1.



During the two phases of combustion of either liquid droplet or spheres, disintegration or disruptions of either the droplet or the char into fragments were not observed. However, jets of devolatilized gases and steam leaving the surface through a number of tiny pores without cracking or fragmenting of the outer surface were seen in the case of large droplets.

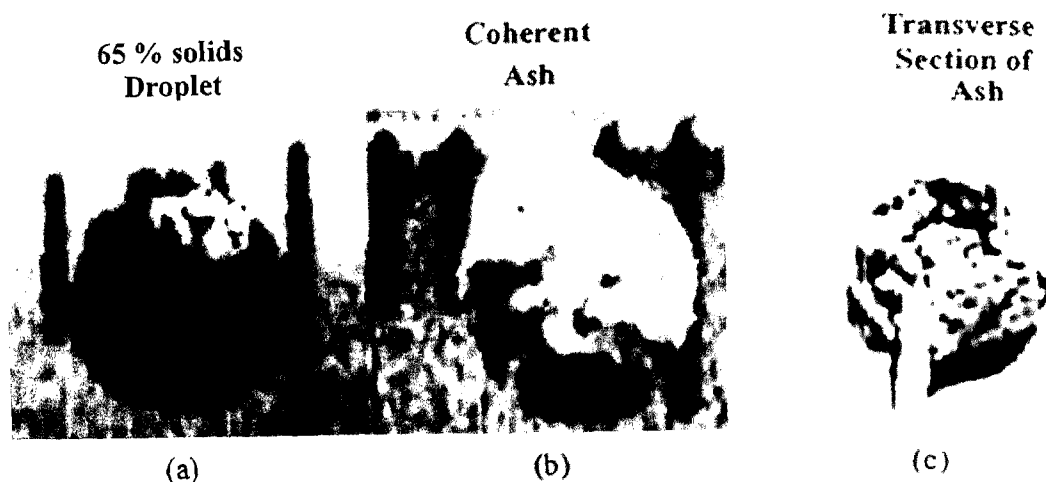


Figure 3.7: Initial effluent droplet and coherent ash of the same droplet suspended on quartz fiber

In the case of 65 % solids droplet, volatile combustion was not seen below ambient temperature 1073 K. However, jets of volatile matter ejecting through the surface could be seen. During this, glowing due to surface reaction could be seen in small zone where surface had dried. The transient was observed for short duration and would end with the gradual spread of the reaction glowing throughout the spherical droplet surface. For the droplets of size larger than 3 mm and ambient temperature above 1073 K, similar observations were made with exception that the asymmetric ejection of volatile as jets ignited homogeneously and later the flame surface enveloped the droplet. Prior to flaming while swelling occurred, repeated bubble bursting on the droplet surface was prominent. This was not very prominent in the case of droplet consisting of 77 % solids.

3.5.5. Structure of fresh sample, char and ash

The scanning electron micrograph (SEM) of fresh sample and sample obtained during flaming reveals the formation of small cavities under the surface of droplet leading to appearance of a porous material. The SEM 1 and 2 shown in Fig 3.10a reveal these features. There appeared no significant morphological change during the course of combustion in unburned char. To determine this, combusting spheres of almost same initial diameter and density were quenched and their bisected halves were observed under microscope. *There appeared a distinct, thin quenched reaction front zone separating ash and char.* This feature implies a shrinking core behavior of the combustion process. The color of this zone ($\sim 100 \mu\text{m}$) was pale black and was distinctly different from the deep black color of char and totally different, brown colors of ash. The material maintained sphericity throughout the

combustion and therefore radial distance of reaction front from center was same in all directions indicating one-dimensional progress of reaction towards center.

The coherent ash remains almost spherical in shape. In the case of liquid droplet the ash shrinks back and attains the initial diameter as shown in the Fig 3.7; however, the ash of dry solid droplets shrinks by about 18 to 19 %. The ash does not coalesce or fuse and become droplet of molten material even at a temperature above 1268 K as is found in the case of black liquor. The effluent droplet with 80 % solid and $d_o = 2.95$ mm is shown suspended on quartz fiber of $250 \mu\text{m}$, in Fig. 3.7a super-imposed on scale with 1mm graduation. The droplet is combusted in quiescent air at $T_a = 973$ K and the residual ash obtained after combustion is shown in the Fig. 3.7b. The porous ash dissected into two half with core exposed is shown in Fig 3.7c.

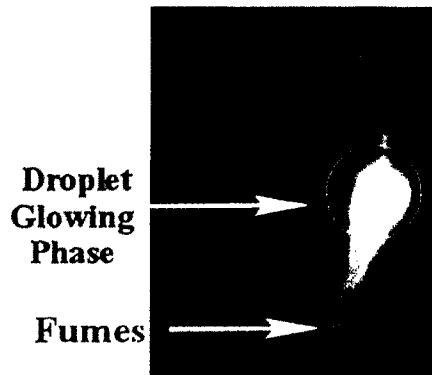


Figure 3.8: Fume releasing during char glowing at $T_o = 973$ K of effluent droplet

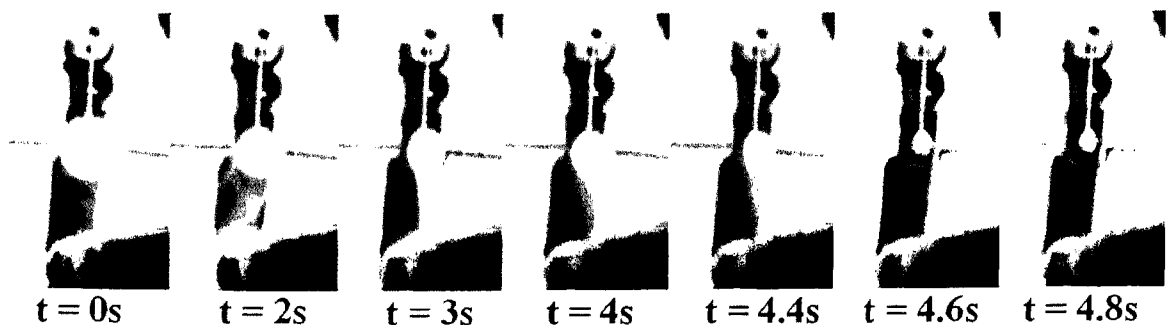


Figure 3.9: Fumes releasing from combusting effluent droplet ($d_o=2.0$ mm, 65 % solids) suspended on quartz fiber at 1173 K.

3.5.6. Fumes During Combustion

White fumes exuding from the droplet are seen during liquid droplet (as shown in Fig 3.8 and Fig. 3.9) as well as effluent spheres combustion. The $t=0\text{s}$ frame in Fig 3.9 shows

fuming during flaming and subsequent frames are of char glowing till the end of combustion. Also shown is the decrease in fuming intensity towards the end of combustion. In the case of liquid effluent its release is quite severe. It was inferred after performing qualitative analysis on the collected fumes, that it is composed of sulfate, sulfide, chloride, and carbonate of alkali are sublimated or transformed to gas phase as a consequence of high temperatures. Fuming starts some time after ignition and continues till the drop is completely consumed. The intensity of fuming increases with temperature and reduces towards the end of combustion. The fuming during char oxidation is basically due to sulfide oxidation and will be discussed in section 3.9.3 (see discussions on weight loss experiments). The fumes were found getting deposited on colder surfaces basically due to thermophoresis. Figure 3.9 also shows the dense fume flowing downwards towards the ceramic holder. The fume release is also reported to be present in case of black liquor (Verrill and Dickenson., 1998).

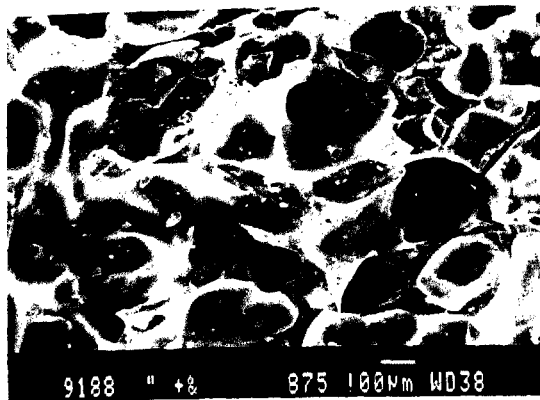
3.6 Scanning electron micrograph

Some of the parameters of one of the char samples are as follows: The BET surface area

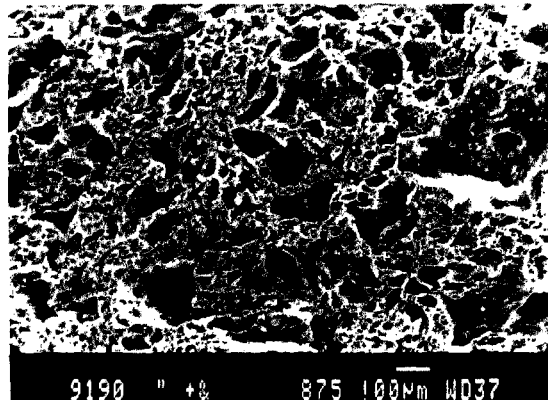
SEM No.	Magnifications	Initial Sample			Sample Burn Time (Ignition. at 4-6 s; Flaming from 5 to 39 s; Glowing 39 to 200 s) (s)	Combustion Phase at the time of Quenching
		Features				
		Dia. (mm)	Mass (gm)	Density (kg/m ³)		
1	75	8.48	0.2300	720	0	Initial Sample
2	75	8.35	0.2196	721	20	Flaming
3	500	8.35	0.2196	721	20	Flaming
4	75	8.25	0.2210	750	38.84	End of Flaming
5	700	8.25	0.2210	750	38.84	End of Flaming
6	800	8.25	0.2210	750	38.84	End of Flaming
7	850	8.52	0.2300	708	110	During Glowing
8	2500	8.52	0.2300	708	110	During Glowing
9	850	8.25	0.2220	757	200	End of glowing (Ash)
10	3000	8.25	0.2220	757	200	End of glowing (Ash)

Table 3.3: Details of samples prepared for SEM and magnification of micrograph

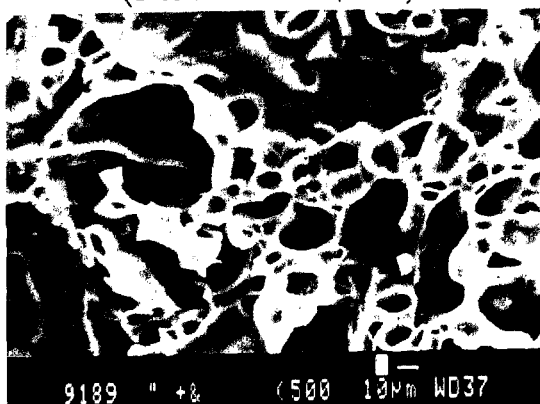
of the char obtained at the end of flame at $T_a = 973$ K was determined to be $3.68 \text{ m}^2/\text{g}$. The fresh sample sphere when dissected into two halves showed internal porous structure



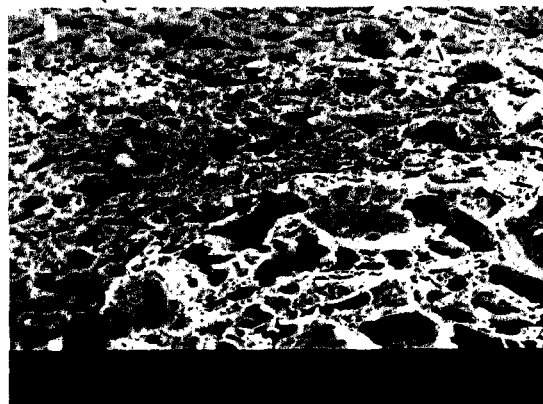
SEM No. 1
(0 % conversion, 75X)



SEM No 2
(Devolatilization 45%, 75X)



SEM No. 3
(Devolatilization 45%, 500X))



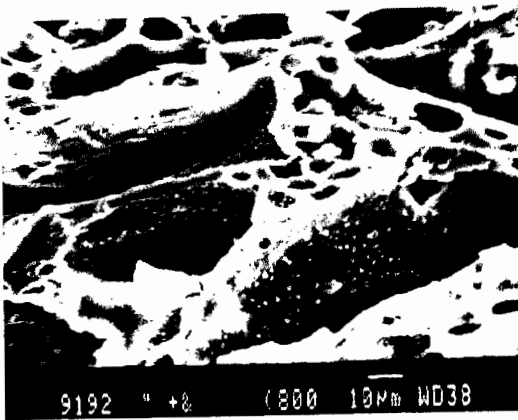
SEM No.4
(Devolatilization 100%, 75X)

Figure 3.10a: SEM of fresh sample (SEM No. 1), partly devolatilized sample (SEM No. 2 & 3) and of char (SEM No. 4) of dry effluent sphere obtained at $T_a = 973$ K.

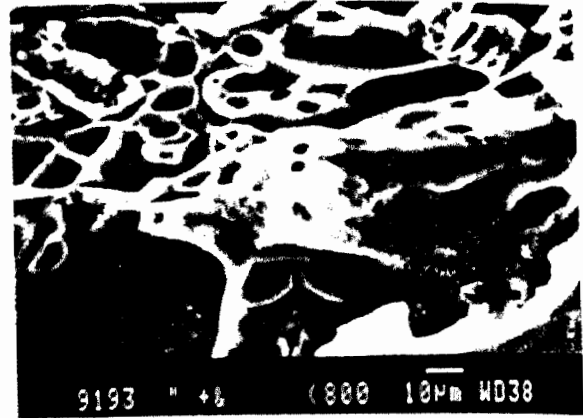
formed during moisture evaporation. The pore has typical dimensions of 10 to 200 μm . Dry sample spheres of $d_0 = 8.37 \pm 0.12$ mm and density 731 ± 21 kg/m^3 , initial mass 0.2236 ± 0.005 gm were used to obtain scanning electron micrograph (SEM) at various stages of combustion.

The figure shows 10 SEM of the 5 samples obtained at different conversions obtained at 973 K ambient temperature in quiescent air. SEM 1 depicts the internal structure of fresh sample at a magnification of 75 X. It shows pores of the size in the range of 50 and 200 μm . Except for small amount of dispersed particles, the material seems to be homogeneous. The pores seen are formed due to evaporation process.

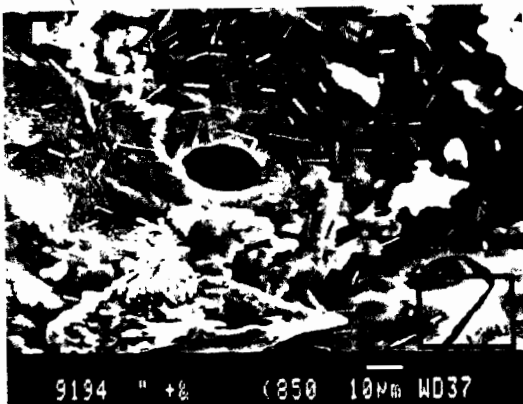
SEM 2 is of sample quenched during flaming at after 45 % of total devolatilization time. The magnification is same as for SEM 1. Depicted zone is of already devolatilized material.



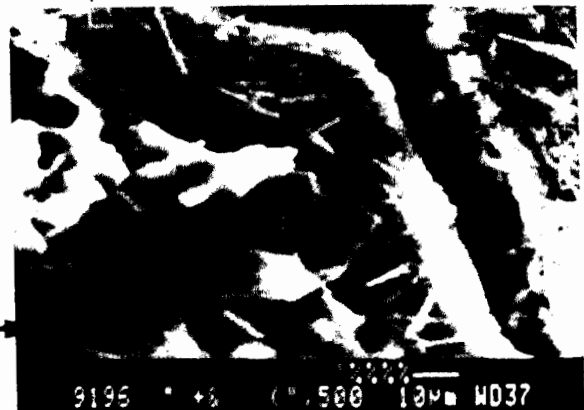
SEM No. 5
(Devolatilization 100%, 700 X)



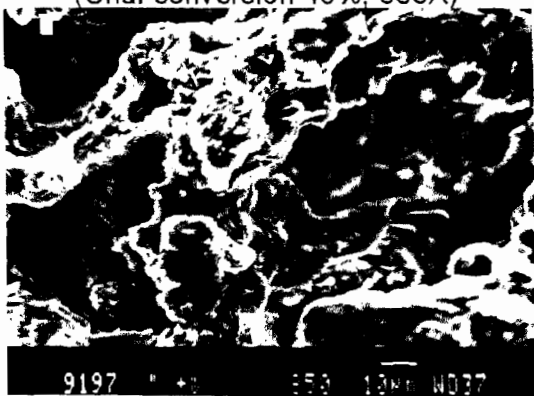
SEM No. 6
(Devolatilization 100%, 800X)



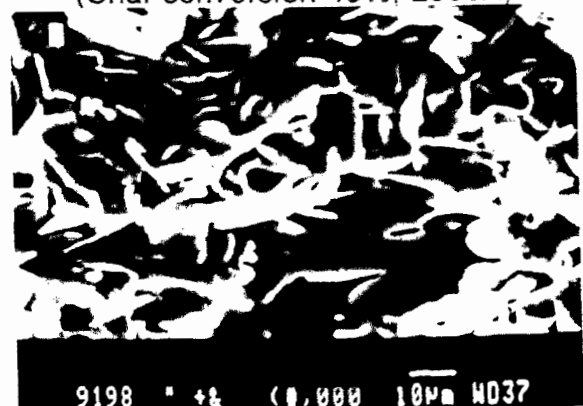
SEM No. 7
(Char conversion 45%, 850X)



SEM No. 8
(Char conversion 45%, 2500X)



SEM No. 9
(Ash, 850X)



SEM No. 10
(Ash, 3000X)

Figure 3.10b: SEM of char (SEM No. 5, 6), partly converted char (SEM No. 7 & 8) and of ash (SEM No. 9, 10) of dry effluent sphere obtained at $T_s = 973$ K.

Zone close to the center resembled that of SEM 1. It is clearly seen that with devolatilization the structure becomes porous. SEM 3 is of same sample but at higher magnification (500 X), which reveals the size of irregularly formed pores that are even

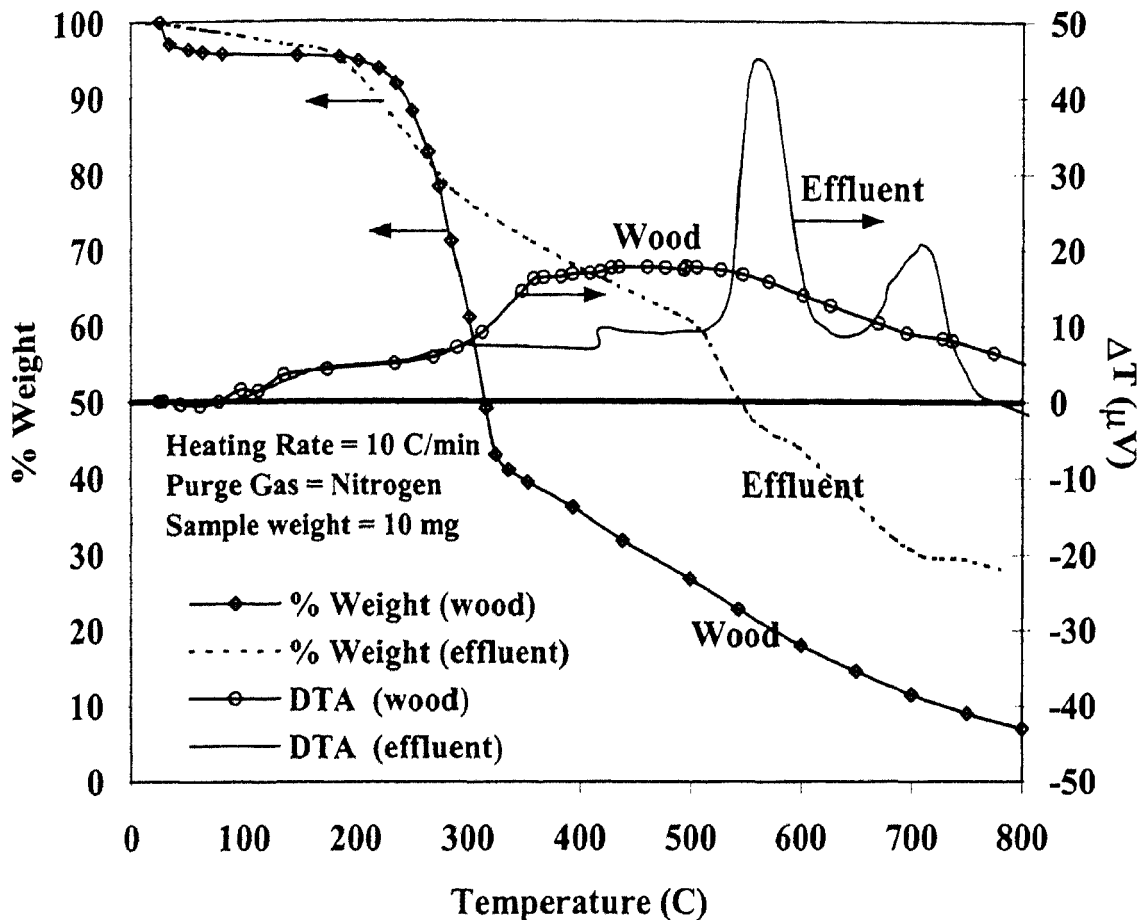


Figure 3. 11: TG and DTA of distillery effluent and wood

smaller than $1 \mu m$. There is no major difference between SEM 2 and SEM 4 of sample obtained after complete devolatilization at 973 K ambient temperature.

The SEM 4, SEM 5 and SEM 6 are also of the same sample. The size of the pores remains in the same range and the uniformly dispersed particles are more clearly visible. SEM 7 is of sample obtained by quenching during char glowing. The structural changes in the virgin char, at the end of 45 % char conversion, seems to be negligible and is seen as in SEM 5 or 6. The only exception is that of the coherent ash accumulation around the pores but does not seem to be blocking them. Slender cylindrical fibrous structures are seen scattered on the surface in SEM 7 and 8. A magnified view of a fine fissure and fibrous bodies as seen in SEM 7, is shown in SEM 8 SEM 9 and 10 are of highly porous coherent ash. The fibrous bodies seen in SEM 7 & 8 have disappeared in ash indicating post-conversion inorganic transformation.

3.7 DTA/TGA

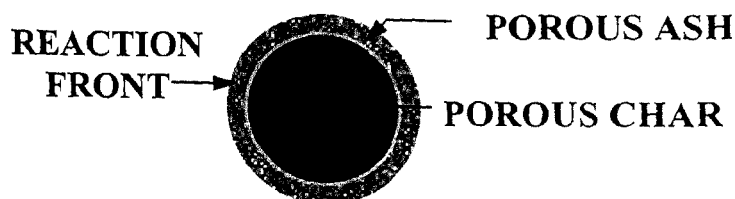
One question that became important was to determine if the condensed phase pyrolysis/phase transformation was exothermic as it happens with wood. To explore this thermogravimetric (TG) analysis was carried out on the samples of effluent and wood in inert condition. Thermogram of effluent shown in the Fig 3.11 clearly depicts sharp peak at 723 K and 833 K indicating a spontaneous exothermic reaction in contrast to that of a broad exotherm, in the case of wood over a range of 573 and 773 K. While the precise implications of this behavior for combustion are unclear, the reason for sharper exothermicity in the effluent are suspected to be due to the carbohydrate structures in the effluent coming from the basic biomass, which would have been processed leading the effluent material augmented by the presence of inorganic materials.

3.8 Mathematical Model

The processes taking place during flaming are the combustion of volatiles similar to wood sphere–diffusion limited gas phase combustion modeled by the Burke-Schumann theory with appropriate initial and boundary conditions as in Mukunda et al. (1984). This work is directly utilized in the treatment of the flaming process and therefore not addressed here.

3.8.1. Char combustion process

The heterogeneous combustion of porous spherical effluent char in quiescent air in furnace condition is modeled. The model aims at estimating the mass loss rate of the spherical effluent char. Consistent with the physical observation noted earlier that the char sample quenched during glowing has a thin spherical reaction zone on the surface of the unburnt



char. The processes taking place during combustion of porous char spheres are similar to those treated in Dasappa et al. (1994) involving diffusion and convection of the species and energy in the porous medium and the heterogeneous reaction between gaseous species and the char. These are modeled in the present analysis using the unsteady spherically symmetric one–dimensional conservation equations. Since the initial porosity was large (see SEM 6) the resistance offered by pores to diffusion was small in all cases.

Also sintering or blocking of pore was not seen during burn out. The porous structure does not greatly change with conversion as seen in scanning electron microscope.

The processes modeled in the present analysis with the assumption of (1) one-dimensional conversion process, (2) No pressure gradient within the particle owing to highly porous structure of the char (3) same local temperature of carbon and gas, (4) change in surface area with conversion is negligible.

3.8.2. The Governing Equation

The char glowing process is modeled using the un-steady spherically symmetric one – dimensional conservation equations. The Conservation equations are:

$$\frac{\partial}{\partial t}(\rho\varepsilon) = \frac{1}{r^2} \frac{\partial}{\partial r}(-\rho v r^2) + \dot{\omega}_c^m \quad 3.1$$

$$\frac{\partial}{\partial t}(\rho\varepsilon Y_i) = \frac{1}{r^2} \frac{\partial}{\partial r} \left(-\rho v r^2 Y_i + r^2 D_e \rho \frac{\partial Y_i}{\partial r} \right) + \dot{\omega}_i^m \quad 3.2$$

$$\frac{\partial}{\partial t}(\bar{\rho} C_p T) = \frac{1}{r^2} \frac{\partial}{\partial r} \left(-\rho v r^2 C_p T + r^2 \bar{k} \frac{\partial T}{\partial r} \right) - H_c \dot{\omega}_c^m \quad 3.3$$

$$\frac{\partial \varepsilon}{\partial t} = \frac{-\dot{\omega}_c^m}{\rho_c} \quad 3.4$$

where $\bar{\rho} = \rho_c(1 - \varepsilon) + \rho\varepsilon$ is the average density of porous char, ρ_c is non-porous char density, ε is the porosity of the char, and $\dot{\omega}_c^m$ is volumetric reaction rate of char with O₂ and CO₂ including contribution due to growing pores.

$$\dot{\omega}_c^m = \dot{\omega}_{cO_2}^m + \dot{\omega}_{cCO_2}^m \quad 3.5$$

The subscripts $i = 1, 2, 3$ refer to species CO, CO₂, and N₂ respectively.

The volumetric reaction rate is related to the heterogeneous reaction rate per unit surface area by

$$\dot{\omega}_c^m = \dot{\omega}_c^s S_g \rho_{ap} \quad 3.6$$

where ρ_{ap} is the apparent density of the char and S_g is the surface area per unit volume of the char, which is given by Howard (1967) as $S_g \rho_{ap} = 2\varepsilon/r_p$,

The surface reaction rate is given by Howard as

$$\dot{\omega}_{CO_2}^m = -\frac{M_c S_1 S_2 X_{O_2}}{(S_1 X_{O_2} + S_2)} \quad 3.7$$

where X_{O_2} is the mole fraction of oxygen at the surface and S_1 and S_2 are the rate constants for absorption and desorption respectively given by

$$S_1 = A_c P \exp\left(\frac{-E_1}{RT}\right) / \left(\sqrt{2\pi M_{O_2} RT}\right) \quad 3.8$$

$$S_2 = A_f \exp\left(\frac{-E_2}{RT}\right) \quad 3.9$$

The reaction rate of carbon with CO_2 proposed by Semechkova and Frank-Kamenetskii and referred to in Blackwood is given by

$$\dot{\omega}_{CO_2}^m = \frac{k_1 p_{CO_2} - k_2 p_{CO_2}^2}{1 + k_3 p_{CO} + k_4 p_{CO_2}} \quad 3.10$$

No gas-phase reactions are considered. The oxidation of CO is neglected because the mass fraction of CO inside the sphere during the reaction process is too low to contribute toward any heat release.

The reaction rate per unit area $\dot{\omega}_c^m$ is related to $\dot{\omega}_c^m$ by $\dot{\omega}_c^m = \dot{\omega}_c^m 2\varepsilon / r_p$

3.8.3. Initial, interface and boundary conditions

The initial conditions at $t = 0$ are the temperature and concentration profile within the porous char. The temperature is set at the furnace condition as per the experimental condition. The precise nature of the temperature profile does not matter as the transients die down in a small fraction of the conversion time. This is due to the diffusion dependence of the heterogeneous reaction. The interface conditions at $r = r_s$ are the continuity of heat and mass fluxes. These are as in Mukunda et al. (1984).

$$D_g \rho \left. \frac{\partial Y_i}{\partial r} \right|_{r_s} = Q(Y_{i\infty} - Y_{is}) \quad ; \quad k \left. \frac{\partial T}{\partial r} \right|_{r_s} = c_p Q(T_\infty - T_s) - \dot{R}'' \quad 3.11$$

where \dot{R}'' is the radiative heat flux and the surface from the sphere and

$$Q = \frac{\dot{m}}{4\pi r_s^2} \frac{\exp(-B_o)}{[1 - \exp(B_o)]} \quad B_o = \frac{\dot{m} c_p}{4\pi r_s k} \quad 3.12$$

Equation 3.11 is obtained from the solution of spherically symmetric one-dimensional conservation equation for the gas phase (Mukunda et al. 1984), and the effect of free and/or forced convection is accounted for, by choosing the appropriate value of the Nusselt number

(Nu). $Nu = 2$ in the absence of either free or forced convection but increases in the presence of convection. In the present case the char sphere encounters only free convection.

3.8.4. Method of Solution

The solution calls for integration of the parabolic system of partial differential equations subject to the initial and boundary conditions noted above. The transformation of independent variable r into 'V' defined as $V = \frac{4}{3}\pi r^3$ was carried out in order to eliminating singularity at $r = 0$ and render the difference equation into a conservative form. The above equation was integrated by using implicit Crank–Nicholson scheme (Mukunda et al, 1984)

3.8.5. Choice of Parameters

The choice of physical, thermodynamic and transport properties of dry effluent material and char based on measured and literature information are as follows:

Dry effluent:

$$\rho_c = 730 \text{ kg/m}^3 \quad c_p = 1.40 \text{ kJ/kgK}$$

$$k_c = 2.1 \text{ W/mK} \quad k_g = 0.063 \text{ W/mK}$$

Char:

$$\rho_c = 1650 \text{ kg/m}^3 \quad r_p(t=0) = 50 \mu\text{m} \quad c_p = 1.25 \text{ kJ/kgK}$$

$$H_c = 32.60 \text{ MJ/kg} \quad k_c = 1.85 \text{ W/mK} \quad k_g = 0.071 \text{ W/mK}$$

Rate parameters for the C + O₂ reaction:

$$A_c = 1/150, E_1/R = 1700 \text{ K}, E_2/R = 20,000 \text{ K}$$

$$A_f = 0.0875 \text{ mol/m}^2\text{s}$$

where, ρ_c is the non-porous carbon density and H_c calorific value of carbon, k_c is the conductivity of solid phase at temperatures of 1000–1200 K. The presence of a large amount of inorganic material affects the conductivity of the porous carbon-inorganic matrix. It must be brought out that the char is composed of nearly equal amounts of carbon, inorganic matter—oxides and sulfates of potassium, sodium, magnesium and calcium. The thermal conductivity data of several inorganics and char were examined from standard literature. These indicate values anywhere between 0.5 to 2 W/mK. The conductivity of porous carbon is also in the same range of values at high temperature. In light of this and the known significant influence of thermal conductivity, it was decided to choose a value to match the burn time at one point. This value turned out to be 1.25 W/mK. The initial radius

of the pore is obtained from Groeneveld (1980) where wood char was used for measurements. The parameters in the kinetic expression used presently were not altered from those of wood char (*Blackwood, 1960*) due to inadequate information on better value for the effluent like material. The rate of backward reaction k_2 is obtained from appropriate equilibrium constants. The emissivity of the sphere surface, used for radiant heat loss calculation, is taken as 0.95.

3.9 Results and Discussion

3.9.1 Ignition Delay

Ignition delay is defined as the period between the exposure of droplet or sphere to high temperature quiescent air and the flash of light on its surface owing to either visible flame or beginning of smoldering, whichever appears first. As the effluent droplet or sphere is exposed to high ambient temperature, heat from hot ambience is transported radially inward, while the volatiles or pyrolysis products are transported radially outward. Volatile diffuses and mixes with the oxidizer forming flammable mixture and reacts, leading to a flame. The ignition event is significantly affected by concentration and temperature variations, due to their influence on the rates at which heat and mass are transported. The necessary two conditions for flaming of volatiles to occur are: a) attainment of a least lower-limit by volatile/air mixture and b) attainment of minimum ignition temperature of the mixture. Failure to satisfy either of these conditions will lead to flame-less combustion or smoldering. The rate of devolatilization is also an important parameter deciding ignition delay.

The dependence of ignition features described on diameter vs. ambient temperature plot is shown in Fig. 3.12. A clear boundary is seen between flaming and non-flaming zone, depending on ambient temperature and diameter of dry effluent sphere. At a fixed ambient temperature there exists a critical diameter of effluent sphere, below which volatile does not ignite into flame but instead, after about the same weight loss as in the case of flaming, ignites heterogeneously with a low intensity red glow quickly spreading over the surface from one or more ignition points. This feature is attributed to the low volatile matter concentration created in the gas phase, *incapable* of reaching ignition limit of the mixture at the ambient gas temperature involved. This can also be explained in as: the diffusion time of volatiles scales with r^2/D (where, 'r' is particle radius and 'D' is diffusion coefficient) while

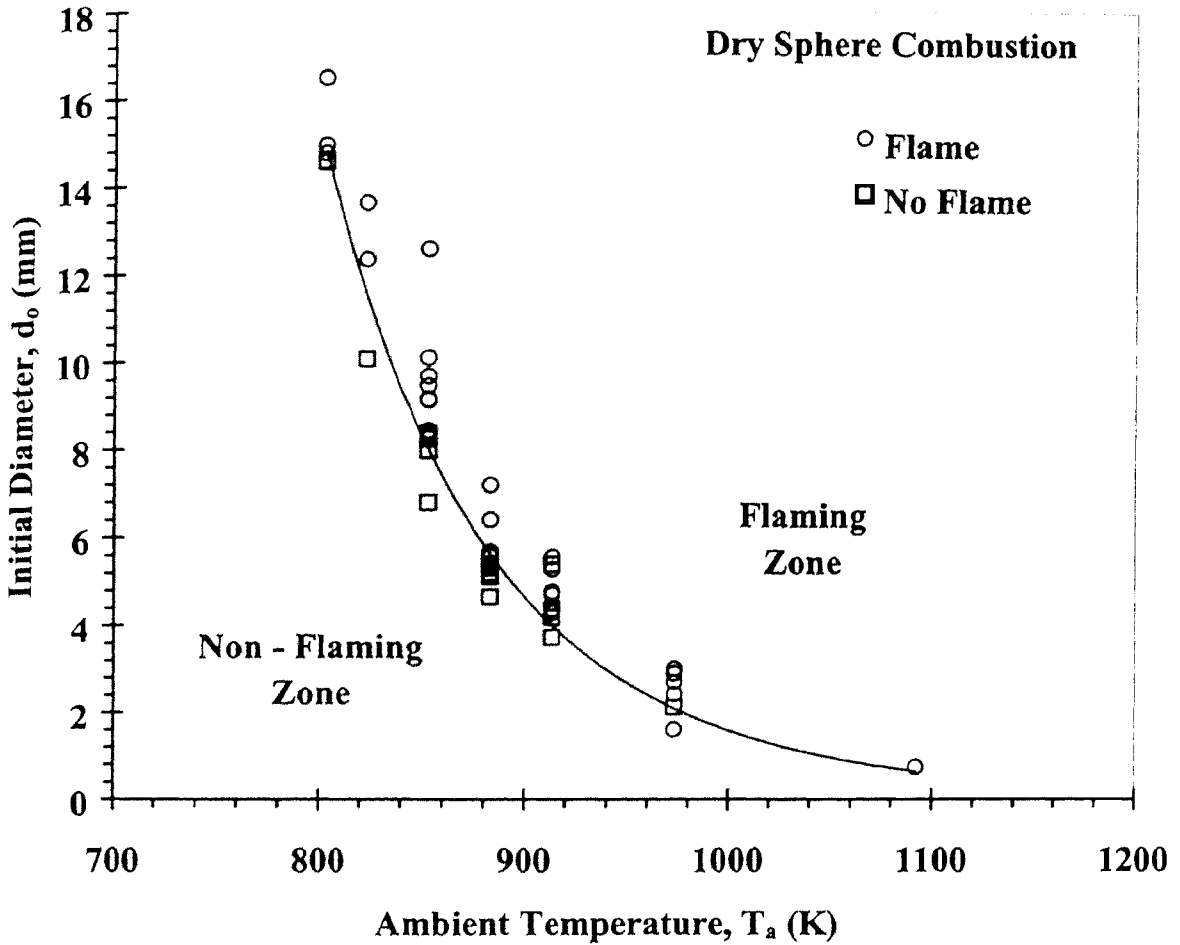
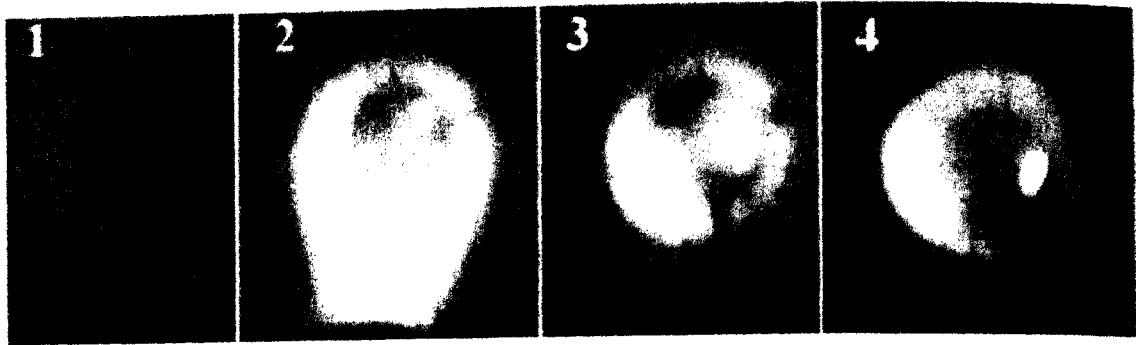


Figure 3.12: Dependence of primary ignition as flaming or glowing on the effluent initial diameter and ambient temperature

the gas phase reaction time scales like $\sim 1/A \exp(-E/RT)$. While the reaction time is relatively fixed the diffusion or residence time for smaller particle is too small to balance with reaction time. Hence, the small particle will never ignite homogeneously.

Essenhigh (1958) also noted similar features in the case of coal in which particles below $650 \mu\text{m}$ had no volatiles flame. Annamalai and Ryan (1993) had also recorded that homogeneous ignition is favored for high volatile coal and large particle diameters ($d_0 > 1 \text{ mm}$), This feature again has been observed earlier by Takei et al (1993) explained as due to a competition between chemical heat release rate and diffusion of reactants in space.

Figure 3.13 shows direct pictures of occurrence of ignition of dry sphere and droplets at various ambient temperatures. Fig. 3.13a depicts clearly the ignition of volatile in the space enveloping the dry effluent sphere at $T_a = 973 \text{ K}$. The time period between consecutive frames is 40 ms. The ignition delay ' t_i ', could be easily timed due to sharp rise in the light



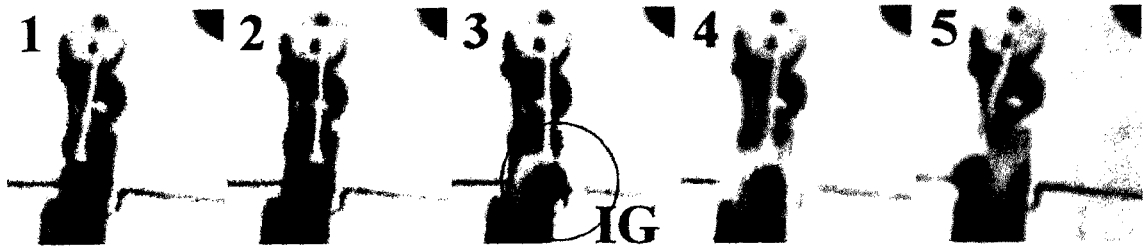
$\Delta t = 40 \text{ ms}$

(3.13a) Homogeneous ignition of sphere $T_a = 973 \text{ K}$



$\Delta t = 400 \text{ ms}$

(3.13b) Flameless or heterogeneous ignition of 65 % solids droplet $T_a = 973 \text{ K}$,



$\Delta t = 40 \text{ ms}$

(3.13c) Homogeneous ignition of 65 % solids droplet $T_a = 1173 \text{ K}$

Figure 3.13 : Ignition feature of sphere and liquid droplet with 65 % solids at various T_a .

intensity as can be seen in frame 2. Swelling during devolatilization is negligible. These data are plotted in Fig. 3.17 for different diameter and T_a . It is also clearly seen that the surface temperature increases sharply following ignition due to circumambient flame. The release of volatiles is seen to be axisymmetric since the flame is almost symmetrical about the sphere surface.

Fig. 3.13b shows heterogeneous ignition of effluent droplet (with 65 % solid, $d_o = 2.5 \text{ mm}$) suspended on quartz fiber at $T_a \sim 973 \text{ K}$. The ignition starts with a glow, brighter than the ambient, on the surface as shown in the frame 4. The heating and ignition is at a slow rate and therefore the frames shown are at larger time intervals in order to accommodate both features. In frame 2 and 3, the heating of surface is seen as the dark surface become red (the

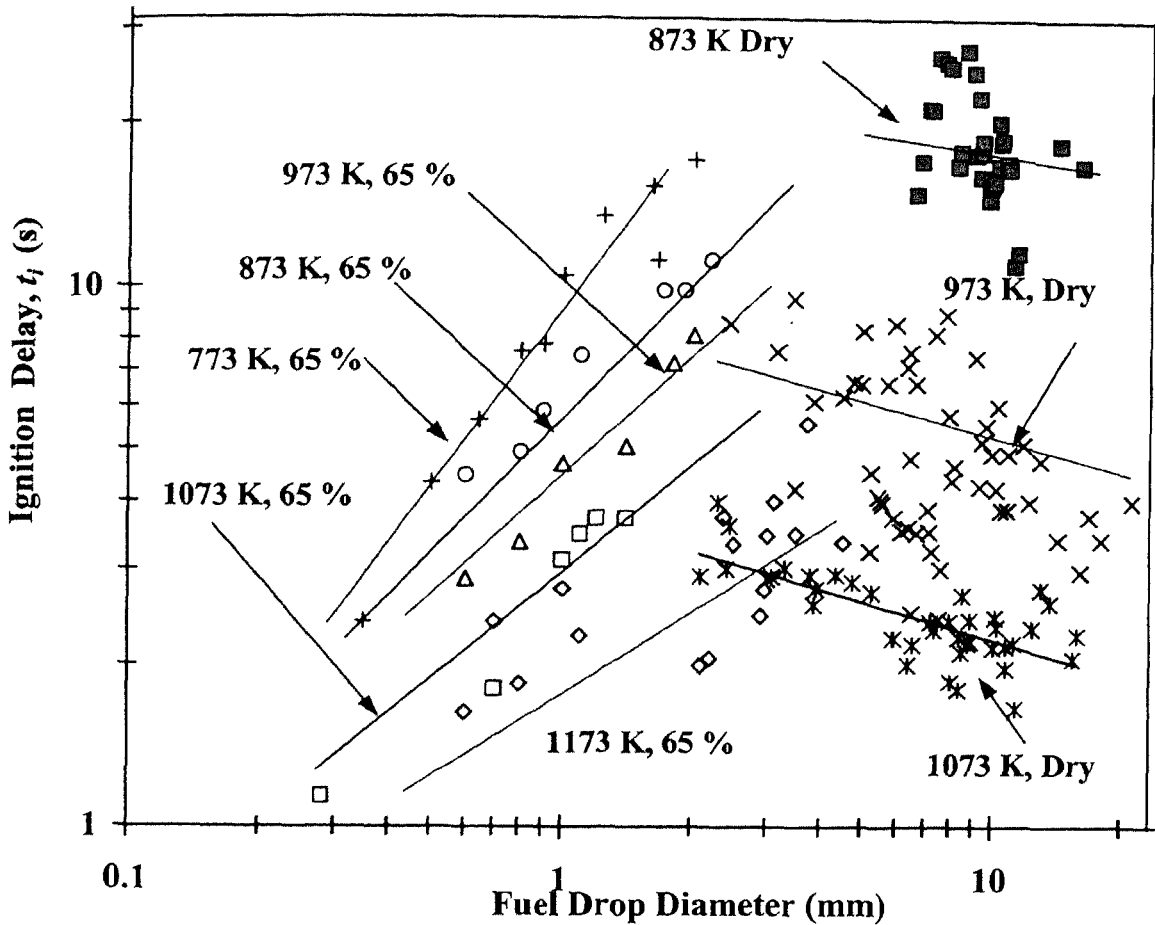


Figure 3.14: Ignition delay of liquid effluent droplets with 65 % solid concentration and dry spheres vs. diameter

intensity is low and may not be clear in the print). The ignition is seen to occur uniformly on the surface and happens after the devolatilization is almost complete. Since the quartz fibre is freely hung in the ceramic holder, the release of gases gives slight random deflections to the droplets (observed with the naked eyes) and therefore the end of devolatilization can be judged from the complete seizure of the deflection.

At $T_a = 1173$ K, the droplet ignites like in the case of dry sphere with near spherical enveloping flame as seen in frame 3 of Fig 3.13c. However, in the initial phase of flaming, the release of accumulated volatile matter is in the form of a jet, which is capable of deflecting the droplet in the direction opposite of its release. The volatile matter accumulates due to formation of hard layer from the evaporated surface material and acts as a barrier to uniform volatile release in the initial phase. The plot depicted in Fig. 3.14 presents the dependence of ignition delay on the diameter of the effluent containing 65 % solids and dry spheres (100 % solids).

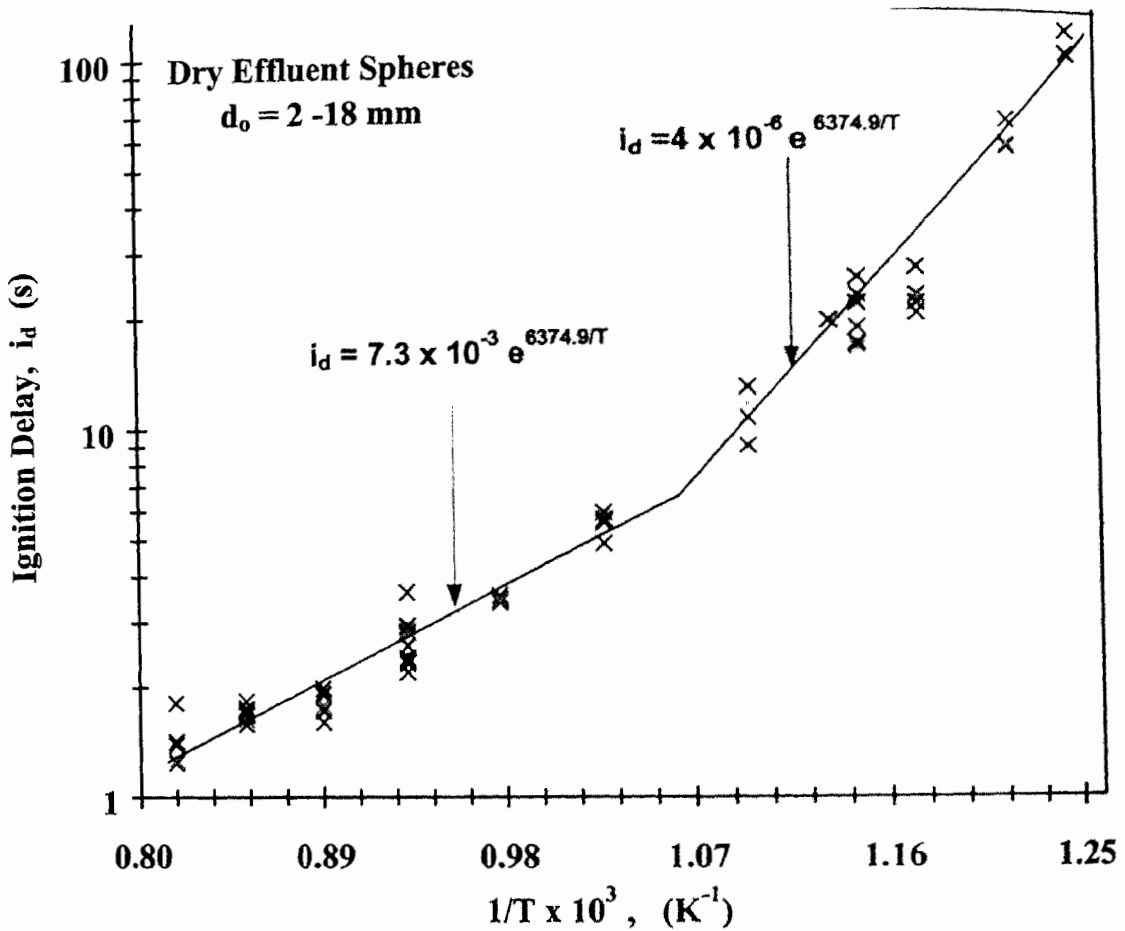


Figure 3.15: Dependence of ignition delay of dry effluent spheres of various diameters on ambient temperature

3.9.1.1 Ignition delay of dry effluent spheres

In the case of dry spheres, even though there is scatter of data (see Fig. 3.14), it appears reasonable to conclude that the delay time decreases slightly with increase in size. Earlier experimental data on highly volatile fuels, non-volatile fuels, as well as their blends (*Takei et al, 1993; Kumagai et al, 1972*), suggest that the decreasing trend of ignition delay with size is due to volatility of the fuels. *The dry effluent appears similar to volatile fuels in regard to ignition delay.* Ragland and Weiss (1979) also report results of the above kind for bituminous coal and Sakai and Saito (1983) for coal oil slurry. Ignition delay has a strong dependence on ambient temperature, understandably decreasing with increase in temperature.

Data of ignition delay vs. inverse of the ambient temperature T_a of effluent spheres of different diameter has been plotted in Fig 3.15. The figure shows that the ignition delay

correlates well with temperature in an Arrhenius law and has two distinct slopes depending on T_a .

3.9.1.2 Ignition delay of liquid droplets

65 % solids

In the case of liquid droplets with 65 % solid concentration, the pre-ignition events occurring are droplet heating, evaporation of water and vaporization of organic acids with low boiling point followed by pyrolysis. Heterogeneous ignition occurs in the case of $d_0 < 2$ mm and $T_a < 1173$ K. This was single stage combustion. However, water vapor and volatiles were released unignited prior to heterogeneous ignition, as seen from the deflection of the suspended droplet on the quartz fiber. This indicated that devolatilized droplet was ignited heterogeneously.

Following are the observations on ignition delay.

- a) Ignition delay is proportional to the initial diameter at any given ambient temperature as is seen in the case of black liquor (*Hupa et al., 1987*) and coal-water-slurry (*Burgess and Gaffari, 1988; Yavuz et al., 1998*).
- b) Ambient temperature has strong dependence on ignition delay. It decreases with increase in temperature. The slope of line decreases with increase in T_a from 773 to 1173 K.

77 % solids

In case of droplets of effluent with 77 % solid, primary ignition was heterogeneous for T_a in the range of 833–873 K. The combustion was a single stage process without any flaming. At T_a of 963 K and above, primary ignition was homogeneous resulting in a flame at the end of which char glowing took place till complete conversion. The ignition delay vs. droplet initial diameter shown on a log–log plot as shown in Fig. 3.16, indicates an increase in the ignition delay with increase in diameter, as is the case with 65 % solids. However, at the same T_a , ignition delay of droplet with 65 % solids is higher than 77 % solids. At $T_a = 873$ K, ignition delay of droplets of 65 % solids is 40 % higher compared to 77 % solids and at 973 and 1073 K it is 127 % higher. At $T_a > 1073$ K the difference tapers down, but the delay will always be lower in the case of 77 % solid droplets.

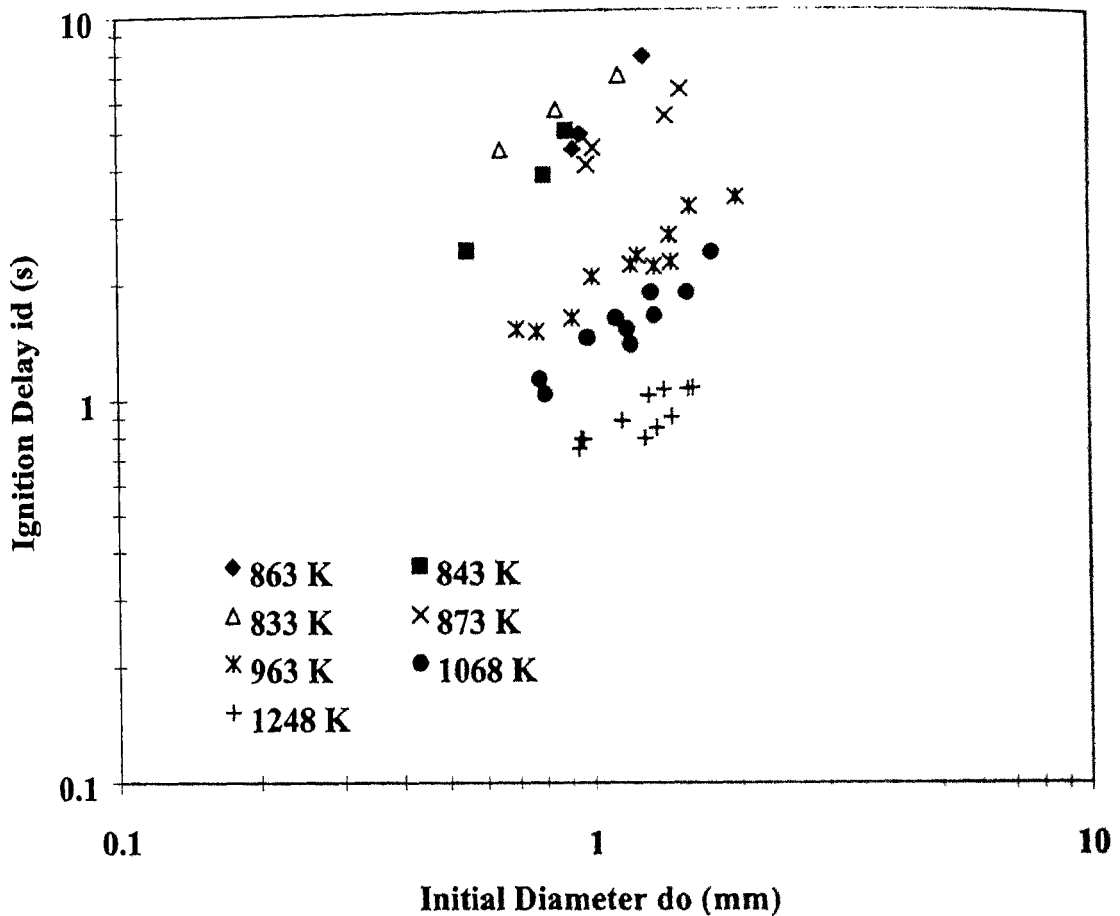


Figure 3.16. Variation of ignition delay with droplet initial diameter of effluent (77 % solid).

3.9.2 Pre-ignition heating phase

3.9.2.1 Dry Effluent Sphere

The surface temperature and mass loss history vs. time of dry effluent sphere of $d_0 = 8.5$ mm, combusted at $T_a = 973$ and 1073 K are presented in Fig. 3.17. The release of volatile that forms the combustible mixture in the gas phase prior to ignition is seen in the plot. Surface temperature and percent volatile material pyrolysed and diffused in the quiescent air at the instance of ignition at two different temperatures are shown. It is seen that at 1073 K ambient temperature ignition can occur at a lower ratio of volatile and air mixture compared to that at 973 K temperature owing to higher heat flux. Sphere surface temperatures at ignition are 573 and 673 K for T_a of 1037 and 973 K respectively. These indicate the invalidity of a single ignition temperature concept for these fuels.

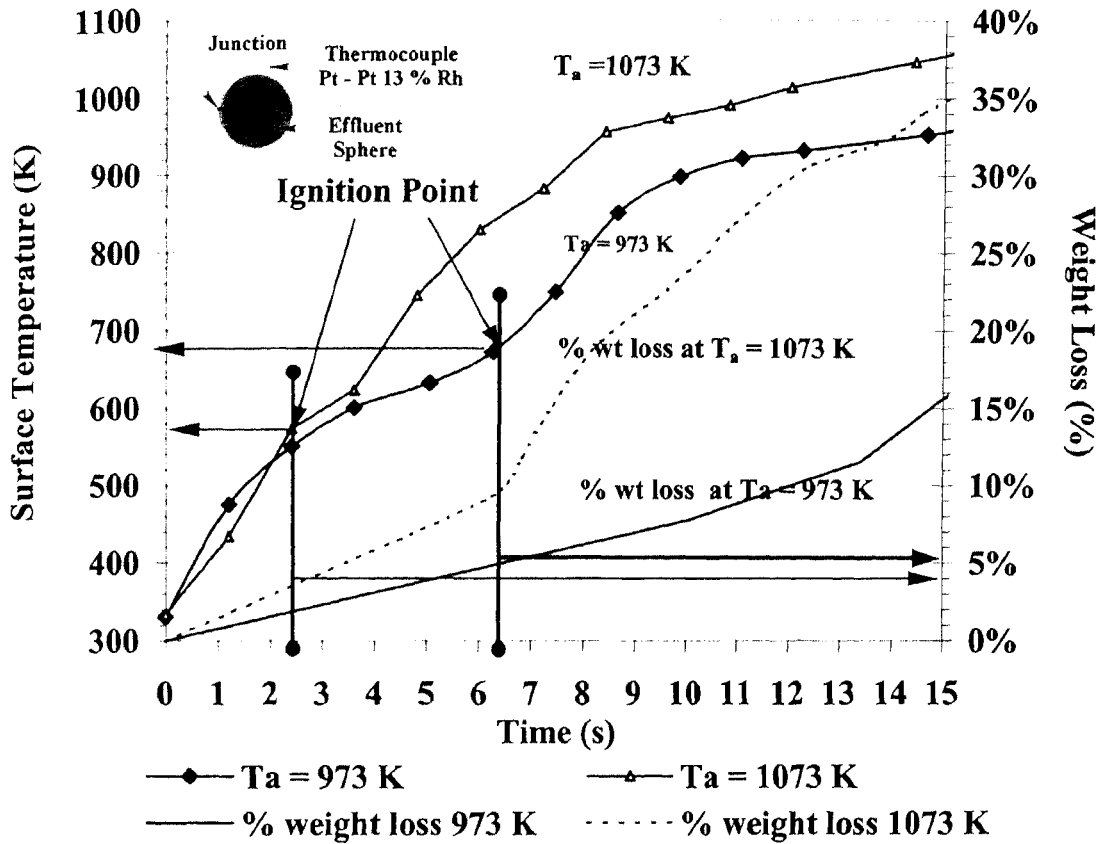


Figure 3.17: Experimentally obtained profile of surface temperature and percent weight loss vs. time of 8.5 mm dry effluent spheres at $T_a = 973$ K and 1073 K.

65 % solids droplet

Fig. 3.18 depicts pre-ignition history of core temperature of a 1.1mm diameter effluent droplet at different ambient temperatures. The profile terminates right at the point of ignition. Heating rate of droplet of the same diameter increases with temperature. The ignition point was determined by observing a step change in light intensity very close to the surface of the droplet.

The absence of identifiable plateau at 373 K indicates lack of distinction between drying and devolatilization stages; however, there is a steep change in slope at temperature 470 K for furnace with $T_a = 873, 973$ and 1073 K and at 395 K for $T_a = 1173$ K. These are thought to be due to the surface getting dry immediately after loss of water and getting heated-up to temperatures much higher than the boiling point of water. In this case, heat transfer occurs radially inward, converting water to super heated steam and vapors of volatile organic acids mainly acetic acid (b.p.391 K), lactic acid (b.p. 395 K), and other organic acids (whose boiling points are close to water) escaping through tiny pores formed in the dried effluent as

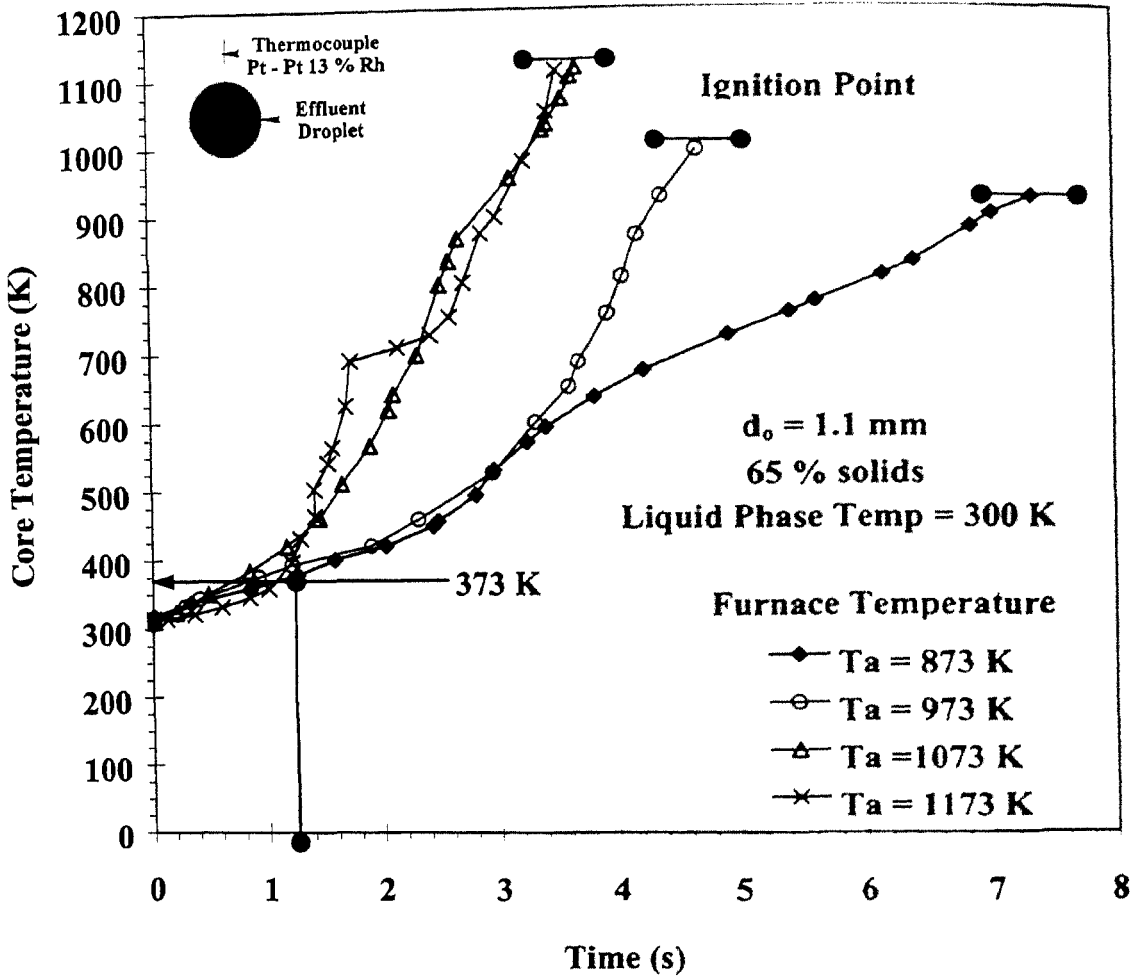


Figure 3.18: Measured pre-ignition core temperature profile of 65 % effluent droplets of 1.1 mm diameter at different ambient temperature.

shown in the Fig. 3.6. Yao et al. (1983) have also reported similar observations in the case of coal water slurry prepared with high volatile lignite, unlike that prepared from bituminous coal. Ignition delay is a function of T_a decreasing with increase in T_a . Gas phase ignition occurs at ambient temperature 1123 K and higher, and at lower temperatures heterogeneous ignition occurs without flaming. This is due to the fast depletion of volatiles of organic acid and decomposed sugar products along with water which acts as a major diluent, hindering gas phase ignition for the fuel mixture at available heat flux. About 25 to 40 % of ignition delay time is taken up only to heat up the liquid to the boiling point of water.

This indicates that ignition delay will be substantially reduced if the effluent is heated to temperature close to the boiling point of water (378 K). Fig. 3.19 depicts pre-ignition core temperature history of droplet of different d_o obtained at 873 K in quiescent air. Heating rate

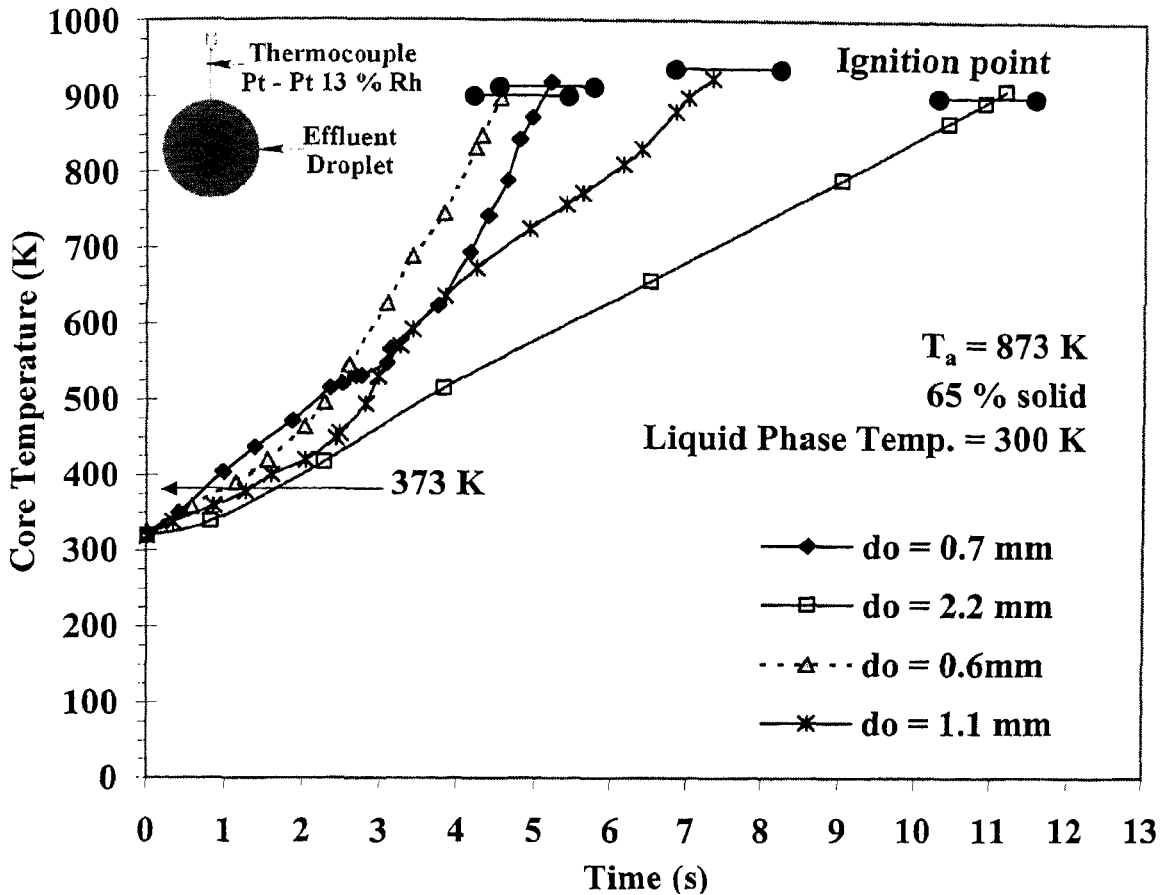


Figure 3.19: Measured pre-ignition core temperature profile of 65 % effluent droplet of different diameter at 873K ambient temperatures.

decreases with increase in droplet diameter at same temperature. As was observed earlier, ignition delay rapidly increases with increase in the droplet diameter. This was also seen in the case of 77 % solid droplet for the same temperature.

3.9.3 Weight Loss

The weight loss of effluent droplet or spheres is the function of ambient temperature. Figure 3.20 depicts weight loss of dry effluent sphere at the end of flaming or devolatilization and at the end of char glowing. The weight loss is determined by taking the difference in the weights of initial effluent sphere and char obtained at the end of flaming or ash obtained after complete combustion. End of flaming is considered as the end of volatilization phase at a given T_a . The term volatilization covers both the chemical depolymerization and the physical evaporation processes. Figure 3.20 was constructed from a large number of tests for flaming and glowing separately on various diameters of dry spheres. The portion marked 'no flame zone' shows the domain in which the weight loss is mainly due to pyrolysis.

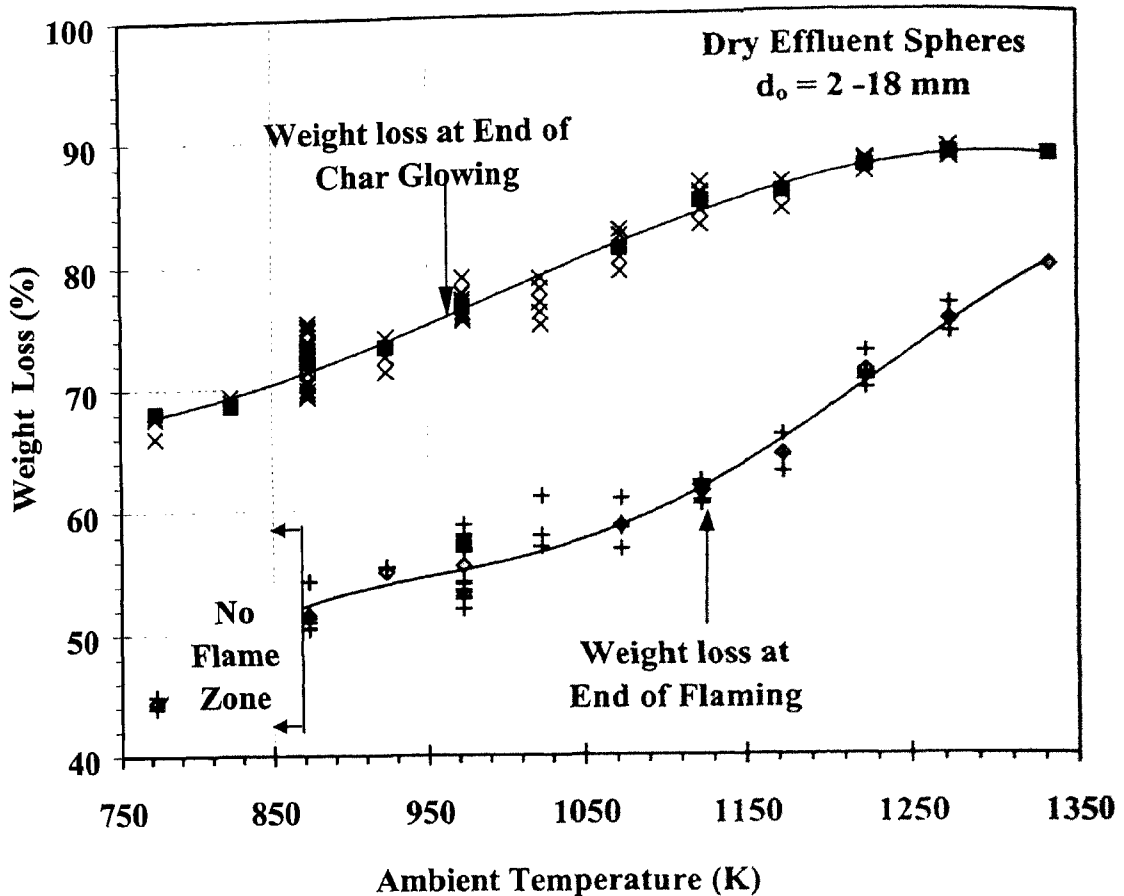


Figure 3.20: Weight losses vs. ambient temperature of dry effluent spheres obtained at the end of flaming and char glowing.

Volatiles, however, do not get into the flaming mode since gaseous mixture (volatile + ambient air) cannot not reach flammability limits. At this temperature (or below 823 K) uncertainty remains concerning the occurrence of flaming – sphere of the same diameter may or may not flame – but after a fixed weight loss (always about 5–6 % lower in the case of no flame), char glowing certainly gets initiated on the sphere surface. It was observed that as the devolatilization rate decreases, the sphere gets slowly heated (but certainly does not glow) and as devolatilization ends (takes 6–8 s more than that in the case of flaming) glowing begins as can be seen by sudden change in the light intensity. Even for temperature above 823 K, if flaming of volatilized products does not occur due to the diameter of spheres being lower than critical diameter (see Fig. 3.12) weight loss will be in the range of 44–48.5 % of initial value. Typical weight loss at the end of flaming increases from 50 % to as high as 80 % for T_a varying from 800 K to 1330 K. This increase, as a function of T_a , is consistent with the observations made by Kobayashi et al., (1976) in the case of coal

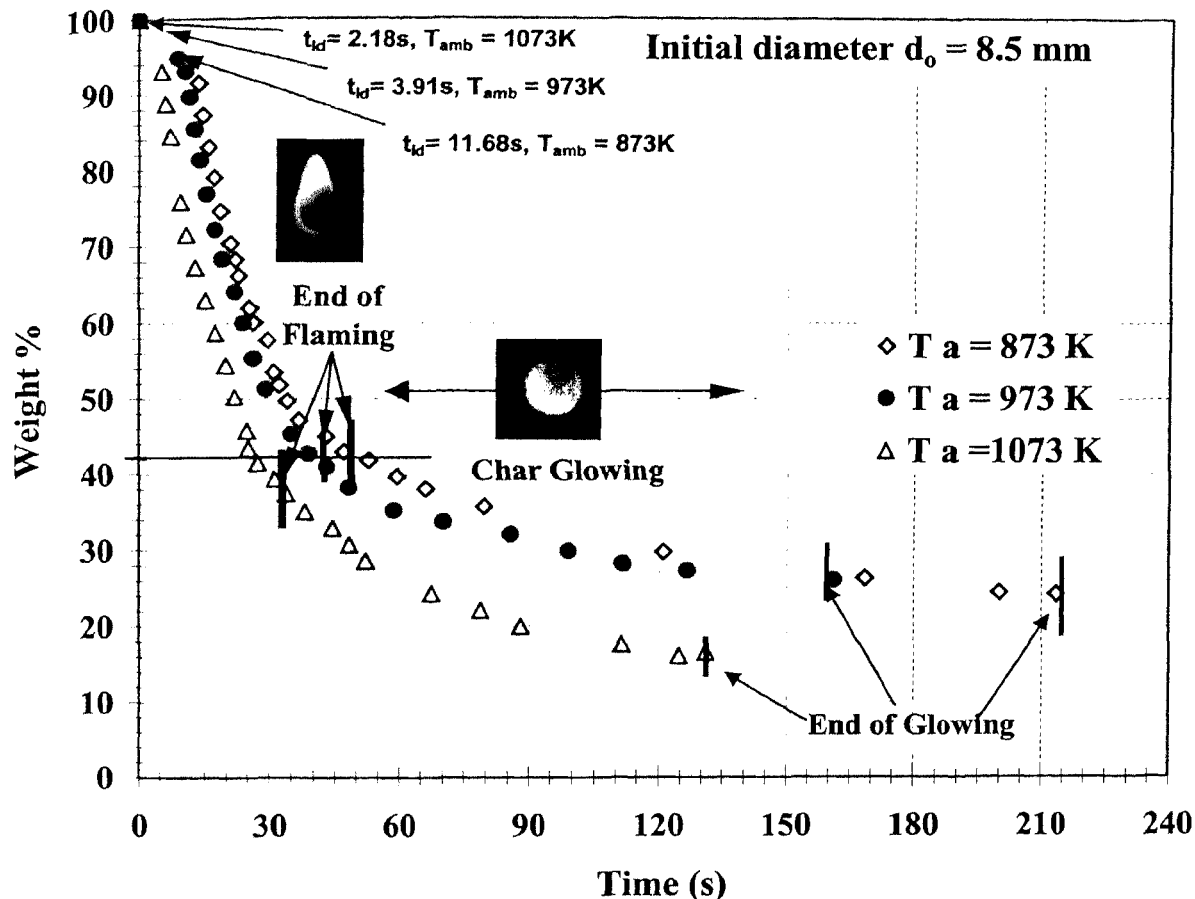


Figure 3.21: The plot shows weight loss–time history of an 8.5 mm diameter combusting sphere vs. time at 873, 973 and 1073 K ambient temperature in quiescent air.

combustion. A fair amount of inorganic material is also lost during the combustion process since the analysis of the dry samples indicated an organic content of only 60 %. The observed white fume exuding from the burning spheres also supports the arguments in favor of inorganic material loss (see Fig. 3.8 – 3.9).

3.9.3.1 Weight vs. time profile of combusting effluents at various T_a

Figure 3.21 show the weight vs. time history of a dry effluent sphere of $d_0 = 8.5$ mm, combusted at $T_a = 873, 973$ and 1073 K. Weight loss prior to ignition decreases with ambient temperature as seen in Fig. 3.17. Steep weight loss is recorded with ignition during flaming.

The rate of devolatilization is not very different once the flame envelops the sphere. In the case of $T_a = 1073$ K, flaming and char glowing overlapped for about 3–4 s. Char conversion

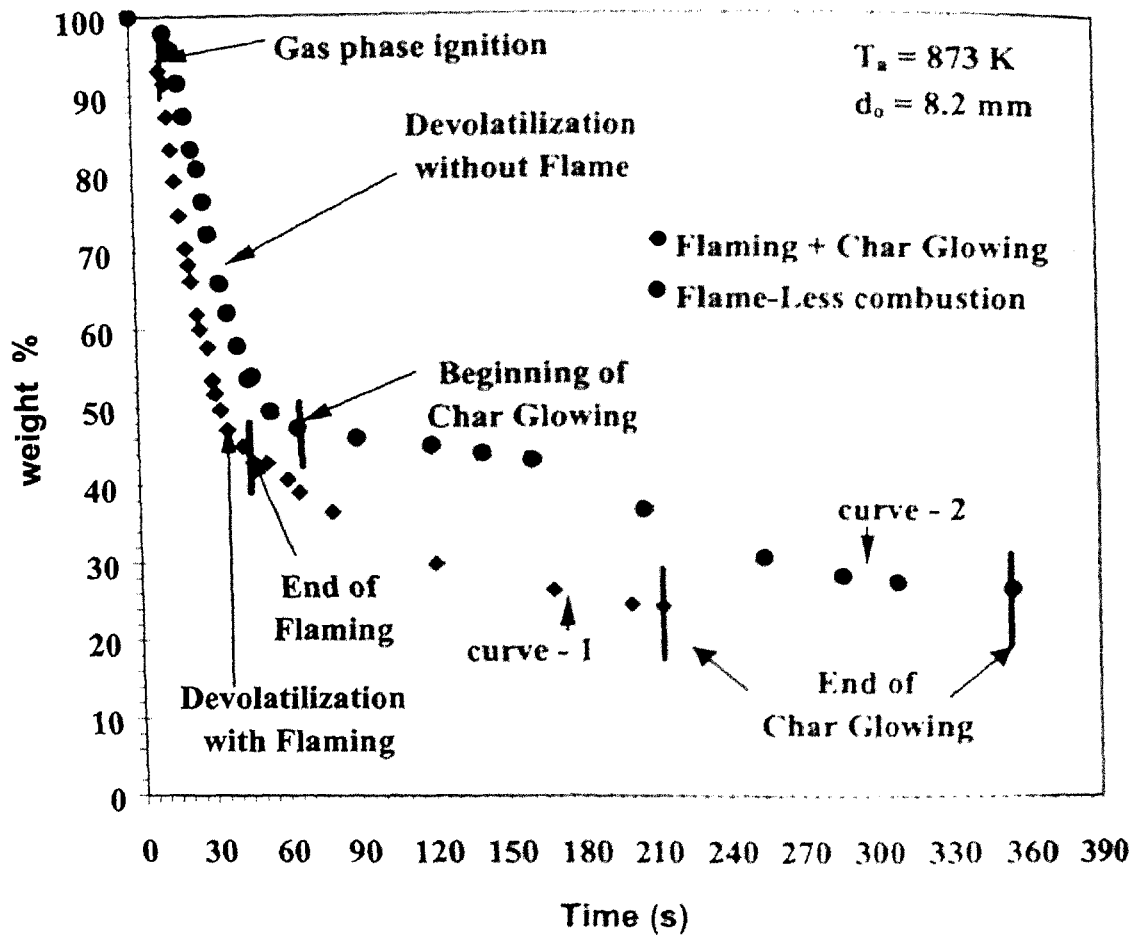


Figure 3.22: Percent weight vs. time history of two effluent spheres of 8.2 mm diameter, combusting at 873 K, one having primary homogeneous ignition and other having heterogeneous ignition.

rate is high for $T_a = 1073 \text{ K}$ compared to T_a of 973 K and 873 K. The obvious reason for higher reaction rate in the former case is the higher surface temperature as can be seen from the surface temperature profiles of 1073 K and 973 K depicted in Fig. 3.32.

3.9.3.2 Weight vs. time profile of sphere combusted with and without flaming.

The effect of circumambient flame on the overall weight loss vs. time profile of dry effluent sphere is depicted in Fig. 3.22. Two spheres of same initial diameter of 8.2 mm were burnt in quiescent air at 873 K. The flaming of devolatilized gases at this T_a is highly uncertain for $d_o > 6.5 \text{ mm}$; however, homogeneous ignition certainly does not occur below this diameter. In addition the ignition delay range is large, from 7.5–28 s with standard deviation of 5.3. If flaming does not occur in this range then it will not occur at all. The interesting feature is the weight loss vs. time profile in both the cases where flaming does and does not occur. In

order to have comparison between the two cases, weight vs. time profile of two separate spheres of $d_0 = 8.2$ mm with one devolatilized with flame and other without it are plotted.

In both the cases, after devolatilization is over, the char glowing occurs and continues till the end of conversion. During devolatilization phase, glowing does not occur in either case since the surface will not receive any oxygen: in the first case, it is due to the presence of circumambient flame, and in the second case of flameless devolatilization, the bulk gas close to surface would be devoid of oxygen, due to outward volatile degassing. Therefore, char glowing commences at the end of flaming or devolatilization.

The weight loss at the end of devolatilization in the first case (with flaming) is 52–56 % and in the second case (with out flame) is 44–49 %. The pointer indicating 'beginning of char glowing' is the instant where char glowing initiates on one side of the sphere, and in about 8–10 s for the complete sphere to glow.

The presence of circumambient flame has a clear impact on the higher char conversion rate compared to the case with no flaming and this is clearly seen from the slope of profiles during glowing. This is expected due to difference in heating rates. The heating rate of the spheres in both the cases prior to devolatilization is 40 K/s up to 473 K. However in the case of flaming the surface heating rate increases to 60 K/s until the surface temperature is 873 K (ambient temperature) and then decreases again to 8–10 K/s until the end of flaming where the surface temperature is 320 K above T_a . In the case of no-flaming, the heating rate decreases to 10 K/s after initial sphere heating and the maximum temperature attained by the surface is close to ambient.

Thus the enveloping flame causes the surface to get heated more rapidly and at higher temperatures compared to that in the latter case and this has significant effects on the total burn time and final weight loss. This observation is similar to that of pyrolyzing polymer where higher temperature promotes more de-substitution and de-polymerization reactions and also enhances secondary breakdown of the primary products. Though the effluent has complex polymeric organic materials, temperature effect on depolymerization is similar to that on any other polymer. In the case of coal, it is known that the reactivity of char prepared by rapid heating to 1073K is much more than the char prepared by slow heating to 773 K despite the weight loss upon pyrolysis being found similar in two cases.

	Initial (gm)	Char (gm)	Ash (gm)	% Loss During Flaming	% Loss During Glowing	Total loss %
<i>Ambient Temperature = 973 K</i>						
Organics	60.3	22.8	0.5	62.2	97.9	99.2
Inorganics	39.7	21.6	22.8	45.5	-5.6	42.5
<i>Ambient Temperature = 873 K</i>						
Organics	60.3	24.3	0.6	59.7	97.8	99.1
Inorganics	39.7	23.1	26.4	41.9	-14.3	33.5
<i>Ambient Temperature = 773 K</i>						
Organics	60.3	27.9	0.6	53.6	97.7	98.9
Inorganics	39.7	26.6	30.2	33.1	-13.6	24.0

Table 3.4 Organic and inorganic composition of dry effluent and its char produced at various temperatures.

3.9.4 Chemical Transformation

A fair amount of inorganics are lost during combustion process as the white fumes are observed getting released from the burning sphere. The weight loss during flaming increases from 45 % to as high as 80 % for T_a ranging between 800 and 1330 K, though the total organic content is only 60 %. In order to shed more light on the chemical transformation occurring during the combustion process, chemical analyses of dry effluent sphere char and ash were carried out at 773, 873 and 973 K and the results are summarized in Tables 3.4 and 3.5. The char and ash were obtained from individual effluent spheres (d_p in the range of 8 to 10 mm) after devolatilization and quenching it or, allowing it to burn completely to form ash in quiescent air at prescribed T_a .

The organic material loss *during flaming* increases from 53.6 % to 62.2 % of total organic content for an ambient temperature rise from 773 K to 973 K. This loss is significantly high at higher temperatures as can be seen from Fig. 3.20. This is true even in the case of inorganics. Substantial amounts of inorganics are lost during flaming (gas phase release, physical ejection, reduction reaction). The weight loss increases from 33 % to 45.5 % of total inorganic material with rise in temperature from 773 to 973 K. Total organic losses till the end of char glowing is 97.8 %. The inorganic material, however, gains weight during char glowing and this is primarily due to formation of alkali oxides and oxidation of alkali sulfides to alkali sulfates. A comprehensive analysis of the release of inorganics during the

	100 % solids (g)	T _o = 973K Char	Weight loss %	T _o = 973K Ash	Percent Weight-loss %	Total Weight Loss %
Potassium as K	14.8049	7.3205	50.6	6.0520	17.33	59.12
Magnesium	3.1979	1.1537	63.9	1.1329	1.80	64.57
Calcium Ca	2.3688	2.1499	9.2	2.1112	1.80	10.88
Carbonate CO ₃ ⁻²	----	3.2249	----	3.1667	1.80	----
Sodium as Na	2.3133	0.5143	77.8	0.6267	-21.85	72.91
Total chloride as Cl	12.5842	6.5672	47.8	5.5401	15.64	55.98
SO ₄	4.4600	0.6563	85.3	4.5491	-593.2	-2.00
PO ₄	0.00004	0.0005	0.0	0.0000	0.00	0.00
Organic Solids	60.2709	22.9228	62.0	0.4211	98.16	99.30
Inorganic	39.7	21.5872	45.7	23.1789	-7.37	41.66
TOTAL (gm)	100.0	44.51	55.5	23.60	46.98	76.40

Table 3.5: Compositions of dry effluent and its char and ash obtained by combusting dry effluent spheres at 973 K ambient temperature.

conversion of organics is required in order to understand and design a combustion system that has low carryover and low emissions. Gasification is a low temperature process compared to incineration and is carried out in reducing atmosphere. This condition has great impact on the release of inorganics during combustion and is discussed based on chemical analysis presented in Table 3.4.

3.9.4.1 Reduction of sulfate

During flaming, no oxygen reaches the surface of the sphere and the heat transferred from the surrounding flame causes the surface to attain temperatures from 723 to 1153 K. This causes a strong reducing condition inside the sphere due to high temperature, presence of various carbonaceous material and devolatilized reducing gases like CO, H₂. The presence of sulfide would catalyze this reduction, as is found in the literature which was experimentally determined by Dunks et al. (1982). Any alkali sulfate especially potassium sulfate gets reduced to alkali sulfide and alkali oxide contributing towards the inorganic weight loss. The sulfate loss during flaming is found to be 85.3 % (obtained through chemical analysis of char). This loss is higher than that obtained by Kikuchi et al. (1983) (see Fig. 3.23) where K₂SO₄ was heated in different stream of reducing gases H₂, CO or inert He in the presence of graphite.

Figure 3.23 shows thermogravimetric analysis carried out by Kikuchi et al. (1983) with respect to the reduction reaction of K₂SO₄. Heating rate was 10 K/s and flow rate of each

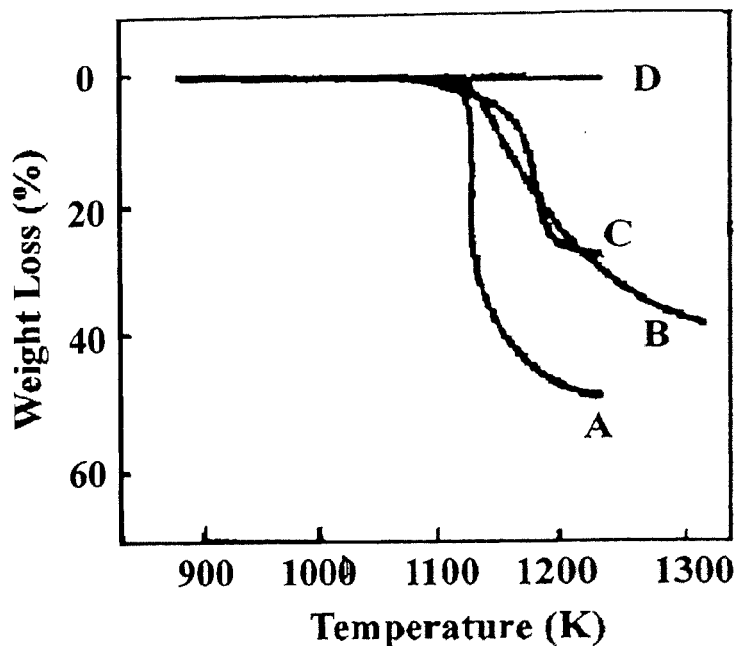
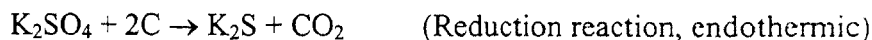


Figure 3.23: Thermogravimetric analysis with respect to the reduction reaction of K_2SO_4 . Temperature rate, 10 C/min; flow rate of each gas 1 ml/s. A): K_2SO_4 in H_2 ; B) K_2SO_4 in CO ; C) 1:1 graphite- K_2SO_4 mixture in He ; D) K_2SO_4 in He . (Kikuchi *et al.*, 1983)

reducing gas (H_2 , CO , He) was 1 ml/s. Reduction in carbon (graphite) was carried out in 1:1 of C and K_2SO_4 .

During char combustion, sulfide gets reoxidized to sulfate and gains back weight almost equal to the initial weight and completes the cycle. The reduction of sulfate in presence of carbon and the oxidation of sulfide can be written as



The first reaction may occur predominantly during flaming where no oxygen reaches the surface of the sphere while the second reaction predominantly occurs during char glowing. Sulfide oxidation is extremely fast in the temperature range 1050 - 1200 K, the typical temperature range occurring during the char glowing phase. During char glowing both the above reactions may be in a dynamic equilibrium till the last fraction of carbon existing in the char remains. Thus sulfate to sulfide redox couple may help accelerating char conversion; it was found during weight loss versus time experiment that the effluent char conversion rate is equal to or little higher than of wood char (without redox couple) at the

same temperature (see Fig. 3.28), inspite of the BET surface area of wood char being 100 times higher than effluent char.

As seen in the Table 3.5, during devolatilization phase, sulfate reduction is associated with carbonate formation. The char analysis shows presence of 3.2 % carbonate that can exist as alkali carbonate since they are stable at high temperatures. Carbonates of calcium and magnesium decompose at 1170 and 593 K respectively. Hence the possibility of the existence of calcium and magnesium as oxides is far more than the carbonates. Therefore, it is clear that in the effluent char, alkali sulfide, alkali sulfate and alkali carbonate can coexist.

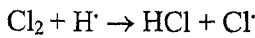
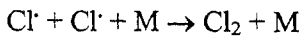
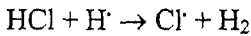
Stellman et al. (1976) have shown that the oxidation of graphite was faster in a sodium carbonate-sodium sulfate melt than in a pure sodium carbonate melt and established the catalytic effect of sodium sulfate in the graphite oxidation by sulfate-sulfide redox cycle. Similar sulfate-sulfide redox mechanism was also shown to exist in the case of oxidation of black liquor char by Cameron (1987). The author has demonstrated higher oxidation rate of black liquor char in air as compared to that of soda char in air and the effect was attributed to the presence of sulfur in char. Therefore it is also expected in the case of effluent char.

3.9.4.2 Release of chlorine

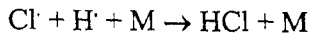
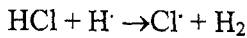
Qualitative analysis of the char formed after devolatilization reveals loss of about 47.8 % of total chlorine. The surface temperature vs. time profile of effluent sphere plotted during combustion reveals that the maximum temperature experienced by the particle is below 1000 K up to the end of devolatilization phase. This temperature is lower than the melting point of potassium chloride (1043 K) or sodium chloride (1073 K). Therefore, the loss of chlorine is much more than expected, if predominantly, the chlorine were to exist as chlorides of alkali metals since their vapor pressure is very low at these temperatures. Experiments were carried out on oven dried effluent (100 % solids) and liquid effluent (75 % solids) prepared by adding distilled water to dry effluent solids separately, to determine the release of chlorine at low temperatures. Effluent samples were heated by electrically heated paraffin wax bath in glass tubes with an arrangement to divert the vapor evolved into AgNO_3 solution. White precipitate of silver chloride was observed when bath temperature reached 463 K and the amount of precipitate increased with time. At higher bath temperature (up to 498 K) rate of precipitate formation increased and at temperatures above 523 K the release of pyrolysis products interfered with the color of the silver chloride

precipitate. These qualitative observations confirm that part of the chlorine in the effluent exists as organic chloride and gets released during early devolatilization phase itself.

The characteristic of HCl oxidation in post-combustion conditions and the effect of HCl on the other gas emissions like CO and NO_x are poorly understood. It is, however, known that in high temperature flames, compounds containing halogen atoms act as inhibitors for the combustion process by catalyzing the recombination of radicals and thus decreasing the radical pool causing extinction of flame.



and



The overall effect for both schemes is $\text{H} \cdot + \text{H} \cdot \rightarrow \text{H}_2$

Char loses about 15.6 % of its chlorine content during char glowing and this amount to only 8 % of total chlorine in dry effluent.

3.9.4.3 Release of alkali metal

The effluent contains high amounts of alkali metal and chlorine and they exist in molecularly dispersed form. The occurrence is highly complex due to the presence of mixture of organic compounds basically sugars, organic acids, gums (polysaccharides), phenolic compounds, lignin and many other non sugar compounds (see Table 1.1). They are in ionic form in sugar-cane plant and play an important role in the plant metabolism. All soluble non-clarifiable inorganic compounds in the cane juice remains in molasses and finally in the effluent. Their high proportions has immense impact on the pathways for the release of alkali metal and fume formation during devolatilization and char combustion phase. Alkali can be primarily as alkali chloride in solution, alkali sulfate and as organically bound material directly attached to carboxylic acid group. Early release of chlorine as HCl is an indication of their occurrence also as non-alkali chloride form. During devolatilization phase, the potassium release is found to be 50.6 % by weight of the original amount present in 100 % dry solids (dry effluent has 14.8 % K) at 973 K furnace temperature. In the char

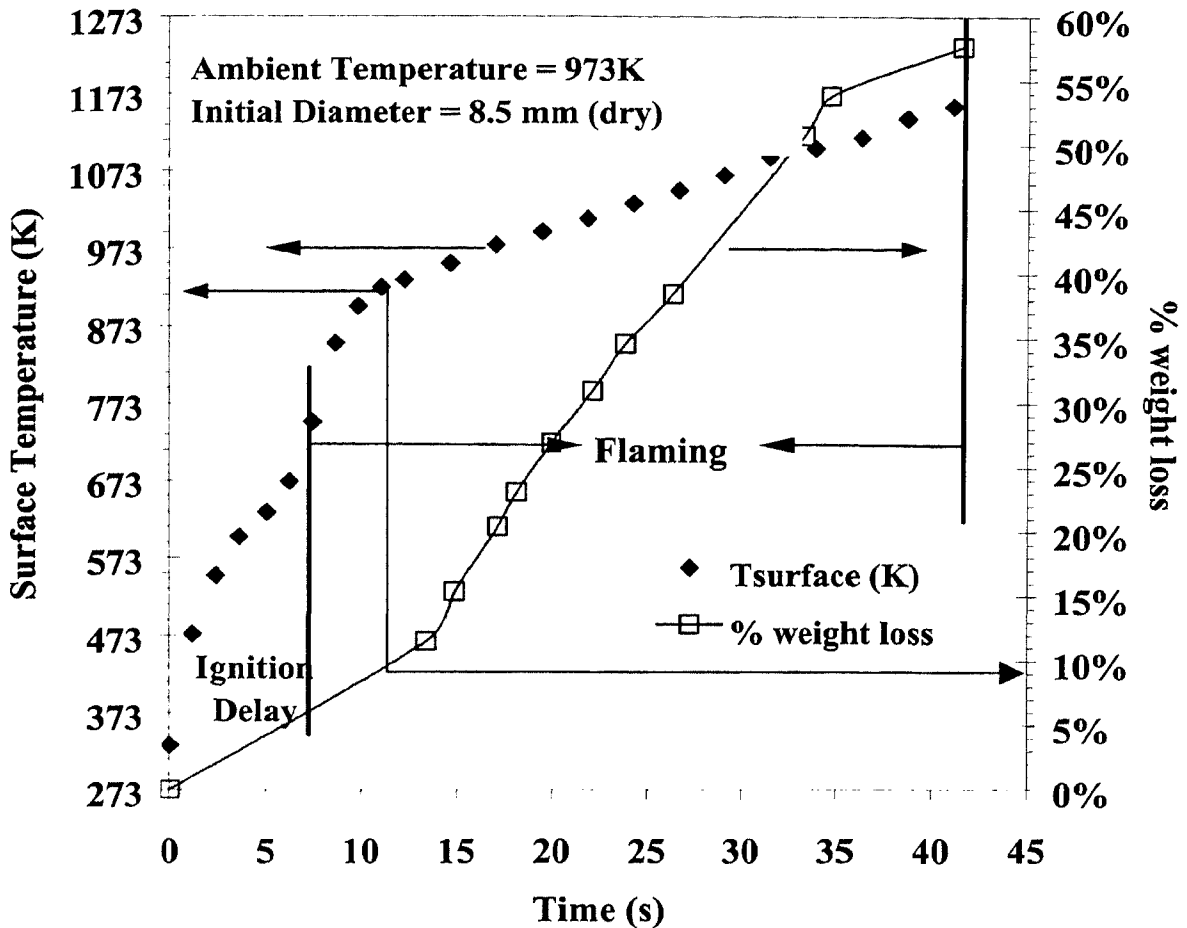


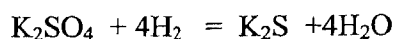
Figure 3.24: Surface temperature and weight loss vs. time profile obtained up to end of devolatilization of dry effluent sphere of $d_0 = 8.5$ mm, combusted in quiescent air at $T_a = 973$ K.

glowing process, potassium release is 17.3 % from the char and total loss in the over all combustion process is 59.1 %. The alkali release can be divided in two parts. Part I: release during devolatilization phase (in strong reducing condition) and Part II: release during char glowing phase (oxidizing condition). These two processes are discussed below.

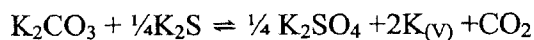
Part I - Alkali release during flaming (strong reducing condition)

Figure 3.24 shows surface temperature and corresponding weight loss profile of 8.5 mm diameter, dry effluent sphere, combusting at furnace temperature of 973 K during flaming. By 4 s after ignition, the surface temperature goes up by 473 K. The weight loss at a rate of 1.94 % per second of the initial weight is observed till the end of devolatilization phase. As the surface temperature of the droplet goes up from 893 K to 1153 K, partial melting of salts can occur. During the devolatilization phase, alkali metal exists as sulfate, carbonate, sulfide and chloride. The eutectic mixture of alkali sulfide and alkali sulfate has very low melting

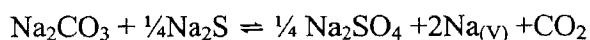
point (883 K) as compared to that of pure individual components in an inert atmosphere and favors the release of alkali metal vapor. Huttinger and Minges (1985) in their study on catalyst for water vapor gasification of carbon, have observed that melting point of pure K_2SO_4 in H_2 - H_2O atmosphere is 1028 K much below the melting point in an inert atmosphere (~1342 K). This depression in melting point in the hydrogen atmosphere (reducing conditions) is caused by the presence of K_2S formed by the reduction of the K_2SO_4 .



K_2S melts at 1113 K, but a mixture of the two has a melting point as low as 883 K, which may enhance the possibility of the following liquid phase reaction:



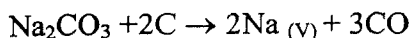
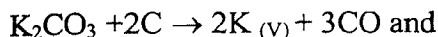
and



Cameron (1987) has proposed a mechanism of alkali vapor release due to oxidation of sulfide in a melt of alkali carbonate-sulfide. During devolatilization, however, no oxidation of alkali vapor is possible since the flame is enveloping the sphere. Hence the alkali vapor release mechanism proposed by Cameron (1987) cannot be applied in this case. The release of chlorine, however, may have some effect on the release of alkali. Dayton and Frederick (1996) has found that high levels of chlorine tend to facilitate alkali metal release in biomass combustion. It is known that the effect of chlorine in combustion environment is to lower the temperature at which there is transition between vapor and condensed metal species. This indicates that chlorine will enhance vaporization of metals at low temperatures and subsequently delay their nucleation and condensation. This behavior is observed in the combustion of waste containing chromium, nickel and lead and known to have similar effect on alkali metals. The pathway of the alkali release may be very complex; however, at combustion temperatures, the release of alkali is predominantly as alkali chlorides due to high chlorine content of the feed. A qualitative analysis of fume deposited on colder surfaces of the reactor sight glass showed the presence of alkali chloride along with alkali carbonate and alkali sulfate.

Another plausible mechanism for such high amount of alkali loss during devolatilization could be due to the ejection of pyrolysis gases from the surface of the heated droplet.

Another set of reactions that can be applied to explain the alkali release are:



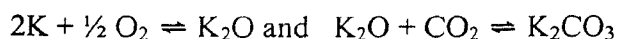
These reactions require strong reducing conditions and high temperature of 1173 K. Reductive fuming at 1473 K was an early commercial process for sodium production (Clay et al., 1984; McKeough et al., 1995). The formation of alkali carbonate is found from chemical analysis of char. The possible pathways involved in its formation can be explained based on the decomposition of low molecular weight alkali carboxylates, which is considered likely at low temperatures (673–773 K).

Part II – Alkali Release during char glowing (oxidizing conditions)

Alkali loss during char glowing is an order of magnitude lower as compared to that released during devolatilization in spite of comparatively higher temperatures experienced during char glowing. Hence, it is clear that the pathways of alkali release in both the cases are different.

Fig. 3.25 shows surface temperature and weight loss profile obtained during char oxidation in air. This plot is a continuation of surface temperature variation beyond 1153 K from the previously plot which was for flaming period. The total weight loss is 17.7 % and the surface temperature varies in the range of 1153–1373 K and reaches 1143 K at the end of char glowing phase. The surface temperature crossed 1273 K for a brief period of 17 s. During this phase of combustion, sulfide gets oxidized back to sulfate to an amount almost equal to initial amount. Alkali carbonate is also present in the char. Fuming is also observed during this period. Particle condensed on cold surface was found to have chloride, carbonate and sulfate of alkali as confirmed by AgNO_3 , HCl and BaCl_2 tests respectively.

The formation of carbonate in the gas phase may be as follows:



However, alkali oxide will exist only at lower temperature ranges (< 973 K) and at low CO_2 partial pressures. The presence of sodium oxides in carbonate melt has been reported by Anderson (1977). These oxides are Na_2O , Na_2O_2 and NaO_2 in decreasing order of concentration in liquid phase and may contribute in the formation of fume. Also, NaO , a

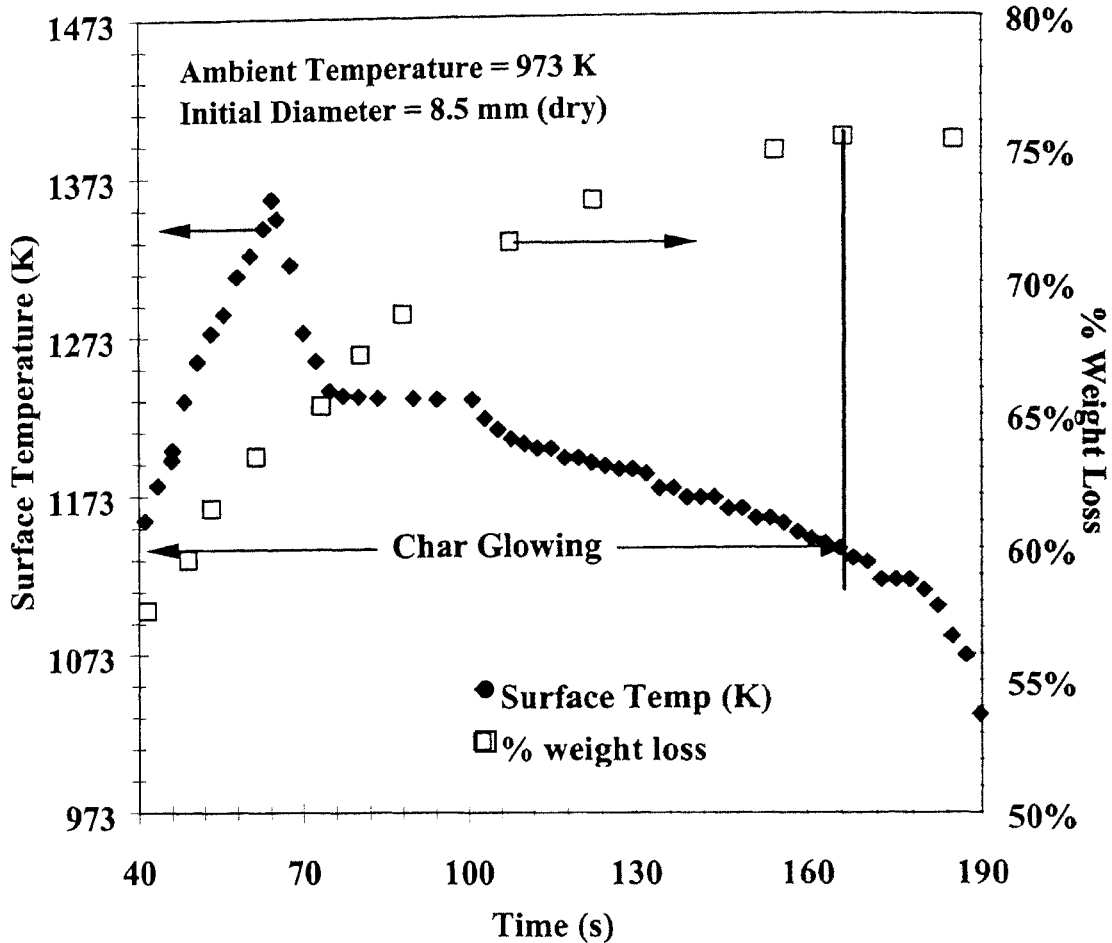
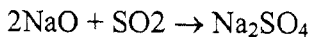
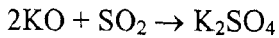


Figure 3.25: Surface temperature and weight loss vs. time profile obtained for char glowing of dry effluent sphere of $d_0 = 8.5$ mm, combusted in quiescent air at $T_a = 973$ K.

volatile and highly reactive oxide is present and may act as initial fuming species. Alkali sulfate may have formed by following reaction:



Alkali Chloride found could have released as alkali chloride vapor or may have formed in the gas phase. The increase in fuming intensity can be physically seen with increases in ambient temperature and this reflects on higher total weight loss at higher temperature as can be seen in Fig 3.20.

Potassium loss during this char oxidation is 17.3 % amounting to 8.6 % of initial amount and chlorine loss is 15.6 % amounting to 8 % of initial amount present in dry solids. Fume

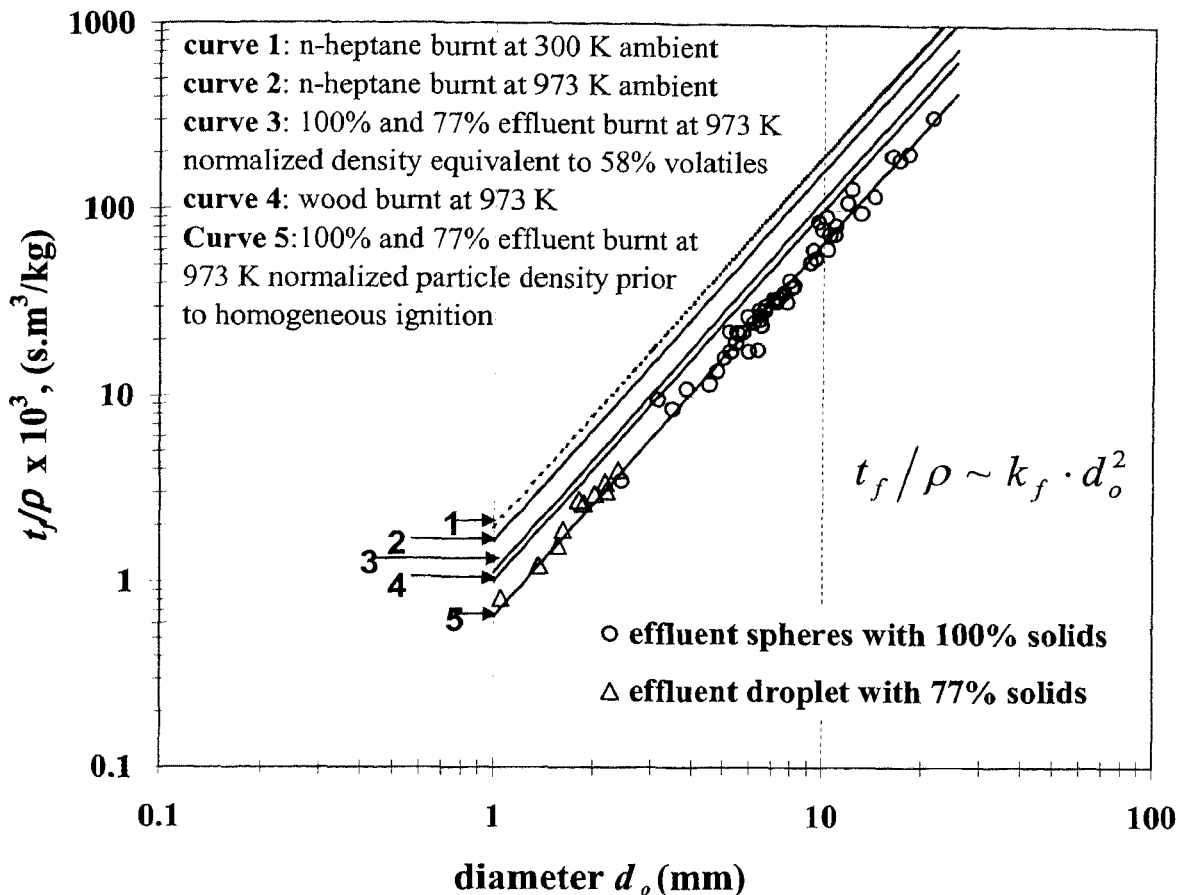


Figure 3.26: Normalized flaming time vs. diameter for effluent spheres (100 % solids) and droplets (77 % solids). Results of n-heptane and wood are also shown.

release during char glowing is clearly due to the alkali sulfide oxidation in ambient air, however, during flaming, the release of fume can be due to alkali evaporation.

3.9.5 Flaming of effluent droplet and dry spheres

Figure 3.26 shows the relationship between flaming time normalized with density and diameter of dried effluent spheres (100 % solids) and effluent droplets (77 % solids) on a log-log plot. The value of density used for normalizing flaming time in the case of spheres, is the density of unburnt sphere or initial density. This is to account for variations in density that occurs in the process of making dry effluent spheres and the expectation that the combustion time varies linearly with density. In the case of liquid droplets, the flaming time is normalized with density of the dried effluent droplet that is in the range of 350–400 kg/m³. Similar data for wood by Mukunda (1984) and n-heptane by Kumagai (1971) burnt at an ambient temperature of 973 K are also shown for comparison purposes. Curves 1 and 2 are for n-heptane burnt at ambient temperatures 300K and 973 K respectively. Curve 2 for

973 K is presented to exhibit a comparison with dried effluent combustion and is obtained using standard liquid droplet combustion calculation procedure, taking into account burning constant dependence on thermodynamic and transport properties.

Curve 4 is for wood burnt at 973 K. Curves 3 and 5 are for effluent burnt at 973 K. Curve 3 is obtained by normalizing burn time with density that is equivalent to 58 % fuel mass that devolatilized during the flaming process and curve 5 is normalized with initial density of the dried effluent sphere and droplet. A curve fit to this data leads to $t_f \sim d_o^2$ indicating the diffusion-dominated combustion. The value of $\dot{m}/d = 0.45$ g/m.s for combusting dry spheres at 973 K and is 0.55 g/m.s for wood. As can be seen, flaming time in the case of n-heptane is larger since it gets completely consumed to zero diameter and zero weight unlike that of for effluent and wood. These data can be understood in another manner. If one constructs a non-dimensional burn time, ' τ ' defined by

$$\tau = t_f \frac{k_w}{\rho_w \cdot c_{pw}} \cdot \frac{1}{d_o^2}$$

where the quantities subscripted by w refer to solid phase, the quantity τ is given in the Table 3.6:

Fuel	τ
Effluent	0.1170
Wood	0.1050
n-heptane	0.1003

Table 3.6: Non-dimensional burn time for effluent, wood and n-heptane

The table indicates that effluent volatile burn time compares well with that of wood.

3.9.6 Char Glowing: experimental and computational results

Figure 3.27 depicts the experimental data of char glowing times normalized with char density of the effluent and of wood char with its initial diameter d_o for combustion in quiescent air with T_a of 873, 973 and 1073 K. Glowing time data of char formed after drying and devolatilization of initial concentrated droplet effluent are also presented.

Computations of char combustion in air at 973 K and 1073 K with the data indicated earlier are shown in the same figure by the lines. The slope of the line leads to the exponent in $t_c/\rho_c \sim d_o^m$ as $m = 2$ ($t_c \approx 2.13 d_o^2$) for effluent at $T_a = 973$ K and $t_c \approx 2.5 d_o^2$ for wood) indicating diffusion dominated combustion. The line remains straight up to a lower end

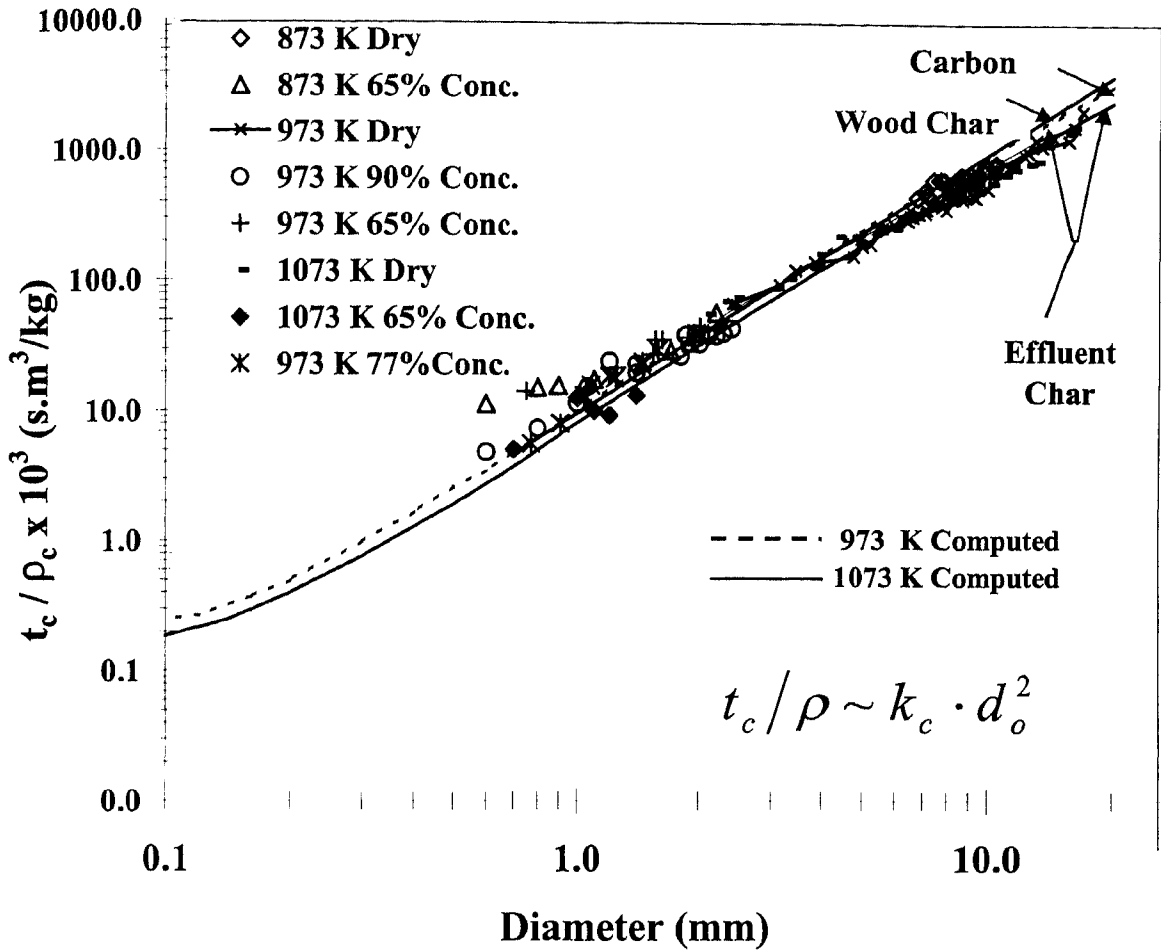


Figure 3.27: Char glowing time vs diameter for concentrated liquid droplets and dried effluent material at different temperatures. Results for wood char and pure carbon are also shown. Comparison with model prediction is shown as continuous lines in the figure.

diameter of 0.6 mm. Below this the line becomes curved with slope decreasing with decrease in diameter indicating increasing reaction control at lower diameters. The burn time of the effluent and wood char are comparable even though the effluent has about 39 % inorganics in comparison to wood with only 1 % ash. Besides, the BET surface area of wood is two order of magnitude larger than effluent surface area. This indicates that there is no obvious correlation between BET surface areas and reactivity of the char in both the cases, however, the presence of large fraction of alkali/inorganics, expected to be in the molecular matrix, may act as catalyst, and contribute to the compensating effect. Similar results were found by Spiro (1983) in the case of Illinois No. 6 coal char obtained by charring for 2 hours at 973 K and treated with 5 % K_2CO_3 and has CO_2 surface area $4.6 \text{ m}^2\text{/g}$ as compared to a less reactive char prepared under same conditions and has large

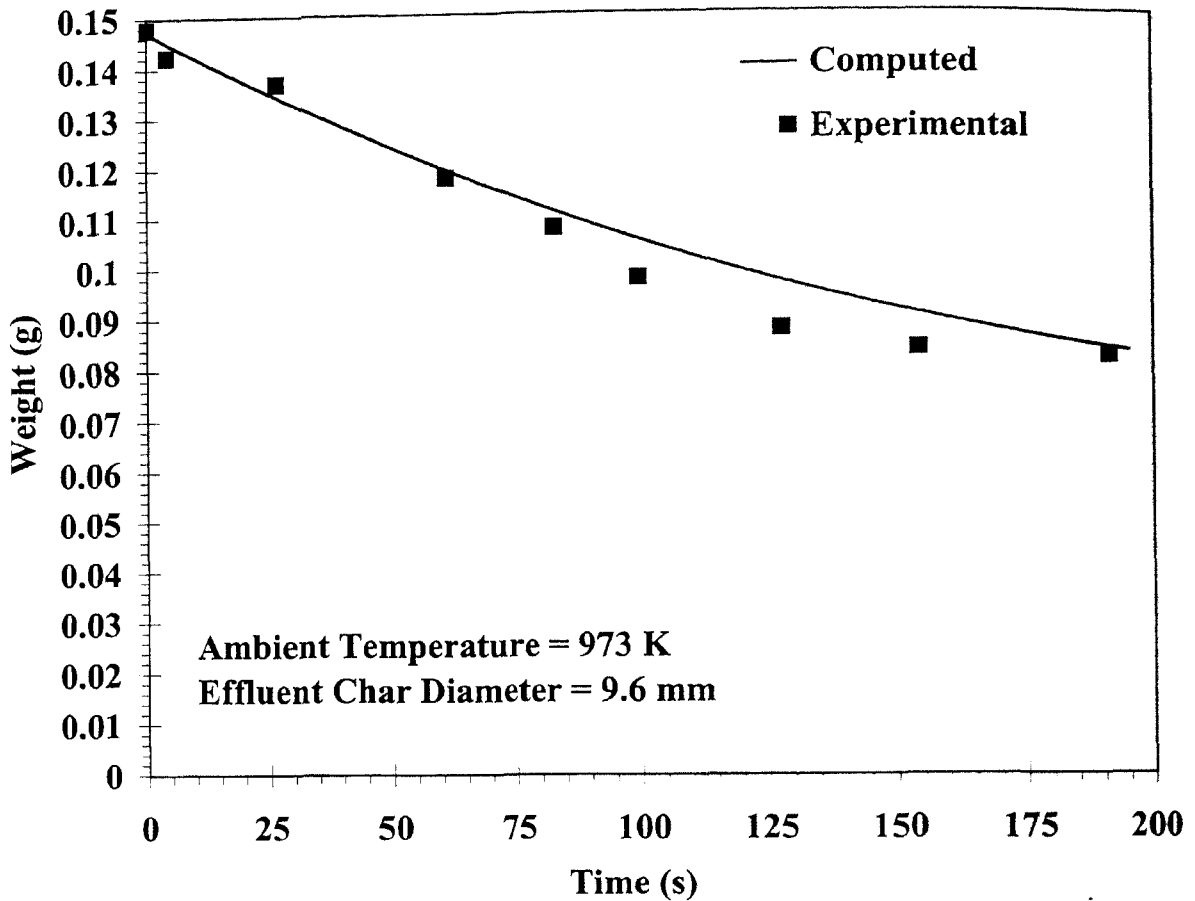


Figure 3.28: Experimental and computed weight–time profile of 9.6 mm diameter char combusted at ambient 973 K.

surface area of $233 \text{ m}^2/\text{g}$.

3.9.6.1 Weight – time profile of char: experimental and computed results

Continuous weight of combusting effluent sphere of 9.6 mm diameter was recorded with respect to time in quiescent air at 973 K. The data of char glowing was extracted and is plotted in Fig. 3.28 represented by square dot along with the computed result represented by line. The physical, thermodynamic and transport properties used in the computation are the same as that in section 3.8.5.

The computed results compare well with the experimental data. The data of char glowing extracted from the weight–time profile of effluent sphere at 873 K for 8.2 mm and 8.5 mm diameter is plotted in Fig. 3.29. The devolatilization in both the cases was flameless. Computed results for both the cases represented by line are also plotted along with experimental results. The computed results compare well with the experimental data.

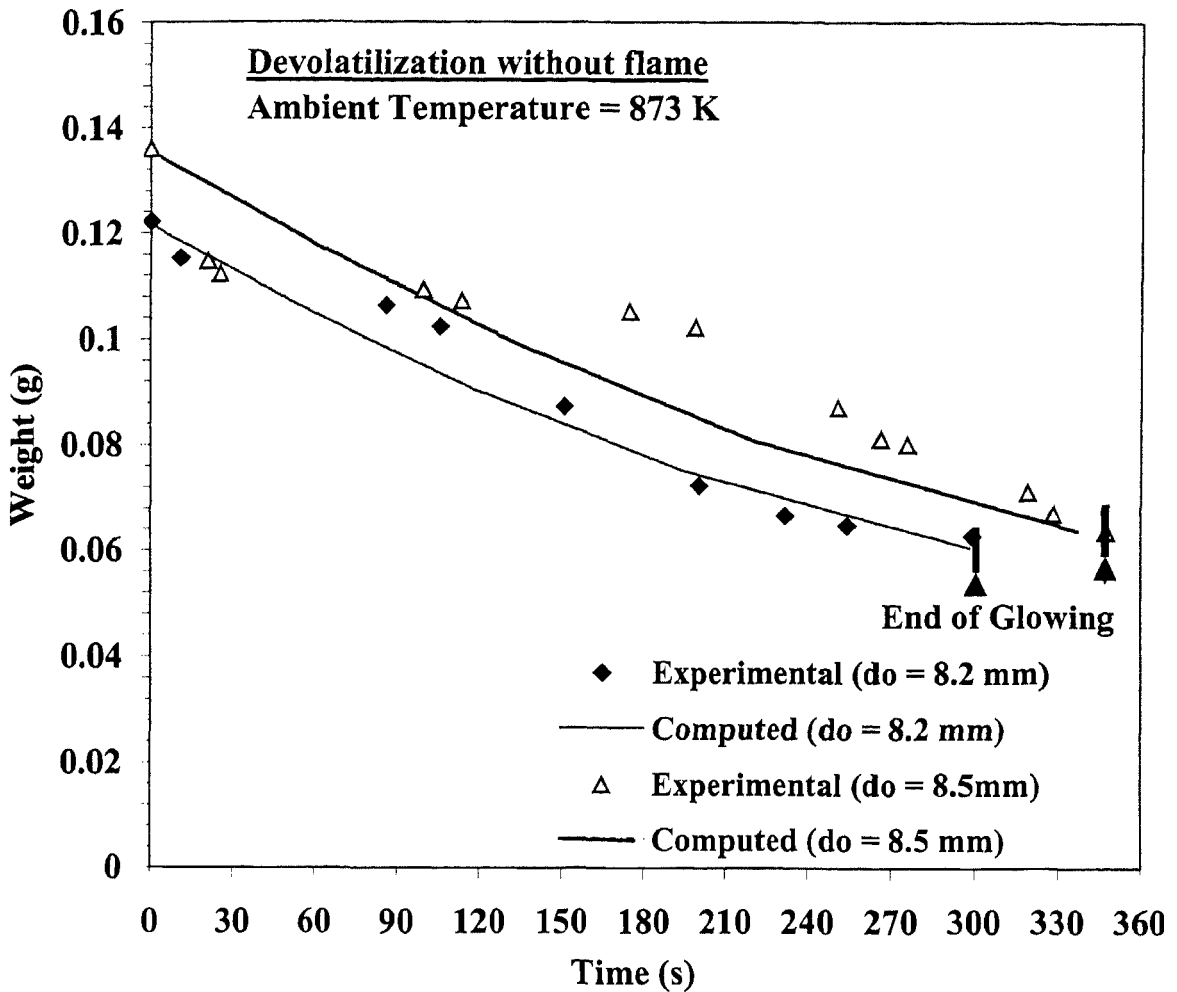


Figure 3.29: Experimental and computed weight–time profile of 8.2 and 8.5 mm diameter char combusted at ambient 873 K.

3.9.7 Flaming and char glowing time as a function of ambient temperature

Figure 3.30 shows the burn time (both flaming and glowing) of a 6.5 mm diameter sphere as a function of temperature. The computed flaming and glowing times are also shown in the figure. As seen in Fig. 3.20 and discussed earlier, there is a small increase in the mass loss during flaming as T_a increases, however, the burn time remains almost same. This compensation is due to slight increase in the burn rate owing to increase in the heat flux with T_a , and as a result, the flaming time remains nearly independent of ambient temperature up to 1150 K. Beyond this temperature, the percentage weight loss increases steeply with ambient temperature (Fig. 3.20) causing increase in flaming time. At higher ambient temperature increase in volatile yield more than the proximate yield was found in the case of coal combustion (Kobayashi et al, 1976).

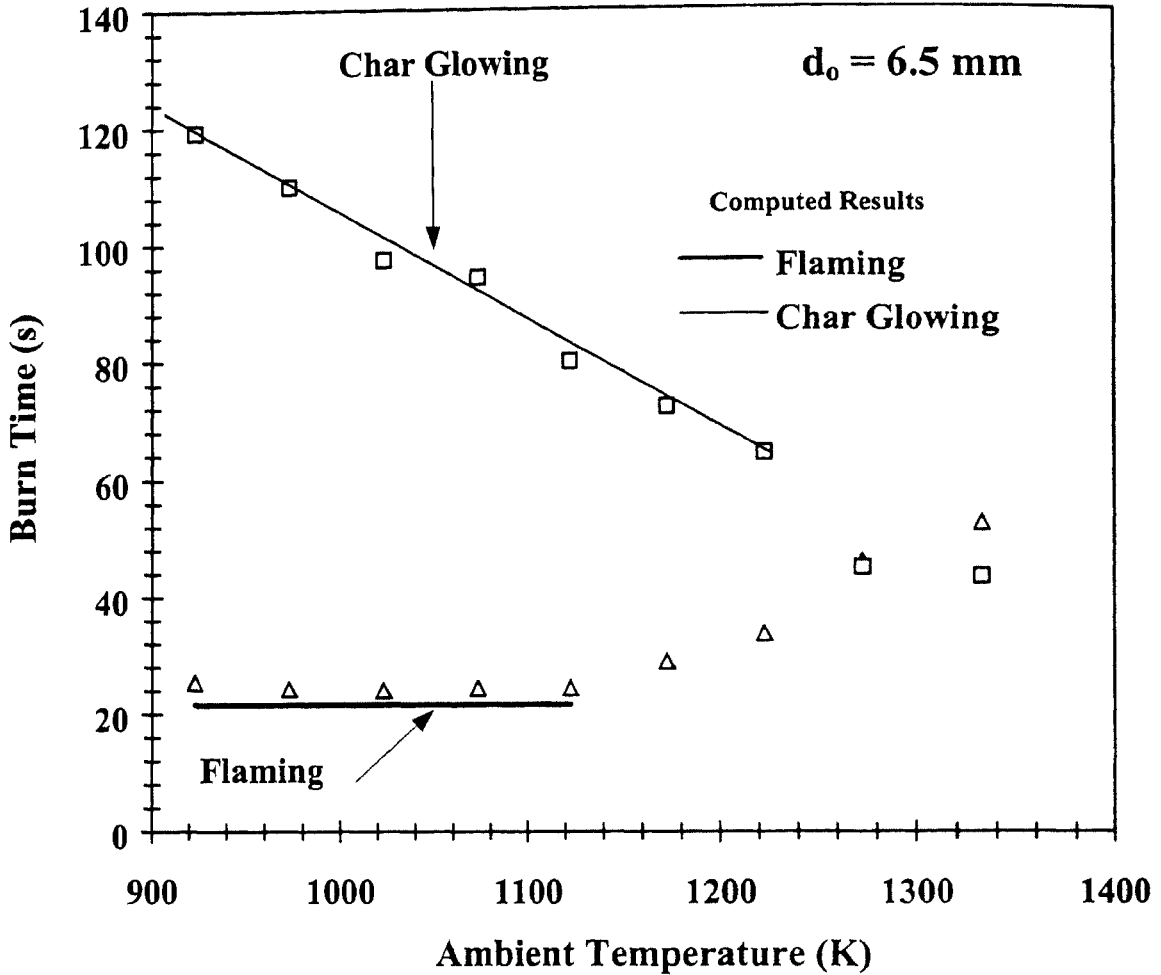


Figure 3.30: Flaming and char glowing time as a function of ambient temperature for dried effluent sphere of diameter 6.5 mm

Char glowing time decreases with ambient temperature because of the increase in reaction rate and to a certain extent due to increase in the transport properties. Even though the oxygen-carbon reaction is essentially diffusion controlled and consequently insensitive to changes in the rate constants, the increase in the rate of the reduction reaction between CO and carbon causes decrease in the overall char glowing time with increasing ambient temperature. It is observed from the computational result that as the temperature increases CO₂ fraction decreases and CO fraction increases at the center of the sphere, indicating increasing C—CO reaction rate.

Above 1250 K there is step decrease in glowing time. This is attributable to decrease in combustible char due to higher volatile yield. This was investigated by determining weight loss incurred by char combusted at 973 K ambient temperature that was lower by 300 K at

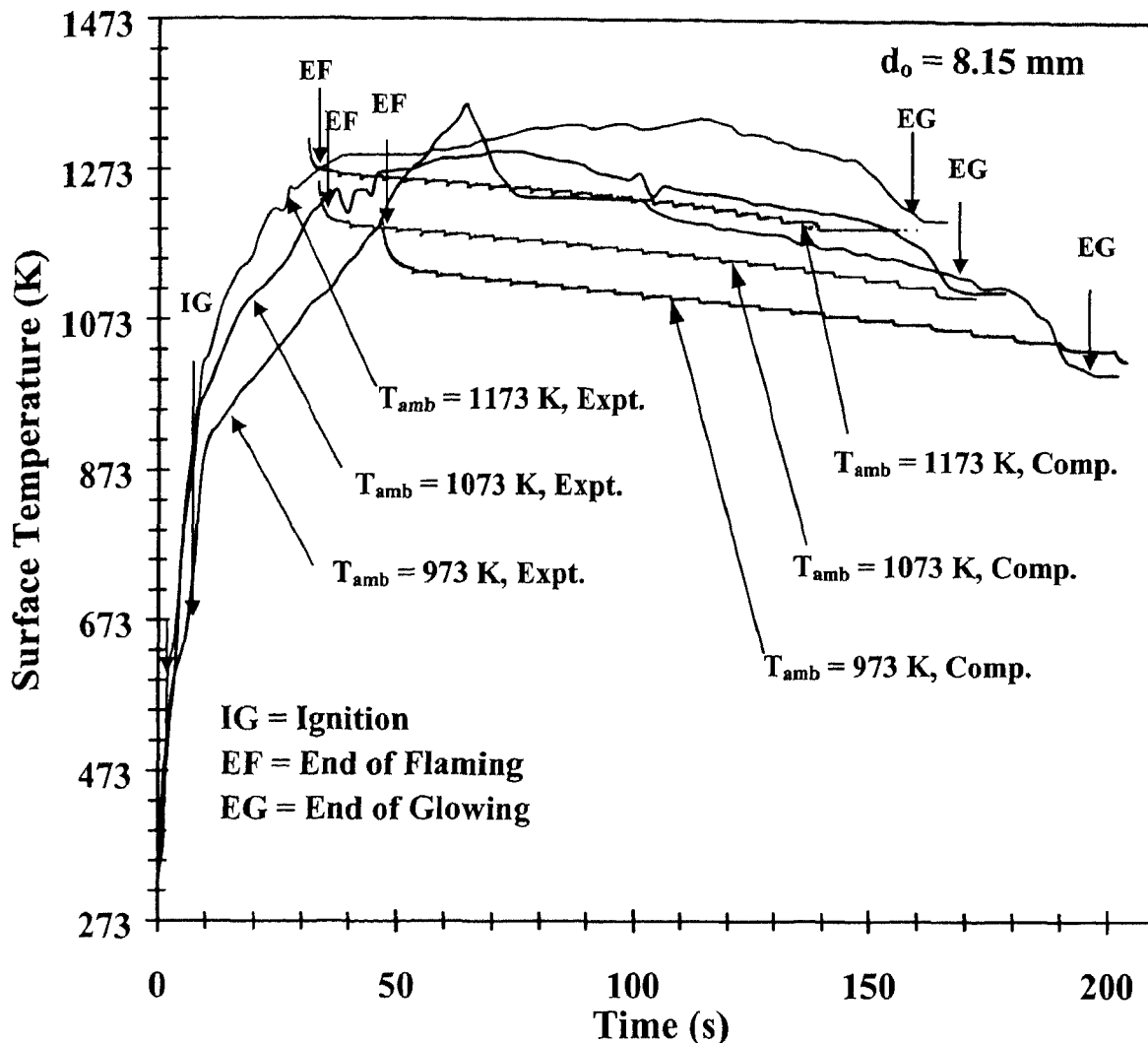


Figure 3.31: Surface temperature–time history of combusting dry effluent sphere of 8.15 mm diameter at 973, 1073 and 1173 K ambient temperature. Computed results of char glowing are also shown.

which char was obtained by quenching spheres at the end of flaming period.

3.9.8 Core and surface temperature vs. time history

Measurement of surface temperature of large size spheres ($d_o = 5 - 10 \text{ mm}$) and core temperature of liquid effluent droplets ($= 0.55 \text{ to } 2.2 \text{ mm}$) during the period between their exposure to high ambient temperature (823 to 1248 K) in quiescent air and their complete combustion were made and are presented on temperature–time history plots. These plots are extremely useful in keeping track of evaporation, devolatilization, flaming, glowing and end of combustion precisely along with their exothermicity, with respect to the time.

3.9.8.1 Dry spheres: experimental and computed results

The result of the thermal probing is presented in Fig. 3.31, which contains the surface temperature variation with time during combustion of effluent sphere of 8.15 mm diameter and 715 kg/m^3 at 973, 1073 and 1173 K. The ignition is marked by the onset of visible flame around the sphere. The surface temperature at the point of ignition decreased with increase in T_a and the heating rate remains the same. After primary homogeneous ignition, a steep rise in surface temperature is observed due to circumambient flame. This is followed by slow rise until the peak temperature is achieved. This peak is observed during char glowing and is 650 K, 500 K and 440 K higher than $T_a = 973, 1073$ and 1173 K respectively since the reaction front is shifted to the surface where ambient oxygen reacts with char. This is followed by gradual fall in surface temperature until the end of char glowing.

Predictions for the temperature profile during char combustion obtained from the model calculations are also presented in the figure. The difference in the two results is about 100 K in all the three cases. This is suspected to be due to oxidation of product gases mainly carbon monoxide, on the surface or close to the surface depending on the sphere diameter. This conclusion is based on the physical observation in which a faint bluish flame could be seen very close to the surface in the case of sphere with diameter larger than 5mm. It is likely that the inorganic compounds in ash catalyze the exothermic reactions in the gas phase. Roberts and Smith (1973) made similar observations in the case of large size carbon sphere in which the primary product CO burnt close to the surface.

3.9.8.2 Droplet Combustion

65 % solids

Droplets combusting at 873 K

Figure 3.32 depicts typical temperature histories of effluent droplets of different size at the 873 K ambient temperature. The mixture of devolatilized gases does not ignite into flame and after almost complete devolatilization char begins to glow. Prior to ignition the droplet swells to 1.45–1.5 times initial diameter. During initial heating stage, effluent droplet does not have flat step in the profile at 373 K as found in many cases of bituminous coal–water slurry (CWS) droplet, which is primarily due to water evaporation (*Yao and Lin., 1983*). Instead, there is a slight change in slope only at 450 K for diameter 1.9 mm and at 400 K, for diameters > 2.2 mm beyond which heating rate has increased. This is due to high rate of

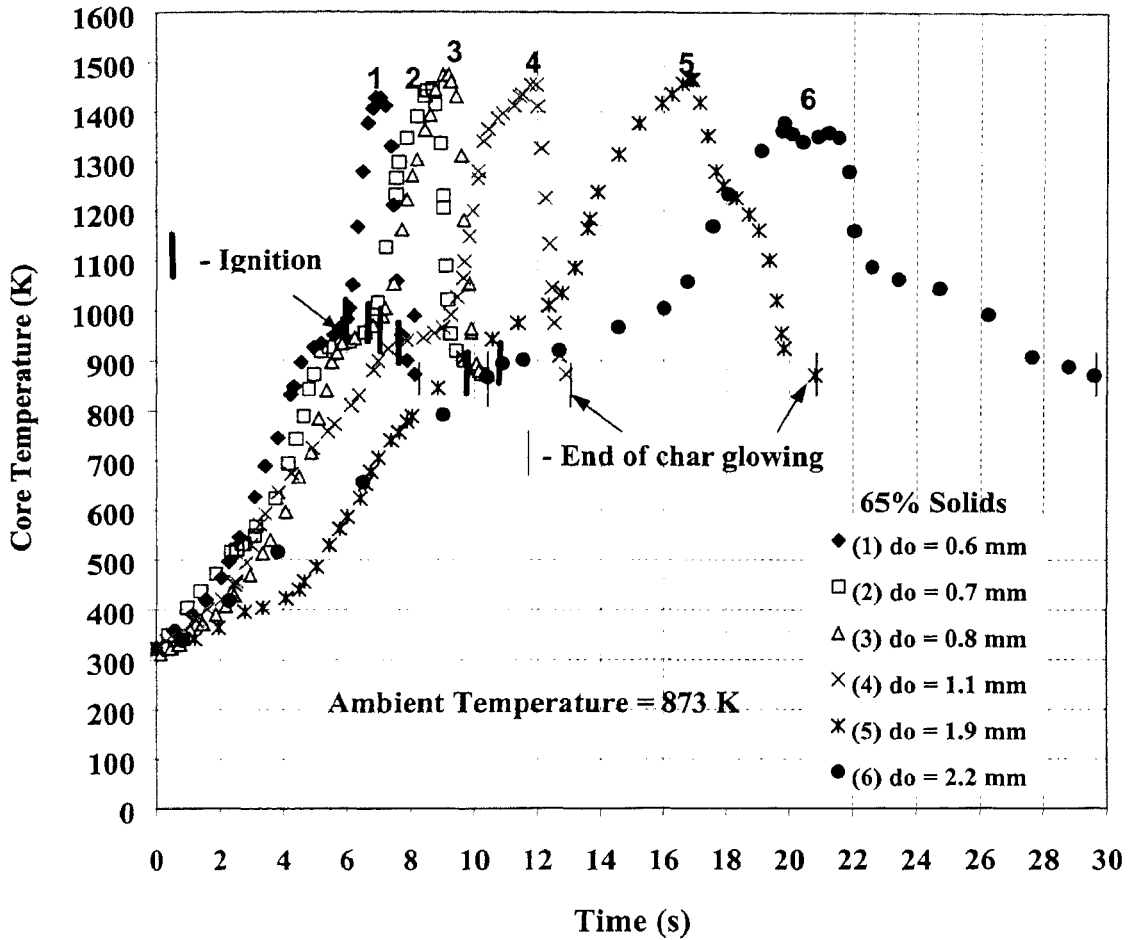


Figure 3.32: Core temperature profile of droplets of effluent with 65 % solids of different diameter combusted at 873 K ambient temperature.

water evaporation in the early phase, which is endothermic and therefore, has low heating rate. Beyond this point, the surface becomes dry and the thermal front progresses towards the center simultaneously with evaporation and devolatilization front. Volatiles get released continuously all along but do not get ignited into flame in all the cases. This is due to the concentration of ignitable volatiles generated being lower than the ignitable limits. Core temperature at the time of ignition decreases with increase in diameter. Ignition delay (at 873 K, heterogeneous ignition) increases with increase in diameter.

Prior to ignition, as was physically observed in the case of quenched droplets, the total weight loss ($\sim 60\text{--}70\%$) corresponded to the sum of weight of water and volatiles plus inorganics as was in the case of dry spheres. Therefore, it is concluded that the heterogeneous ignition of effluent char (containing small undetermined amount of volatile) and not of dried effluent occurs, as oxygen is available to the char surface. After ignition,

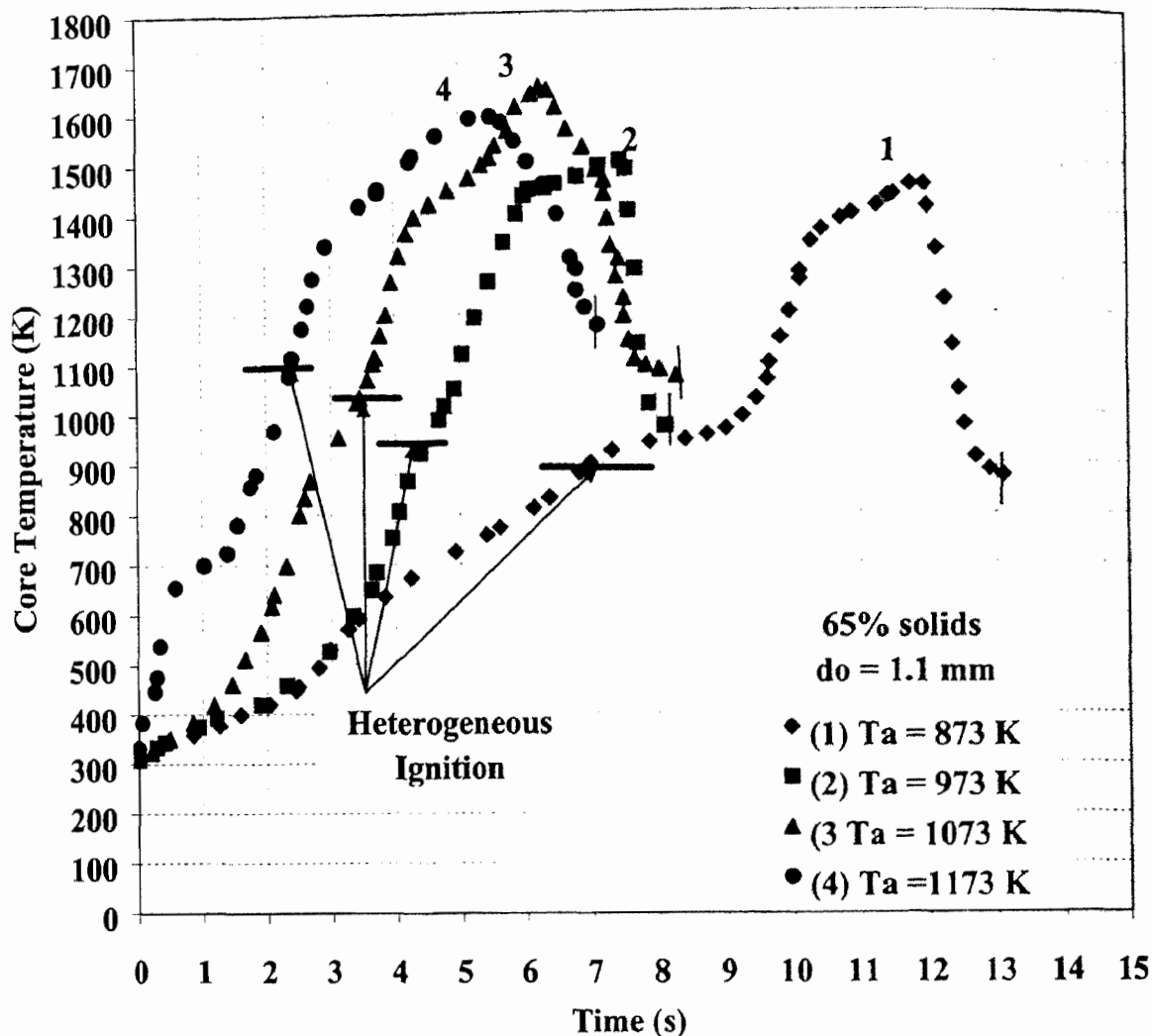


Figure 3.33: Core temperature history of 1.1 mm initial diameter of effluent with 65 % solids combusted at various ambient temperatures in quiescent air.

there is a sudden rise in temperature and peak in temperature is attained as the reaction front approaches the core where thermocouple junction is located. Prior to ignition, due to heating of the outer droplet, surface is seen to be red hot; however, with ignition the light intensity steeply increases and therefore, there was no ambiguity in determining ignition point. This is clearly visible in Fig. 3.13b (p. 63). Once the peak temperature is reached, the temperature drops immediately indicating the end of char glowing. However, there is some delay in reaching ambient temperature and this is attributed to the exothermic oxidation of inorganic ash (mainly sulfide oxidation). Peak core temperature attained remains same up to 1.9 mm diameter and then decreases with further increase in diameter.

Effect of T_a on the burn time ($d_o = 1.1$ mm)

Effect of ambient temperature on burn time of effluent droplet of 1.1 mm initial diameter is shown in Fig. 3.33 on a temperature–time plot. The ignition delay (the time duration up to the ignition marker in time) decreases with increase in T_a as also shown earlier in Fig. 3.14.

The ignition is heterogeneous and volatile flame is not seen in all depicted cases (see Table 3.2, p. 48). With ignition at $T_a = 873$ K, the glowing proceeds at slow rate with relatively weak oxidation (inferred from physical observation and the plateau in the temperature–time profile of curve 1). Glowing intensity is high (indicating strong exothermic reaction) with droplet ignition at $T_a = 973, 1073$ and 1173 K. The core temperature gradually increases and then reaches peak temperature. The heating rate also has effect on pyrolysis and char formation of as was found in the case of coal combustion (*Annamali et al., 1993; Kobayashi, 1976*). The fall in the core temperature is more gradual at higher temperature. This is expected, due to exothermic oxidation of inorganics in ash, particularly sulfide to sulfate as is found in the case of black liquor droplet combustion (*Frederick et al., 1994*).

77 % Solids

The combustion features of 77 % solids were investigated by direct observation and by obtaining temperature–time history of suspended droplets.

Droplet combustion at 823 K

Figure 3.34 shows core temperature–time history of effluent droplet subjected to quiescent hot air at 823 K ambient temperature. It is seen that after initial high heating rate up to 525 K (460 K/s for $d_o = 0.65$ mm, 375 K/s for $d_o = 1.14$ mm), the heating rate decreases (115 K/s for $d_o = 0.65$ mm, 65 K/s for $d_o = 1.14$ mm) indicated by decrease in slope in the temperature profile till ignition occurs. The sudden change in slope is due to out-gassing of pyrolysis products and superheated steam. The point of ignition was not very clear due to negligible difference between glowing intensities of droplet surface and furnace wall. If the ignition point is taken approximately as the point when the measured temperature attains the value equal to T_a , the delay can be noted to be increasing, with an increase in initial diameter.

The ignition of droplet occurs with weak heterogeneous combustion. This occurs as the rate of devolatilization reduces and ambient oxygen reacts heterogeneously with the surface, giving rise to temperature higher than ambient. This reaction continues for very long time

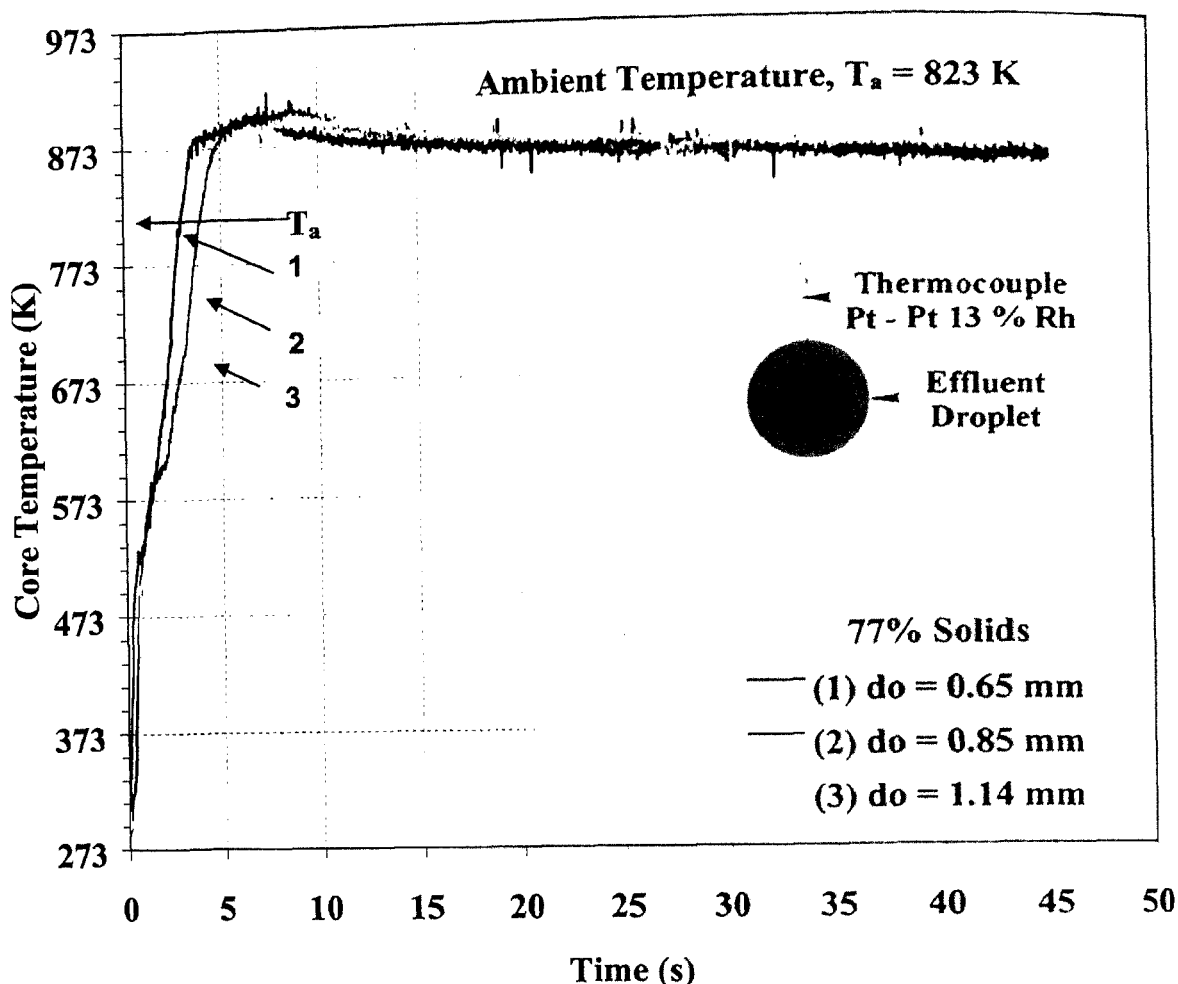


Figure 3.34: Temperature-time history of combusting effluent (77 % solids) droplet of initial diameter $d_o = 0.65, 0.85$ and 1.14 mm at 823 K ambient temperature.

(200–300 s) until the core temperature is reduced to almost that of ambient. The conversion was found to be incomplete as was indicated by the presence of carbon in the residue. The surface of the spherical residue remained stiff and within it were hollow spaces. It takes about 120 minutes for complete carbon conversion because of extremely low reaction rates at this ambient temperature. The maximum peak temperature attained was 900 K soon after ignition and gradually decreased subsequently.

Droplet combustion at $T_a = 863$ K

The Fig. 3.35 shows the core temperature of combusting effluent droplet with initial diameters varying from $0.6 - 1.62$ mm at $T_a = 863$ K (40 K higher than the previous case). Droplets ignited heterogeneously with weak exothermic reaction (or glowing), followed by strong glowing. Peak temperature of about 1300 K was attained during strong glowing.

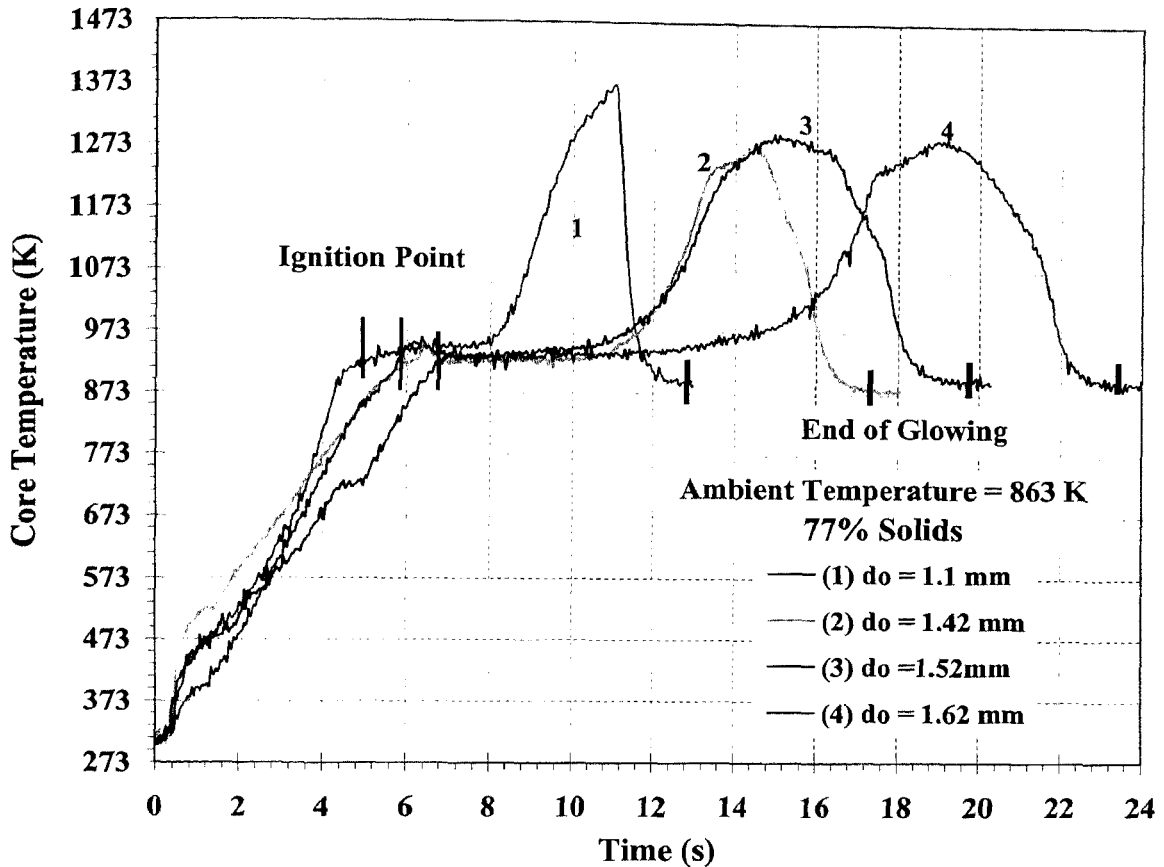


Figure 3.35: Core temperature–time history of effluent droplet with 77 % solids combusting at 863 K ambient temperature.

During primary glowing the profile for all diameter droplets have a plateau and its duration increases with diameter. It is important to note that the value of temperature during plateau is above ambient temperature indicating it to be exothermic. The plateau is primarily due to surface reaction along with devolatilization. The devolatilization will have twofold contributing effects on heat and mass transfer resulting in weak exothermic reaction 1) reduced oxygen concentration in the bulk gas close to the droplet surface and 2) heat loss due to convection. As the devolatilization is reduced or stopped, the above effects are correspondingly reduced or stopped and surface oxygen concentration approaches the free-stream resulting in increased reaction rate and thus the temperature. Exothermic devolatilization, as was earlier recorded in DTA (see Fig 3.11) and DSC performed in inert environment could also be a contributing factor. The gradual rise in the core temperature towards the end of plateau is a subtle indication of gradual decrease in devolatilization rate and increase in oxygen concentration in the bulk gas. The rise in core temperature becomes more gradual for droplet with $do > 1.1$ mm. With the end of glowing, the fall in temperature

is abrupt for small diameter droplet and is gradual for larger diameter. The ambient temperature is not reached immediately with the end of glowing due to strongly exothermic oxidation of alkali sulfide as discussed earlier in section 3.9.3. Conversion was found complete in all the cases as no carbon was detected in the residual ash adhering around thermocouple junction. It was physically observed that the junction was little off-center but was well within the porous surface of ash.

Droplet combustion at $T_a = 963$ K

Figure 3.36 depicts temperature–time history of effluent droplet combustion in which the primary ignition was found to be homogeneous. The initial heating rate is about 1300 K/s and when core temperature is in the range of 873 and 930 K the profile shows a dip. The initial heat-up profile does not have variations in slope unlike those seen in the previous cases (Figs. 3.34 and Fig. 3.35). This is an indication of little or no out-gassing except for surface water evaporation and heating of the surface. Though devolatilization rate may not be low due to observed high heating rate, out-gassing of volatiles may not occur immediately as the gases may get contained in the droplet. This will cause swelling up to a critical diameter, beyond which sudden out-gassing takes place as was also noted earlier in the case of 65 % solid effluent (see Fig. 3.13c frame 1 and 2, droplet deflects due to out-gassing). The dip in the temperature profile as shown in Fig 3.36 is a clear indication of abrupt out-gassing, occurring through the pores and resulting heat loss. The dip was observed in the case of droplets of all sizes. The magnified view of the portion of temperature profile depicting dip is also shown in the same figure. The out-gassing is severe and therefore, the domain close to the surface will be devoid of oxygen, leading to the stoppage of the heterogeneous reaction. Beyond the dip in the profile, the temperature rises but at a very small rate compared to the initial heating period due to continued devolatilization. This continues till the homogeneous ignition of volatiles occurs at core temperature lower than T_a and the temperature abruptly rises. This is a common feature in the case of droplets of different sizes. The flaming time normalized with the density of dried and swelled droplet is plotted against diameter as shown in the Fig. 3.26 (p. 85) along with similar data of 100 % effluent spheres.

It was physically observed that the flame diameter was approximately 1.5–2 times the diameter of droplet. The flame standoff distance was not clear as was in the case of dry spheres. The probed temperature was close to adiabatic flame temperature, which was too

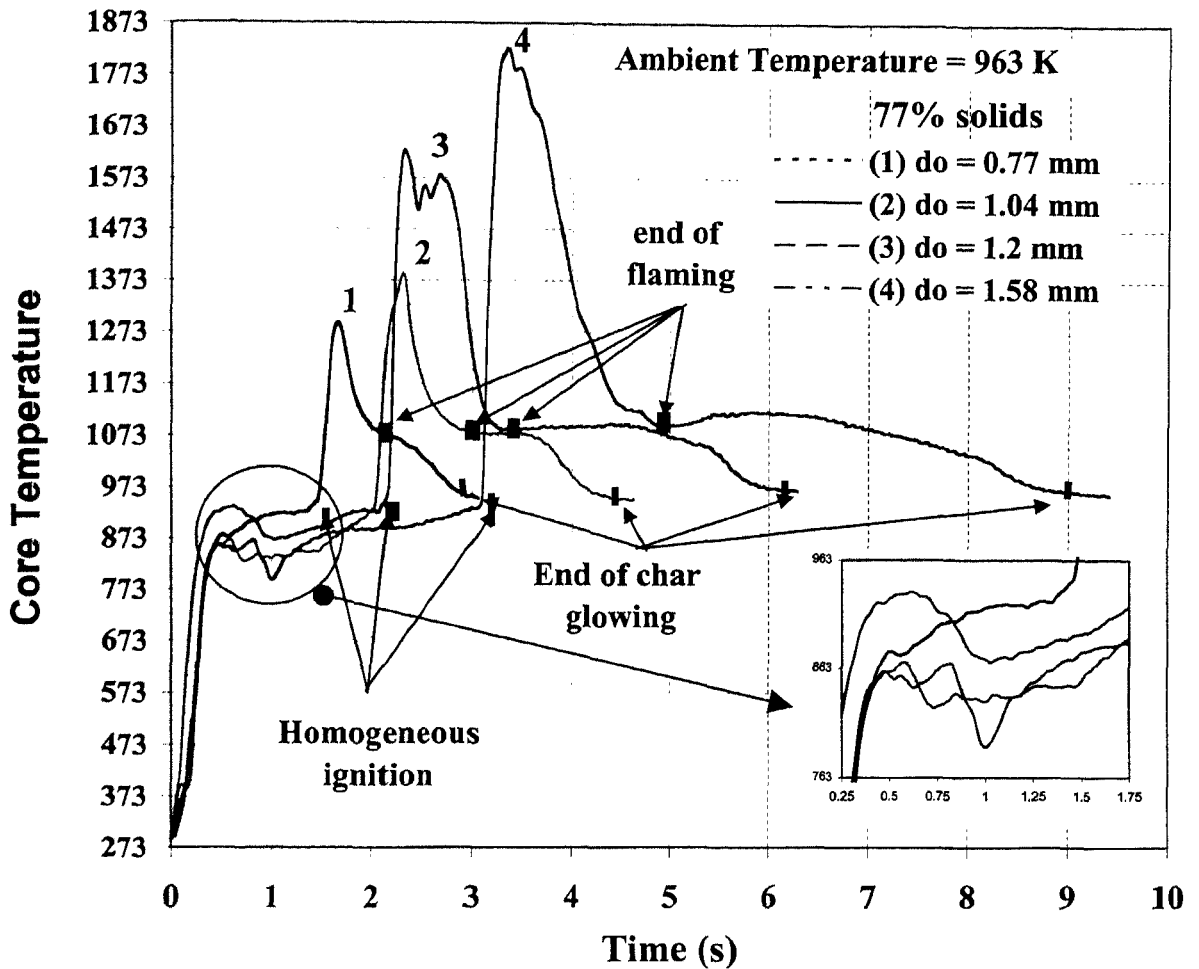


Figure 3.36: Temperature–time profiles of 77% effluent droplets of different size combusting at 963 K ambient temperature.

high if thermocouple junction were located close to the droplet center. This needs investigation for the cause of junction sensing high temperature which otherwise should have been much lower during devolatilization phase. It may be because of 1) heat conduction from the gas phase to the junction through thermocouple wire 2) of internal reaction 3) or due to the shift in the location of the junction from droplet center to close to porous outer surface. Experimentally it was determined that the temperature rise due to heat conduction in thermocouple wire was negligibly small. It was also physically observed, as in the previous cases, the thermocouple junction was located well beneath the porous ash surface. The possibility of internal reaction is also ruled out as there was an enveloping diffusion flame that would consume oxygen. Therefore, the most probable reason is the migration of the junction, close to the porous surface and its exposure to the flame through pores. This may occur during out-gassing of volatile vapors.

There is a sharp drop in temperature with the end of flaming; however due to the preceding char glowing phase, the temperature remains either steady at about 125–150 K above ambient for short duration or increases gradually first to about 170 K above ambient and then again gradually decreases till the end of glowing. Due to exothermic alkali sulfide oxidation, the temperature takes some time to attain ambient temperature. The relationship between char glowing time t_c , initial diameter d_o is $t_c \sim d_o^m$ where $m = 2$. The data is plotted in Fig. 3.26 along with similar data of char glowing of sphere.

Droplet combustion at $T_a = 1063$ K

Figure 3.37 depicts temperature–time history profile of droplet heating phase, pre-ignition violent devolatilization, causing dips in the profile, flaming and char glowing. The profile has features similar to the case of droplet combusting at $T_a = 963$ K. The primary ignition is homogeneous, occurring after violent devolatilization that caused dips in the profile. Flaming is followed by char glowing, which ends after complete conversion. At the time of ignition, the internal temperature is 1035 K for 0.78 mm droplet and 995 K for 1.56 mm droplet. Initial heating rate is same as in the cases of 963 K ambient temperature, but the pre-ignition devolatilization time is small in the present case. Flaming time is larger compared to the previous case for the droplet of the same diameter (eg for $d_o = 1.2$ mm, $t_f = 0.958$ s and 1.385 s for droplet flaming at 963 and 1063 K respectively) due to higher volatile yield. This observation is consistent with those made in the case of large sphere ($d_o = 6.5$ mm) combustion where flaming time and weight loss increase with temperature (see Figs. 3.30 and 3.20) somewhat similar results have been reported for coal volatile yield by Kobayashi et al (1976). The peak temperature measured during flaming is in the range of 1573 to 1840 K very close to the adiabatic flame temperature, though the expected temperature is much lower than the measured one if the junction was to be located in the core of the combusting sphere.

This discrepancy, as discussed earlier, is due to the migration of the junction close to the porous surface and getting exposure to the flame. Flaming is followed by char glowing as in the previous case; however, the peak temperature during glowing in the case of initial diameter droplet 0.78 and 1.56 mm is 1178 K which is about 90–100 K higher than in the case of glowing at 973 K. Both flaming and char glowing time normalized with initial density follow d^2 -law in this case as well.

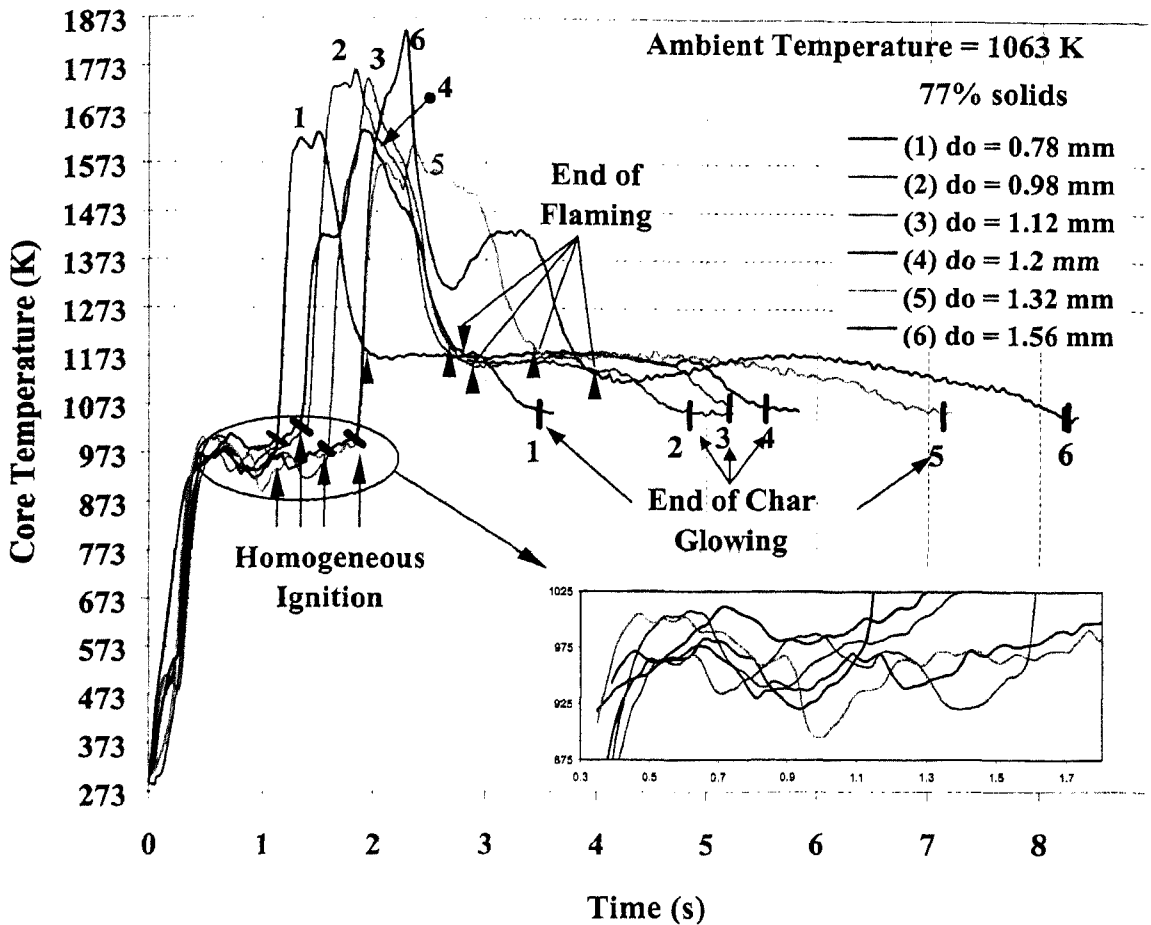


Figure 3.37: Temperature–time history of effluent droplet of different sizes combusting at 1063 K ambient temperature. Magnified view of pre–ignition temperature profile depicting dips in it is also shown.

Droplet combustion at $T_a = 1123$ K

The temperature–time profile of combusting effluent droplet at ambient temperature 1123 K has features similar to those in the case of droplet combusting at 973 K. The primary ignition is homogeneous, occurring after violent devolatilization that causes dips in the profile. Flaming is followed by char glowing and finally ends after complete conversion. At the time of ignition, the internal temperature is 1090 K for 0.86 mm droplet and 1050 K for 1.82 mm droplet. Initial heating rate is same in both the cases but the pre–ignition devolatilization time is short in the present case. Flaming time is longer as compared to that determined in previous cases for same diameter droplet, due to higher volatile yield. The peak temperature measured during flaming is in the range of 1500 to 1820 K close to the adiabatic flame temperature and justification for the discrepancy from expected core temperature is also the same as in previous cases.

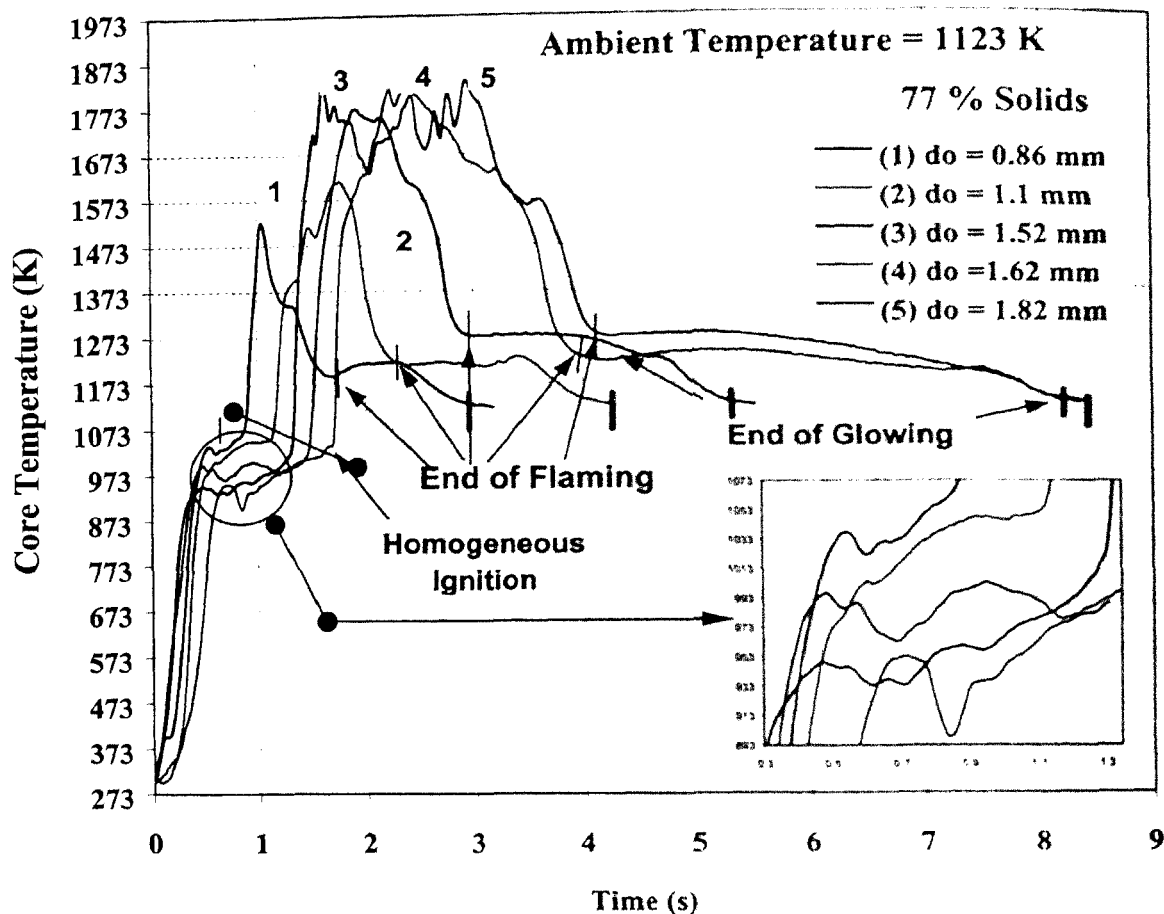


Figure 3.38: Temperature–time history of effluent droplet of different sizes combusting at 1123 K ambient temperature. Magnified view of pre–ignition temperature profile depicting a dip is also shown.

Flaming is followed by char glowing as in the previous cases, however, the peak temperature during glowing in the case of initial diameter droplet 0.86 and 1.82 mm is 1234 K and 1274 K respectively which is 150 K and 80 K higher than that in the case of glowing at 963 and 1063 K respectively. Both flaming and char glowing time normalized with initial density flows d^2 -law in this case as well.

Droplet combustion at $T_a = 1248$ K

Figure 3.39 depicts temperature-time history of effluent droplet combusting at 1248 K. The initial heating rate is 2050 K/s and pre–ignition dip in the temperature profile due to violent devolatilization, though for short period, is similar to those for droplet heated at 973 and 1143 K. Ignition is homogeneous and the temperature at the time of ignition is 1200 and 1100 K for droplet of size 0.98 and 1.35 mm respectively. The peak temperature recorded during flaming is in the range of 1725 and 1845 K. The flaming time is higher as compared

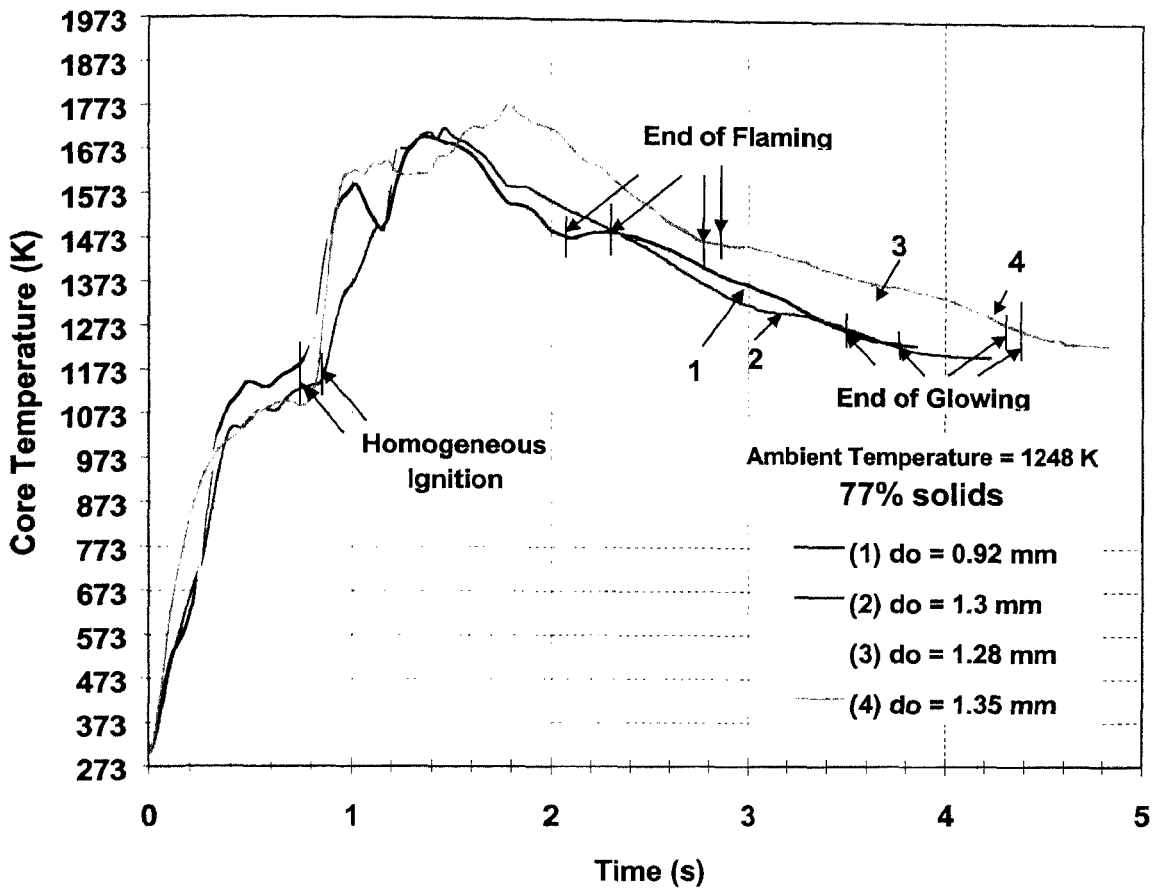


Figure 3.39: Temperature–time history of effluent droplets of different sizes combusting at 1248 K.

to that recorded in the previous cases of flaming attributable to higher volatile yield. Char glowing begins with the end of flaming and continues till the end of conversion. The peak temperature during glowing is recorded immediately after ignition.

Droplet combustion with and without flame

There exists a critical droplet diameter for homogeneous ignition to take place. Droplet of diameter smaller than a critical value will ignite heterogeneously. Experimental investigation of burn time of the droplet of the same diameter, ignited either homogeneously (case 1) or heterogeneously (case 2) at same ambient temperature (963 K) was carried out and temperature–time history of both the cases are shown in the Fig. 3.40. Profile 1 is of the droplet ignited homogeneously and profile 2 is of the one that ignited heterogeneously. The maximum temperature recorded is in case 1 and is during flaming. This temperature is 200 K higher than that recorded during strong exothermic oxidation, which is 1090 K. The initial heating rate is same in both the cases and therefore the devolatilization rate will also

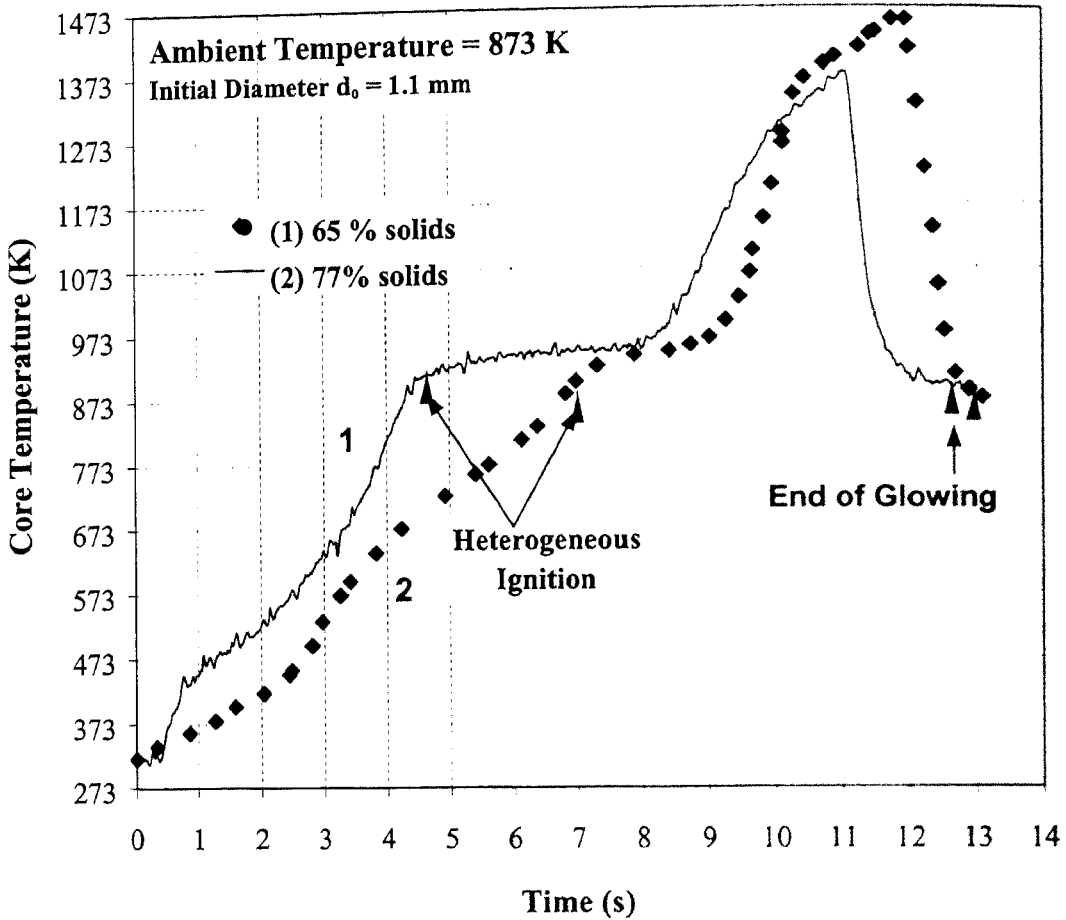


Figure 3.40: Effect of solid concentration on temperature–time profile of 1.1 mm diameter effluent combusting at 873 K.

be the same; however, volatiles in one case ignite and in other case do not. The obvious difference observed due to this behavior is in the total burn time of the droplet. In the latter case the burn time is 1.7 times higher than for the former case with flaming combustion. Ignition in later case is heterogeneous and glowing is weak due to continued devolatilization. As devolatilization stops, strong char glowing occurs resulting into complete conversion. In the former case the droplet experiences high temperature due to circumambient flame and as a result the char formed will be different. The maximum temperature recorded during glowing in both the cases is 1090 K. It was found in the case of dry sphere of critical diameter combusting with flame and without flame that the weight loss measured at the beginning of glowing in both the cases was same. Therefore, in either case, the same weight of char is converted but at different rates and this is attributed to the difference in char formed under different conditions of ambient temperature.

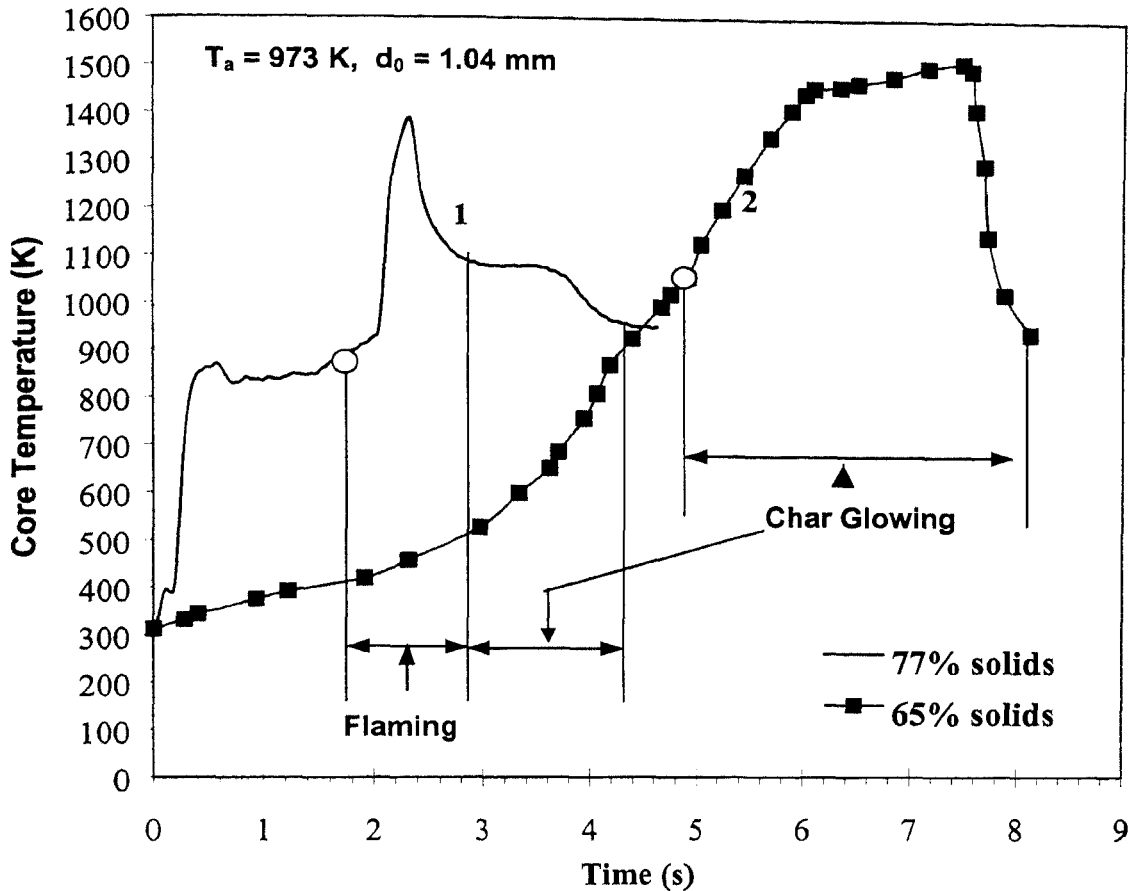


Figure 3.41: Comparison core temperature vs. time profiles of droplet of effluent with 77 % and 65 % solids

Effect of solid concentration on combustion

$T_a = 963 \text{ K}$

Figure 3.41 shows the temperature profiles of the same diameter droplet at two solid concentrations. It is clear from the figure that though the ignition delay is 2.3 s earlier in the case of 77 % solids droplet, the overall burn time in both the cases is about the same.

Although, the content of combustible material is 16 % higher in the first case, the burn rate is higher at $T_a = 873 \text{ K}$.

$T_a = 973 \text{ K}$

Figure 3.42 depicts the core temperature vs. time profile of the combustion of effluent droplet with 77 % and 65 % solids as curve 1 and 2 respectively. The effect of solid concentration on the temperature profile is prominent at $T_a = 973 \text{ K}$. The ignition in the case of 77 % solids effluent is homogeneous and in the case of 65 % solids effluent is

heterogeneous. Ignition delay in the first case is small after initial high rate heating and brief devolatilization phase. In the later case, ignition is much delayed and pre-ignition heating rate is low. The overall burn time in the first case is almost half compared to the case of 65 % solids. The char glowing period is also almost half. Short ignition delay and enveloping flame in the case of 77 % solids droplets are the causes of short burn time and hence the difference in the temperature profiles which was not seen in the earlier experiments of droplet combusted at $T_a = 873$ K. It is therefore concluded that the homogeneous ignition of effluent droplets is necessary in order to achieve overall faster burnout and higher solids concentration is favorable.

3.10 Conclusions

Basic experimental data on the principal features of effluent combustion in quiescent air are presented. Suspended droplet technique is used in the present study so that continuous observation of droplet burnout starting with ignition can be recorded for effluent with 65 %, 77 % and 100 % solids. Experiments were performed on a) dry spheres (100 % solids) with diameter ranging between 2 mm to 20 mm b) liquid droplets containing 65 % and 77 % solids (mass concentration) with diameter ranging between 0.5 mm to 3.5 mm and effect of droplet size on combustion features are obtained. Surface and core temperature and continuous mass loss history of combusting effluent particle at various ambient temperatures are presented.

- Effluent droplets burn with two distinct regimes of combustion, flaming and char glowing.
- The ignition delay of the droplets increases with size as in the case of non-volatile droplets, while that of bone dry spheres are independent of size.
- The ignition delay decreases with increase in solids concentration.
- About 25 to 40 % of ignition delay time is taken up only to heat up the liquid to the boiling point of water therefore heating effluent close to its boiling point utilizing waste heat is essential for achieving a compact practical combustion system.
- The ignition delay has Arrhenius dependence on temperature.
- The initial ignition of the droplets and dry spheres occurred either as homogeneous or heterogeneous (flame less), depending on the ambient temperature in the case of sphere and on solid concentration and ambient temperature, in the case of liquid droplets. The first type of initial ignition leads to faster char combustion as compared to the case of

flame less ignition and therefore in the case of practical spray combustion, higher solids concentration is preferred.

The weight loss found during flaming combustion was 50 – 80 % while during char glowing it was 10 – 20 % depending on the ambient temperature.

The flaming time ' t_f ' is given by $t_f \sim d_o^2$, as in the case of liquid fuel droplets and wood spheres.

The char glowing time ' t_c ' is given by $t_c \sim d_o^2$ as in the case of wood char, even though the inert content of effluent char is as large as 50 % compared to 2 – 3 % in wood char and the BET surface area is 3 – 5 m²/g against 250 – 300 m²/g in the case of wood.

The heterogeneous char combustion in quiescent air in furnace condition has been modeled, and the results of this model compare well with the experimental results.

Homogeneous ignition of effluent droplets is necessary in order to achieve overall faster burnout and higher solids concentration is favourable

The measured surface and core temperature measured during char glowing is typically 200 to 400 K higher than the furnace temperature.

Combustion Experiments in a Vertical Cylindrical Reactor

4.1. Introduction

This chapter is concerned with the spray combustion of effluent. This effort is based on the consideration that droplet combustion, an aspect addressed in great detail in the earlier chapter – Chapter 3 – will provide a compact solution to the problem of the organic material conversion. For a premium fuel (with heating value in excess of 40 MJ/kg) stable flame with good atomization can be easily achieved. However, if the fuel is the distillery effluent, which is similar to coal water slurry or emulsions of water and heavy oil, achieving stable flame is challenging due to the presence of water and inorganics. The amount of heat consumed in water evaporation can be a substantial fraction of the total heat required to ignite the droplets. For distillery effluent, the heating value is about one-third that of coal water slurry with same solid concentration, therefore, it is more challenging to establish a stable flame compared to even coal water slurry assuming good atomization. In addition effluent contains dissolved materials in water and therefore the evaporation rate is smaller than for pure water or water slurry containing insoluble coal particles which results in longer ignition delay.

Hot ambient ($T_a > 773$ K) is essentially required for ignition as was also found in the case of 100 % solids sphere that remained unignited at $T_a \sim 773$ K. The present chapter is therefore, concerned with experimentally investigating autoignition and subsequent combustion processes of fine spray of distillery effluent, when injected in a hot oxidizing environment. The series of processes expected to occur after injection as spray of fine droplets in the high temperature environment are those observed in single particle combustion study (heating, swelling, devolatilization, char glowing). However, as in the case of hydrocarbon fuel, the rate of burning of droplets of slurry fuel in the spray will be much different from those of isolated droplets. Further, the difference between a traditional

liquid fuel spray and distillery effluent spray injected into a high temperature ambient is that in the first case, evaporation occurs at low temperature and has large enthalpy of vaporization and in the second case evaporation of water occurs first at low temperature and then pyrolysis occurs at higher temperatures.

Effluent is a heterogeneous mixture of combustible organic and inert inorganic compounds (Ref. Table 1.1 for composition) consisting of about 40 to 45 % dissolved solids and 50 to 60 % suspended solids in finely dispersed state in water. It is non-Newtonian liquid at room temperature for solids greater than 50 %. Unlike most coal water slurry, distillery effluent is scale forming and swelling liquid. Therefore the methodology used for obtaining fine atomization of effluent and injecting in the high temperature environment is expected to be complex.

4.2. Objective of the experiments

The ignition of devolatilized products in the flame is a prerequisite for providing sustained high temperature environment for heating, drying and pyrolysis of the fine effluent droplets in the spray. This is primarily required in order to achieve self-sustained gasification where heat required for endothermic reaction steps is made available from the zone where strong exothermic oxidative processes occur. The three processes, therefore, should preferably occur at the shortest distance from the point of injection. The primary objective of the experiments is to verify conditions under which this can be achieved. Fine atomization of effluent is imperative in order to achieve large surface area to augment heat transfer to the droplets.

Fine spray combustion of black liquor, which has resemblance to distillery effluent, is not used in the traditional recovery boilers. Instead, coarse spray with average droplet size of 2 - 4 mm is injected and most droplets are expected to burn on the bed of the furnace (Macek, 1999, Adams and Frederick, 1988). Therefore, spray combustion of black liquor droplets has not been investigated earlier essentially due to the lack of motivation.

The recirculation of hot product gases and the combusting particles either due to spray aerodynamics or due to the geometry of the reactor itself, could be employed such that hot oxidative environment is available for ignition for steady state spray combustion. This needs investigation because the droplets being non-volatile and high in density, even after achieving the best atomization, may escape from the recirculation zone unburnt due to their high momentum.

Need for auxiliary heat input for sustained spray combustion is required to be experimentally verified, although the heating value at 50 % solids (~ 7 MJ/kg) appears sufficient to maintain reactor temperature and the inevitable heat loss.

Self-sustained flame combustion is necessary to conduct studies on the effect of solid concentration and stoichiometry on flame appearance, blow-off, flame size, temperature profile, and gaseous species concentration and therefore are not considered in the present experiments.

The objective of the experiments can be restated as:

- (i) To investigate pre-ignition, ignition and combustion process of the effluent spray injected into a high temperature oxidative environment in a pilot scale vertical cylindrical reactor with and without the support of auxiliary fuel burner and thus determine the ambient condition at which complete combustion is accomplished.
- (ii) To investigate effluent spray combustion when injected into a confined turbulent kerosene flame.

Effluent with 50 % and 60 % solids are used in the experiment conducted. Concentrating effluent to these levels in commonly used evaporators is found relatively economical in the small-scale distilleries. More importantly, fine atomization of effluent at these solid concentrations is relatively simple (viscosity is 10 – 20 mPa.s at 343 K) which at 75 % solids is much higher (8 Pa s at 343 K)

Plan of the chapter

Section 4.3 describes the design basis of the experimental set up. Section 4.4 describes the experimental set up. The details of the setup are relegated to Appendix A4. The instrumentation employed in the experiments and related details are presented in the section 4.4.1. The method of operating the gasification facility is briefly discussed in section 4.5 and the detail procedure is presented in Appendix A4.2. Section 4.6 outlines the seventeen experiments conducted with several configurations and flow parameters in essentially three categories 1) Effluent injection from the wall with no auxiliary heat input, 2) injection with auxiliary heat input and 3) injection within kerosene enveloping flame. The results and discussion of all these experiments with of 50 and 60 % solids are presented in the sub-sections of section 4.6. Self-sustained flaming combustion of effluent spray is not obtained at both the concentrations in any of the experiments conducted. Analysis showed that ignition delay of the droplets in the spray core is large due to continuously reducing

temperature, attributed to inadequacy in the heat flux to take care of the large evaporation load and this established the need of providing higher heat flux and residence time. To substantiate this conjecture, another experiment is conducted in which sustained combustion with complete carbon conversion of the pool of effluent resulted from the accumulated spray droplets at the downstream of the atomizer, is accomplished. These findings led to a new approach of combusting effluent, which is presented in the next chapter.

4.3. The design of experimental set-up

The experimental setup is fixed by considering the direction of flow of input and reacted material (effluent, ash and product gases). The combustion residue (ash) is expected to be collected largely under gravity and therefore the collection point is chosen to be at the lower most part in the reactor. The exhaust gases could be vented from the top most part of the reactor. The simplest reactor configuration would be a vertical one with cylindrical geometry having exhaust of the product gases from the top most point in the reactor and solid residue collected and removed from the bottom most part of the reactor.

The auxiliary heat input required for initial heating of the reactor and during effluent injection is fixed tangentially to the bottom of the reactor walls so as to have higher gas residence time. The dimensions (diameter and length) of the reactor could be fixed based on the approximate quantitative data (obtained from effluent atomization experiments in cold quiescent air) such as the length of spray, range of initial droplet diameter in the spray, mass distribution etc. The length of spray is based on not only the relative kinetic energy of the atomized droplets in the spray (which gradually dissipates) but also depends on the degree of aerodynamic resistance offered by the surrounding gas in the reactor. In the present case, the important criterion is the availability of large heat flux; this would enable the spray fine droplets to heat, dry and devolatilize fast in order to effectively reduce ignition delay, which is large at low solid concentrations. Too large a reactor diameter would require longer heating period and the large thermal inertia would have detrimental effect on the control over the phenomenon. On the other hand, too small a diameter and power level will have higher heat loss and it is difficult to accommodate the spray if radially injected. The first approximation of reactor diameter is obtained based on the residence time involving in ignition delay (t_i) and flaming time (t_f) (calculated from non-dimensional burn time ' τ ', p. 86, Chapter 3) for experimentally obtained average droplets size of range of 200–215 μm , at ambient temperature of 1100 K with the approximated gas velocity of 10 m/s. The diameter value works out to be 390 mm and finally chosen value is 400 mm. The height of the reactor could be fixed on the basis of the trajectory of the glowing ($t_i + t_f < t_c$) droplets in

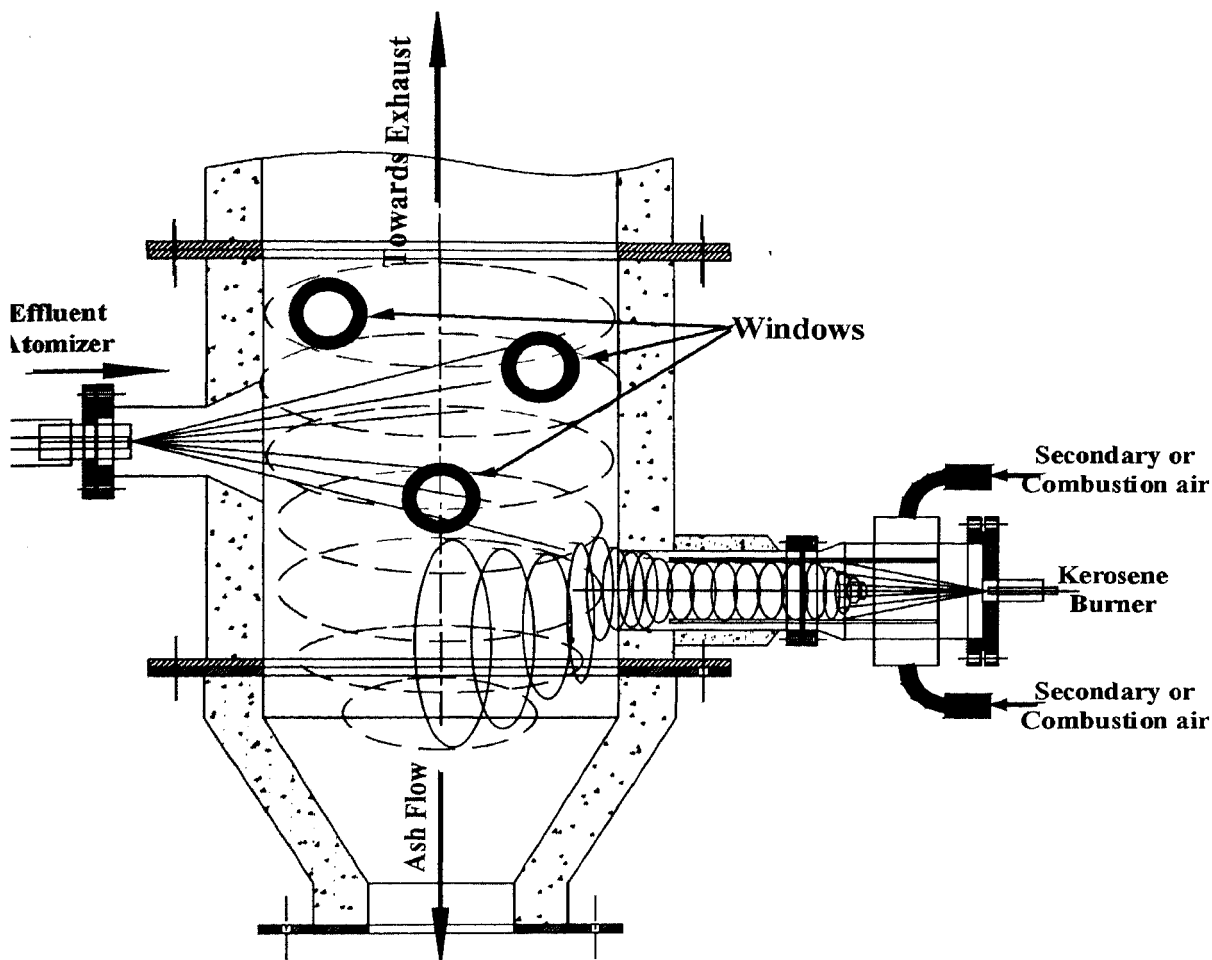


Figure 4.1: Conceptual view of the reactor and location of effluent injector and burner.

the spray. Droplet trajectory depends on the droplet size which itself depends on the atomizer performance and internal reactor aerodynamics. If atomization is good and if the hot oxidizing gases have tangential velocity larger than for the combusting droplets preferably in the char glowing phase or towards the end of it) the droplets would go to wall and depending on their remaining mass, may either get entrained in the gas and leave through the exhaust port (which is not favorable) or may fall back into the lower part of the reactor. If the droplets continue to burn in the entrained mode then larger length (from point of injection) would be needed. This issue could be examined based on the observations from the first set of experiments and hence the length of the reactor was fixed as 1500 mm (from the first injection point).

Effluent spray injector should be located in the zone of highest temperature to minimize the ignition delay. This location should therefore be in the vicinity of auxiliary burner where the

reactor walls are the hottest. Figure 4.1 depicts the conceptual view of the reactor including the location of burner, effluent atomizer and direction of the flow of the gases and residue (ash).

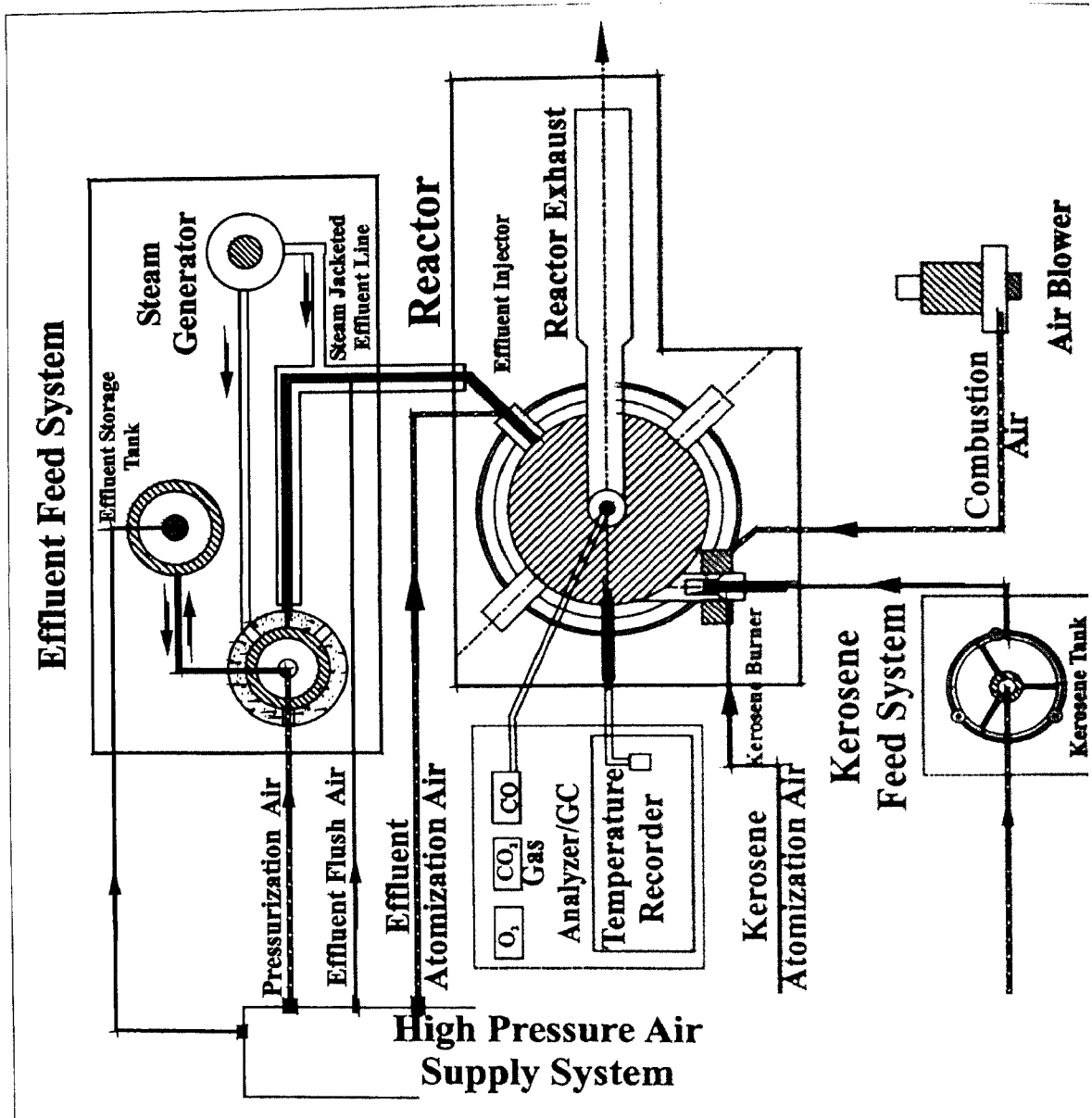


Figure 4.2: Schematic view of the experimental set-up

4.4. The Experimental Setup

The schematic of experiment setup is shown in the Fig. 4.2. The setup consists of a vertical cylindrical reactor, effluent feed system, kerosene or (auxiliary) fuel feed, and high-pressure air feed system, air blower and instrumentation. The unit components of the systems are modular, a typical requirement necessary to accommodate changes, due to expected

variation in the experimental plan. All the experiments performed in the vertical reactor were with reactor walls preheated to temperature in the range of 973 to 1373 K. The heating was carried out using kerosene as auxiliary fuel in swirl stabilized kerosene burner, which was fixed in the lower part of the reactor such that the hot gases and flame entered the reactor tangentially. The burner received kerosene from the *kerosene feed system*. It consisted of a feed tank with level meter, filters, local fine pressure regulators for pressurizing air and flow meter. It supplied kerosene to the burner at known flow rate (0.5 to 5.5 g/s) to obtain required power level (20 – 250 kW).

Effluent atomizer is part of the reactor and its location could be varied along the vertical axis of the reactor, always kept down stream of the kerosene burner. Hot effluent is fed into the atomizer at known flow rate from the effluent feed system. Effluent was preheated and maintained at a temperature close to its boiling point by providing steam jacketed feed tank and feed line until the point of injection. The *high-pressure air feed system* supplied regulated pressurization air required by both the feed systems and atomization air required for atomizing effluent as well as kerosene. The same air feed system supplies air for flushing and cleaning effluent feed lines and aerodynamically scraping the combustion residues, mostly ash, from the reactor walls. The *air blower* supplied low-pressure and high volume flow rate combustion air to the reactor. Combustion gases were exhausted from the top end of the reactor. The gaseous products were ejected into an annular tube of exhaust system and under ejection effect entrained atmospheric air and the resultant mixture was flared with support of LPG flame. K-Type thermocouples were used to measure gas as well as inside wall temperatures at selected locations on the reactor. The exhaust gas composition was analyzed for CO, CO₂ and O₂ to monitor the combustion process. The air and fuel mass flow rates leaving the feed system were measured prior to their entry into the reactor. The combustion residue accumulated in the lower part of the reactor and was removed by opening a specially designed valve fixed to the bottom most flange. The details of the reactor, reactor heating system, kerosene effluent and air feed systems are described in the Appendix A4.

4.4.1. Instrumentation

4.4.1.1. Pressure Measurement

Reactor pressure was measured by a manometer fixed to the static pressure taps made on the reactor walls. Effluent and kerosene flow rate was calibrated with respect to pressurization

air pressure in the feed tank. Bourdon tube gauges in the range of 0 – 2 and 0 – 5 bar were used for the purpose. Atomization air pressures were measured using gauges fitted at the downstream of the pressure regulator.

4.4.1.2. Flow Measurement

a. Air flow rate

The effluent and kerosene atomization airflow rates were in the range of 0 – 5 g/s and 0 – 2 g/s respectively and were measured using venturi meters. The effluent injector was air-cooled and the cooling air was introduced in the reactor. The airflow rate (of 5 – 20 g/s) was measured using an orifice plate meter. The total air flow rate (combustion + cooling air) in fully developed flow was determined using total-static pitot tube and correlated to the center line velocity at a fixed point (40 times diameter) in the flow pipe. The airflow rate was later obtained from the correlation by using the central line velocity.

b. Kerosene and effluent flow rate

The kerosene and effluent flow rates were calibrated with respect to the applied feed pressure. In the calibration procedure, the fluid (kerosene or effluent) was allowed to flow through the atomizer nozzle under known feed pressure. The fluid was collected in a container and the collection duration was timed. This was repeated at various feed pressures and flow rate was obtained by taking the ratio of weight of fluid mass and collection duration in seconds. The data of the flow rate vs. feed pressure were plotted and precise co-relationship between these data was used to determine flow rates. In the case of kerosene, a capillary flow meter with inverted kerosene filled manometer was later introduced in the feed line (shown in Fig 4.6) in order to accurately determine flow rate in the range of 0.1 – 3 g/s.

Level gauges were fitted on the feed tanks of effluent and kerosene. The flow rate could be obtained by determining the drop in the fluid level in the tube corresponding to the weight consumed in known time. The mass flow rate could thus be obtained intermittently. In the case of effluent, since it is an opaque fluid, the internal surface of transparent level gauge tube was made non-wetting by coating it with thin oil film.

4.4.1.3. Temperature Measurement

Effluent and combustion air temperature were measured using bimetallic-stem dial thermometers in the range of 0 – 160 C.

Chromel–Alumel (type K) thermocouples were used to measure reactor wall and gas temperatures up to 1500 K. Though 16 thermocouples were provided, the signals from eight selected locations were connected for digital read outs in the present experiment. The thermocouple wires were embedded in ceramic bead over which there was a protective stainless steel sheath. Except for the part of the junction, the bare protruding wire was molded in a thin sodium silicate paste that was first dried and baked at 873 K. This protected the thermocouple from the reducing gases. Figure 4.3 depicts the thermocouple wire and protective sheath.

In the case of gas temperature measurement, the tip of thermocouple junction was exposed to the gas and for measuring wall temperature; the junction was embedded 5 mm within the wall of the reactor.

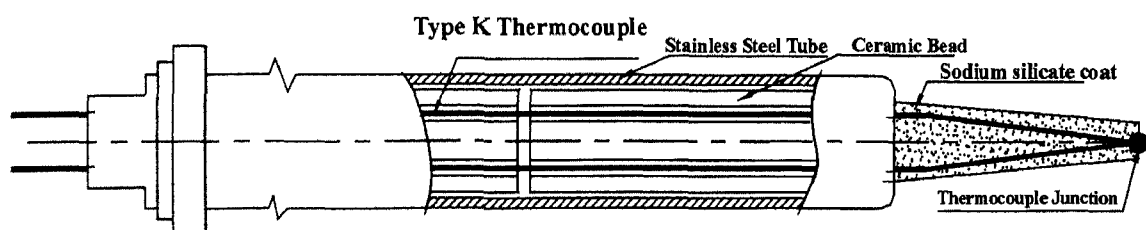


Figure 4.3: Type K thermocouple

4.4.1.4. Gas Composition Measurement

Volume percent of oxygen, carbon dioxide and carbon monoxide were measured continuously (on line) on the dry basis. The sample gas was drawn from the exhaust gas tube, downstream of the reactor. Prior to gas analysis, it was scrubbed with water and subsequently dried by passing it through series of cylindrical containers, the first containing calcium chloride granules and second containing phosphorus pentoxide. The oxygen analyzer used was chemical cell based and CO and CO₂ were measured by Riken Infrared Gas Analyzers, model RI – 550A.

4.5. Experimental Procedure

The experimental procedure is divided into two parts: 1) initial setup procedure includes preparation of feed systems, reactor, instrumentation and 2) startup procedure. Both parts of the experimental procedure are described in Appendix A4

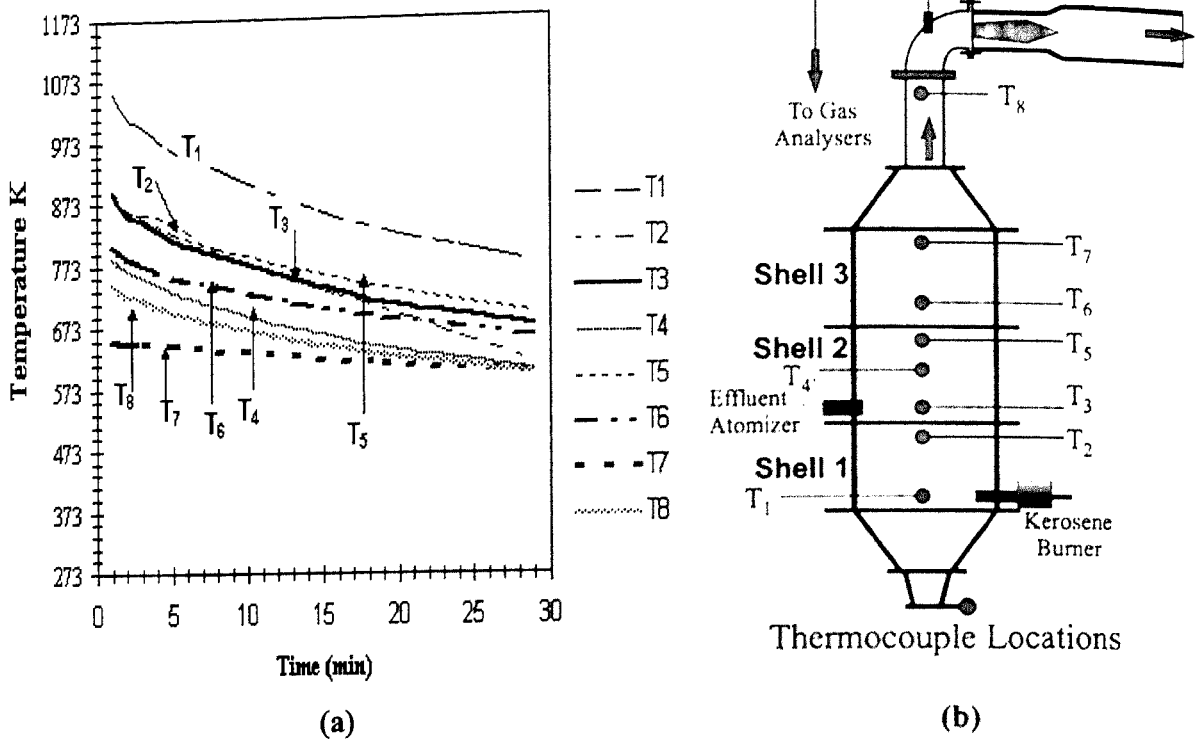


Figure 4.4: (a) Typical plot of temperature history vs. time obtained during reactor cooling, (b) Thermocouple location in the reactor

Reactor Shell No	1	2	3	Exhaust duct
Temperature (K)	T_w	T_w	T_w	T_g
	1123 – 1223	1023 – 1073	1023 – 1050	1050 – 1100

Table 4.1: Shell temperature at the end of heat up phase.

The startup procedure of the experiment is divided into two phases: **phase I** is ‘reactor heat up phase’ and **phase II** is effluent injection phase. These phases are timed and are in a sequence.

They are carried out only after initial setup procedure is completed. Effluent is injected only after different section of the reactor attains minimum temperature as depicted in table 4.1. Typical kerosene flow rate during the heat up phase of all the experiments is 2.0 - 2.1 g/s and airflow rate is stoichiometric. The gas composition obtained is: $O_2 = 0.5 \%$, $CO = 13.5 \%$, $CO < 0.1 \%$ (dry basis).

4.6. Observations, Results and Discussions

Three sets of experiments were conducted with similar heat up phase (phase I) and variations in the effluent injection phase (phase II). The duration of phase I is 50 – 55 minutes while the duration of phase II varied between 30 – 45 minutes. Reactor wall temperatures at the end of phase I, are given in Table 4.1. The different injection methodologies, which distinguished the three sets of experiments, were designed based on the results of the preceding experiments, in the light of attaining sustained spray combustion. Table 4.2 shows the results of the 16 experiments conducted.

Separate experiments were also conducted to determine temperature time profile (cooling) without injecting effluent (see Fig 4.4). These profiles were subsequently compared with those obtained with the effluent injection into the hot reactor.

The observations and results of each set of experiments are discussed in the following sections:

4.6.1. Experiment set I (V_I – 1 to V_I – 4): With zero auxiliary heat input

Effluent spray is injected from a port located on the wall of the shell no.1, diametrically opposite to the location of the burner as shown in Fig. 4.1. Stoichiometric air is injected from the burner fixed to the tangential port to the reactor and effluent (2.5 g/s) atomizer and kerosene (1 g/s) atomizers.

With spray injection, flaming is seen at the reactor center but *it did not sustain for more than 2 minutes*. During this short flaming period, individual particles glowed brighter than the wall, such that their trajectories in the swirling flow are seen. Except for experiment No. V_I-4, the reactor wall temperatures dropped by 200 K at rate of 25 – 30 K/minute, a rate much faster than previously obtained profile during cooling (See Fig. 4.4). Oxygen concentration increased from near zero value during heat up phase to 8 – 10 %, which also indicated the failure of achieving sustained combustion. Figure 4.5 is constructed from the observations. The flaming depicted in the figure disappeared while individual particle at spray periphery glowed until effluent supply is cut-off. The droplet in the core penetrated the swirling hot air and struck the wall, gradually forming a patch from which, later, effluent dripped. Spray injection is continued until the reactor wall temperature dropped to 823 K (shell #1).

Experiment Number		Solids %	Effluent Injection (phase II)		Flow Rates \dot{m}_s g/s			Sustained Combustion or gasification		Complete Combustion	Remarks
			Effluent Flow rate (g/s) \dot{m}_e	Injection Methodology	Phase II			Combustion	Gasification		
					Kerosene	Total Air	Eq. Ratio				
Set I Auxiliary Fuel Burner 'OFF'	V_I-1	50	12.0	#1 wall ¹	0.0	24	1.0	No	—	No	Reactor temperature dropped
	V_I-2	50	8.5	#1 wall ¹	0.0	18	1.0	No	—	No	
	V_I-3	50	10.0	#1 wall ¹	0.0	21	1.0	No	—	No	
	V_I-4	50	3.0	#1 wall ¹	0.0	9	1.0	No	—	Yes	
Set II Auxiliary Fuel Burner 'ON'	V_II-1	50	8.5	#1 wall ¹	1.2	35	1.0	No	—	No	Reactor temperature dropped
	V_II-2	50	8.1	#1 wall ¹	1.2	34	1.0	No	—	No	
	V_II-3	50	8.0	#1 wall ¹	1.2	34	1.0	No	—	No	Reactor temperature drop arrested
	V_II-4	60	7.5	#1 wall ¹	1.2	32	1.0	No	—	No	
	V_II-5	60	4.4	#1 wall ¹	1.3	29	1.0	Yes	—	Yes	
Set III Injection in Kerosene flame	V_III-1	50	10.0	Burner ²	1.8	45	1.0	No	No	No	
	V_III-2	50	8.0	Burner ²	1.8	45	1.0	No	No	No	
	V_III-3	60	7.0	Burner ²	1.8	43	1.0	Yes	No	No	
	V_III-4	50	7.0	Burner ³	1.7	26	1.0	—	No	No	
	V_III-5	60	8.0	Burner ³	1.7	30	1.0	—	No	No	
	V_III-6	60	8.0	Burner ³	1.7	30	1.0	—	No	No	
	V_III-7	50	10.0	Burner ⁴	1.8	21	0.5	Yes	No	Yes	
	V_III-8	60	10.0	Burner ⁴	1.8	24	0.43	Yes	No	Yes	

Table 4.2: Details of experiments conducted.

No micro-explosion or disruptive burning of the droplets was observed, an observation consistent with that of single droplet combustion.

Improving atomization by increasing atomizing air flow rate was found to have no effect in sustaining combustion either by ignition of fine spray (as seen initially for short duration) or by ignition of spray droplets after getting entrained in the swirling air and traversing close to the hot wall. This is due to following reasons: 1) increase in the ignition delay for the droplets with same spray characteristics due to the fall in reactor wall temperature (below

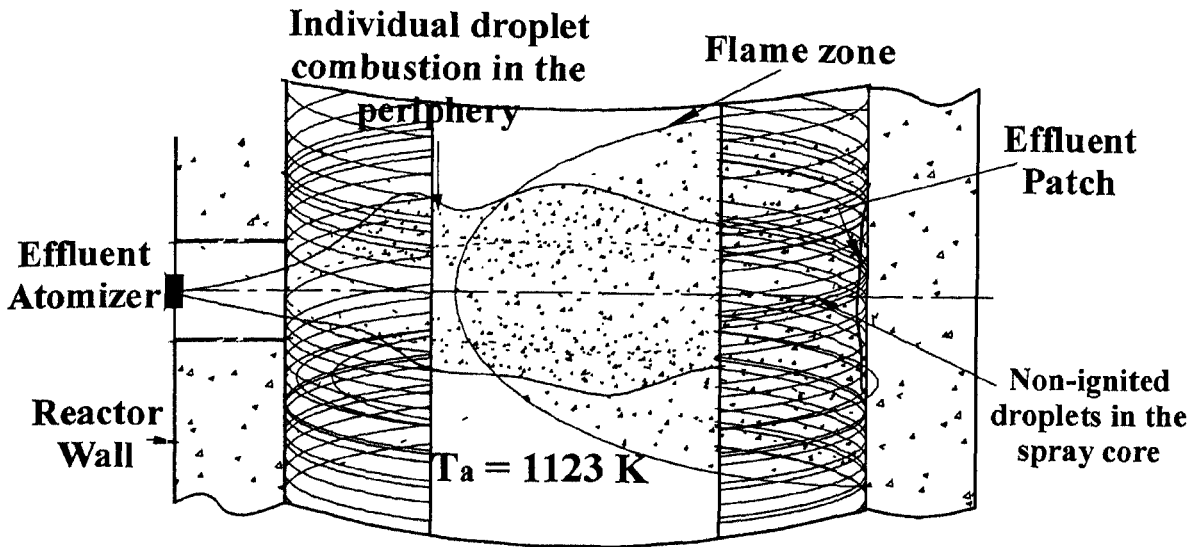


Figure 4.5: Spray of effluent and combustion processes as was observed from the view port.

973 K) caused by injection of cold combustion air and the evaporation load. 2) Spray penetrating the swirling air and striking the opposite wall at the same spot.

The spray injection at reduced \dot{m}_e of 3.0 g/s (expt. No. V I-4) lead to complete carbon conversion. However, the heat released by its combustion did not sustain temperature in the reactor.

The ash dump opened during the initial phase of injection, contained accumulated fine ash particles and after completion of experiment, partly devolatilized char lumps and thick mass of concentrated effluent were found.

Following inferences are drawn from the above experiments:

Sustained combustion of effluent cannot be obtained at 50 % solids even with good atomization. The heat release from the initial short duration flame or droplets combusting in the spray periphery is inadequate to maintain critical heat balance, needed to maintain reactor temperature and consequently it dropped causing increase in ignition delay. Effluent spray struck the wall and dripped without combusting. The amount of heat required for evaporation and heating the vapor to reactor temperature (1173 K) is about 30 % and 20 % of the heating value of the effluent feed for 50 and 60 % solids respectively. In the present experiments combustion air injected in the reactor is at room temperature therefore about 20 % and 30 % of the effluent heat content is required to heat the air to reactor temperature considering stoichiometric air injection to combust 50 % and 60 % solids effluent.

It is therefore concluded that auxiliary heat input of at least 50 % of the feed heating value is required to be provided to achieve sustained combustion. The following sets of experiments are planned with providing auxiliary heat input in order to achieve sustained combustion.

4.6.2. Experiment Set II (V_{II} – 1 to V_{II} – 5): With auxiliary heat input

Effluent was injected from the same location as in the previous experiment. The kerosene burner was kept operational at reduced power level (50 ~ 55 kW) from ~ 95 kW and effluent combustion air was introduced through the same burner. The kerosene burner gas exit temperature dropped due to change in local equivalence ratio and remained steady at around 1273 - 1353 K. The vitiated swirling hot air interacted with the spray as shown in the Fig. 4.5. The heating, drying and devolatilization processes are unaffected by vitiated air. The atomization air was increased from a usual value of 10 – 12 % to about 20 % of stoichiometric value in order to provide more air in the spray core to assist combustion.

The spray ignition was not clearly visible however; discontinued puffs of flame due to volatile oxidation were seen during initial period (about 5 minutes) and temperature remained same. Subsequently, the temperature gradually reduces by about 150 K in the upper shells and about 200 to 250 K in the shell # 1. It was physically investigated that a large number of the glowing droplets were seen on the spray periphery. Oxygen concentration that was found to be ranging between 3 – 4 % prior to injection, reduced to 0.3 – 1 % range, although the exhaust gases were sooty. As the temperature dropped, the spray penetrating the swirling gas flow could be seen clearly (earlier it was not visible) extending till the opposite wall. The penetration did not decrease even with increase in the atomization air (to reduce droplet size). The excess effluent dripped into the lower part of the reactor.

The dump contained fine ash, char particles (single and small lumps) with varied carbon content. Small amount of non-devolatilized effluent mass was also found.

The fall in the reactor temperature was arrested in a similar experiment by increasing the burner power level or decreasing effluent flow rate below 5 g/s (Expt.V_{II}-5). Carbon conversion is found complete and individual droplet combusting in gas-entrained mode is clearly visible through the view port. Effluent spray combustion was not obtained even by improving atomization, or by increasing solid concentration from 50 to 60 %.

It is inferred from this set of experiments that sustained effluent combustion is difficult to obtain even if the air is preheated and its effect is restricted to increase in single droplet combustion on the spray periphery as compared to the previous set of experiments. The ignition delay of the droplet in the spray core is not affected due to the evaporation load that causes decrease in the local temperature. To avert this, it is necessary to either increase the solid concentration in excess of 70 % or provide higher localized heat flux by injecting effluent into a turbulent flame or injecting in space with hot walls. Injecting effluent at higher solid is found to be a difficult alternate than injecting spray in turbulent flame and therefore the last option is considered and set III experiments were conducted.

4.6.3. Experiment Set III (from Expt. No. VIII-1 to VIII-7): Injection in turbulent flame

The combined burner is shown in described in section A4.1.2 The average gas temperature at the burner exit plane is measured in the range of 1273 – 1373 K and the average axial gas velocity is approximated in the range of 25 – 35 m/s. Effluent spray injected into flame envelope providing high convective heat transfer is expected to accelerate the pre-ignition processes, reducing ignition delay and ignition distance.

Three different sets of experiments were performed: 1) combined injection in the reactor 2) combined injection outside the reactor and 3) combined injection in inclined reactor. The results of these experiments are discussed in the following sections.

4.6.3.1. Combined injection in the reactor (from Expt. No. VIII-1 to VIII-3)

The burner was fixed tangential to the reactor as shown in Fig. 4.1. with the expecting of the effluent spray to tangentially brush the wall of the shell and ignite on or close to the wall.

With effluent injection, the luminous kerosene flame became dull and the flame temperatures drastically reduced at the rate of about 2 K/s from 1373 K before stabilizing at 1223 – 1273 K. The glowing droplets are seen emerging out of the flame along with a lot of un-ignited droplets that struck the wall, rebounded and then got entrained and burnt close to the wall in entrained mode. The helical trajectory of the glowing char droplets could be seen and large numbers of droplets were found entrained in the swirl flow. The droplets seemed large in the core since it penetrated the flame and its residence time in flame was relatively short. The atomization airflow rate was increased in order to obtain finer atomization. However a lot of unburnt particles were seen in the core of the spray striking the wall. The

temperature in shell #1 dropped to value lower than 943 K in 10 minutes and effluent adhered and then dripped. The smoke was sooty and oxygen concentration ranged between 4 - 5 %. At no point of time, was there a formation of the spray flame or the volatiles combusted in sustained manner.

The residue in the dump contained 15 – 20 % of total carbon fraction. The residue consisted of mostly ash and partly devolatilized material.

In order to further investigate the extent of droplet conversion taking place in the flame zone, separate experiments were conducted which are described below.

4.6.3.2. Combined injection outside the reactor

The burner unit was fixed on a metal stand and injection was carried out in room air outside the reactor. The primary aim was to observe more carefully the processes occurring with effluent injection as fine spray in the absence of complex aerodynamic interaction due to presence of reactor boundaries. A stainless steel sheet (1200 X 1200 mm) with surface coated with oil was kept under the spray. The length of flame was varied (150 --200 mm) by slightly varying swirl intensity without affecting stoichiometry.

Effluent was injected once the power level of the burner was stabilized. Gas temperature was measured in the perpendicular plane 150 mm downstream of the burner exit plane. With the beginning of effluent injection, the gas temperature invariably dropped from about 1350 K to 1150 K at the outer periphery and to 1000 – 1073 K on the centerline of the burner. The drop in temperature is primarily due to heat being removed by heating and evaporation processes, excessive dilution and increased competition for oxygen in the flame core. The processes occurring in the droplet would freeze once they left the flame envelope and those ignited, completed conversion. Therefore, the history of the droplets would be useful in drawing conclusions.

The first set of the experiments was with burner power level of 75 kW. With the injection of effluent (8 g/s effluent flow, 2 g/s atomization air), the flame length increased and its colour changed from bright yellow to a mixture of orange and crimson with reduced luminosity. The droplets in the spray core penetrated the flame and traveled straight at a horizontal length of about 800 mm. The droplet diameter of major fraction of liquid was estimated to be in the range of 200 - 500 μm (obtained by projecting scale gradation) along with a number of much finer droplets. The droplets on the periphery completed combustion and the glowing could be seen in the dark. Fine ash particles and partly dried and devolatilized

droplets were found on thin oil film sticking on the sheet (approximate diameter $< 200 \mu\text{m}$, which is about the same as initial diameter). The spray ignition did not take place in this experiment except for the glowing individual char particles. The product gases were not smoky as in the earlier experiments. An important feature observed was the ignition of fine droplets and the continuation of glowing in their trajectory through air at near room temperature condition.

In similar experiments conducted by improving atomization (by increasing atomization air), the droplets penetrating flame reduced and more ash and dried (and partly devolatilized) particles were seen on the metal sheet. Similar effects were obtained even with reduced effluent flow rate of 3.5 g/s (burner power level of 75 kW).

The ignition delay, in the case of single droplet combustion, increases with decrease in ambient temperature (refer to section 3.9.2 – chapter –3) and therefore, the drop in localized temperature found after injecting effluent in flame has greater impact in increasing ignition delay. This makes it necessary to provide spray droplets with longer residence time either in the flame or hot zone. The incomplete combustion of the droplet is therefore attributed to the inadequate spray residence time. One possible way to avert this is to decrease ignition delay by increasing solid concentration of the feed and improving atomization. Since the preferred solid concentration is 60 % or lower (owing to the limitation of one industry to concentrate effluent to higher solids) and from the inferences drawn from the results of above experiments, it becomes imperative to provide higher heat flux at the downstream to convert partly evaporated and partly devolatilized droplets. Effective control of the residence time is also necessary to achieve complete combustion. Separate experiments were conducted with the aim of obtaining complete combustion and are discussed below.

4.6.4. Injection in confined hot cylinder

The combined burner is fitted to a stainless steel cylinder of 300 mm internal diameter and 2500 mm long with external surface insulated with ceramic wool as shown in Fig.4.6. This makes the spray confined within a hot cylindrical space such that the droplets penetrating the flame fall on the hot cylindrical wall over which hot gases flow causing augmented heat transfer. This causes increase in the rate of heating, evaporation and reduction in ignition

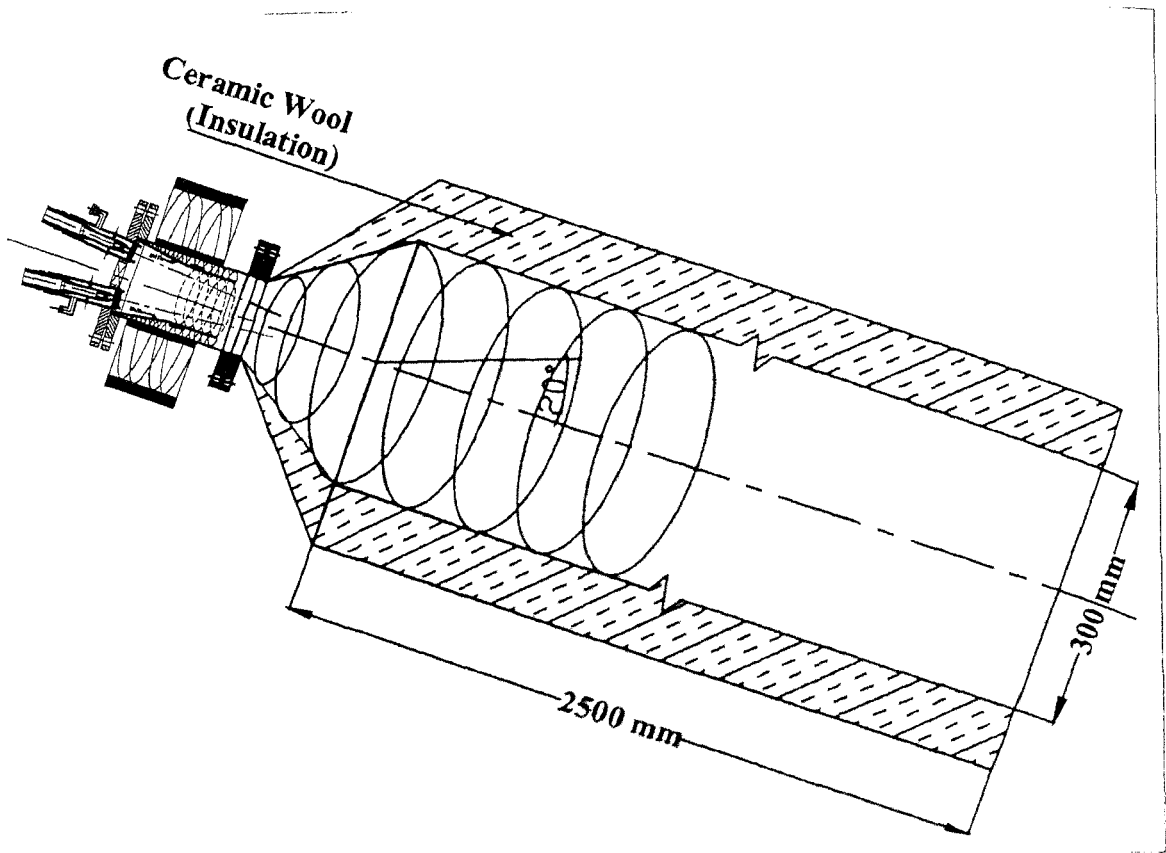


Figure 4.6: Effluent injection in kerosene flame in a confined cylindrical reactor.

delay of the droplets. The limitations found in the earlier experiments due to inadequate residence time and heat flux were overcome in this configuration. The cylinder is kept inclined so as to control the mass flow of combusting effluent falling on the surface under gravity and aerodynamic forces.

Prior to injecting the effluent, the cylindrical shell was heated to 1273 - 1173 K (at $T_a \sim 1273$ K, single droplet ignites in the flame). Hot effluent with 50 or 60 % solids is injected in the kerosene flame. The difference in the observation was that more glowing single droplets, could be seen close to the wall though spray ignition did not occur inspite of fine atomization. The un-burnt droplets falling on the wall accumulated after some time of injection and formed a pool of effluent that flowed under gravity to some distance. It became immobile as water evaporated and then the solid matter ignited into the flame. Char glowing also started downstream. Except for the location close to injection port where temperature dropped, the temperature downstream remained in the range of 923 - 973 K. In order to verify self-sustained combustion of the effluent, kerosene burner was completely shut off and injection was continued along with stoichiometric air. The 400 mm zone

downstream of the effluent injection cooled down to temperatures in the range of 573 K – 753 K; however, the flaming occurred at the downstream portion of the cylinder with intense char glowing. In this portion (1200 mm) the temperature remained in the range of 973 - 1073 K while the gas temperature was in the range of 1123 – 1223 K. This indicated that volatile and char oxidation contributed to sustaining the local temperature and combustion process in this zone. The cold domain increased as effluent injection continued. Therefore auxiliary heat input was necessary in this zone. Effluent injection was stopped while combustion air was being continuously injected. Flaming continued for 5 - 10 minutes after stopping effluent injection and slowly diminished but continued for about 5 minutes. The flame color was pale yellow and had a distinct tinge of crimson. Char glowing continued even after combustion air was stopped since the end was open to the atmosphere. The ash remained on the inclined surface of the cylinder. The carbon conversion was almost complete (> 99 %) and residue contained very little carbon in it.

It is inferred from the above experiments that sustained spray combustion of effluent with 50 % to 60 % solids, even with fine atomization, is not possible; however, complete conversion with sustained combustion is attainable, provided the residence time of the effluent in the hot zone is controlled and the enthalpy of product gases is utilized to sustain pre-ignition endothermic processes. In addition, since the unburnt effluent droplets in the case of both the solid concentrations fall on the wall, form liquid pool, and flow under gravity, it was thought that the effluent can be injected as thin film over the heated surface instead of injecting it as atomized spray and this will simplify injection process.

4.7. Conclusions

Effluents with 50 % and 60 % solids were injected as spray in hot oxidizing environment to determine conditions (ambient temperature and air ratio) at which auto-ignition occurred and subsequently investigate pre-ignition, ignition and combustion processes. Three classes of experiments were conducted: 1) Effluent injection from the wall with no auxiliary heat input, 2) injection with auxiliary heat input and 3) injection within kerosene enveloping flame.

- The heat release from the combustion of individual particles on the spray periphery is inadequate to maintain heat balance in the core due to evaporation because of which, the core remained unignited. Therefore, the sustained spray combustion of effluent with 50

and 60 % solids, even with fine atomization, is not achieved in all the three sets of experiments.

The effluent pool resulted from the spray injection in the heated cylinder leads to complete and sustained carbon conversion. It is found that the control of residence time of the effluent flowing under gravity on the heated plate by subjecting the plate to variable inclination is achievable. Since the heat required by pre-ignition endothermic process is large (30 % and 20 % of heat content of the feed for effluent with 50 % and 60 % solids), auxiliary heat input is found necessary. However, this requirement can be minimized if the transfer of the enthalpy of the product gases ($T_g \sim 1123 \text{ K} - 1223 \text{ K}$) to the evaporation zone occurs.

Since sustained combustion is necessary to provide heat to gasification reactions, a new experimental reactor is called for. The design of such a reactor should be able to control the residence time by changing inclination and the evaporation zone is regeneratively heated by circulating high temperature gases.

Inclined plain sheet reactor: Experiments and Results

5.1. Introduction

Achieving sustained combustion of effluent pool, flowing under gravity over inclined heated surface, as described in chapter 4, led to a new approach to provide effluent conversion with adequate residence time. By varying the inclination of the plate over which effluent is injected as a thin film, residence time of the fixed range of effluent flow can be varied. In addition, it is realized from the same experiments that the enthalpy of hot gases can be transferred as regenerative heat (from $T_g = 1073$ to 1173 K) to a relatively colder zone where endothermic processes occur and thus minimize the auxiliary heat input. These concepts are utilized in the construction of experimental reactor to obtain sustained effluent combustion, which is primarily essential to achieve gasification. The experiments conducted in such a reactor are described in the present chapter. The combustion air in the reactor can flow over the effluent film at relatively high velocity such that it can serve the purpose of transporting the combustion residue to the dump located at the end of the reactor and enhance heat convection from product gases flowing over the film. Evaporation and devolatilization rate are enhanced due to intense heat conduction and radiation from the hot surface. Higher surface area is required and hence, rectangular cross-section is preferred to the circular one.

The conceptual reactor is shown in the Fig. 5.1. It consists of a plate separating upper and lower chamber of the reactor that would form a long continuous bed over which effluent can be injected as a thin film. All combustion processes are expected to occur on the bed. The bed will be at a temperature lower than the gas temperature since endothermic evaporation and gasification reactions occur on the bed. Therefore, the bed can be heated, as in

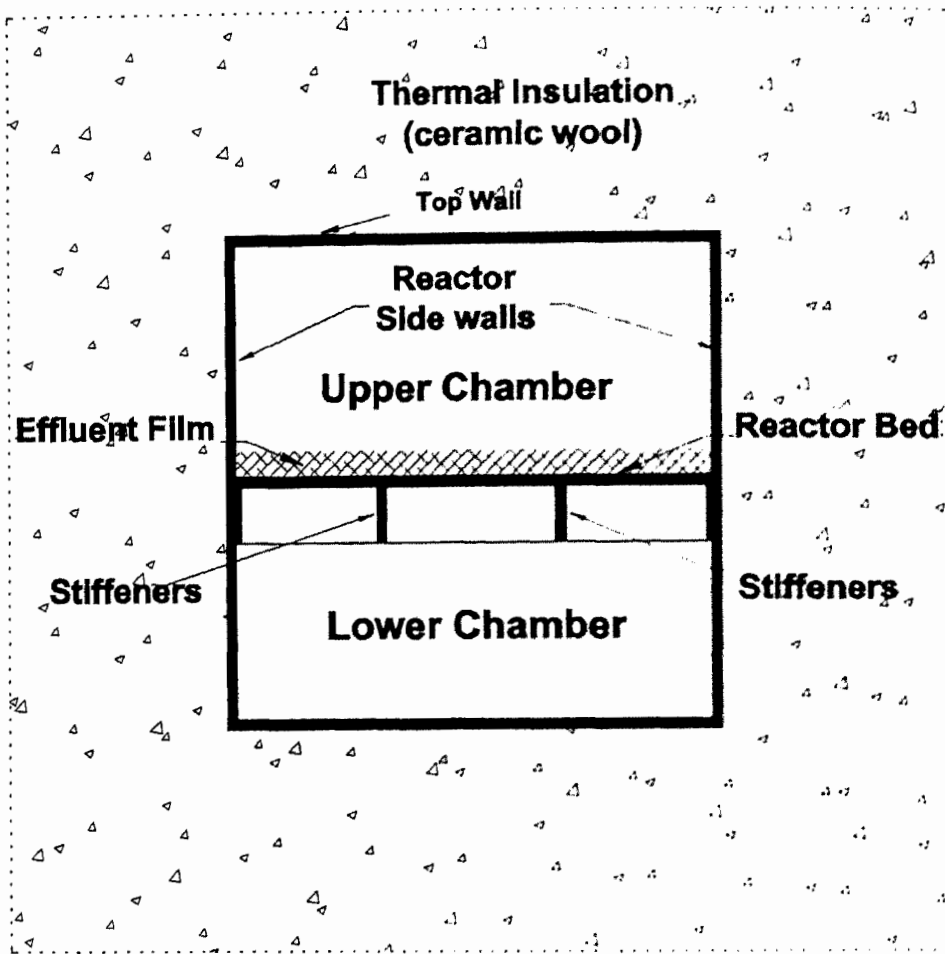


Figure 5.1: The conceptual rectangular cross section reactor.

regenerative heat exchanger, by allowing the product gases to pass through the underside of the bed before reaching the exhaust port. Therefore, the reactor space is divided by the bed into two separate ducts – upper and lower – through which gases flow in opposite directions.

In the upper duct hot product gases flow over the combusting effluent film with velocity in the range of 5 - 15 m/s to aerodynamically scrape residual ash and move it till the edge of the duct that terminates abruptly into residue (ash) dump. The reactor is kept inclined such that the effluent conversion occurs while traversing downstream under gravity. The top and side wall (with temperature higher than the bed) will contribute radiant heat flux with high ambient temperature. The reactor can be made adiabatic by enclosing it in a blanket of insulation. A kerosene burner is used to initially heat up the reactor and then give a low powered pilot flame during sustained operation compensating the input of cold combustion air. This is an alternate to pre-heating the air.

Plan of the experiment

Section 5.2 describes the experimental set up. The details of the experimental setup and instrumentation employed in the experiments are relegated into Appendix A5. The experimental procedure is presented in Appendix A5.2. Three sets of experiments were conducted. The table 5.2 outlines thirteen experiments conducted with various flow parameters and injection methodologies. This section and its sub-sections present the results and discussion on the experiments conducted with effluent with 60 % and 73 % solids. Self-sustained combustion of effluent, injected as film on the inclined bed with the help of film injector, splash injector, and atomizer, is achieved at sub-stoichiometric conditions. The gas composition obtained is an indication of effluent gasification. Experiments conducted for visual investigation of concentrated effluent spray combustion, in an open-end reactor is presented in section 5.3.1.3. The small cross sectional area of the present reactor obstructs the interaction of the spray with the hot ambient gases resulting in un-sustained spray combustion. These findings established the need for injecting effluent in a reactor with wider cross section area and high thermal inertia.

5.2. Experiment Setup

The main components of experimental setup consist of a plain sheet reactor, wet scrubber and product gas flare and an exhaust duct are as depicted in Fig 5.2. Fig 5.3 depicts the side view of the experimental setup and clearly indicates the locations of the thermocouples. The setup also include the systems for air supply and effluent feed, an injector with kerosene feed system and burner, and instrumentation for measurement of temperature, pressure, flow rates, gas composition and data logging system.

The modular reactor has three sections. The first section consists of effluent injection ports and the kerosene burner port; the second section, upper and lower ducts, divided by the reactor bed. This section has two inlets and two outlets and the product gases exhaust through this section to the wet scrubber section. The third section has the main function of directing the product gas in the lower duct of the second section and transfer the entrained residue particles and residue on the reactor bed into the dump. The exhaust gas is water scrubbed in two vertical pipes containing close cycle water spray and connected through a water seal. The aerodynamic ejector at the downstream of the wet scrubber is used to maintain reactor pressure to sub-atmospheric level and provide mixture of air and gas to flare it downstream. Blower supplies primary air. The flare has multiple tube outlets and a

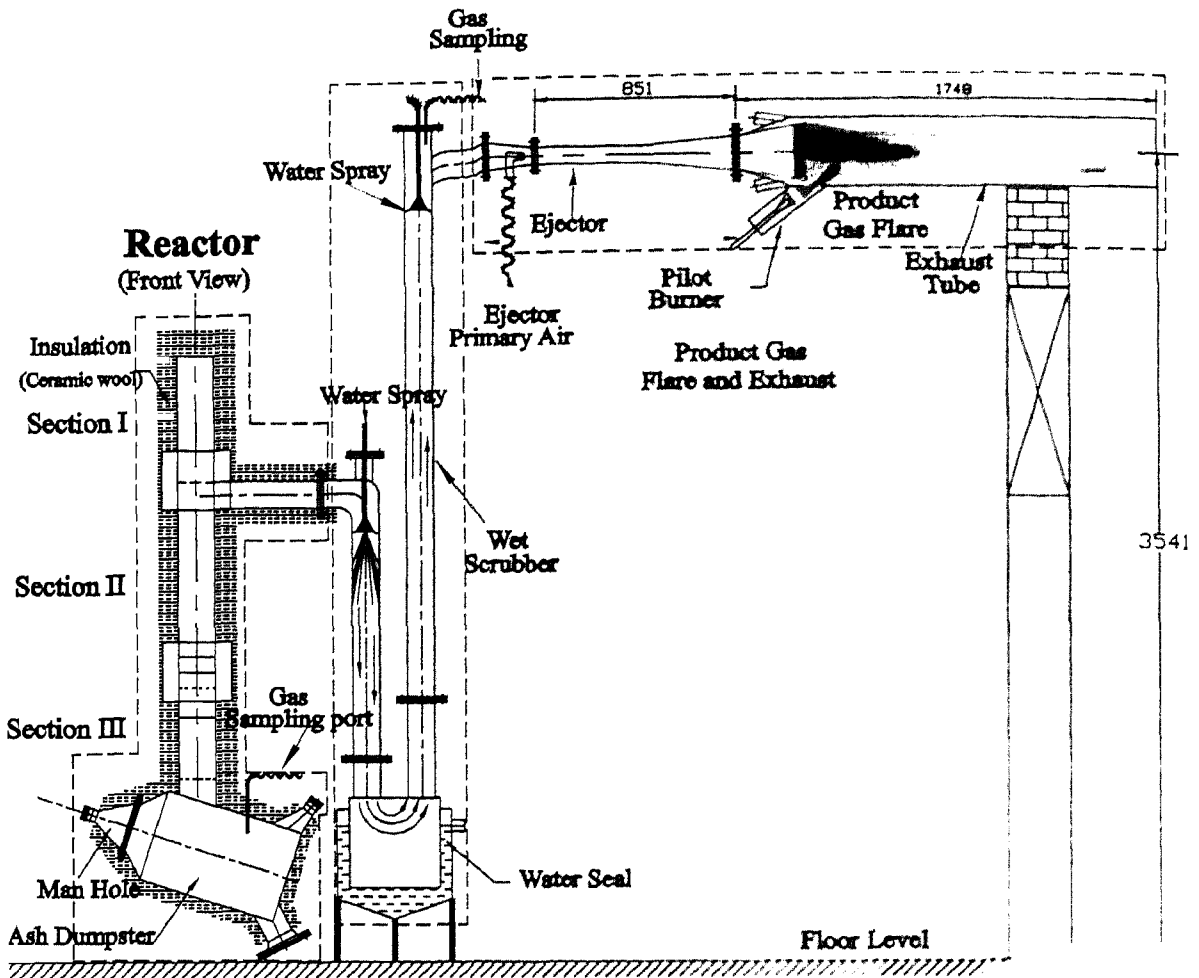


Figure 5.2: Scaled front view of the experimental setup.

pilot LPG burner to ignite the product combustible gas and air mixture. The combustion products are exhausted into the atmosphere.

The effluent feed system essentially consists of effluent storage and a feed tank, pressurizing air pipeline, effluent feed lines, purge and flush lines, electrical heaters or heat exchanger. The effluent is fed at a predetermined flow rate into the injector fixed to the reactor. Reactor temperature is measured using thermocouples, and the effluent temperature using bimetallic thermometer. The details of the reactor, reactor heating system, kerosene effluent and air feed systems are described in the Appendix A4. Measurement systems are similar to those discussed in Chapter 4.

5.3. Observations and Results

Three sets of experiments were conducted with similar heat up phase (phase I) and variations in the effluent injection methodology in phase II. The duration of phase I is

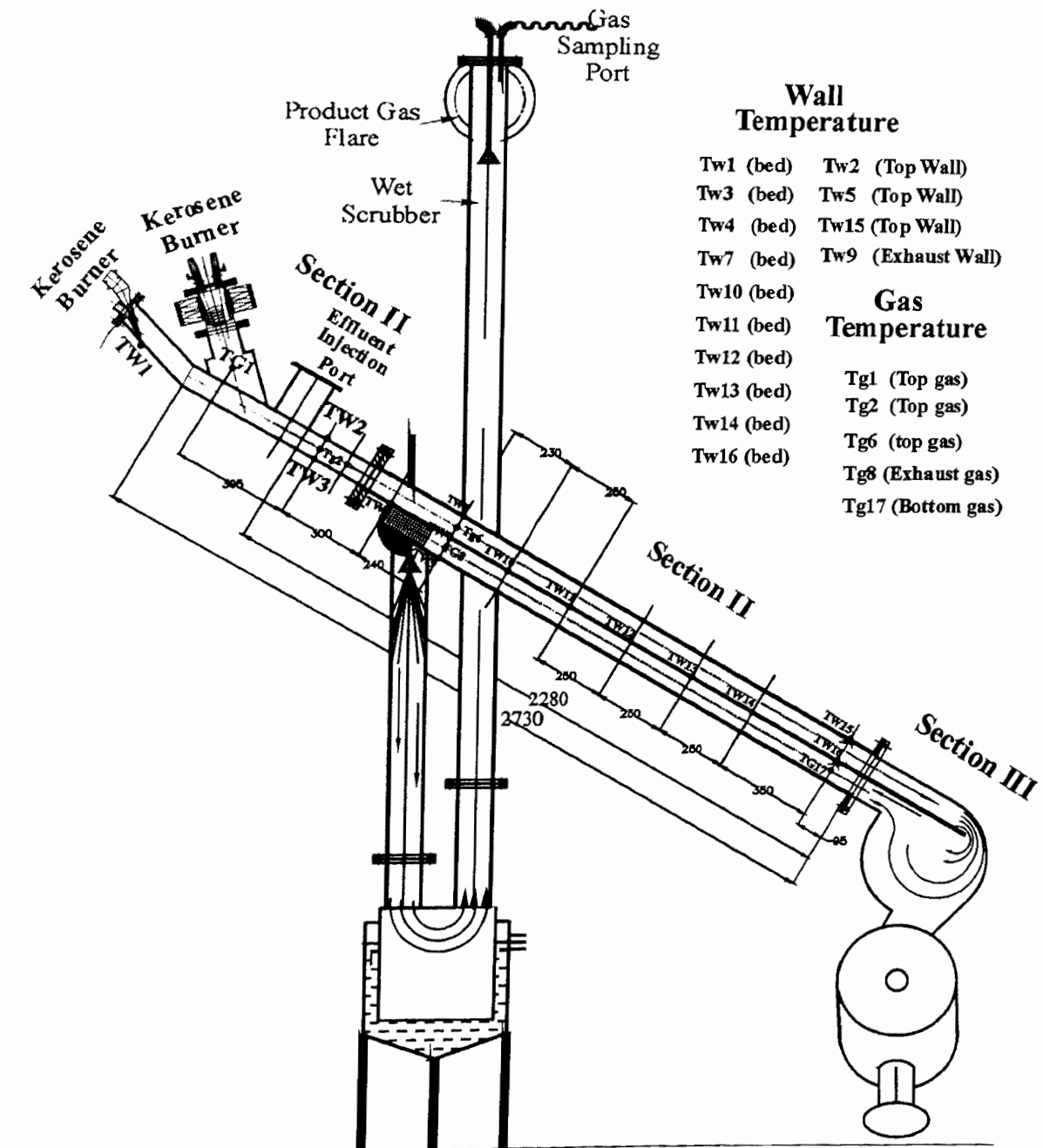


Figure 5.3: Schematic view of the reactor depicting the location of thermocouple used to measure gas and wall temperature.

recorded to be 18 – 22 minutes while the duration of phase II varied between 25 – 30 minutes. Reactor wall and gas temperatures at the end of phase I, are given in table 5.1. The name of the thermocouple location starts with ‘T’ and the subscript ‘g’ and ‘w’ corresponds to gas and wall temperature respectively. Effluent is injected once temperature at the end of section II (T_{w16}) is in the range of 1073 - 1123 K. The location of the thermocouples is shown in Fig 5.3 and those of view ports in Fig 5.4.

Time	T_{g1}	T_{g2}	T_{g6}	T_{g8}	T_{g17}	T_{w2}	T_{w3}
t (min)	1335 K	1328 K	1183 K	1023 K	903 K	1303 K	1103 K
18 - 20	~ 1535 K	~ 1528 K	~ 1330 K	~ 1164 K	~ 1036 K	~ 1400 K	~ 1353 K
	T_{w4}	T_{w10}	T_{w11}	T_{w12}	T_{w9}	T_{w14}	T_{w16}
t (min)	1153 K	1153 K	1133 K	1083 K	983 K	1053 K	1003 K
18 - 20	~ 1165 K	~ 1335 K	~ 1306 K	~ 1265 K	1053 K	~ 1207 K	~ 1110 K

Table 5.1: Bed and gas temperatures prior to effluent injection

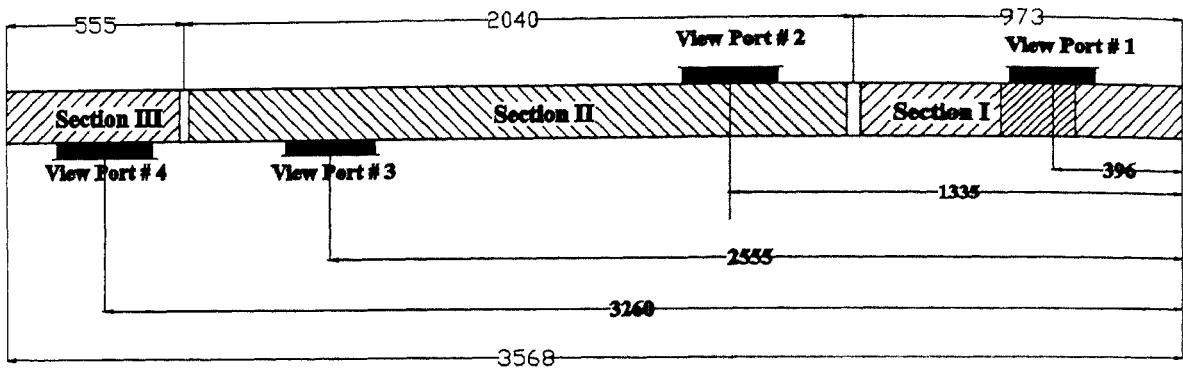


Figure 5.4: Top view of the reactor depicting the location of the view ports

The residence time of liquid effluent film and partly converted solids traversing in the reactor towards the dump depended largely on reactor inclination and to an extent on the gas velocity. Separate experiments were conducted on cold as well as hot plate at inclination ranging from 15° – 60° and effluent flowing at the rate of 5 – 10 g/s (throughput) and air flow rate ranging from 5 – 25 g/s (stoichiometric air). At low inclinations (< 20°), effluent gradually choked reactor passage in section I, since it became immobile due to evaporation. At higher inclinations (45° and higher), effluent reached the dump (section III) before completing evaporation. The optimum inclination emerged as an outcome of these experiments was 30°. At this inclination, effluent film remained mobile (with velocity of 1.2 – 1.3 m/s) till it reached hot zone (see Fig. A5.7) and continued to flow over its own vapor (spheroidal evaporation) and later charred. The char and ash was found non-sticking on the hot surface and moved towards dump under gravity and aerodynamic drag exerted by hot gases.

Figure 5.5 depicts the reactor cooling profile with and without airflow in absence of effluent flow and zero auxiliary heat input. The rate of temperature fall in the case of (a) is about 75 K/min and that in case (b) is about 10 K/min. These profiles are compared with those

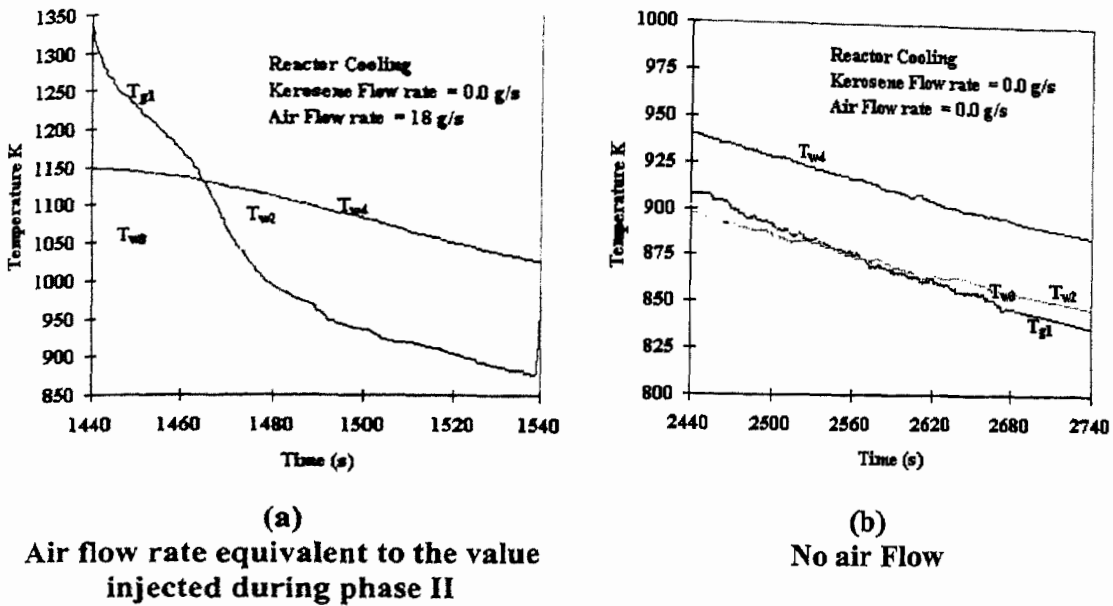


Figure 5.5: Reactor cooling profile

obtained during effluent injection phase to determine the exothermicity of the reaction occurring on the bed.

The different injection methodologies, distinguishing the three sets of experiments, were designed based on the results of the preceding experiments, in the light of attaining sustained combustion and gasification. Table 5.2 shows the results of all the 13 experiments conducted in the inclined reactor.

5.3.1. Phase II : Effluent Injection

5.3.1.1. Experiment set 1 (I – 1 to I – 5): Injection as film on flat plate

The first experiment (I-1) was conducted in the inclined reactor, set at an inclination of 30° . This was the first reactor without gas scrubber or cooler. The effluent injected as film at 15 g/s flow rate and with sub-stoichiometric air. The product gas was ignited and diffusion flame extending beyond the exit plane of the exhaust tube (extending to about 1.5 m long) was seen without any support flame. Temperature in the reactor dropped even though the exhaust duct temperature was found high due to product gas oxidation (the wet gas scrubber was installed after this experiment). The residue in the ash dump contained ash (~ 50 %), devolatilization char (~ 40 %) and partly evaporated liquid effluent (~ 10 %). The significance of the present experiment is that, although, sustained behavior was not obtained, the fact that the material is combustible as well as gasifiable at correct effluent and airflow rate was established.

Experimental Reactor	Experiment Number	Solids %	Effluent Injection (phase II)		Flow Rates \dot{m}_s g/s			Sustained Combustion or Gasification		Complete Combustion
			\dot{m}_{eff} g/s	Injection Methodology	Phase II			Combustion	Gasification	
					Kerosene	Total Air	Eq. Ratio			
First Inclined Reactor	I-1	60	15	Film	1.5	20	0.3	No	Nc*	No
	I-2	60	7	Film	1.5	34	0.79	Yes	Nc	Yes
	I-3	60	7	Film	1.2	28	0.73	Yes	Nc	Yes
Second Inclined Reactor	I-4	60	5.0	Film	1.0	20	0.71	Yes	No	Yes
	I-5	60	7.0	Film	0.55	21	0.70	Yes	Nc	Yes
	I-6	60	4.0	Splash	1.1	27	0.96	Yes	No	Yes
	I-7	60	5.3	Splash	1.6	29	0.73	Yes	No	Yes
	I-8	60	5.0	Splash	1.4	22.5	0.63	Yes	Nc	Yes
	I-9	60	5.8	Splash	1.0	18	0.54	Yes	Nc	Yes
	I-10	60	10.0	Splash	1.4	21	0.42	Yes	Nc	Yes
	I-11	60	8.0	Spray	0.55	12	0.38	Yes	Nc	Yes
	I-12	73	6.0	Spray	--	15	0.67	Yes	Nc	Yes
	I-13	73	8.0	Spray	0.0	12.5	0.42	Yes	No	Yes

*Nc = Uncertain gasification

Table 5.2: Details of the experiments conducted

In contrast to these results, in the subsequent experiments (Expts. No. 1 - 2 and 1 - 3) effluent combustion sustained with high carbon conversion along with the support of auxiliary heat input. The oxygen fraction in product gas sampled from the end of duct was measured zero (or undetectably small value) indicating it to gasification condition, although CO and H₂ were less than 5 % and hence is treated as 'uncertain gasification' (Nc).

In the subsequent experiments (not tabulated), the flat bed of the reactor gradually deformed due to thermal stresses and self load. A new reactor was therefore constructed with same cross sectional dimensions but with higher sheet-metal thickness (3.6 mm) and adequately reinforced with same metal stiffeners.

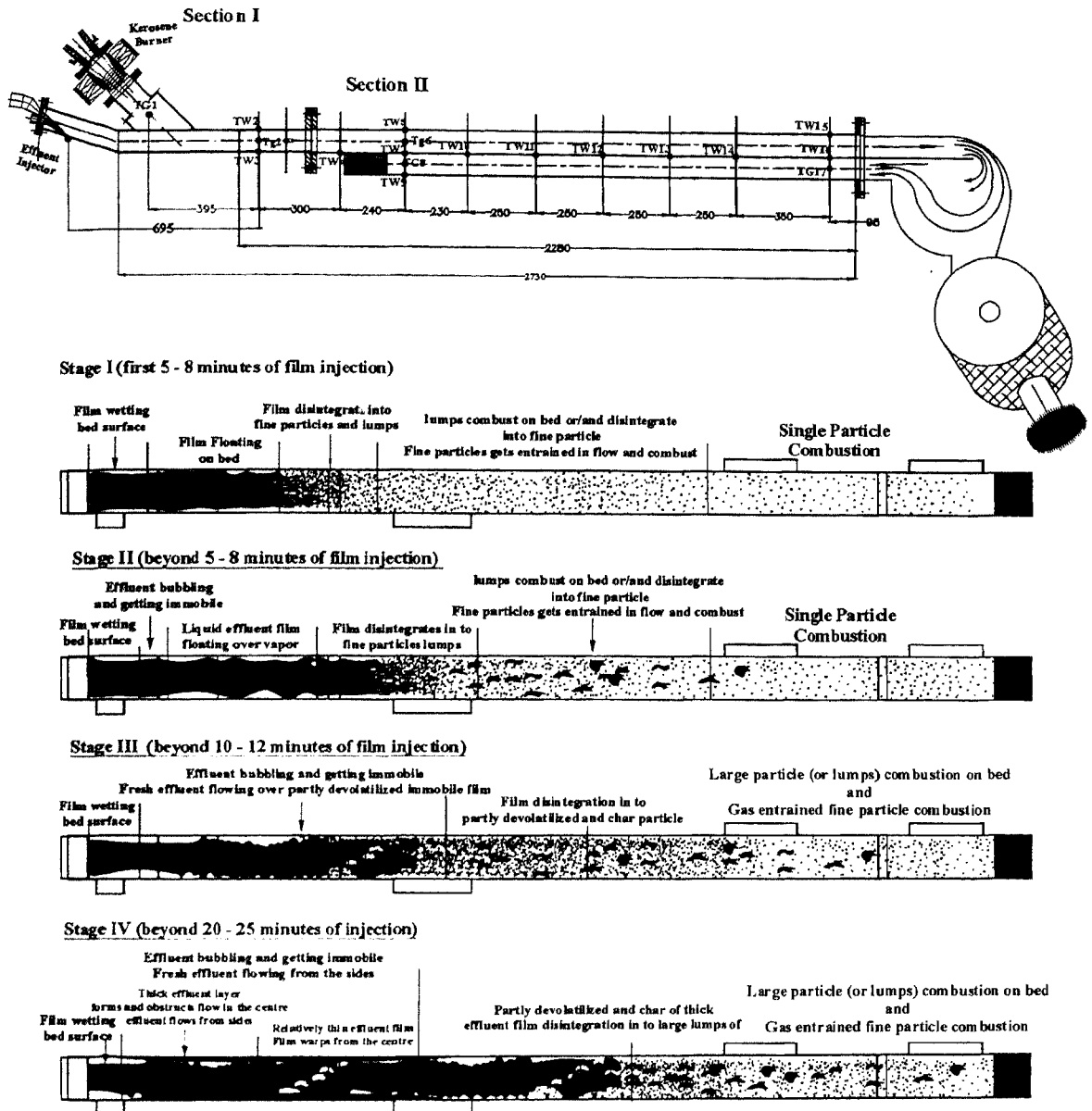


Figure 5.7: Observations of sequence of processes occurring after injecting effluent as film in the inclined reactor.

After 8 minutes of injection (stage II (a)) effluent film was seen bubbling and becoming immobile in the zone upstream of kerosene burner. This changed the initial behavior observed in stage I. Liquid effluent flowed over immobile effluent film surface and spilled on the fresh bed surface and floated as film. The film disintegrated into fine particles as in the stage I as well as lumps (ligaments of effluent). Lumps burnt on the bed or disintegrated due to impact and fine particles combusted in gas entrained mode. The temperature of gases flowing over the film was in the range of 1253 –1273 K (T_{g2}).

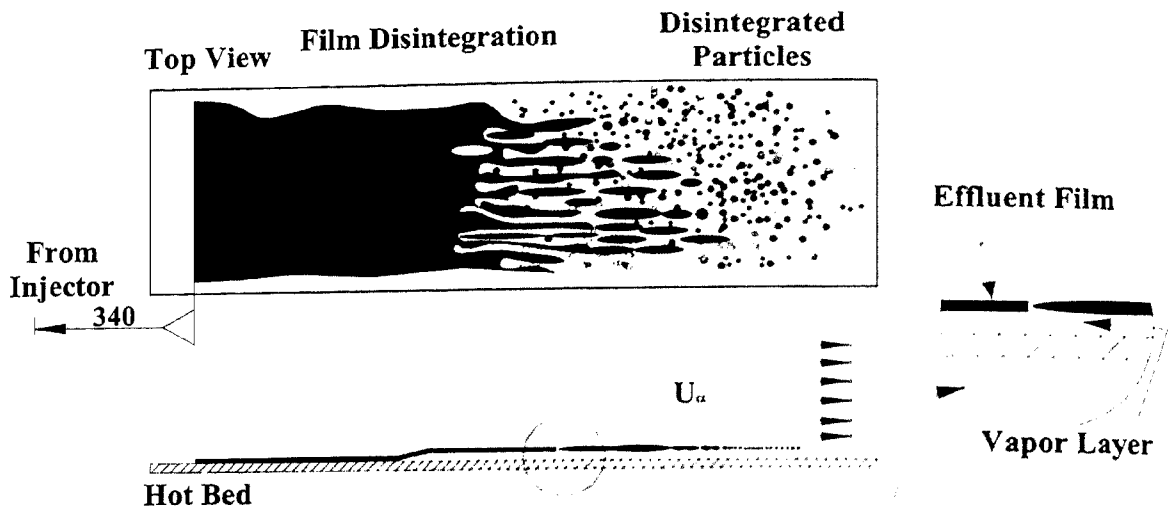


Figure 5.6: Schematic of the effluent film flowing over hot bed and subsequent disintegration into particles due to stretching and shear stripping.

Physical Observations (Expt No. I – 2 to I – 5)

The observations are summarized in Fig. 5.7. All the observations are divided into four stages. In *Stage I* (first 8 - 10 minutes), the effluent film flowed towards the hot zone of the reactor where the top wall and bed temperatures were in the range of 1300 K (T_{w2}) and 1100 K (T_{w3}). As was seen from view port # 1 (see Fig 5.4), the effluent film wetted the reactor bed as shown in the Fig. 5.6, however, as it approached hot zone, it swiftly rolled towards downstream of the bed without wetting the hot surface. This was because of the beginning of intense evaporation (commonly known as spheroidal evaporation) as it approached hot zone (see Fig. A5.7) and the vapors filled the space under the film lifting it from the surface reducing the friction between film and surface. The transition between end of wetting and floating is very rapid. No film was visible from the view port #2 even after five minutes of injection, but instead, large number of gas entrained particles combusted with higher luminance compared to ambient gas and reactor walls. Similar observation was made even through view ports # 3 and 4. Most particles completed combustion and were carried away into the dump as negligible amount of combusting gas-entrained particles were seen in the reversed gas flow under the bed, as seen from view port # 4. From this observation, it was clear that effluent film disintegrated under aerodynamic forces with a process of stretching and shear stripping as would prevail commonly in the case of non-Newtonian fluids (Arcoumanis et al., 1994). The gas flow velocity was 8-10 m/s and temperatures in the range of 1223 – 1273 K.

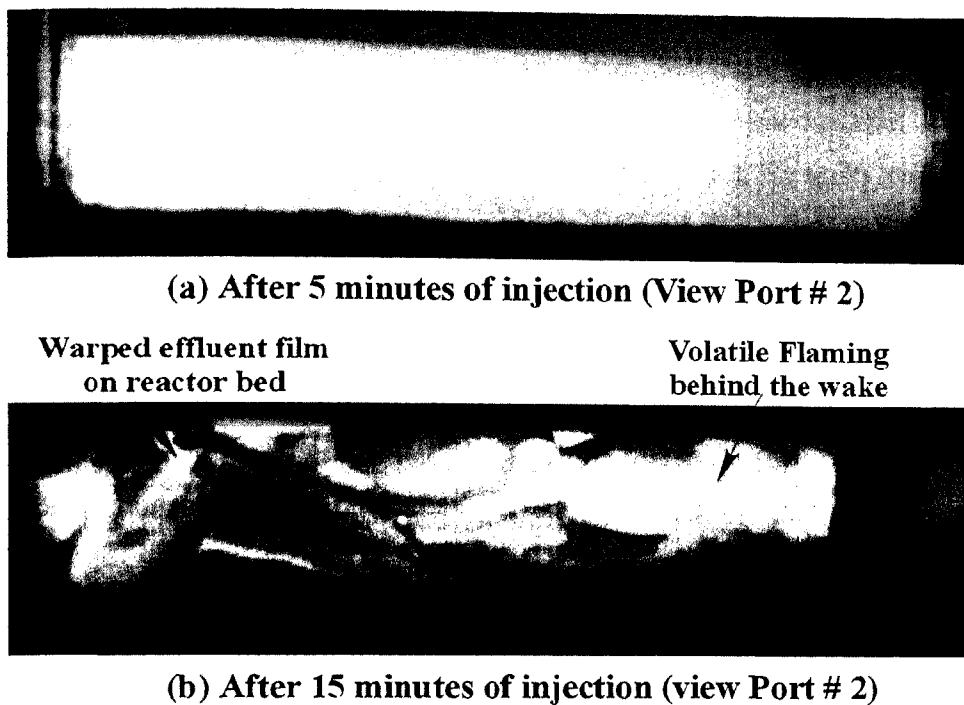


Figure 5.8: Direct photographs of effluent combustion during phase II as viewed from view port # 2.

Beyond 10 – 12 minutes of injection (stage II (b)), the zone of immobile effluent grew extending up to port # 2; however, along with the liquid effluent, the dried and partly devolatilized and char particles also disintegrated and traversed downstream.

In the stage III, the piling up of the fresh effluent over the dried and partly devolatilized effluent grew to an extent that the pile or thick effluent film (40 – 50 mm thick) obstructed the effluent film from traversing downstream. Therefore, the incoming effluent flowed from the sides and stage II process occurred downstream of the burner location. More of partly devolatilized and char lumps were fragmented while the fresh incoming effluent could not uniformly flow on the bed as was possible up to stage III process. Large particles or lumps combusted on the bed while gas entrained particles combusted in gas-entrained mode. Beyond this stage the effluent flow was not uniform due to clogging of its passages and there the effluent injection was discontinued.

During stage III, the effluent film would undergo expansion with initial heating and then contraction as devolatilization progresses, as observed in effluent sphere combustion, as a result the film warped as depicted in Fig. 5.8(b). Volatile flaming occurs in the wake region of the film. The partly devolatilized film gets detached from the surface and gets dragged downstream.

The peculiar behavior of effluent getting strongly adhered to heated surface and subsequently getting detached with time was carefully studied through separate experiments. Effluent with different (60 % and 70 %) solids concentrations was injected on a stainless steel plate set at an inclination of 30° to the horizontal and heated uniformly to different temperatures. Cold liquid column was injected on the upstream cold surface. Observations are in Table 5.3.

Expt No.	Effluent Solids, %	Surface Temp., K	Observations
1	60	623	Effluent spread out and formed patch, began to boil and adhere to the bed. Bond between metal and effluent surface is strong. Mechanical scraping is required to detach it from the surface. Warping does not occur with time.
2	60	723	Effluent spread out a little but then rolls down on the surface. Providing a small obstruction on the plate would prevent column from rolling down, it would wet surface and boil and stick to the surface. The bond between surfaces gets weaker with time. Aerodynamic scraping (10–15 m/s cold air) was still inadequate. Effluent warps with time.
3	60	823	It rolls down and when obstructed, it boils and sticks onto surface. Immediately after drying, it warps, gets scraped aerodynamically.
4	70	> 850	The difference between obs. No. 1, 2 and 3 and corresponding 4, 5, and 6 was the evaporation times that was shorter in higher solids effluent. Other observations are the same.
5	70	> 850	
6	70	> 850	

Table 5.3: Experimental observations of effluent injected on hot stainless steel bed

Figure 5.9 depicts top wall (T_{w2}) and bed (T_{w3} , T_{w4} , T_{w7} , T_{w16}) temperatures measured at different locations shown in Fig. 5.3. Downstream of the film injector, bed temperature (T_{w1}) remained within 423 K with continuous effluent injection. During stage I, temperature in the Section I varied more than in Section II and III. T_{w2} and T_{w3} would drop by 70–75 K and 120–130 K respectively while T_{w4} and T_{w7} remain constant or slightly increase and T_{w16} increased by 160 K. The fall in temperature was inferred as due to heating and evaporation processes occurring on the bed while the increase in temperature was due to the exothermic oxidation of disintegrated effluent material. During Stage II, T_{w2} and T_{w3} further drop while towards the end, T_{w4} and T_{w7} also drops indicating that the liquid effluent has

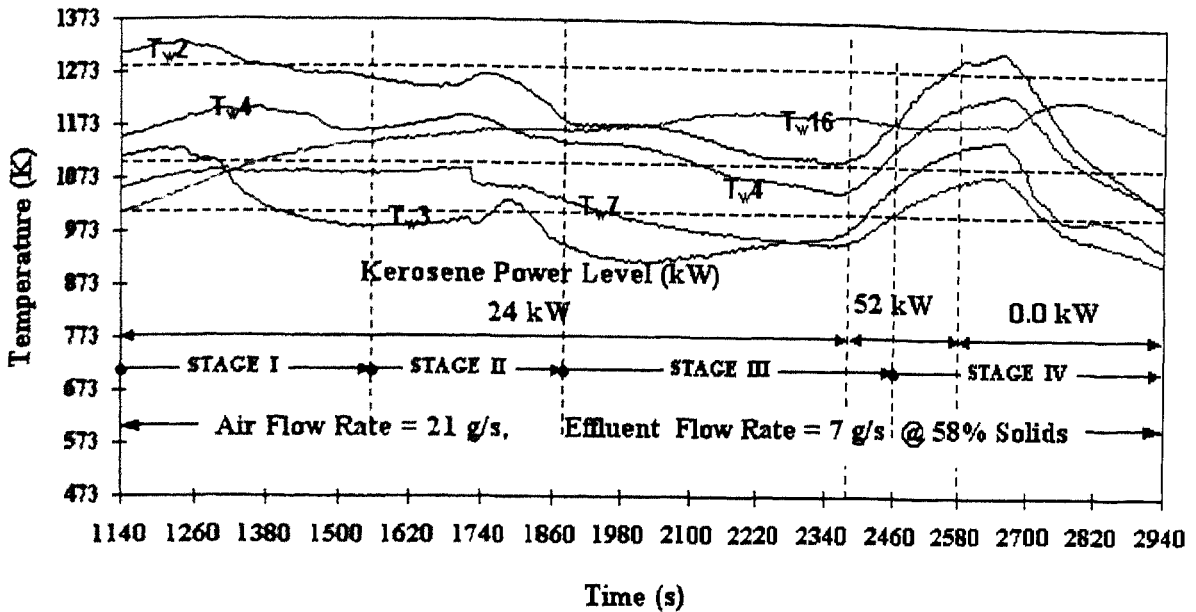


Figure 5.9: Temperature vs. time history obtained at various locations in the reactor during Phase II obtained during effluent film injection experiment

reached these zones, where endothermic processes have been initiated. T_{w16} continues to rise throughout the experiment.

During stage III, temperature T_{w3} does not drop since the effluent flows over the existing dried and immobile film and it does not wet the surface. It actually increases due to devolatilization and volatile combustion under side of the film surface, heating the bed. The top wall temperature falls continuously from 1330 – 1110 K in 20 minutes due to endothermic processes in that zone.

Figure 5.10 depicts gas temperatures, T_{g6} (top duct) and T_{g8} (bottom duct or exhaust gas) and wall temperature T_{w5} (top wall), T_{w7} (bed) and T_{w9} (bottom wall). The temperature in this zone remained almost constant during Stage I, unlike that in the case of T_{w1} and T_{w3} , which decreased.

Beyond 10 minutes, T_{w5} , T_{g6} and T_{w7} (except for T_{g8}) decreased due to the liquid effluent film reaching this zone where endothermic pre-ignition processes occur. The exhaust gas temperature T_{g8} (see Fig. 5.3 for location) remained above T_{w7} soon after effluent injection and exceeded upstream (upper duct) gas temperatures after stage II. This clearly indicated that the combustion of volatiles and entrained particles occur in downstream zones. During stage IV of injection the burner power level was increased from 24 to 52 kWth for 200

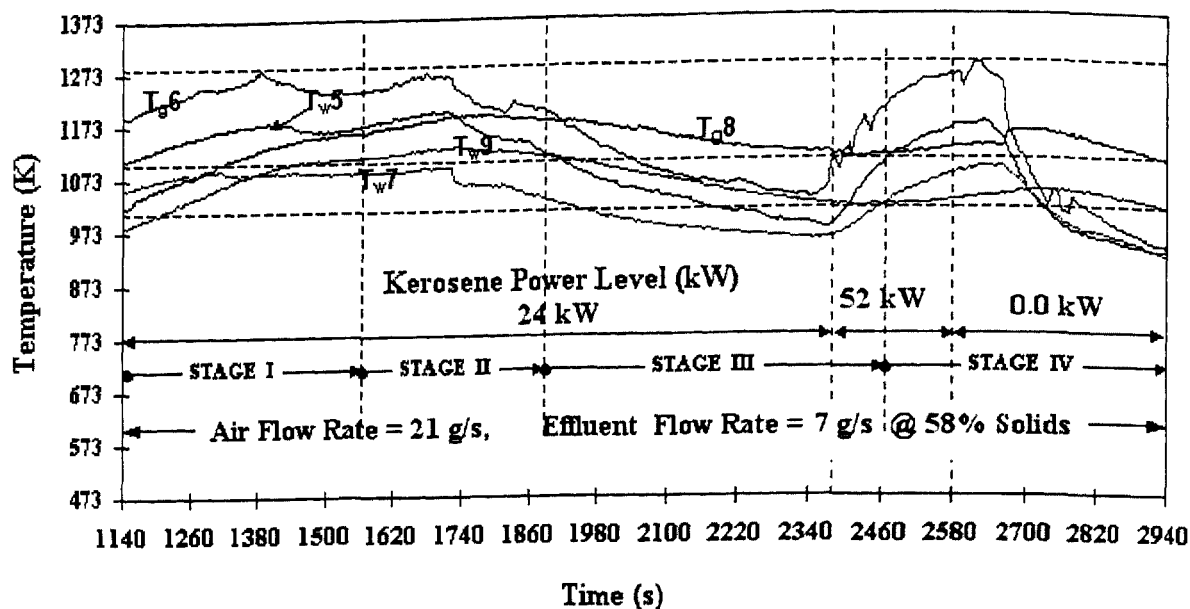


Figure 5.10: Wall and gas temperature vs. time history obtained at a plane perpendicular to the reactor, located at 1235 mm from injector during the Phase II of effluent film injection experiment.

seconds, after which it was switched off. This resulted in sudden rise in the gas and bed temperatures. However, temperatures at the downstream locations were not much affected.

Effluent was injected till the end of the 30th minute. Injection was stopped when it was found that the liquid effluent entered view port # 2 and obstructed the view. The combustion air was switched off and the combustion process in the reactor was frozen.

The above observations were representative of all film injection experiments.

Post-experimental observations

Physical inspection of section I through the sight, injection and burner port showed that the thick effluent film blocked the passage upstream of the burner, although the residue was ash with negligible carbon in it. The film was weakly adhering the surface. View port # 2 box contained lumps of ash and char obstructing the vision. Once cleared, the reactor bed could be seen to be containing smaller ash lumps of thin effluent film. View port # 3 and #4 box was found to contain finer ash particles as shown in Fig. 5.11 (b). The dump contained large fraction of fine ash particles along with small irregular shaped soft lumps [broken multi layered film, Fig. 5.11 (a)]. The lower duct (underside of the bed) contained negligible

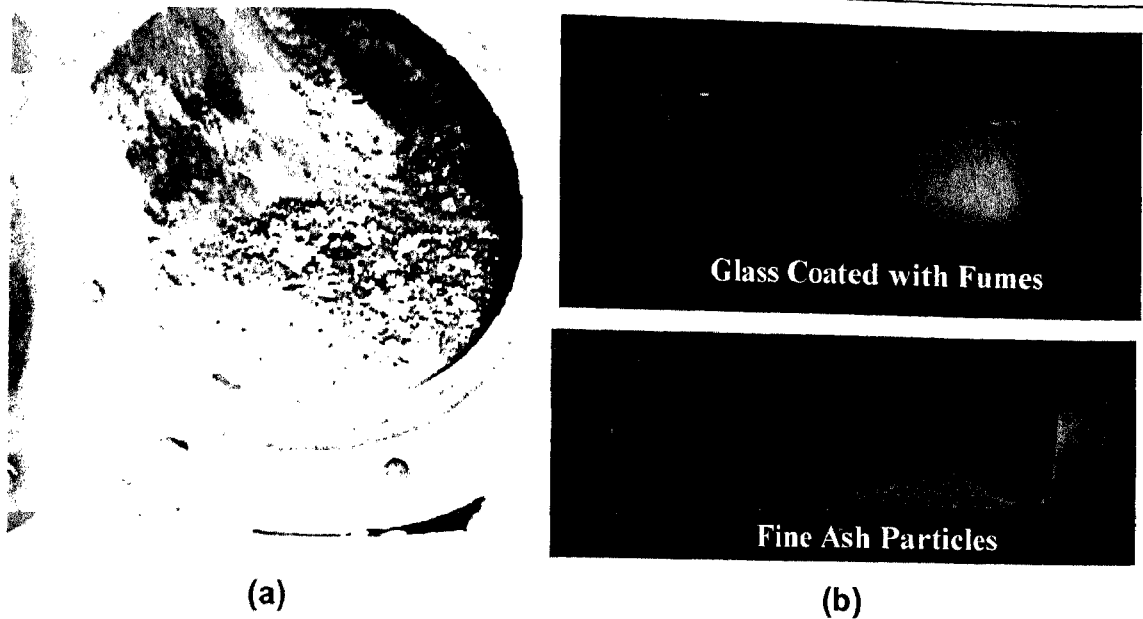
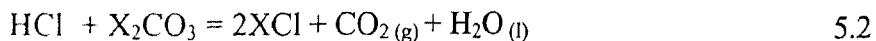


Figure 5.11: (a) Fine ash in the dump (b) View port glass coated with fumes and accumulation of fine ash behind glass.

amount of fine ash. The ash in the dump was about 13.5 % of the total weight of the solids. The color of the ash was pale brown and contained negligibly small amount of carbon (< 0.5 %, by analysis). 65 % of the ash could pass through 1.0 mm sieve. Qualitative analysis of ash indicated presence of large amount of alkali sulfide and carbonate. Pungent smell of hydrogen sulfide and effervescence were detected with the addition of hydrochloric acid to ash, undergoing reaction 5.1 and 5.2, indicating expected presence of large amount of alkali sulfide and alkali carbonate



The sight glass was coated with white layer of fine fume particles as shown in Fig 5.11 (b). Chloride test for fume was positive indicating fumes of alkali chlorides. The scrubbing water temperature after experiment was 350 K and had gained a little turbidity with weak sulfurous odor. This water was pH neutral. The sample gas scrubbing water was also found neutral and contained chlorides. The oxygen concentration during all the stages of phase II of the experiment was found to be near zero, carbon dioxide would ranged between 13.5 – 17 % and $\text{CO} = 5 - 6 \%$, $\text{H}_2 = 3 - 4 \%$.

Results and discussion: (Expt. I – 1 to I – 5)

The Leidenfrost point in the case of effluent is unknown; however, the minimum surface temperature above which effluent would float is in the range of 673 – 773 K. Temperature lower than this would cause effluent to wet surface and initiate nucleate boiling, resulting in intense heat transfer. Since the bed temperature in the hot zone is 1353 K (T_{w3}) the film rapidly attains spheroidal evaporation state. In comparison to nucleate boiling, the evaporation rate during spheroidal evaporation is reduced and therefore, effluent traverses downstream prior to getting dried and become immobile. The disintegration of film into ligaments and subsequently finer particles (or droplets) is due to the complex effect of aerodynamic forces exerted by hot gases causing stretching and shearing of the film top surface and the surface tension efforts to minimize the surface area.

The steady state processes observed during stage I could have been maintained only if the bed temperature gradient between the cold and hot zone (see Fig. A5.7, p. 188) remained sharp. However, with time, as seen in subsequent stages, this gradient tapered off due to heat transfer from hot to cold zone. This rendered effluent film, close to the hot zone to boil in the nucleate regime resulting in intense heat transfer, causing effluent film to dry up and become immobile. In addition to this, the bed temperature also reduced due to endothermic evaporation and contributed in increasing the length of nucleate boiling zone over which effluent became immobile. Liquid effluent flowed over the immobile effluent film and flowed in the hot zone metal surface subsequently following stage I process of disintegration. The immobile effluent zone increased at a faster rate downstream of the hot zone than at the upstream of cold zone since the continuous effluent injection kept the surface below boiling point.

Effluent lumps observed during stage II, III and VI were fragmented pieces of partly devolatilized effluent film that were disintegrated under aerodynamic forces. Immobile effluent film undergoes phases of expansion and contraction resulting in warping as shown in the Fig. 5.11(b). This causes the liquid effluent to flow from the sides as was seen at the end of stage III and stage IV.

A continuous heat input of 20 – 25 kWth was found necessary in order to provide heat flux to sustain endothermic evaporation in section I of the reactor and also because non-preheated combustion air introduced through this section.

The ash did not fuse or melt on the bed, an observation consistent with single particle combustion. The ash from the reactor dump contained sulfide unlike the ash obtained from single particle combustion. This is due to supply of sub-stoichiometric air quantity.

However, since the effluent was flooding the top bed surface and the heat source (auxiliary kerosene burner) was located over the bed, the effluent film itself resisted the heat transfer to the bed. Air injection over the film, which was effective in assisting film formation, however, remained ineffective to scrape the adhering film.

Film formation and disintegration into particles leads to gas entrained single particle combustion. The available residence time is adequate for almost complete combustion as found from ash analysis even under confirmed gasification conditions.

Cold zone is necessary for effluent to form thin film on the surface; however, the intermediate zone between hot and cold zone will have temperature in the range of 573 – 673 K. Effluent wetting the surface would boil in nucleate boiling regime and most water would evaporate at a high rate rendering effluent immobile, adhering to the bed with strong bond. Injected effluent film clog due to obstructing immobile effluent layer.

Sharp gradient (as observed during stage I) would prevent clogging and allow effluent to penetrate deeper in the reactor. Cooling the cold zone and maintaining temperature of the hot zone would maintain sharp gradient however, thermodynamically it is not a favorable solution. Temperature vs. time profile obtained (see Fig. 5.9, 5.10) gives a clear picture of the zone where endothermic and exothermic processes occurred on the bed, by comparing temperature at different locations at a particular instance.

5.3.1.2. Experiment set 2 (I – 6 to I – 10): Splash Injection in hot zone

In this experiments effluent is injected directly into the hot zone (as liquid column is broken into small ligaments and/or 2 – 3 mm diameter droplets) using air as shown in the Fig. 5.12. The bed temperature is the highest at the point of injection where hot burner exhaust gas deflector is located. The splashed ligaments liquid column rolls over the hot surface and penetrates deeper into the reactor as compared to film injector without causing any clogging. The injection location was cyclically changed in lateral direction using a quick return mechanism to which injector was fixed. Effluent was injected after the reactor wall attained temperature as in Table 5.1.

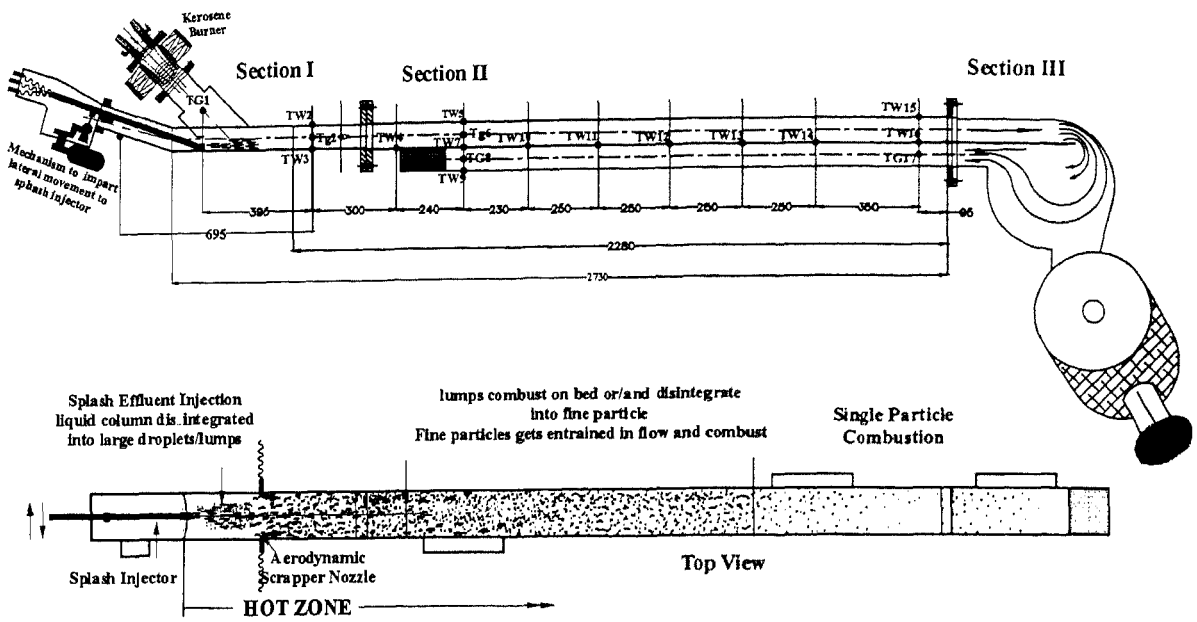


Figure 5.12 Observations of process occurring after injecting from splash injector in inclined reactor

Physical Observations

As was seen from the top end of the reactor, the splashed effluent in the form of large droplets or ligaments floated over the hot bed and traversed downstream without wetting the surface. However, there was no accumulation of the fresh effluent and the steady state processes of evaporation, film drying-warping and subsequent scrapping of partly devolatilized effluent soon established owing to the cyclic change in the injection locations, avoiding localized flooding and allowing even heat flux distribution.

From the view port #2, large and small sized, single particle combustion was seen (as seen during stage I of film injection experiment). Particles glowed brighter than the reactor walls. Small effluent lumps (~5 mm diameter) were seen glowing on the bed, being pushed downstream of the reactor. From the view port # 3 and #4, gas entrained combusting particles were seen. Porous ash was seen on the bed even though there was no flow of molten ash. Gradual deposition of the fumes on the cold glass surface blurred the view. Most observations were found similar as compared in case of all the experiments.

Figure 5.13 depicts the bed temperature, gas composition and air flow rate vs. time history measured during effluent injection. Air flow rate was maintained to sub-stoichiometric value (air ratio = 0.54 or $\Phi = 1.85$) after 3 minutes of injection and was kept constant during

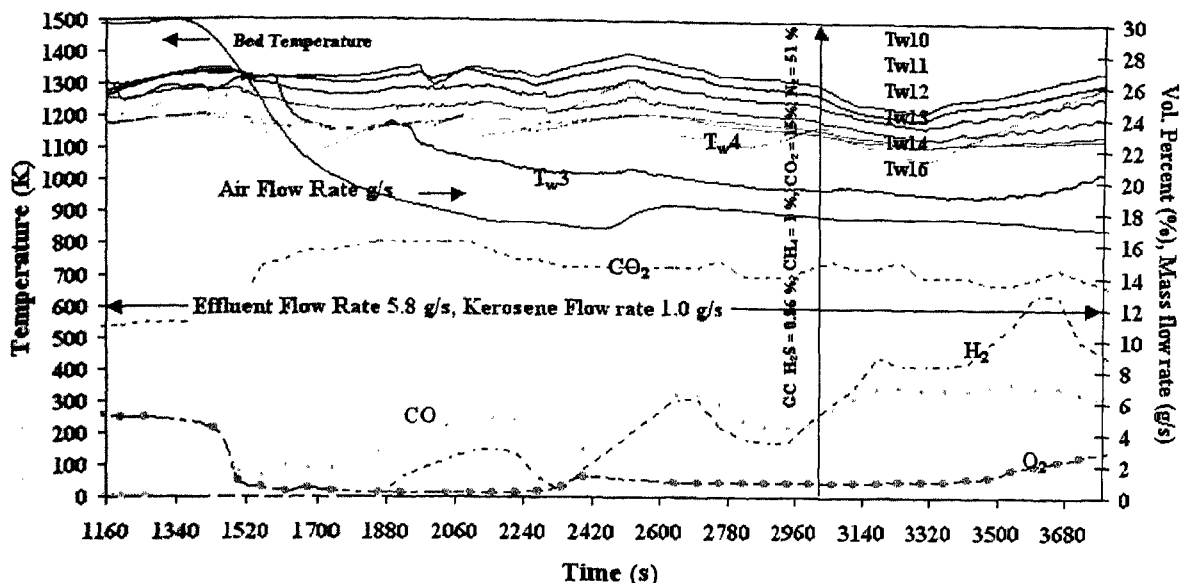


Figure 5.13: Bed temperature, gas composition and air mass flow rate vs. time history obtained at various locations in the reactor during effluent injection phase (Phase II) (Expt. No. I – 9)

this phase. The stoichiometric air requirement was calculated based on combined fuel input (effluent + kerosene), the kerosene combustion was provided with stoichiometric air.

Temperature T_{w3} and T_{w4} decreased by 200 K due to effluent injection. Evaporation seems to have been completed in this zone (within 700 mm downstream of injection) since the downstream bed temperatures does not fall rapidly as in the case of T_{w3} . In fact T_{w10} and T_{w11} increased by 130 and 90 K respectively.

Gasification condition could be attained (oxygen concentration less than 1 %) as the air flow rate was reduced. The dry gas composition obtained showed increase in CO and H_2 concentration. The CO_2 concentration ranged between 14.5 and 15 % during gasification. Owing to variation in the bed temperature, the CO and H_2 gas composition fluctuated. The maximum value of CO and H_2 was measured to be 7 and 12.9 % respectively. The H_2S and CH_4 composition obtained (using gas chromatography) were 0.86 and 1.0 % respectively (at $t = 3000$ s, and $t = 3600$ s). During the first phase the total $O_2 + CO_2$ concentration varied between 13 – 15 % while CO and H_2 remained zero.

Post experimental observations

Upper duct of the reactor contained negligible ash. Ash sample was removed immediately after experiment and it contained 4.83 % carbon (of total carbon injected), which is higher

compared to that found during film injection experiment (contained less than 1 % carbon). Ash was fragile and its fusion or agglomeration was not seen in the dump. About 35 % of ash could be passed through a 1.0 mm sieve. Most observations made are same as those made for film injection experiment.

Results and discussion (Expt. I – 6 to I – 10)

The temperature drop in the zone of injection (T_{w3}) indicates excess heat loss due to water evaporation. Reducing water content in the effluent could alleviate this problem. Table 5.4 depicts gas composition obtained from the equilibrium calculation (using NASA SP-273 code) and measured from the gas sampled from the exhaust, at the upstream of the water scrubber and cooled to room temperature.

Equilibrium calculation for combined fuel was carried out because the sample gas was drawn from the exhaust, far downstream of the reaction zone. Kerosene is expected to nearly completely burn up, immediately downstream of the dump combustor exit plane and only effluent gasification is expected to occur. Since, the equilibrium gas composition is sensitive to temperature variation, near steady composition could not be obtained. Temperature variation,

Gas Components	CO_2	CO	H_2	CH_4	H_2S	N_2	H_2O
Measured values	14.0 %	7.0 %	12.9 %	1.0 %	0.84 %	By diff	< 5 %*
Equilibrium calculation (Effluent + Kerosene)	8.8 %	9.16 %	12.76 %	---	---	50.17 %	17.0 %

* value at saturation pressure

Table 5.4: Equilibrium and measured gas composition for combined fuel injected in the reactor at $\phi = 1.85$.

even with small variation in flow condition due to self generating irregularity in effluent flow is inevitable in the case of this reactor because of negligible thermal inertia of the reactor walls. However, the gas composition obtained is a proof of effluent gasification.

The H_2S and CH_4 concentration deviates from equilibrium composition as was reported in case of black liquor gasification (Larson et al., 1996). Since H_2S is sparingly soluble in water, sample was drawn from the upstream of the gas scrubber.

The relative lower carbon conversion found in film injection case is because of higher residence time available to film adhering to the bed, prior to disintegration into finer particles which did not happen when effluent was splash injected.

The present technique of injecting effluent, although was successful, was found more complicated owing to involved moving parts and fluids transfer tubes.

Steady state wall temperature is essential for achieving steady gas composition, which could not be obtained in the present set of experiments. This can be achieved by either increasing the thermal inertia of the reactor or prevent flow variations. The first option is not opted for since the reactor (experimental setup) needs to be changed. However, flow variations can be brought under control by injecting effluent as spray with distribution over large surface area and prevent effluent flowing over the bed prior to evaporation. Therefore, effluent spray injection is considered in the next experiment.

5.3.1.3. Experiment Set 3 (I – 11 to I – 13): Spray injection

Separate experiments were conducted in transparent reactor (Scale 1:1) made of perspex sheet. The spray distribution over the plate is similar to that shown in the Fig. 5.14. Effluent with 60 % solids was injected (Expt. No. I – 11) from the location shown in the schematic view depicted in Fig. A5.7. Sustained combustion was obtained (with auxiliary heat input) however, the temperature fluctuated and so the gas composition. Nucleate boiling of effluent wetting the surface and excess effluent flowing over the surface was seen. It was inferred from this experiment that the effluent solid concentration needs to be raised to a level that can be injected without difficulties of feed line or atomizer blockage, poor atomization, caused due to high viscosity, the scaling and foaming characteristic of effluent, when heated close to its boiling point (~375 K). Increasing solid content, as was found in single particle experiments, would shorten evaporation time and avoid localized excess heat loss. Higher heat content and reduced evaporation load would result, combustion processes to occur in relatively hot zone where the particle heating rates are higher. Therefore temperature fluctuations are expected to reduce giving steady gasification. In addition it is thermodynamically more efficient to utilize low grade waste heat to concentrate effluent to higher solids rather than allowing evaporation to occur at higher temperature in the reactor.

In favor of using fuel with higher solid or reduced moisture contents, it was experimentally determined (*Sharan et al., 1996*) that gasification efficiency in the case of wood gasification increases from 64 % to 75 % by reducing wood moisture content from 35 % to 12 % and therefore waste heat from the process is preferentially utilized to remove moisture from the wood prior to gasification.

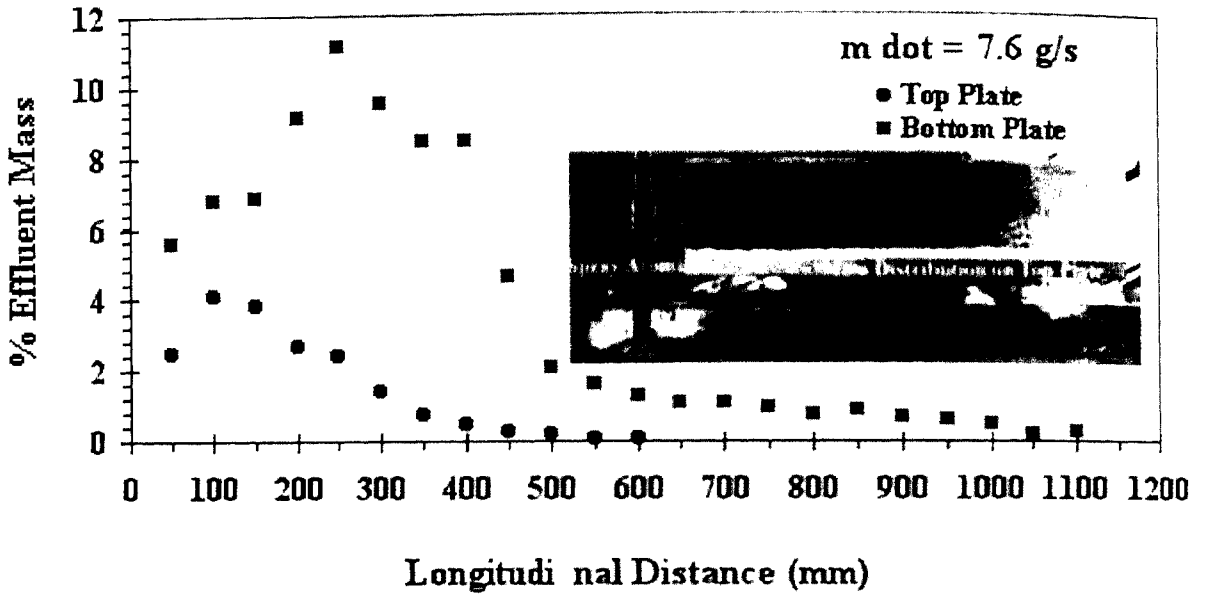


Figure 5.14: Mass distribution of effluent injected as spray on reactor walls

It was determined by conducting separate experiment to determine scaling and flowability of effluent with solid concentration in excess of 70 %. It was found that effluent below 78 % solids does not scale during heating up to 378 K and flows like thick oil or bitumen (at 373 K) but may cause blockage and deteriorate atomization quality, if temperature in the feed line dropped by 5 K. The difficulty may also arise due to blockage at the atomizer outlet if temperature increased. Effluent with 73 % solid was found to be more convenient to work with and was chosen for the experiments. Although the viscosity was about 300 mPa.s, fine atomization could be obtained by using indigenously developed low swirl (swirl no 0.5 ~ 1.0), internal mixing air blast atomizer (see Fig. A5.10). The mass distribution of 73 % solid effluent spray confined in the transparent reactor is shown in the Fig. 5.14.

Physical observations

Effluent was injected at the flow rate of 8 g/s and air at 12.5 g/s (air ratio = 0.42). It is clearly seen from Fig. 5.15(a) that with effluent injection the temperature in the zone of injection does not decrease with or without kerosene burner, except for 80 s transition duration due to switching off of kerosene burner and air flow rate adjustments. This was not seen in the experiments with 60 % solids effluent injection. In fact the local bed temperature increased indicating exothermic self sustained combustion even under sub-stoichiometric condition. As depicted in Fig. 5.15(b), the temperature in the injection zone (T_{w3}) increased or remained constant and rest at the downstream location decreased at the very slow rate of

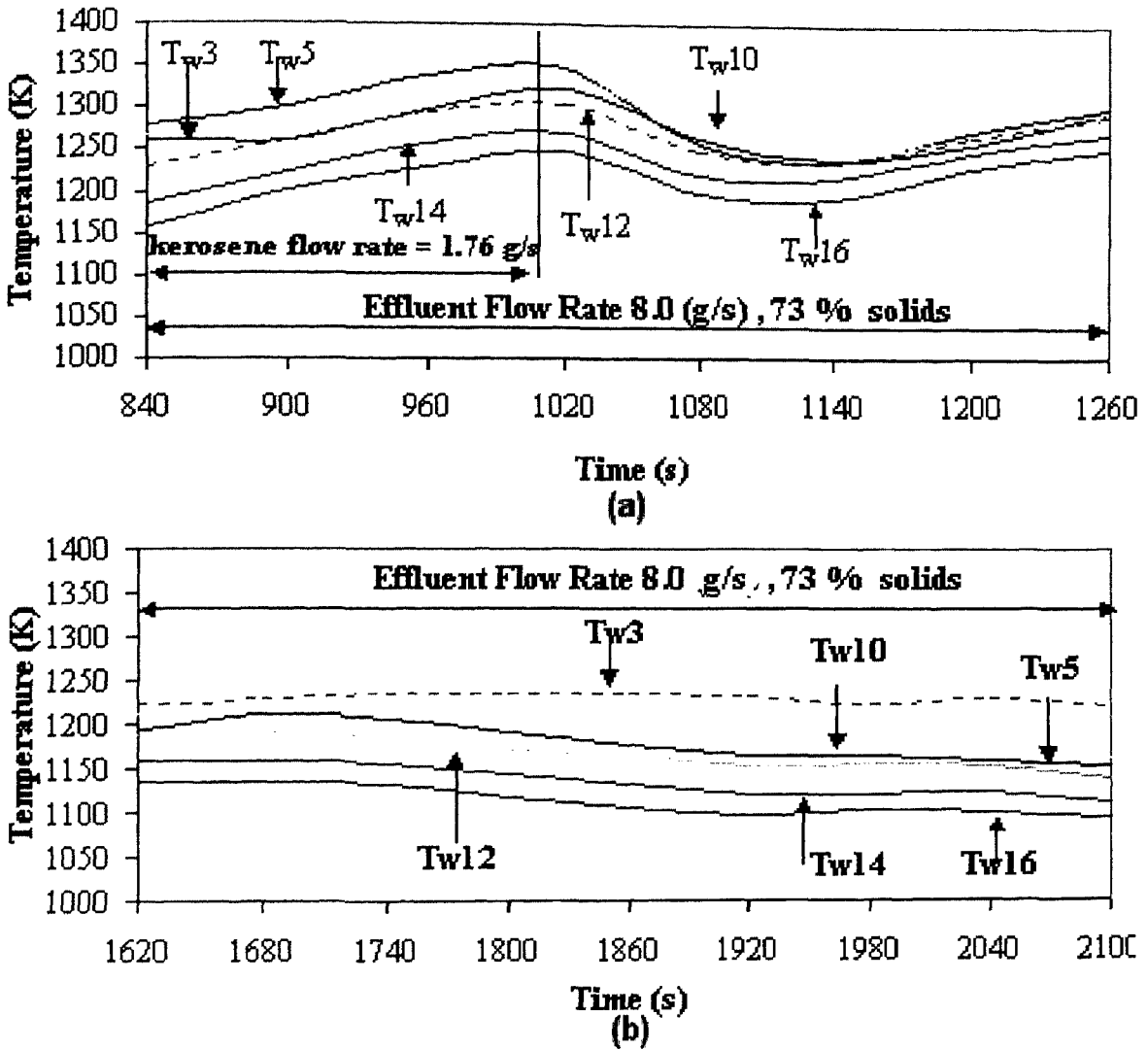


Figure 5.15: Bed temperature vs. time profile of effluent (73 % solid) combustion injected as fine spray.

5 – 6 C/minute. This fall in temperature is at lower rate as compared with ideal cooling profile shown in Fig. 5.5 indicating the exothermicity of the gasification. The fluctuation in temperature is not seen as is in the case of 60 % solid injection. Although, gasification condition was obtained, the gas composition was found poor.

The gas composition obtained is tabulated below:

O ₂	CO ₂	CO	H ₂	CH ₄
0 – 0.3 %	12 – 16 %	4 – 6 %	0 – 3 %	0 – 0.5 %

Through view ports volatile flaming could be seen along with glowing droplets. The confined hot wall of the reactor obstructed the spray and caused the droplets to form film.

This films of partly or fully converted effluent caused obstruction to the gas entrained droplets. Although, the residual ash could be easily scraped off the wall using high-speed air jets, it was found to disturb the steady state operations.

Post-experimental observations

Since the fragile ash found clinging to the wall disintegrated under aerodynamic forces, most ash found in the dump constituted fine particles as in Fig. 5.11(a). The duct passages were not blocked due to the use of high-speed gas jet scraper. The carbon conversion in the ash taken out immediately after experiment was measured to be better than 98 %. The residual ash was about 13 – 14 % of feed solids. The view port glass was coated with fume as shown in Fig 5.11(b). Other observations are similar to those of previous experiments.

Results and Discussion (Expt. I – 11 to I – 13)

For the injection of effluent with 60 % solids (Expt. No. I – 11) sustained combustion was obtained (with auxiliary heat input); however, the temperature fluctuated and so also the gas composition.

The temperature – time history shown in Fig. 5.15(a) indicates that the effluent combusted close to the injection point and contributed to the rise in local temperature (T_{wall}) in this zone. This is because of short ignition delay due to lower water content with reduced endothermic evaporation load. This was experimentally determined in the case of single droplet experiments. The particles therefore pyrolyze in this hottest zone of the reactor at higher heating rates resulting in higher yield of devolatilized products (*Kobayashi et al., 1977*), which are capable of combusting in the flames. The carbon conversion rate will therefore also be higher due to augmented heating rate due to volatile flaming. Higher carbon conversion was verified from the results of ash analysis for carbon. The effluent combustion could be self-sustained and the reactor temperature raised under sub-stoichiometric air with high carbon conversion.

The devolatilization at higher temperature and higher particle heating rate, that can be obtained by increasing solid content can reduce sulfur emission. This was experimentally found by McKeough et al. (1995) in the case of black liquor, which also has as high a sulfur content as distillery effluent (Table 1.1). This is another advantage of injecting effluent at higher solids besides possibility of improving the gasification efficiency as is the case of gasification of wood with low moisture content (*Sharan et al., 1996*).

The rate of decrease of temperature as shown in Fig 5.15 (b) is lower (5 - 6 C/minute) compared to similar experiments with 60 % solids in the same reactor where the fall in temperature is as high as 75 C/minute (see Fig. 5.9) in absence of kerosene flame. Although the fall in temperature is low, a support flame (15 – 20 kW) was found necessary with cold air instead of pre-heated air (as in the present case).

The confined hot walls of the reactor, while providing close proximity to the particles and reduced ignition delay, obstructed the droplets inspite of small spray angle and resulted in effluent blockage. This was detrimental to steady injection or stable spray flame or improved gasification. Therefore, it was found necessary to physically investigate the combustion processes in similar reactor but wider and better view.

Spray injection in open ended inclined reactor

A separate stainless steel reactor (only section II, scale 1:1), with back end open was used. The underside of the bed was heated up to 923 - 973 K using charcoal combustion, prior to injecting effluent with 73 % solids, heated to 373 K in the feed tank (see Fig. A5.11). The reactor did not simulate the exact experimental conditions since the back end was kept open for recording combustion processes. However, combustion air was sucked in the combustion zone under ejection effect caused by the effluent spray itself. Initially, only the lower bed was heated to 973 K; however, the top and two sidewalls of the reactor were heated due to heat release from effluent combustion. During spray injection the volatiles ignited with puff filling the complete reactor. This caused the reactor top wall temperature to increase to 1123 – 1223 K. Figure 5.16 shows the direct pictures (frames of video recording) of the events occurring during injection after the reactor walls temperature rose. A lot of individual particles are seen glowing in the above frames. Tracking a single particle or group of particles or lump, the combustion time could be approximately obtained. The residence time of smaller particles was less than 100 ms. Particles with diameter, $d_p \sim 1.5 - 2$ mm were seen to glow for about a second. Figure 5.16 depicts sequential events of effluent spray combustion. With the wall temperature in the range of 1123 – 1223 K combustion of a large number of single particles is seen. Volatile flame initiation and propagation is also seen; however the flaming was discontinuous unlike most volatile fuel spray flames.

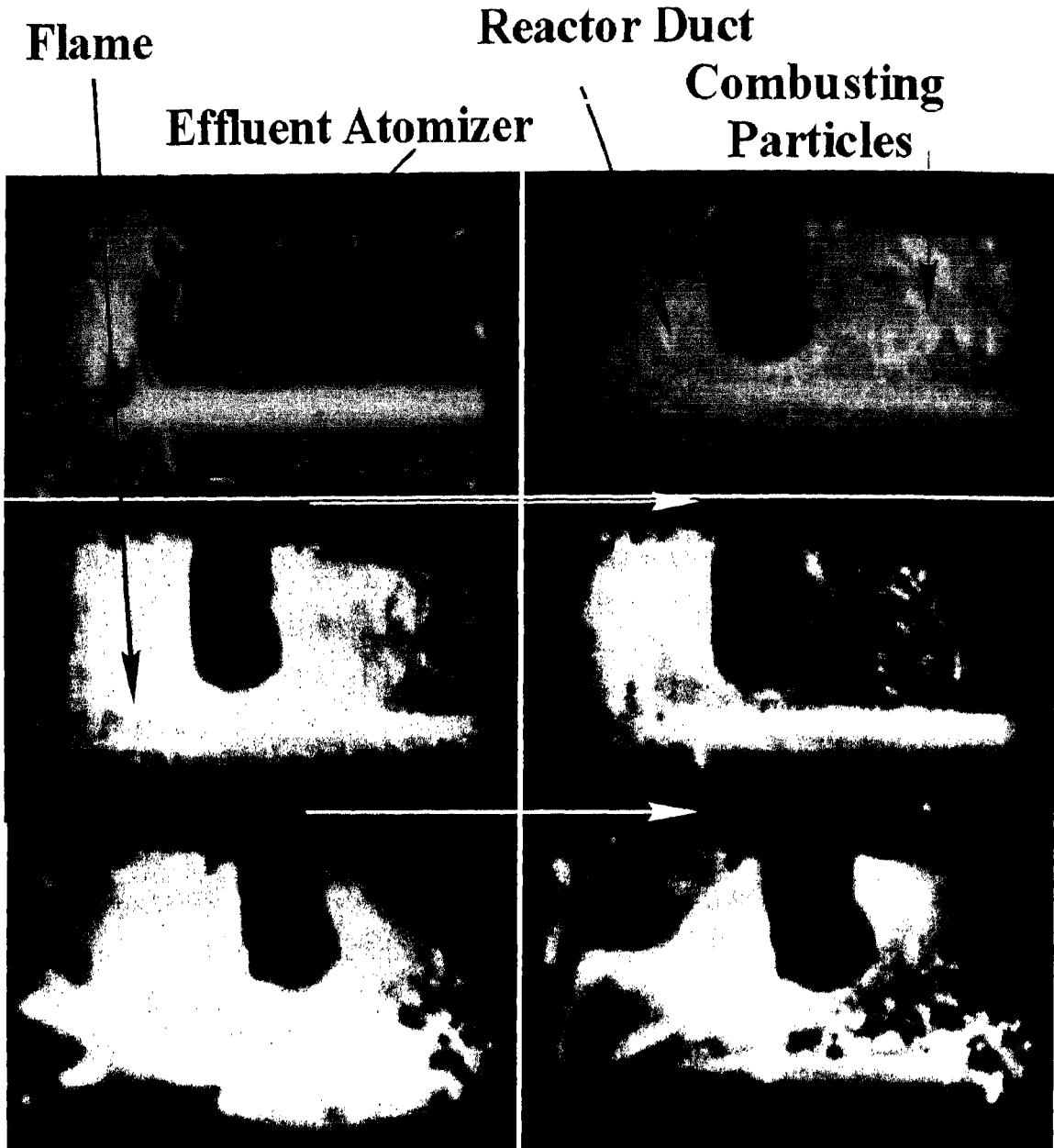


Figure 5.16: Concentrated effluent spray combustion in a heated reactor.

The confined walls of the reactor obstructed the flow and caused partial blockage of already small cross section at the downstream portion of the reactor. It was seen that during the volatile flaming, seen as discontinued puffs, the spray flaming also occurred. This clearly indicated the possibility of spray combustion in hot gas entrained mode. It was found necessary to verify this through experiments conducted in heated space without any wall obstruction.

5.4. Conclusions

Three sets of experiments, classified based on the effluent injection methodology, were performed and their experimental observations and measurements are discussed in the present chapter. Except for the first experiment (I-1) sustained combustion and complete carbon conversion was obtained in all the 12 experiments. A support flame was found necessary in the zone of injection to augment evaporation rate and ignition under gasification conditions. Increasing effluent solids, up till the limits of practicality of injection can help eliminate use of support flame.

The reactor geometry served the purpose of providing adequate heat flux and residence time for heating, drying and subsequent combustion of effluent (with 60 and 73 % solids). The reactor had negligible thermal inertia and was sensitive to small variations in flow conditions responding by variations in temperature and gas composition.

In the film injection experiment, the disintegration of the film into fine particles led to large-scale gas entrained particle combustion and resulted in high carbon conversion (98 – 99 %). However, the initially obtained steady state combustion (stage I, see Fig. 5.7) could not be sustained due to the initiation of effluent clogging process in the cold zone. It was concluded from these experiments that to attain steady state combustion, consistent effluent injection is essential. Through separate experiments it was established that effluent be injected directly in the hot zone to avoid clogging.

Effluent injected directly on the hot surface ($T_s > 873$ K) as coarse droplets, remained mobile on the bed due to spheroidal evaporation, causing particles to float over vapor film. Injection location needed to be varied laterally, in a repetitive cycle, in order to prevent localized fall in temperature due to evaporation and thus avert initiation of clogging process. Effluent could be continuously injected to obtain steady state combustion; however, consistent gas composition could not be obtained because of the variation in reactor bed temperatures. Such small variations are caused due to low thermal inertia of the systems and high evaporation loads and the shift of evaporation zone due to the injection methodology.

Controlling the shifts in evaporation zone by obtaining better effluent distribution on the bed, variation in temperature can be brought under control. It was also found necessary to inject effluent with 73 % solids since 60 % solid spray resulted in spatial and temporal irregularities in the combustion process.

The spray combustion of higher solids (73 % solids), without support flame could provide exothermic heat profile and maintain steady reactor temperature during injection period under sub-stoichiometric conditions; however, the confined reactor space obstructed sustained spray combustion, also investigated through separate experiments with open end reactor.

The possibility of sustained spray combustion of concentrated effluent was seen in this experiment. Since the reactor cross section is small the spray interaction with hot gases is inadequate. To overcome this, spray injection is required to be carried out in a large cross section area reactor. Therefore, a new reactor is proposed which can accommodate the spray of concentrated effluent and unaffected by rapid temperature variations in order to achieve steady state gasification.

Experiments in Modified Vertical Reactor

6.1. Introduction

The heat release from volatile oxidation in an effluent spray is preferred from the point of view of providing exothermic heat envelope for subsequent gasification reactions, which are endothermic in nature and favored at higher temperature. It was also found in the single droplet combustion study that *the yield of the volatile is higher if pyrolysis occurred at higher ambient temperature, rendering higher char conversion rate*. The efforts of spray combustion experiments at 50 % and 60 % solids leading to pool combustion in inclined reactor reported earlier were not successful. However, the possibility of spray combustion of effluent with 73 % solids in the inclined reactor were particularly useful in determining the course of further gasification experiments. Injecting concentrated effluent as spray in the small cross section of inclined reactor prevented droplet interaction with hot gases and the volatiles were seen to be combusting as discontinuous puffs. To overcome this, experiments were planned in a reactor with larger cross section area with the injected spray with appropriate mass distribution subject to aerodynamic interaction. The vertical reactor used in the earlier experiments was found apt for the experiment with the primary aim of achieving steady state gasification.

From a gasification point of view, fine effluent atomization and high degree of air interaction with spray is essential to ensure heat release by (volatiles + char oxidation) and create gasification conditions close to injection point. In such conditions, the heterogeneous gasification reactions occur in gas-entrained particles as well as in the bed if allowed to accumulate. The experiments are planned on these lines.

Plan of the chapter

Section 6.3 describes the design basis of the experimental set up. Section 6.4 describes the experimental set up. The details of the setup including the air blast atomizer and the mass distribution at two different swirl intensities are presented in Appendix A6. The method of operating the gasification facility is briefly discussed in section 6.5 and the detailed procedure is presented in Appendix A6.2. Section 6.5 outlines three experiments conducted with their flow parameters. The results and discussion of all these experiments are presented in section 6.6. *The most important conclusion of the present work is the possibility of self-sustained gasification of effluent spray is obtained at 73 % solids.*

6.2. The Design of experimental set-up

The experimental reactor is designed with considerations given to the following requirements: 1) Cross section to accommodate spray 2) high thermal inertia of the reactor to minimize temperature fluctuations, 3) provide high temperature in the injection zone 4) allow the formation of bed 5) create regenerative heating of the bed by recirculating the product gases, and 6) introduce a wet gas scrubber, an ejector and a flare with a pilot burner.

The first two requirements can be satisfied by the choice of a cylindrical reactor used in the earlier experiment in which effluent spray is injected in a top-down manner. To fulfill the third requirement, auxiliary burner can be fixed to the first shell (from top) with tangential gas outlet. If auxiliary burner is kept operational during injection, the spray gets entrained in the hot gases, augmenting evaporation rate and thus reducing ignition delay. The gasification air can be provided with low intensity swirl to improve spray mass distribution and air interaction. This will push relatively large droplets towards the hot wall. A grate provided at the bottom of reactor with holes (of 4 – 5 mm diameter) can prevent larger char particles (or lumps formed by droplets accumulated on the wall) and form char bed. Although, the largest carbon conversion is expected when the particles are entrained in the gas, the larger particles or lump will be converted on the bed. The bed height can be controlled by removing excess material by operating the grate (by means of an actuating mechanism). This design will ensure higher conversion or (gasification) when hot gases pass through the bed of char. This bed can be regeneratively heated by allowing the product gases to pass through the annular passage provided by inner metallic and outer ceramic wall of the reactor. The details of the setup are given in Appendix A6.

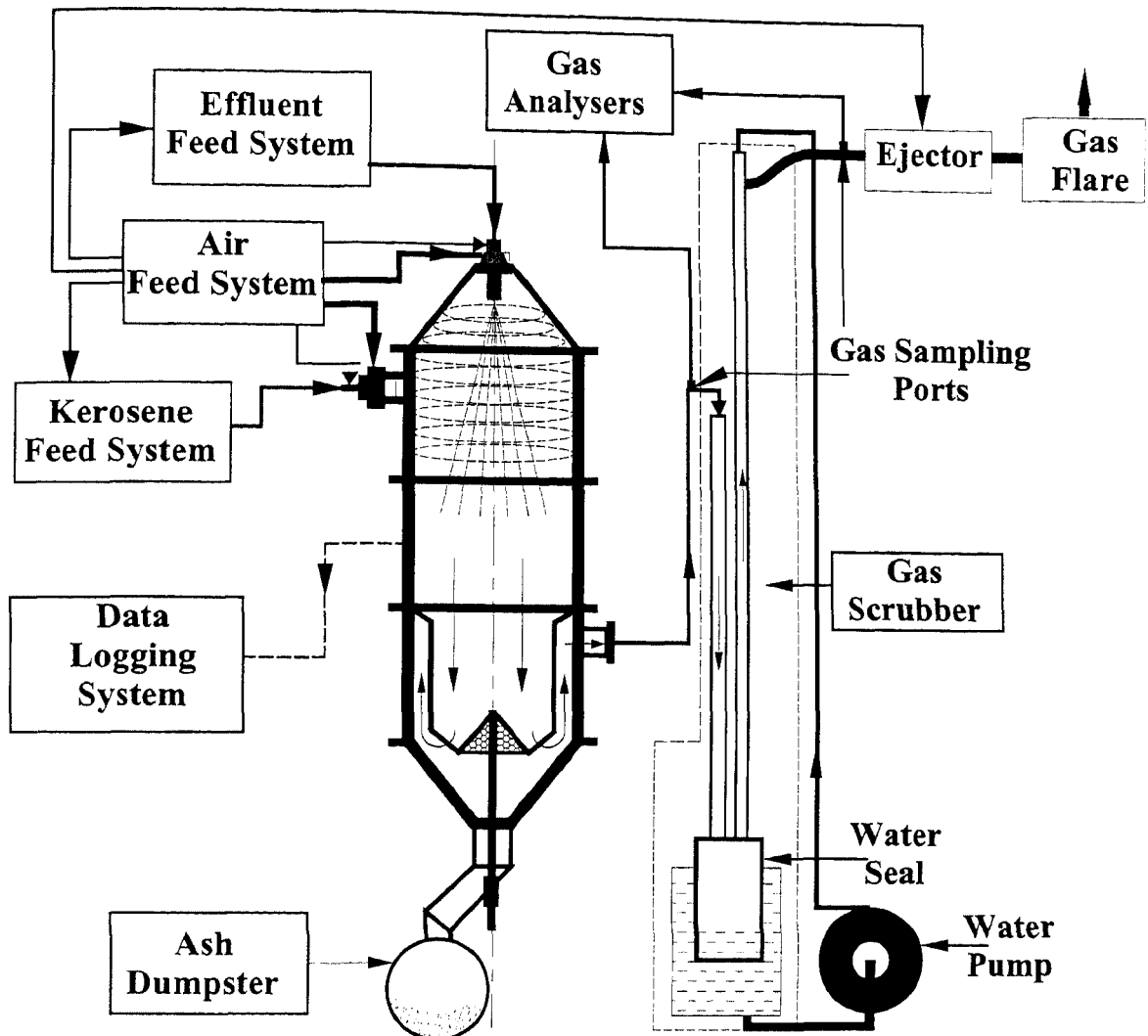


Figure 6.1: Schematic view of the experiment setup

6.3. Experiment Setup

The schematic of the experimental setup is shown in Fig. 6.1. In contrast with the first set of experiments conducted in the vertical reactor, the fine spray of concentrated effluent (73 % solids) is injected vertically down from the top of the reactor. Other components of the experimental setup namely effluent, kerosene (auxiliary fuel) and air feed system, gas scrubber, gas ejector, gas flare, instrumentation are the same as in the earlier experiment on inclined plate reactor. The details of the components are given in Appendix A6.

The auxiliary burner is fixed to the cylindrical top shell such that the hot gases enter tangential into the reactor. The combustion/gasification air is introduced co-axial to the spray and an efficient interaction between the two is ensured. A conical grate with 5 mm

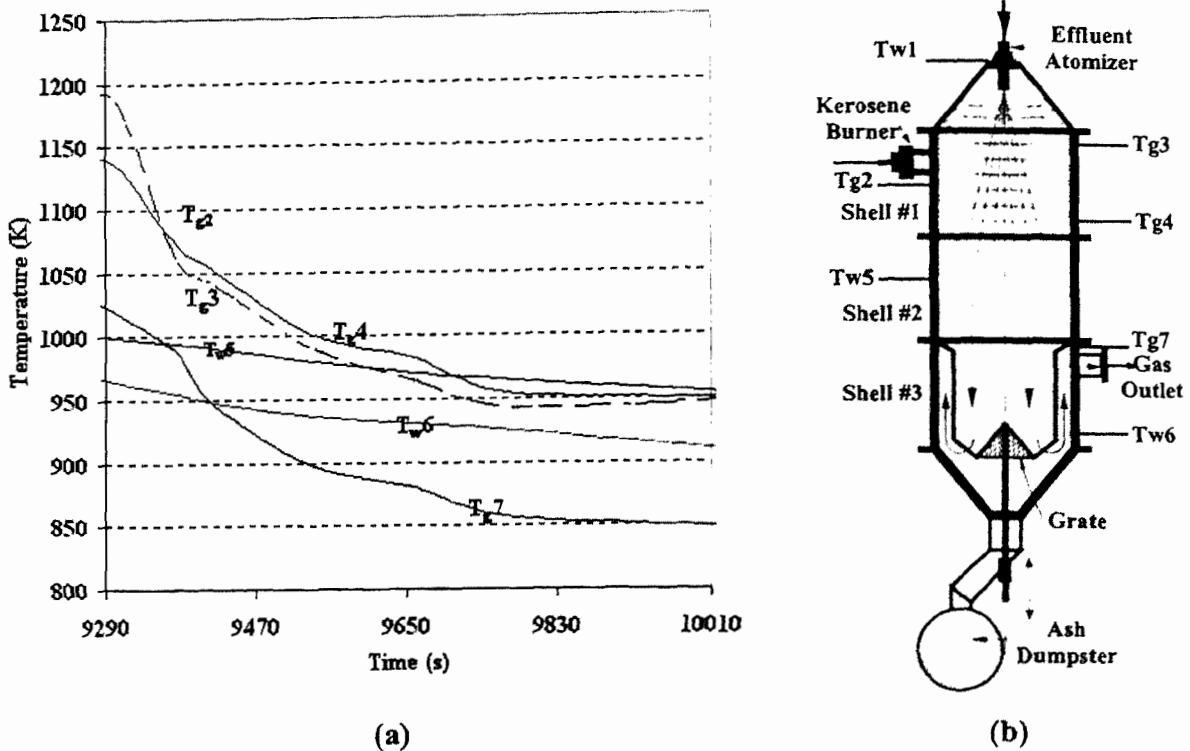


Figure 6.2: (a) Typical plot of reactor cooling history vs. time obtained during trial experiment, (b) Thermocouple locations in the reactor

holes on its surface is provided in the bottom shell with an arrangement to lift and rotate it in order to effectively transfer residue into a 70 litre dump and maintain fixed height of the bed. The product gas flows through the outer annular space in the lower shell and exit the reactor. The gas is scrubbed with water and is burnt in the flare.

6.4. Experimental Procedure

The experimental procedure is divided into two parts as in the case of earlier experiments: (1) initial setup procedure including preparation of feed systems, reactor, instrumentation and (2) startup procedure. The startup procedure of the experiment is divided into two phases: **phase I** is 'reactor heat up phase' and **phase II** is effluent injection phase. These phases are timed and are in a sequence as in earlier experiments. They are carried out only after initial setup procedure is completed. Both the parts of the experimental procedure are described in Appendix A6.2.

Table 6.1 shows typical temperatures measured in different sections of the reactor after an interval of about 10 minutes, at the end of phase I operation. Typical kerosene flow rate during the heat up phase for all the experiments is 2.0 - 2.1 g/s and air flow rate is set at 32

to 33 g/s near stoichiometry. The gas composition obtained is: $O_2 = 0.5 \%$, $CO_2 = 13.5 \%$, $CO < 0.1 \%$ (dry basis).

Reactor Shell	No 1	No 2	No. 3	Exhaust duct
	T_w	T_w	T_w	T_g
re (K)	1133	1073	1023	1050

Table 6.1: Shell temperature prior to effluent injection.

Fig. 6.2 (a) depicts cooling profile of the reactor under no-flow condition. Fig. 6.2 (b) depicts the location of different thermocouples in the reactor. The wall temperature is measured at 25 mm depth from the inner surface of the wall. T_{g7} is the exhaust gas temperature. Variation in gas temperature occurs at a faster rate than wall temperature and therefore its cooling profiles are compared with those obtained during effluent injection to verify exothermicity of volatile and char oxidation reaction.

6.5. Observations and Results and Discussion

Three experiments were recorded with the first phase being the heat up phase and second being injection phase. Table 6.2 shows various flow rates and the results of the three experiments during the injection phase.

Experiments Number	Solids %	Effluent Injection (phase II)		Flow Rates \dot{m}_a g/s			Sustained Combustion or gasification		Complete Combustion	Remarks
		\dot{m}_{eff} g/s	Injection Methodology	Phase II			Combustion	Gasification		
				Kerosene	Total Air	Eq. Ratio				
V-1	73	8.0	Spray	0.7	17.5	0.43	Yes	No	Yes	Carbon conversion 95 – 96 %, $T_w \sim 953 - 1053$ K
V-2	73	9.0	Spray	0.0	9	0.3	Yrs	Yes	Yes	
V-3	73	10	Spray	0.7	15	0.31	Yes	Yes	Yes	

Table 6.2: Details of the experiments conducted

Figure 6.3 depicts the temperature and gas composition plot recorded during effluent gasification. The auxiliary heat input was zero and effluent was injected at 9 g/s with sub-stoichiometric airflow. Three thermocouples located in the first shell respond in a similar

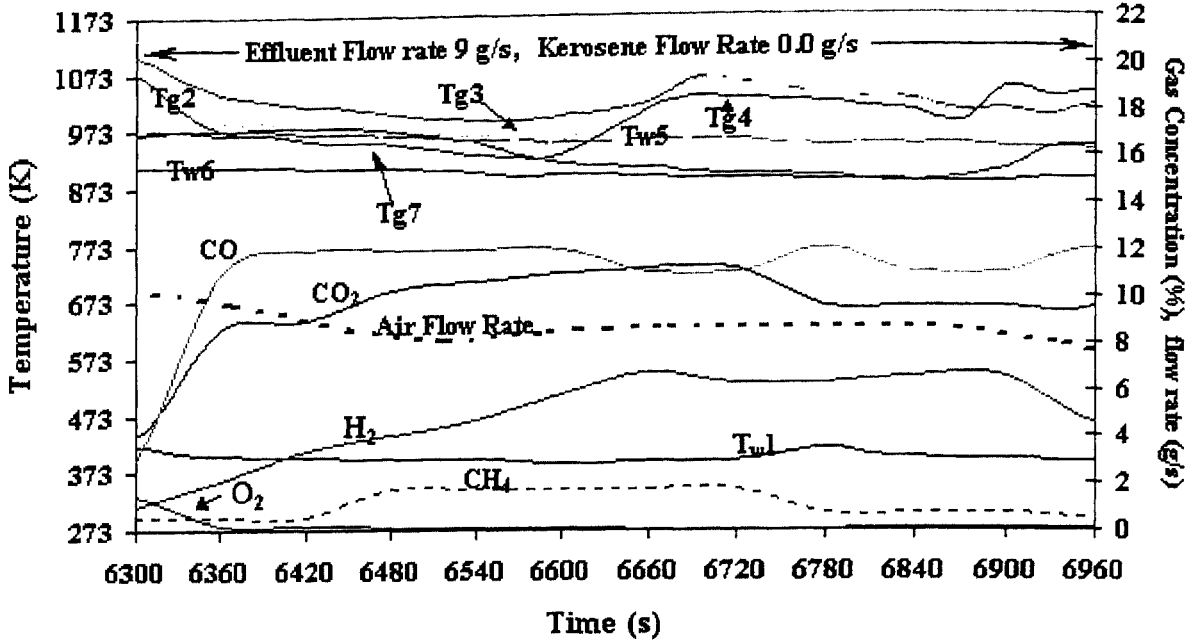
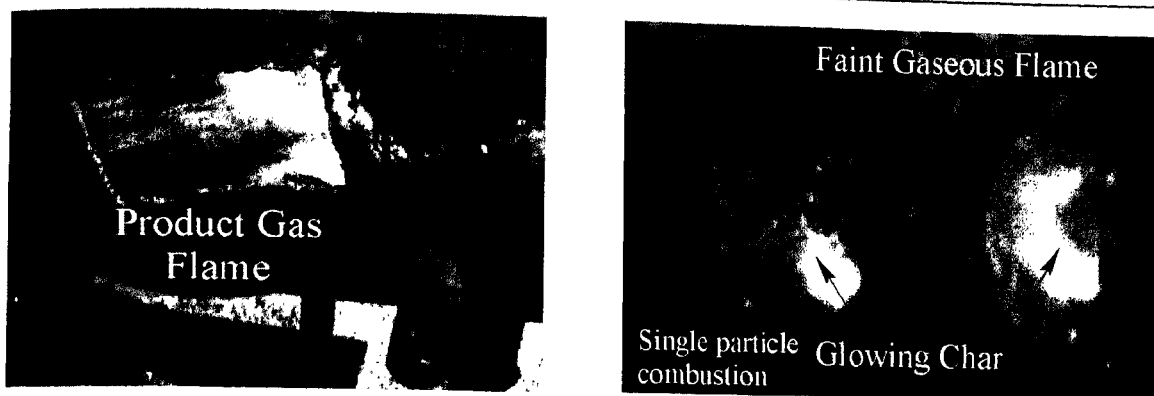


Figure 6.3: Bed temperature, gas composition and air mass flow rate vs. time history obtained at various locations in the reactor during Phase II (Expt. No. V -2)

manner. The initial drop in gas temperature seen is due to stopping of the kerosene flow. However, the volatile and char oxidation in the zone prevented further drop in temperature. This can be seen by comparing the cooling profile, depicted in the Fig. 6.2 with the temperature profile in Fig. 6.3. The wall temperature is nearly constant. Oxygen fraction steeply falls to a value close to zero indicating the attainment of gasification condition. Other gas fractions have sharply increased and in about one minute of injection, the CO has risen to about 12 % and remained almost constant until the effluent injection was discontinued after 11 minutes. H₂ fraction has increased and attained a maximum value of 6.7 %. CH₄ initially has increased to 1.75 % but later dropped to 0.5 %.

The gasification (or cold gas) efficiency, defined as the ratio of the total heat input to the heat content of the producer gas, was found to be in the range of 58 – 55 %.

Fig. 6.4 (a) depicts direct picture of product gases combusting in the flare. The grate is shown in Fig. 6.4 (b). These photographs were taken towards the end of effluent injection. Faint flame and individual glowing char are seen. A small fraction of char, glowing on the grate is also seen. The amount of material on the bed is very little and it indicates that most of the residue passed through the grate and the gasification of char particle occurred in gas-entrained mode.



(a) Sustained combustion of product gas seen from a cutout portion of exhaust flare.

(b) An inside view of the reactor as seen from the top.

Figure 6.4: Direct pictures obtained during gasification phase

The ash dump was maintained at room temperature and therefore no further chemical transformation in the residue could have had occurred. The carbon conversion found was therefore only could have occurred in the gas entrained mode.

Effluent was injected only after it was heated to 373 K. This was necessary in order to have fine atomization. The atomizer performance deteriorates with decrease in effluent temperature below 363 K. Single droplet combustion was more prominent; however, faint broad flame was also visible. This combustion behavior was distinctly different from that of stable flame, as found in the case of the coal-water-slurry, a near precursor to effluent.

6.5.1. Post-Experiment observations

The residue collected in the dump consisted of ash particles with and without carbon. The colour of completely converted ash was pale brown and distinctly different from the pale black of ash containing carbon. A finite sample of residue was sieved through a series of sieves (75 ~ 500 μm) to determine the range of droplet size.

The size distribution is in the following table:

Mesh Size (μm)	600-700	600-425	355-425	250-355	180-250	125-250	< 125
% Weight	6 %	19 %	22 %	17 %	8 %	6 %	14 %

The carbon conversion was determined to be about 94 %, which is low as compared to that found in inclined plate reactor experiment. The total weight loss was found to be 86.5 %. Unconverted particles were found in all the size range; however, when observed under stereomicroscope at 75X magnification, the number of converted particles increased with

the decrease in size. This indicated the need for fine atomization for achieving high carbon conversion. Physical investigation revealed that the completely converted ash particles were spherical and porous with no melt layer on the surface. Those particles containing carbon were hollow with a very thin (less than 20 μm) outer layer that was spherical and swelling was evident. Particles above 300 μm were nearly ellipsoidal.

Severe fuming was found in the upper shell since the sights were found getting smudged blurring the visibility. Tarry substances were not found in either the sample gas line, tubes, including scrubbing water, filter, chemical driers, or surfacing on the scrubber water even after 3 to 4 hours of cumulative experiment.

It was found from separate experiments that if the effluent flow was discontinued, obtaining the gasification condition back was difficult and auxiliary burner was required. From these experiments, it was conjectured that keeping a support burner operational is necessary to facilitate operational aspects and improve gasification.

Experiment V-3 was conducted with auxiliary burner operational at power levels in the range of 25 – 30 kW, which was the minimum value specific to the burner in order to achieve stable flame. The local gas temperature increased by about 150 K and maintained wall temperature in the range of 923 – 973 K. There was no major change found in gas composition measured except for improvement in carbon conversion that was found to be 95.5 - 96 %.

The residue of the experiments was subject to the extraction of potash present in the form of sulfide, sulfate, chloride and carbonate. About 8 – 12 % of the injected effluent formed ash of which 74 – 75 % was soluble in hot water. The filtrate was slightly alkaline and on evaporation, white crystals of potassium salts, consisting of 65 – 68 % potassium sulfate, 15 – 17 % potassium chloride and 8 – 10 % of potassium carbonate were recovered.

6.6. Conclusions

Effluents with 73 % solids were injected as fine spray in a top-down firing mode in a vertical reactor to obtain gasification at low temperature and atmospheric pressure. Single particle combustion with enveloping faint flame was seen unlike stable flame found in coal water slurry spray combustion. Sustained gasification of gas entrained particles occurred at reactor could be achieved without the support of auxiliary fuel. However, additional heat input facilitated operation and improved carbon conversion. The typical gas fractions

obtained during gasification condition (air ratio = 0.3) were $\text{CO}_2 = 10.0 - 11.5 \%$, $\text{CO} = 10.0 - 12.0 \%$, $\text{H}_2 = 6.7 - 8.0 \%$, $\text{CH}_4 = 1.75 \%$ $\text{H}_2\text{S} = 0.2 - 0.4 \%$ and about 2 % of saturated moisture. The carbon conversion obtained was in the range of 95 ~ 96 %. These experiments have provided the conditions for gasification.

The potassium salts extracted from the ash by simple water leaching process can provide additional economic benefits.

Long duration gasification experiments are necessary and can be taken-up as technology development work. Effluent with as high solid concentration as can be injected as fine spray is advocated.

Overview and concluding remarks

The motivation for the present work has come from the necessity of devising an eco-friendly thermochemical conversion technique, that can adequately dispose distillery effluent generated in huge volume to low volume ash, by combining it with a concept of waste-to-energy and hence make it economically attractive. Even though the need for this was realized even during the early part of this century, the seriousness of the magnitude of the problem has enhanced in recent times with the environment regulations becoming more stringent and the control of effluent discharge made mandatory. The lack of understanding of the basic combustion processes associated with the effluent combustion, non-availability of basic data on thermophysical and thermochemical properties of the effluent and dearth of prior experience in practical effluent combustion, have made it appropriate to plan the present work in two parts. The first part is related to developing the understanding of basic effluent combustion processes through experiments on single suspended particle in quiescent hot air and the modeling efforts aimed at predicting the observed results. This was a starting point for studies on ignition and combustion of distillery effluent clarifying the role of solids concentration, drop size and ambient temperature. The second part involved experiments on combustion and gasification of effluent (with 50 %, 60 % and 73 % solids concentration) in laboratory scale reactors with a throughput of 4 – 10 g/s, at atmospheric pressure and reactor temperature of 973 – 1123 K.

It was found from the basic droplet experiments that effluent burns with two distinct regimes of combustion, flaming and char glowing. The ignition delay ' t_i ' of the droplets increased with size as in the case of non-volatile droplets, while that of 100 % dry spheres are independent of size. The ' t_i ' decreased with increase in solids concentration. The ignition delay has shown Arrhenius dependence on temperature. The initial ignition of the droplets and dry spheres led to either flaming or flameless (heterogeneous) combustion, depending on the ambient temperature in the case of sphere and on solid concentration and

ambient temperature, in the case of liquid droplets. The weight loss found during flaming combustion was 50 – 80 % while during char glowing, 10 – 20 % depending on the ambient temperature. The flaming time ' t_f ' is given by $t_f \sim d_o^2$, as in the case of liquid fuel droplets and wood spheres. The char glowing time ' t_c ' is given by $t_c \sim d_o^2$ as in the case of wood char, even though the inert content of effluent char is as large as 50 % as compared to 2 – 3 % in wood char and the surface area two order of magnitude lower. In the case of initial flameless combustion, the char combustion rate is found lower than in the presence of enveloping flame. The heterogeneous char combustion in quiescent air in furnace conditions has been modeled using one-dimensional, spherico-symmetric conservation equations and the model predicts most of the features of char combustion satisfactorily. The measured surface and core temperatures during char glowing are typically 200 to 400 K higher than the furnace temperature.

Based on the results of single droplet combustion studies, effluent spray experiments were conducted in a laboratory scale vertical reactor (throughput - 4 to 10 g/s) with the primary aim of obtaining sustained spray combustion of effluent with 50 % and 60 % solids (calorific value 6.8 – 8.2 MJ/kg). Three sets of experiments were conducted with effluent injection (1) from the wall with no auxiliary heat input, (2) with auxiliary heat input and (3) within kerosene enveloping flame. Although individual particles in the spray periphery were found to combust, the heat release was inadequate to maintain heat balance in the core due to evaporation and therefore, sustained spray combustion was not achieved in all the three sets of experiments even with fine atomization. While conducting the third class of experiments in a separate inclined metallic reactor, sustained combustion of pool of effluent (with 60 % solids), resulted from the accumulated spray, seemed to permit large conversion of carbon. It was therefore concluded from this experiments that complete conversion of effluent with minimum of 60 % solids is possible, perhaps as effluent pool or film spread on hot inclined flat plate. This led to the adoption of a concept of effluent combustion in which the residence time is controlled by varying the plate inclination over which effluent flow as film and the regenerative heat transfer from the product gases supplies heat for endothermic pre-ignition process occurring on the plate.

Combustion and gasification experiments conducted in an inclined plate reactor with rectangular cross section (80 mm height x 160 mm width) and 3000 mm long are presented in chapter 5. A support flame is found necessary in the injection zone in addition to the

regenerative heat transfer. Effluent with 60 % solids was injected as film on the reactor bed. This film disintegrates into fine particles due to stretching and shear stripping induced by aerodynamic force. Combustion of individual particles provided exothermic heat profile and resulted in high carbon conversion. It was found that effluent clogged when injected in the cold zone of the reactor and hindered system from attaining steady state. While effluent injected directly in the hot zone caused it to remain mobile due to the spheroidal evaporation and thus assuaging this problem. Improved mass distribution was achieved by displacing nozzle laterally in a cycle, actuated by a mechanism. Consistent injection led to sustained effluent combustion with resulting carbon conversion in excess of 98 %. It is concluded from these experiments that effluent with minimum 60 % solids can combust in a self-sustained mode. The typical dry gas fractions obtained during gasification condition (air ratio = 0.3) were $\text{CO}_2 = 14.0 \%$, $\text{CO} = 7.0 \%$, $\text{H}_2 = 12.9 \%$, $\text{CH}_4 \sim 1 \%$, $\text{H}_2\text{S} = 0.2 \%$. This composition varied due to variation in temperature ($\pm 30 \text{ K}$) attributed to combined effect of local flow variations, shifting zones of endothermic processes due to flowing of evaporating effluent over a large area. In order to avoid this problem experiments were conducted by injecting effluent at higher solids (73 % solids is found injectable). The effluent was found to combust close to the injection location due to the reduced ignition delay with the lower endothermic evaporation load helping to raise the local temperature. This caused pyrolysis to occur in this hottest zone of the reactor at higher heating rates resulting in larger yield of devolatilized products and improved char conversion rates. The effluent combustion was found to sustain temperature in the reactor under sub-stoichiometric air without support of auxiliary heat input and achieved high carbon conversion besides spray ignition. These results inspired the use of higher concentration effluent, which is also known to have improved gasification efficiency due to reduction in moisture fraction in the case of wood. The recent studies on the effect of the increased solids concentration in the case of black liquor combustion in the recovery furnace have revealed the reduction of sulfur emission. The required concentration can be carried out using low-grade waste heat from the reactor itself. It was found through experiments that, even though spray ignition occurred at this concentration, confined reactor space prevented the spray from attaining sustained combustion. This caused the need for conducting experiments in the new reactor, which has adequate thermal inertia; essential to prevent localized temperature variations to achieve steady state gasification condition and required space to accommodate the spray.

The results presented in chapter 6 relate to experiments conducted in a vertical reactor in which effluents with 73 % solids were injected as a fine spray in a top-down firing mode. Single particle combustion with enveloping faint flame was seen unlike stable flame found in coal water slurry spray combustion. Sustained gasification of gas entrained particles occurred at reactor temperature in the range of 950 K – 1000 K and sub-stoichiometric air ratio 0.3 – 0.35 *without the support of auxiliary fuel*. The carbon conversion obtained was in the range of 95 – 96 % with the typical dry gas fractions obtained during gasification condition (air ratio = 0.3) were $\text{CO}_2 = 10.0 - 11.5 \%$, $\text{CO} = 10.0 - 12.0 \%$, $\text{H}_2 = 6.7 - 8.0 \%$, $\text{CH}_4 = 1.75 \%$ $\text{H}_2\text{S} = 0.2 - 0.4 \%$. These experiments have provided the conditions for gasification.

The potash recovery in the form of potassium sulfate, potassium chloride and potassium carbonate from the ash through simple extraction or water leaching process was found to recover these chemicals to as high an extent as 70 – 75 % of total ash. These chemicals are potential fertilizers and their recovery can contribute to the economic benefits of the process.

In summary it is concluded that increasing the solid concentrations to as high levels as acceptable to the system (~ 75 %) and introducing as a fine spray of heated material (~ 363 K) into furnace with air at sub-stoichiometric conditions in a counter current reactor will provide the conditions of a gasification system for vinasse and similar effluent material.

It is time to reflect on the way research developed over the duration of research. The difference between the initial configuration and the final one is the nature of fuel injection and char management. It would appear one could have skipped the two year effort on the inclined reactor. However, the quirks of thinking process are beyond logical framework; the only satisfaction is that this research has contributed not only to systems, which work, but those which do not. The latter part is quite often as important in a developmental process.

A few words on the scope of future work would be appropriate. The present work is an attempt at constructing the scheme for utilizing distillery effluent as a fuel for gasification. Industrial scale gasification experiments are required to be carried out along with the fundamental and applied research related to the design of unit components of gasification system, imperative to produce gas with consistent composition and capable of being fed into the prime mover is the future work of significance.

Vertical Reactor: The Experimental Setup and Procedure

A4.1. The Experimental Setup – 1

A4.1.1. The Reactor

The experiments carried out on effluent atomization were useful in determining the length of the spray, spray angle, mass distribution and approximate size of the droplets. These data were helpful in approximately deciding the diameter of the reactor based on residence time for heating drying and devolatilization processes that were extrapolated from the single particle combustion experiments.

The direct pictures of the assembled reactor are shown in Fig. A4.2. The reactor outer shell is fabricated of 8 mm thick mild steel plate. The inside surface is lined with 60 mm thick, high temperature refractory material.

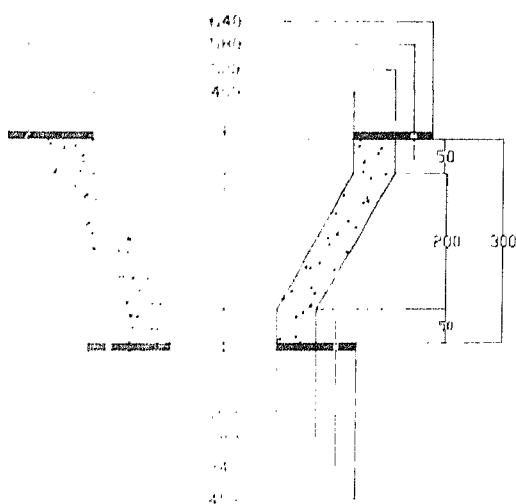


Figure 4.2 a Conical Shell

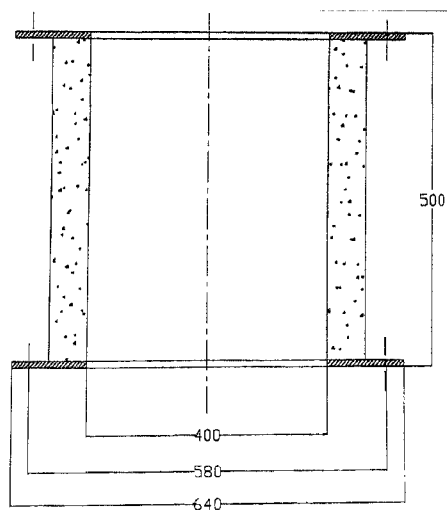


Figure 4.2 b Cylindrical Shell

Figure A4.1 Dimensional view of the conical and the cylindrical shells used in the reactor

The castable refractory material has typical working temperature of 1350 C. Its chemical composition is 60% Al_2O_3 and 5% Fe_2O_3 with calcium aluminate binder as base. This material is inert to most reducing gases. However, the working conditions in the reactor are severe because of the presence of large concentrations of alkali as well as chlorine in the effluent. The average thermal conductivity of the material is in the range of 0.2 to 0.3 W/m

K in the working temperature range (1000-1450K). Maximum heat loss was found to be less than 2.3 kW through all the reactor walls under steady state inside average reactor temperature of 1100K. The reactor shells are provided with holes, view ports and flanged inlets for burner assembly, sight glass, effluent atomizer, thermocouples, pressure tappings, and gas sampling port at appropriate locations.

All joints in the assembly of the reactor were tested for 100% leak proof. Joints with high working temperature were sealed with the help of high temperature resistant gaskets. Reactor was assembled on a robust support structure in vertical position as shown in Fig. A4.2. The assembled reactor was made almost adiabatic by wrapping it with thermal insulation or a blanket of high-density alumino-silicate fibre (Al_2O_3 35%, SiO_2 47%, ZrO_2 18%,) of total thickness of about 100 mm. The thermal conductivity of the insulation material is in the range of 0.05 and 0.1 W/mK and outer skin temperature never exceeded 45 °C.

The product gases were exhausted in the atmosphere. Wet scrubbing of the product gases was not provided in order to simplify the system. The hot product gases were exhausted through bundles of 8 mm internal diameter tubes into an open-end annular tube of larger diameter. This arrangement could produce ejection effect due to which atmospheric air was sucked in and mixed with the product gases into the mixing zone. Down stream of the mixing zone, an LPG burner was fixed such that the flame protruded into the length of the tube and helped in completely oxidizing product gases.

Each shell was provided with set of 4 x 2 holes of ¼" diameter amounting to the total of twenty through holes at different peripheral locations along the vertical axis of the reactor. Threaded end of the thermocouple tube with protruding junctions were fixed on the collars welded on to this holes. Junctions of wall temperature measuring thermocouples were kept embedded to the ceramic wall and those measuring gas temperature were exposed to the reactor ambient. Fifteen thermocouples were fixed into the ports and remaining five ports were plugged. Out of fifteen, the outputs of eight thermocouples were actively recorded during experiments.

The product gas was drawn from exhaust duct for determining volumetric composition of O_2 , and CO_2 . A long stainless steel tube was inserted in the exhaust tube such that the tube end faced the flow. Sample gas was allowed to pass through a train of scrubber, drier and filter prior to its analysis on dry basis.

The Reactor

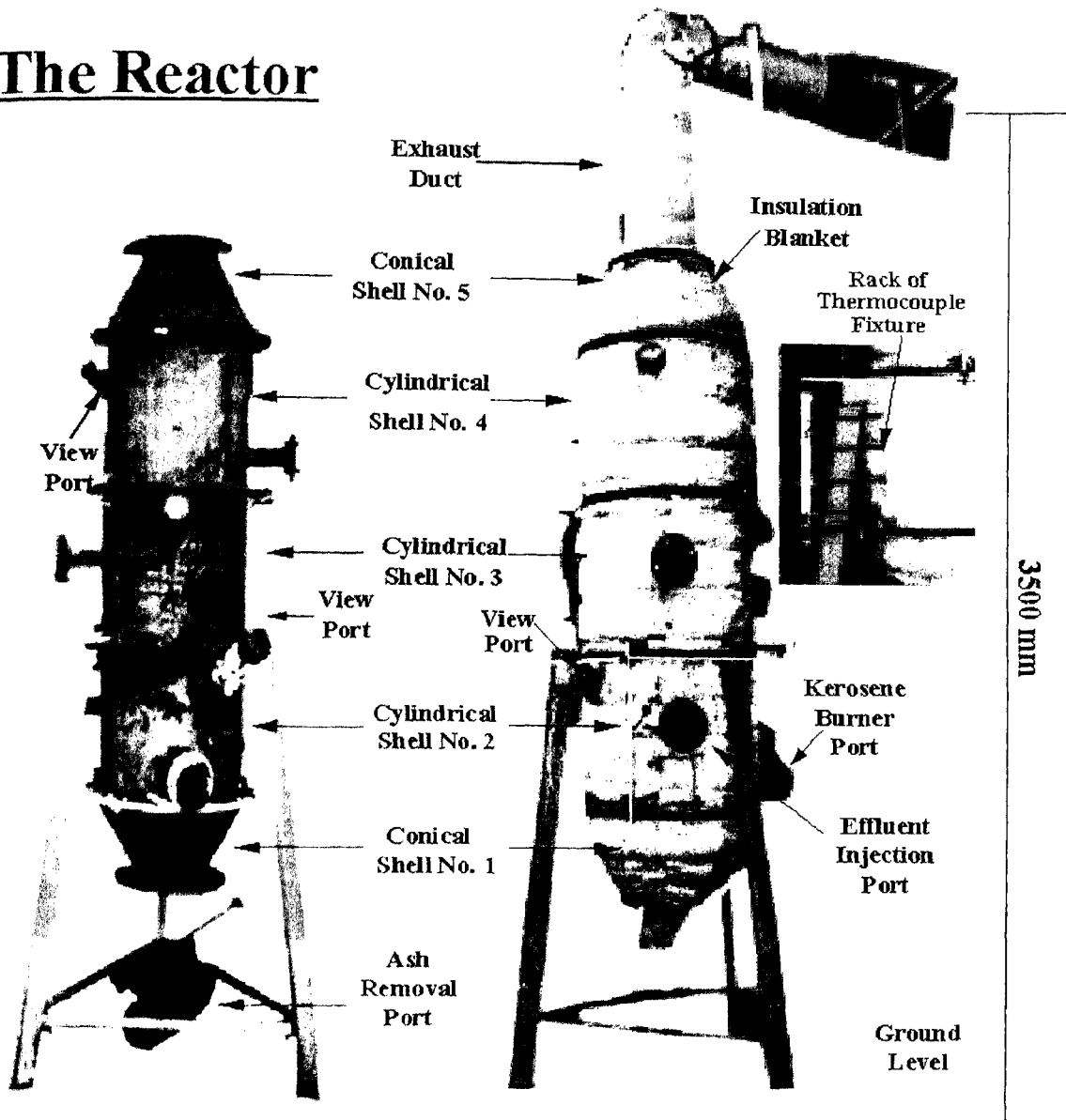


Figure A4.2: Direct pictures of vertical reactor assembled upright on support structure with and without thermal insulation.

A4.1.2. Reactor Heating System

The reactor (wall) is heated to temperature in the range of 973 –1273 K prior to injecting effluent. This was carried out using kerosene burner designed to an output power level of 20 – 250 kWth. The mean gas temperature at the exit plane was measured between 1273 - 1573 K and average gas velocity in the range of 25 –35 m/s. The burner was fixed tangential to the shell no. 1 and therefore was heated to highest temperature due to high convective heat transfer in this section. While effluent was injected, the burner was operated in the lower

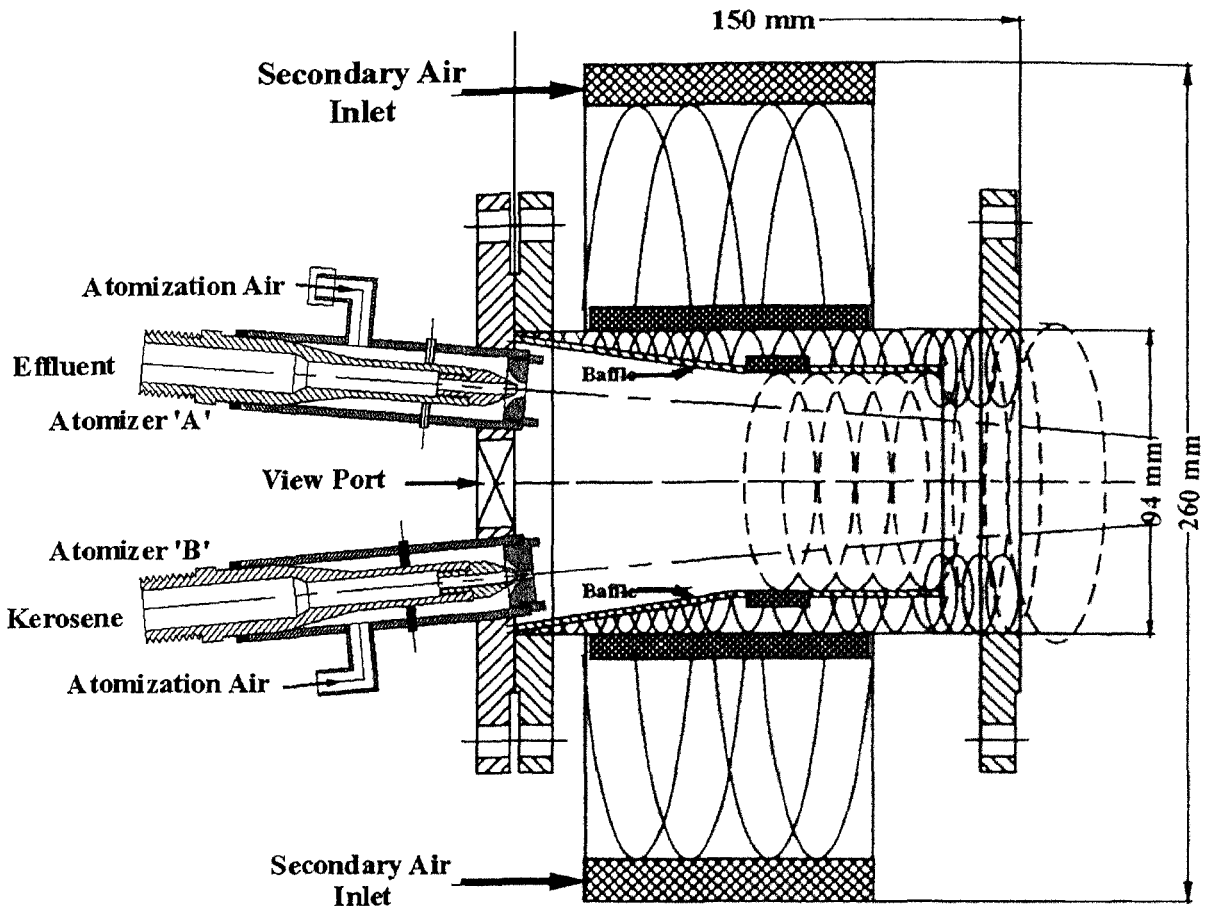


Figure A4.3: Sectional view of burner drawn to the scale depicting atomizers fixed to a flange.

power range or was completely switched off. The burner depicted in Fig. A4.3 could accommodate two atomizers. During tests with the first set of experiments, this burner could be used as kerosene burner by fixing only kerosene atomizer to one of the ports while keeping the other port plugged.

The kerosene atomizer used was an internal mixing air blast atomizer with a solid cone angle of 15° . The amount of atomizer air was limited to 4% of the stoichiometric requirement of the fuel and achieved fine atomization at 1.3 bar air pressure and 3 g/s kerosene flow rate. An annular cylindrical baffle of 75 mm diameter and 100 mm length is provided around the atomizer exit plane as shown in Fig. A4.3. This baffle shielded the kerosene droplets in the spray getting entrained into the swirl air and pushed to the wall, causing blow off and draining of kerosene. It also prevented excess dilution and resulting blow off, especially during effluent injection, when the burner power level was reduced to less than 30 kW and effluent combustion air was allowed through the same burner. The outer edge of the baffle acted as a flame holder. A small part of the secondary air is

admitted tangentially close to the atomizer exit plane that helped forced ignition during startup (or re-ignition) and maintained stoichiometric ratio during low power level operation.

The back end flange contained two atomizer ports and two view ports with toughened glass window, fixed diametrically opposite to each other. The purpose of the view ports was two fold - to ignite the kerosene spray by inserting a pilot flame through a port on the sight tube and to view the core of the of the burner combustion zone. The presence of baffle in the burner provided an aerodynamic effect under all secondary air flow conditions such that it created a negative pressure due to which cold air would be sucked into the reactor even during kerosene spray combustion or would suck the pilot flame into the spray core to facilitate ignition without causing backfire. To determine the effluent spray combustion behavior when injected in a confined turbulent diffusion kerosene flame, effluent atomizers used in the first experiment were fixed into the second port of the same burner (in Fig A4.3 shown as atomizer 'A'). Reactor heating was initially carried out with effluent injection switched off.

A4.1.3. Kerosene Feed System

Accurate kerosene flow rate determination and its control are taken care of by the kerosene feed system. Kerosene was pressure fed to the burner and air was used as pressurant. The kerosene flow rate was calibrated with respect to the air feed pressure. A capillary flow meter was specially designed for measuring flow rate in the range of 0.1 – 3 g/s. Figure A4.4 depicts kerosene feed system. A coarse and a fine pressure regulator were used to adjust air pressure precisely in steps of 0.03 bar. The feed line contained three kerosene filters in tandem to avoid nozzle blockage by suspended particles during burner operation. Feed pipes upstream of the filters were of stainless steel and downstream of it were flexible PTFE tubes to provide non-corroding and smooth internal surface. A level gauge was fitted to 40 L aluminum alloy tank that helped in keeping track of kerosene consumption with time during the operation.

A4.1.4. Effluent Feed System

The effluent with 50% solid concentration is a highly viscous liquid whose zero shear viscosity obtained by extrapolating the experimental result using Williamson model was 17 Pa.s at 308 K and 0.5 Pa.s at 353 K. At 77 % solid concentration the same was 9273 Pa.s at 308 K and was 10 Pa.s at 340 K. The spray combustion experiments at 50% and 60% solids concentration were performed with effluent heated to temperatures close to the boiling point

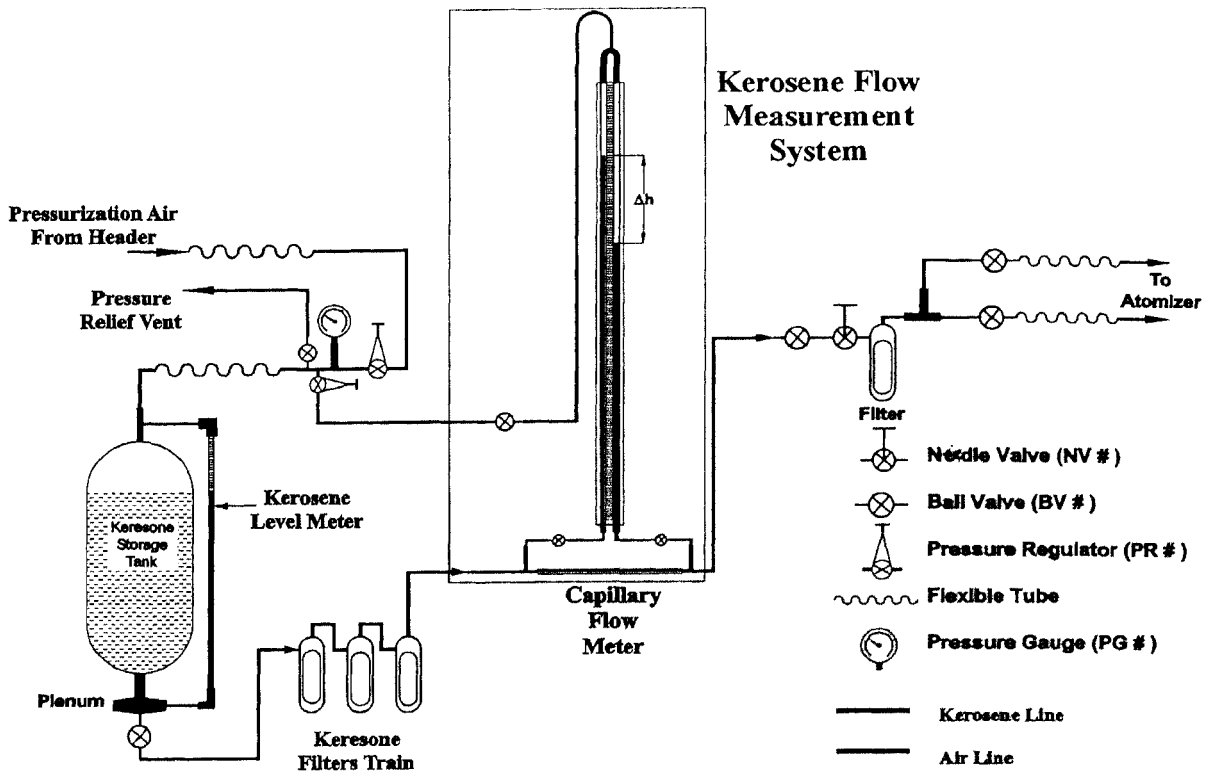
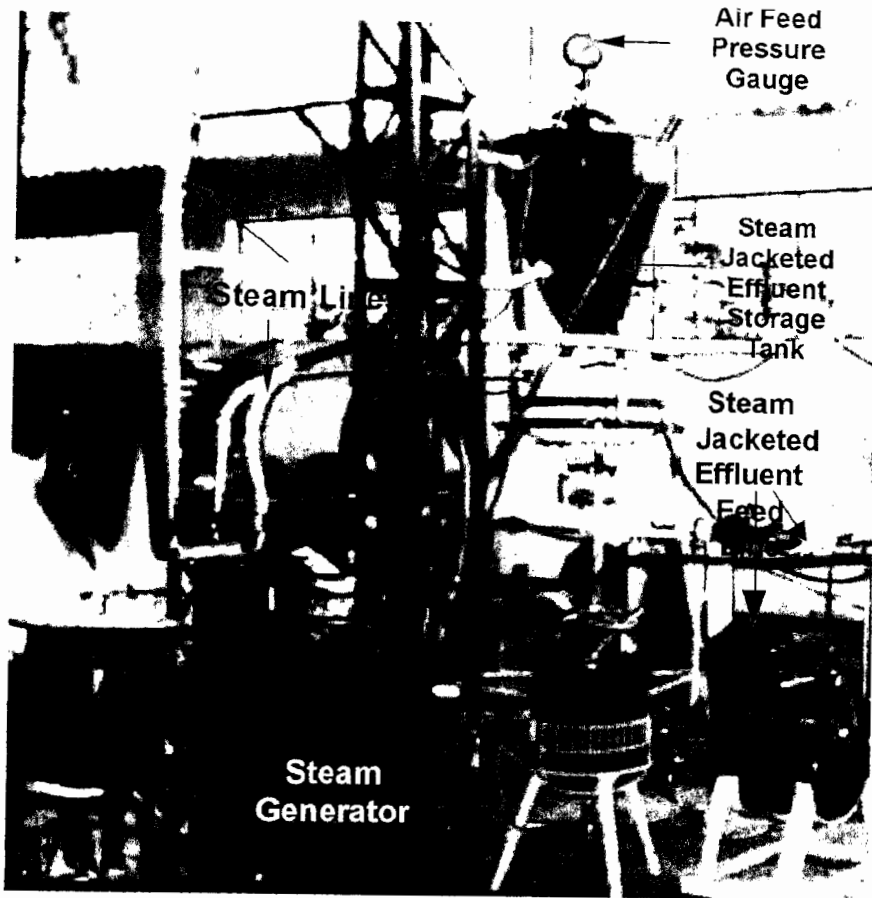


Figure A4.4: Kerosene feed system

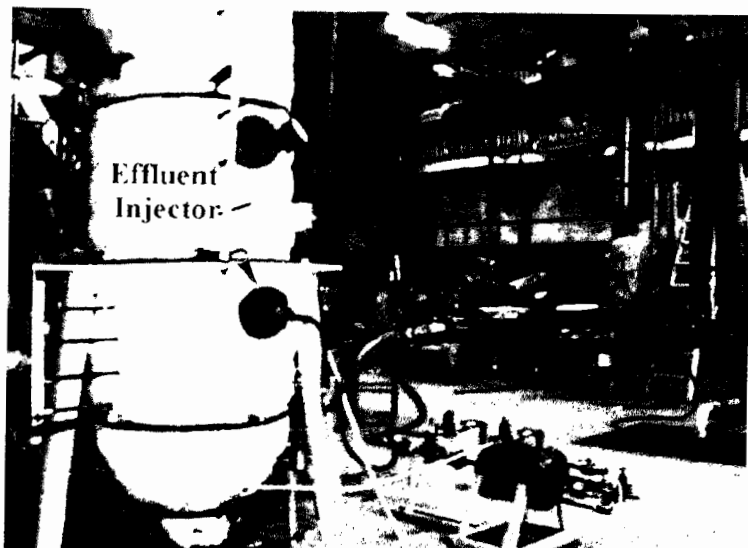
in order to have uniform and fine atomization. A specially designed, modular, steam jacketed feed system was designed and used for the experiments. The feed system comprised of a (i) steam jacketed storage and feed tank and piping (ii) a steam generator and associated piping, and (iii) air pipelines. These are as shown in Fig. A4.5(a) and A4.5(b).

A4.1.5. Steam jacketed storage tank and supply lines

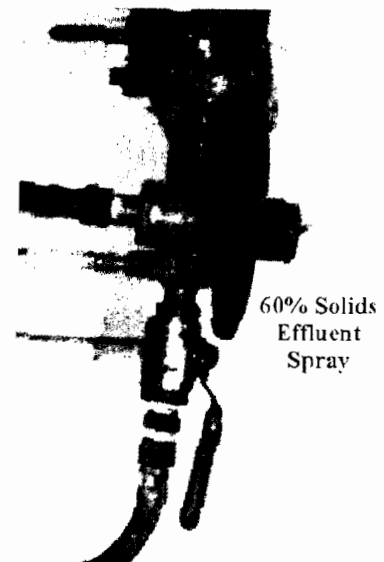
Effluent was pressure fed to the atomizer using air as pressurizing gas. The entire rigid pipeline, storage and feed tank were of stainless steel (SS 304 L) and flexible tubing for effluent was of PTFE braided with stainless steel wire since the effluent is acidic with pH between 4.2 – 4.4. Braided PVC tubes were used for high-pressure air entering the effluent feed system. Effluent was heated to temperature of 360 – 370 K (boiling point is 375 K for 50% solids). Steam generator supplied saturated steam to the outer jackets of feed and storage tank and the pipeline conveying effluent. All the outside hot surfaces were thermally insulated including the short length of the flexible braided tube. Continuous flow of hot effluent could be obtained through the atomizer nozzle of minimum diameter of 1.7 mm. Nozzle diameter smaller than 1.7 mm could not be used due to the problem of blockage, which could disrupt the experiment. Small diameter was preferred in order to have good



(a)



(b)



(c)

Figure A4.5: direct pictures of (a) effluent feed tank and steam generator (b) effluent injection port location and (c) atomization of effluent (with 60 % solid) into fine spray.

atomization and control flow rate at lower values. The nozzle diameter was larger for effluent with higher solids. Figure A4.5 (c) depicts atomization of hot effluent with 50 % solids to fine spray.

The suspended and insoluble solid fraction of the effluent has a tendency to settle down under gravity causing uneven distribution of solids. This could be effectively overcome by agitating effluent vigorously by allowing high-pressure air to bubble through the effluent letting air enter through the far downstream end of feed line so that effluent remaining in the feed line could also be flushed and pushed back into the tank. This exercise was essentially followed prior to each experiment in order to ensure smooth continuous flow proportional to the feed pressure and better atomization.

A4.1.6. Effluent Atomizer

The atomization quality is important for ignition and stable burning with higher combustion efficiency for most fuel including slurry fuels. Atomization quality is mainly indicated by the fineness of effluent spray droplets and its size distribution. Effluent is a difficult liquid to atomize since it is highly viscous with zero shear viscosity determined at 50% solids and at 323 K liquid temperature as 5.6 Pa.s. The effluent is heated close to its boiling point prior to injection to reduce the viscosity. Providing additional sensible enthalpy also helps in reducing overall ignition delay and has an impact on the total conversion time.

A specially designed co-axial, converging, air blast atomizer was used for the experiment with effluent nozzle diameter 3.0 mm and annular gap 0.5 mm. Since effluent is a heterogeneous mixture composed of dissolved and suspended particles it does not flow freely through the nozzle of diameter smaller than 3 mm. This diameter is considerably large for producing fine spray since the fineness of atomization is related to the orifice dimensions. An important feature of the air blast atomizer is that it provides a measure of fuel/air premixing before combustion and improves combustion. It is known that increase in air pressure, air velocity, and air/liquid ratio all tend to lower the mean drop size, experiments were performed with air jet speed in excess of 200 m/s and air/liquid ratio in the range of 0.15 to 0.2. The effluent nozzle exit plane was 1.5 mm inside the annular air nozzle exit plane and hence momentum transfer was better resulting in a finer spray. The breakup length for the converging air blast atomizer configuration was found to be extremely small. The physical appearance showed disintegration of liquid sheet next to the exit plane of the atomizer as if fine spray emerged out of the atomizer. The distance

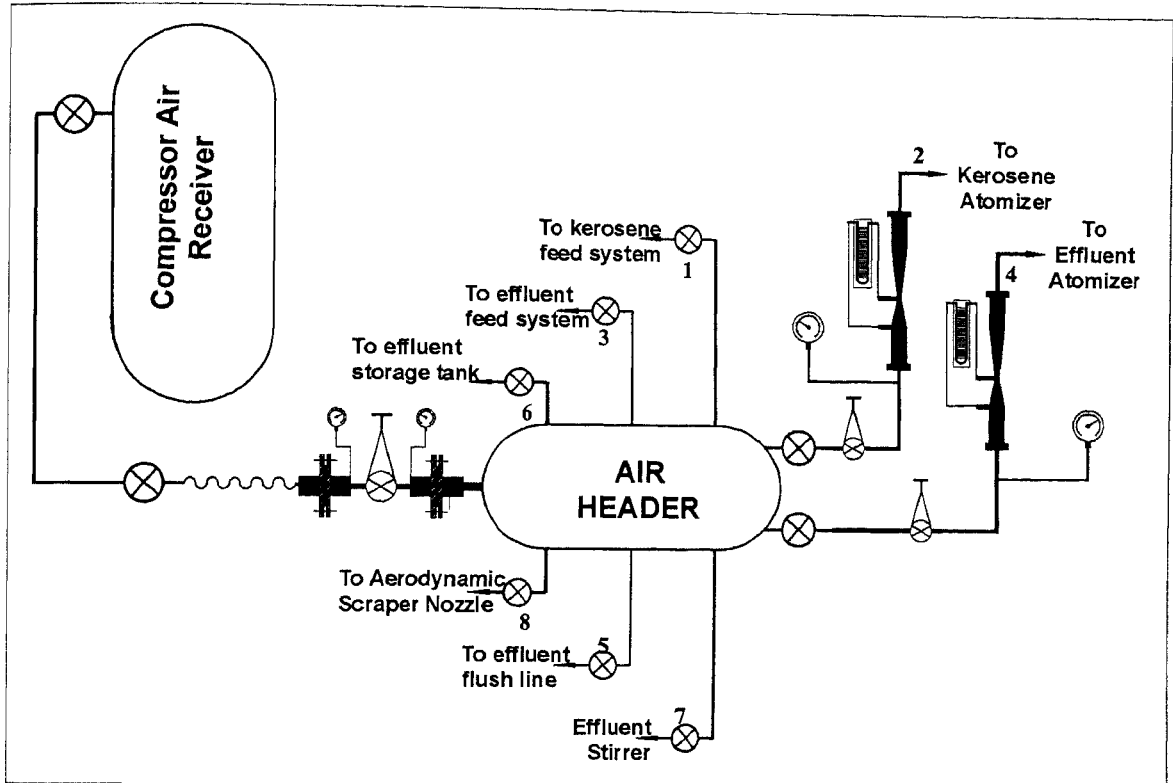


Figure A4.6: Compressed air feed system.

between exit plane of the air and effluent nozzle in the case of coaxial straight flow air blast atomizer where no backpressure is experienced in the effluent tube is called the critical distance. At distance larger than critical distance, positive pressure or back pressure is experienced in the effluent tube and at distance smaller than critical distance negative pressure is experienced. Back pressure would seriously effect the effluent flow and cause disruption in the operation. Therefore, nozzle exit was always positioned at critical distance in the straight portion of the air nozzle where zero back pressure or slight suction is experienced. The minimum possible flow rate was restricted to the minimum effluent nozzle diameter. The restriction on the choice of the diameter is due to the physical property of effluent that is responsible for clogging the nozzle even if the effluent is filtered with 100 μm mesh during filling. Experimentally determined value is 3.5 mm for effluent with 50 % solid concentration at 353 K and minimum flow rate was 3 g/s. and a maximum flow of 35 g/s could be obtained

A4.1.7. Air Feed System

The air required for the experiment was obtained from two sources (i) Air compressor and (ii) Air blower.

A4.1.7.1. Compressed air

Figure A4.6 depicts the schematic of high-pressure compressed air feed system as one of the units in the experimental setup. Compressed air from the main receiver tank is received by a distributor header at a fixed regulated pressure from where it is further distributed to utility points as depicted in Fig A4.6.

There are eight outlets ports connected to application points listed below:

Port # 1: Kerosene feed pressure (regulated pressure)

Port # 2: Kerosene atomizer air (regulated pressure, flow rate measured)

Port # 3: Effluent feed Pressure (regulated Pressure)

Port # 4: Effluent atomizer air (regulated Pressure, flow rate measured)

Port # 5: Effluent flush air

Port # 6: Effluent storage tank.

Port # 7: Effluent agitator / stirrer air

Port # 8: Aerodynamic Ash Scrapper jet air

A4.1.7.2. Blower Air

The combustion and effluent injector cooling air was provided by an air blower delivering air at the flow of rate $500 \text{ m}^3/\text{h}$ at 500 mm of H_2O . The total airflow rate was obtained from an earlier obtained plot of centerline dynamic pressure vs. flow rate. The dynamic pressure is obtained by introducing a total – static pitot tube in the centerline of the tube where the turbulent flow is fully developed (typical Reynolds number of the duct flow are between 0.3 to 0.5 million). The flow rates of combustion air and cooling air (introduced in the reactor) were separately measured using two separate venturi tubes.

A4.2. Experimental Procedure

This section explains the setting up procedure of the feed systems, reactor and instrumentations as pre-requisites for starting experiment and then describes its startup procedures. This section is divided in two parts: 1) the initial setup procedure includes preparations to the setting up of the feed systems and 2) experiment startup procedure. The procedure remains same for all the experiments performed.

A4.2.1. Initial setup procedure

Setting up of effluent and kerosene feed system is imperative for maintaining their consistent desired flow rate throughout the experiment.

A4.2.1.1. Effluent Feed System

Effluent with 50% solids is filled in the storage tank of 50 L water capacity. Cold effluent could flow through a 8 mm diameter tube under gravity at this solid concentration. Since the effluent volume increases while being heated close to its boiling point, only 75 % of the feed tank volume is filled as precautionary measures in order to avoid effluent overflow. In addition, since effluent is pressure fed, any rise in pressure caused by steam generated in the closed tank would drastically alter its flow rate and may upset the experiment. Therefore, the unfilled volume would reduce the rate of change in pressure, which would also further reduce through condensation of the steam in the un-insulated surface in upper part of the tank. Effluent temperature is maintained above 363 K in the feed tank and feed line throughout its spray injection period in order to obtain fine and uniform atomization. Continuous effluent heating is therefore carried out for which steam flow is maintained throughout the experiment. The steam generator is therefore filled with sufficient volume of water. A lot of care is required during effluent heating in the feed tank and feed pipeline due to scaling problems. The dispersed and continuous phase of the effluent are thoroughly mixed prior to heating by allowing high-pressure (4 bar) air to bubble through the liquid by allowing it to flow in the backward direction from the atomizer end of the feed line. Effluent in the tank is first heated and then just prior to its injection, is fed into the line (while displacing air) and heated by steam. The level meter tube connected to the feed tank is thoroughly cleaned and wetted with oil in order to make its surface non-wetting and its meniscus clearly visible. The displacement of effluent mass responsible to cause unit change in the effluent level was initially obtained to be 44 g/mm for the same diameter of the tank and effluent solid concentration.

Effluent atomizer nozzle is thoroughly cleaned with water prior to starting of reactor heating to avoid nozzle choking by dry effluent solids. Since the effluent atomizer was fixed to reactor during heating, an arrangement was provided to cool atomizer below 353 K by passing water through the nozzle and atomization air inlet port.

A4.2.1.2. Kerosene Feed System

The total kerosene consumption could typically range from 8 – 12 L for an average 100 minutes experiment. Hence the kerosene tank is filled up to 20 L. The kerosene nozzle diameter is 0.6 mm and therefore, the kerosene was thoroughly cleaned of fine particulate matter by allowing it to pass through series of filters fixed in tandem. This filters and nozzle

are cleaned prior to the experiments. Capillary tube kerosene flow meter is set for flow rate measurement. The location of the nozzle exit plane with respect to that of the annular air nozzle is adjusted and fine-tuned so as to obtain zero backpressure. The flow rate calibration curve verified prior to starting of the experiment. The level meter also supplemented with obtaining kerosene flow rate and its functioning is verified.

A4.2.1.3. Air Feed system

The maximum air pressure is supplied to effluent flush lines and air bubbled through the cold effluent, therefore, the header pressure is set to this maximum value which is 3.5 bar. The atomization air pressure requirement for the same geometry of effluent atomizer is a function of the effluent flow rate and the solid concentration. Since the effluent spray length (penetration) is restricted to the equivalent of reactor diameter, the fine atomization is essential for which the effluent flow rate range is fixed between 4 – 6 g/s and air flow rate of 1.5 – 2 g/s at 1.7 bar. Kerosene atomization air pressure is between 0.8 and 1.4 bar at flow rate varying between 2 – 4 % of stoichiometric requirement. It was important to note that the air pressure should remain constant in the header during the operation. Drop in pressure from the set atomization pressure would seriously affect the combustion and gas composition would change with immediate effect.

A4.2.1.4. Reactor

Residue of previous experiment collected at the bottom of reactor is removed. The sight glasses are cleaned and replaced. Leak test is invariably carried out particularly in the shell where burner is fixed

A4.2.1.5. Instrumentation

The gas analysis was carried out on the dry basis at room temperature and therefore the gas was cleaned by bubbling it through 1 m water column and then was passed through driers and filter. Water vapour drier and filter were required to be changed prior to the experiment. The calibration of oxygen analyzer was verified against ambient air and pure nitrogen, while CO and CO₂ analyzers were calibrated by passing known composition gas or calibration gas at prescribed flow rate.

The hot and cold thermocouple junctions and wiring were critically inspected for any discontinuity in the circuits as an essential step of the startup procedure.

A4.2.2. Start-up procedure

Effluent is heated to 363 K prior to the starting of phase I in order to maintain the designed flow rate. Temperature recording is started just prior to the first phase and continues till the end of the experiment.

A4.2.2.1. Phase I: Reactor heat up phase

In 70 minutes, parts of the reactor are heated up as follows: Shell #1, 1223 K, shell #2, 1088 K and shell # 3, 1023 K at kerosene burner power of 115 kW [kerosene flow rate: 2.6 g/s, air flow rate 40 g/s, O₂ = 0.5 %, CO₂ = 16%, CO = 0.1 % (dry basis)] burner exit gas temperature = 1500 K and gas velocity is about 32 to 34 m/s.

Operational details

Kerosene burner is generally operated at stoichiometry and the first step to start the procedure is to switch on the atomizer and secondary air at flow rates lower than stoichiometric requirement. Kerosene flow is set only in the presence of ignition source (which is a pilot flame) to avoid accumulation of unburnt explosive mixture in the reactor. Once ignited, the kerosene and airflow rates are tuned to the stoichiometric requirements. The condition of combustion could be verified by inspecting the exhaust gases for entrained carbon particulate matter or soot, oxygen concentration and burner gas temperature. If the exhaust contained soot inspite of stoichiometric combustion air, then atomizer airflow rate is increased in order to improve atomization and thus air – fuel interaction resulting in improved combustion.

The heating is generally carried out at constant burner power level in the range of 100 – 120 kW (kerosene flow rate 2.3 – 2.6 g/s) hence kerosene and air flow rates are maintained constant during this phase until the reactor wall temperature in the shell # 1 is in the range of 1123 and 1223 K and shell #2 and #3 are in the range of 1023 and 1073 K.

A4.2.2.2. Phase II: Spray injection

The first phase remains the same for both sets of experiments that differed due to their injection location viz. for effluent injected from the wall and injected in turbulent kerosene flame. The startup procedure for effluent injection remains same in both the cases.

Injection from the wall

During this phase the kerosene flow rate is reduced to about 1.0 to 1.2 g/s and the hot effluent is injected from the reactor walls. The secondary air is varied such that the combined stoichiometric requirement of effluent and kerosene are met with. There is also

provision of introducing swirl secondary air annular to the effluent atomizer, however, the air temperature could not be kept in excess of 373 K, to avoid effluent choking in the feed line or atomizer nozzle due to loss of water or charring. Therefore, the cold combustion air was introduced through the kerosene burner after few initial experiments, either with or without kerosene flame.

Atomization air is started 2 to 5 minutes prior to injecting effluent in order to cool the effluent feed nozzle, which was heated during the first phase. Continuous effluent flow is essential in order to prevent choking of the nozzle. The effluent flow rate could be varied in the predetermined range of 5 – 12 g/s using air feed pressure ranging from 0.14 to 0.54 bar (2 – 8 psig) which is initially set prior to injection. Effluent level in the tank is determined after applying feed pressure required for obtaining predetermined flow rate.

In the case of re-ignition of kerosene burner, if the reactor wall temperature is above auto-ignition temperature, pilot flame may not be required; however it is useful to ignite using pilot flame since the mixture accumulated during ignition delay period can otherwise explode.

Injection in the turbulent kerosene flame

The procedure to start effluent flow remains same as in the previous case; however, the burner power level is kept higher (in the range of 50 – 100 kW) to avoid flame blow off with effluent injection.

Appendix A5

Inclined Reactor: The experimental setup and procedure

A5.1. The Experimental Setup – 1

A5.1.1. The Reactor

Effluent combustion experiments were performed in a rectangular cross-section, inclined plate reactor of 160 mm width and 80 mm height. The reactor was fabricated using stainless steel (SS 304 L) sheets that offered low thermal inertia for quick response to variation in surface temperature as the effluent is injected and combustion process is initiated. The 3.3 meter long reactor consisted of 3 sections. The area of cross-section was fixed by taking into account the required flow velocity of product gases over the effluent film in the reactor that can assist in transferring residue to the dump through aerodynamic scrapping. The operating temperature ranged from 973 – 1473 K. Large temperature gradients were also observed. Therefore, reactor walls, particularly the bed are reinforced with adequate stiffeners and structures to arrest thermal deformation (linear expansion coefficient of SS 304 L is about twice mild steel) and prevent failure resulting due to thermal stresses. The assembly of all the three sections was mounted on a variable inclination support stand and a structure to prevent reactor deformation under self-load during operation at high temperatures.

A5.1.1.1. Section I

This section has rectangular cross-section of 160 x 80 mm and constructed from 3.5 mm thick stainless steel (SS 316) sheet. Effluent injector and kerosene burner are fixed to this section as shown in A5.1. The A5.2 depicts direct picture of this section along with symmetrical stiffeners and structure support ribs. A swirl stabilized kerosene burner was fixed to a sudden expansion or dump type inlet that will help stabilize flame particularly during low power level operation. Two flame deflectors were provided downstream of the dump port as shown in A5.2. These were provided with a purpose of a) avoiding flame directly impinging on the lower plate causing uneven and excessive heating which may result in high local thermal fatigue and deformations b) avoiding back flow of hot gases which may char effluent in the nozzle and block effluent passage. Section I was coupled with section II using mild steel flange and annealed copper gasket.

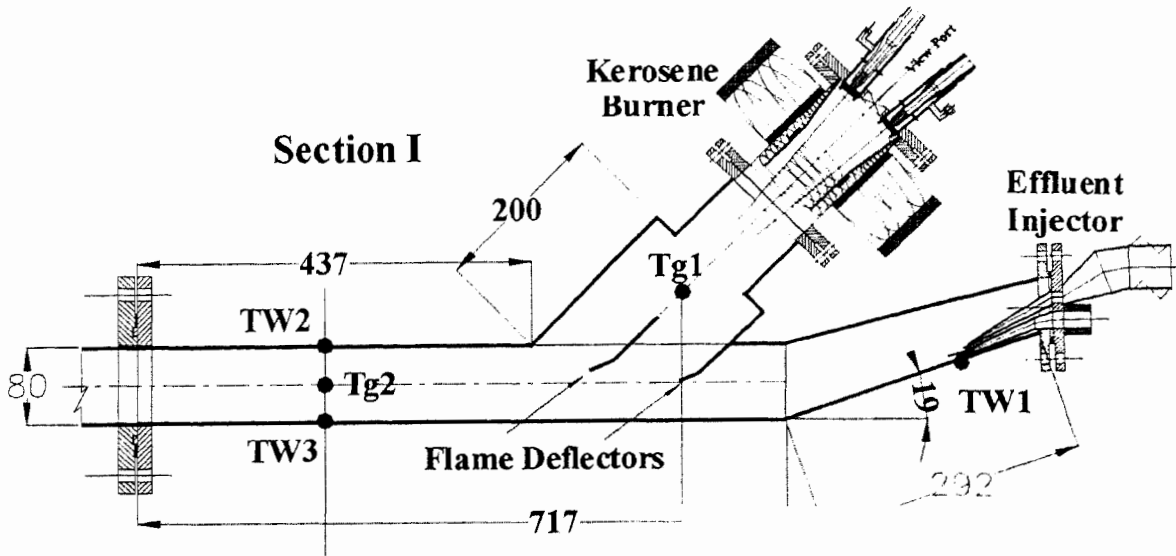


Figure A5.1: Scaled side view of Section I indicating location of effluent injector, kerosene burner and gas and wall thermocouple

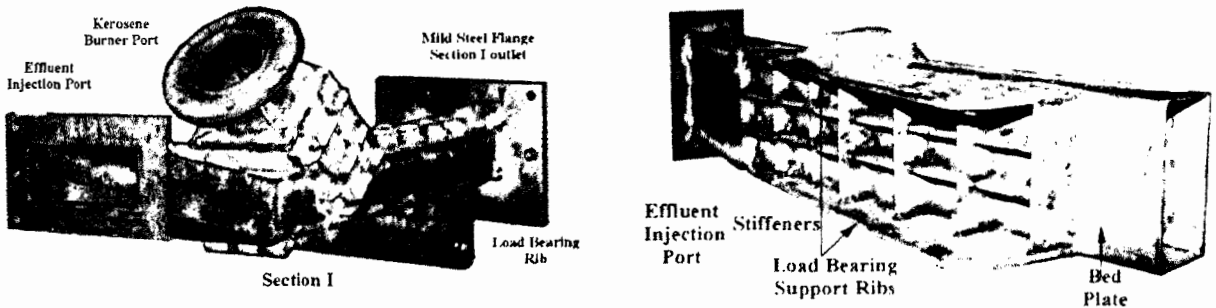


Figure A5.2: Direct picture of section I of inclined plate reactor

A5.1.1.2. Section II

This is the middle section of the reactor. It is 2.2 m long, has a plate (bed) longitudinally separating the section into upper and lower ducts. Cross sectional dimensions of both the ducts are the same at 160 mm width and 80 mm height. The upper port is where effluent combustion processes occur (and on the plate) and acts as a stationary bed. The lower duct transports ash free hot product gases to the exhaust port in the direction opposite to that of upper duct. The long passage of the lower duct also prevents entrained residues from entering the water scrubber. The exhaust port is located perpendicular to the lower duct from where gas enters the wet scrubber as shown in Fig. 5.2 (p. 132). The joints between section II & I and II & III are flanged. Annealed copper gaskets were used to seal these high temperature joints. The sidewall of the upper duct has two view ports as shown in the direct

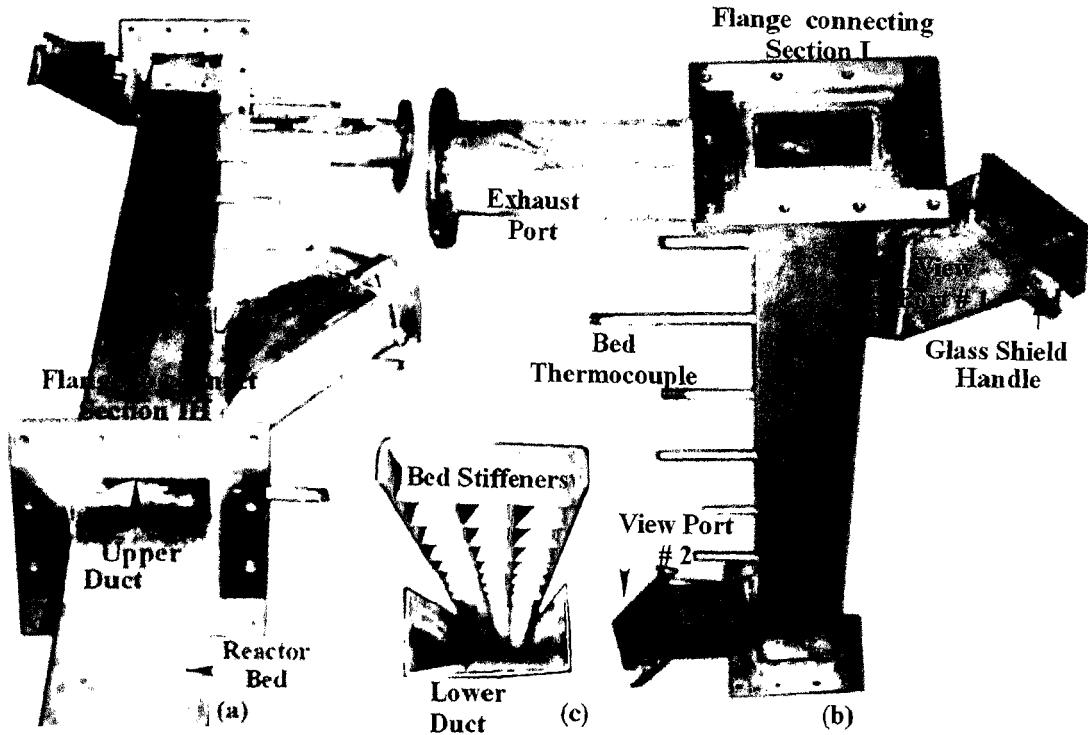


Figure A5.3: View of section II as seen from (a) section III end, (b) section I end and (c) View of lower duct and bed stiffeners

picture A5.3, for the purpose of observing combustion process occurring on the bed. This view ports are located such that the flow field is largely unaffected while providing a wide view field. A metal plate shielded the view port glass when not in use. This arrangement was made in order to prevent the glass plate from getting smudged. The bed experienced maximum temperature gradient because of experimental conditions. Therefore, in order to maintain the bed surface flat, the underside of the plate was provided with symmetrical stiffeners such that residual thermal stresses were evenly transferred on the sidewalls and not on the welded joints that may cause weld joint failure and deformation.

The thermocouple junctions were fixed to the underside of the bed and isolated from reducing gases so that it measured bed temperature at predetermined locations. This arrangement is shown in A5.4. The cold junction ends of the thermocouple wire were extended through the reactor sidewall.

A5.1.1.3. Section III

Section III is fabricated from stainless sheet as shown in Fig. A5.5. The primary function of this section is to divert product gases under the bed and transfer the solid residue into a

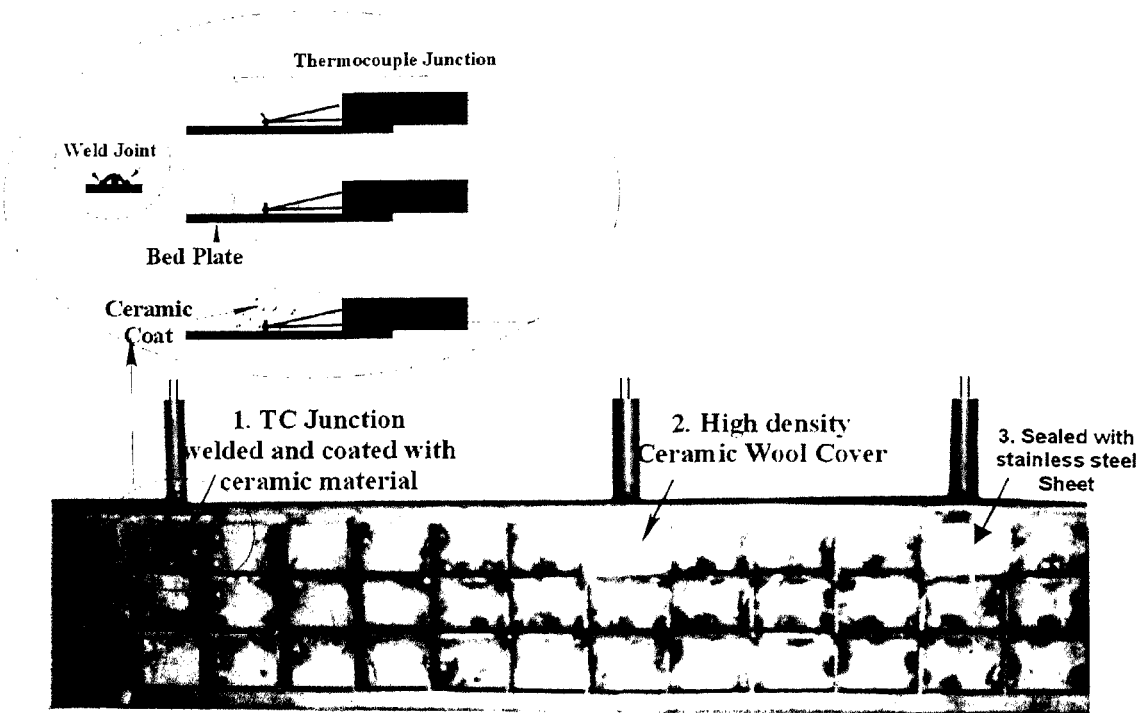


Figure A5.4: Section of the underside of the bedplate with thermocouple junction.

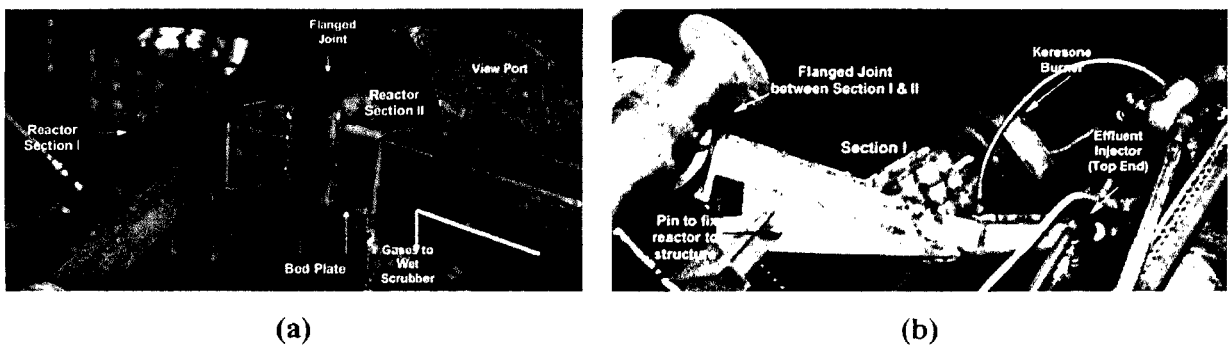


Figure A5.5: (a) Underside view of the reactor, the flange joint between section I & II and telescopic reactor support, (b) Top side view of the reactor.

dump of 85 litres volume. Product gases and ash traversed till the edge of this bedplate and particulate matter would fall into the dump under gravity. Further oxidation of the residue would be prevented once it fell in the cold dumpster zone and hence total carbon converted on the bed could be determined. Product gases take a 180° turn to enter into the lower duct of owing to the pressure gradient in that direction. Due to the centrifugal force, except for very small particles and aerosols all solid residues were expected to fall in the dump.

There are three view ports provided to this section. View port # 3 was located such that the edge of the bed and upper and the lower sides of bed were visible. This gave a clear view of

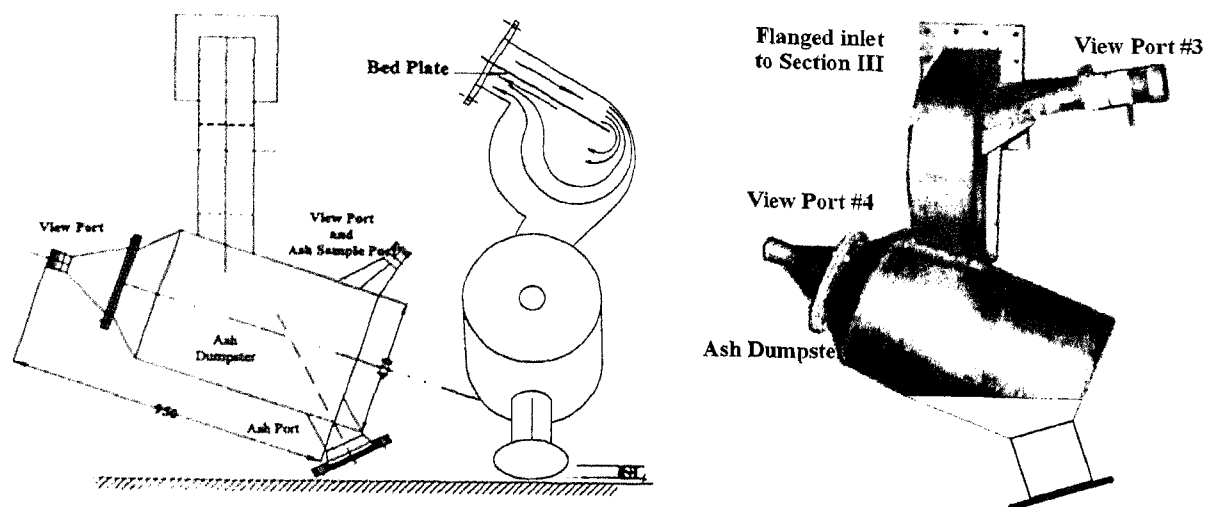


Figure A5.6: Scaled two views and direct picture of section III section II

combustion process on the bed and of the gas entraining particles. Other two view ports are fixed directly on the ash dump as shown in the figure in order to observe physical appearance of residue. Some fume deposition was expected during the experiment and hence arrangement was provided to facilitate easy removal and replacement of glass for cleaning. The dump was provided with an access hole and ash removal port, both sealed with dummy flanges. Sample ash, immediately after the experiment was over, could be removed for physico-chemical analysis with the help of sample collector tube through the view port. Gas sampling port was provided to obtain product gas composition at the end of bed. The joint between section III and II is also flanged as that between section II and I.

A5.1.2. Gas Scrubber

The purpose of providing on-line wet gas scrubber is to remove condensable, odoriferous, water-soluble and other particulate matter from producer gas stream. Plain tap Water was used as the scrubbing medium for all the experiments performed. Product gas enters a vertical co-current and counter-current water spray columns in tandem as shown in Fig. 5.2 (p. 132). The length of co-current and counter current column pipe was 1.3 and 2.93 meter respectively with internal diameter of 112 mm. Both the pipes were fixed vertical above a water seal. Water seal also acted as excess pressure dampener and prevented reactor failure under steep pressure rise condition, which may occur during starting or re-ignition of burner. Co-current column of the scrubber cooled gases to temperature close to water temperature and improved solubility of gaseous component in the long counter-current column. Insulation was provided to all the tubing upstream of the scrubber such that gas remained at high temperature just prior to it entering the co-current section in order to avoid

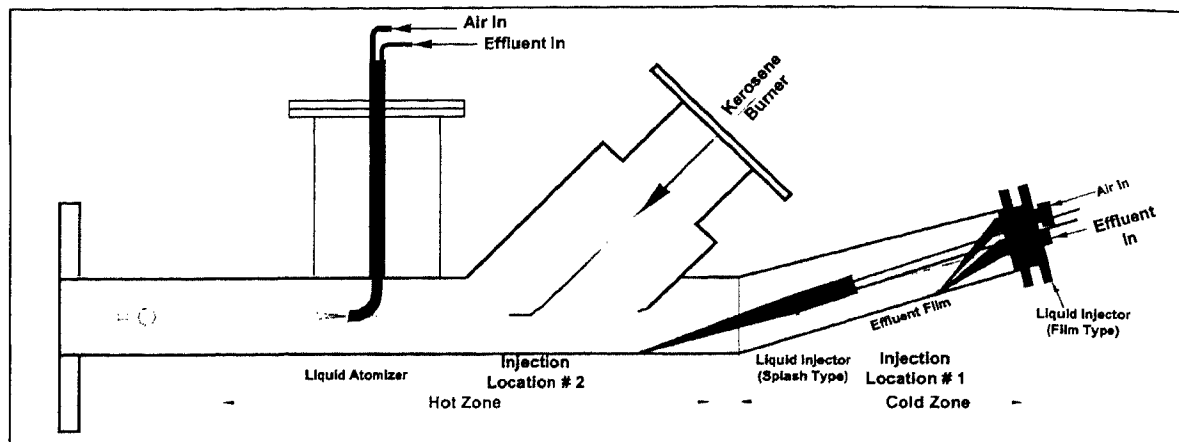


Figure A5.7: Location of different types of injectors in hot and cold zones of the reactor

early fume deposition. Pressure and impinging jet sprays were used for the purpose. Relatively, higher water mass flow rate (4 times) was allowed through co-current scrubber column as compared to counter current column in order to achieve ejection effect to drive product gases in the reactor. Scrubber water flowed in a loop driven by a 1.1 kW centrifugal pump that could deliver fluid pressure of 3 bar. Gas-sampling ports were provided at the upstream and the down stream of the scrubber as shown in Fig. 5.2 (p. 132).

A5.1.3. Ejector and Gas Flare

Aerodynamic ejectors maintain reactor pressure sub-atmospheric (at least 5 mm of H₂O below atmospheric pressure) at all experimental flow rates. This facilitates product gas scavenging. The ejector assembly is as shown in Fig. 5.2. Modular ejector was used to facilitate replacement or cleaning. The primary air flow rate was measured with the help of orifice plate meter and controlled using a gate valve.

A5.1.4. Effluent Injectors

Three types of injectors were used in the experiments; 1) film injector, 2) splash injector and 3) air blast atomizer. Method of injecting effluent was decided with a primary objective of obtaining a definite pattern of effluent distribution on the inclined hot metallic surface so that consistent, steady state combustion and gasification of effluent could be obtained. The location of injector was fixed with respect to the location of the auxiliary fuel burner as shown in the Fig. A5.7. The locations were as follows: cold zone - up stream of the auxiliary kerosene burner and hot zone - little down stream of the kerosene burner.

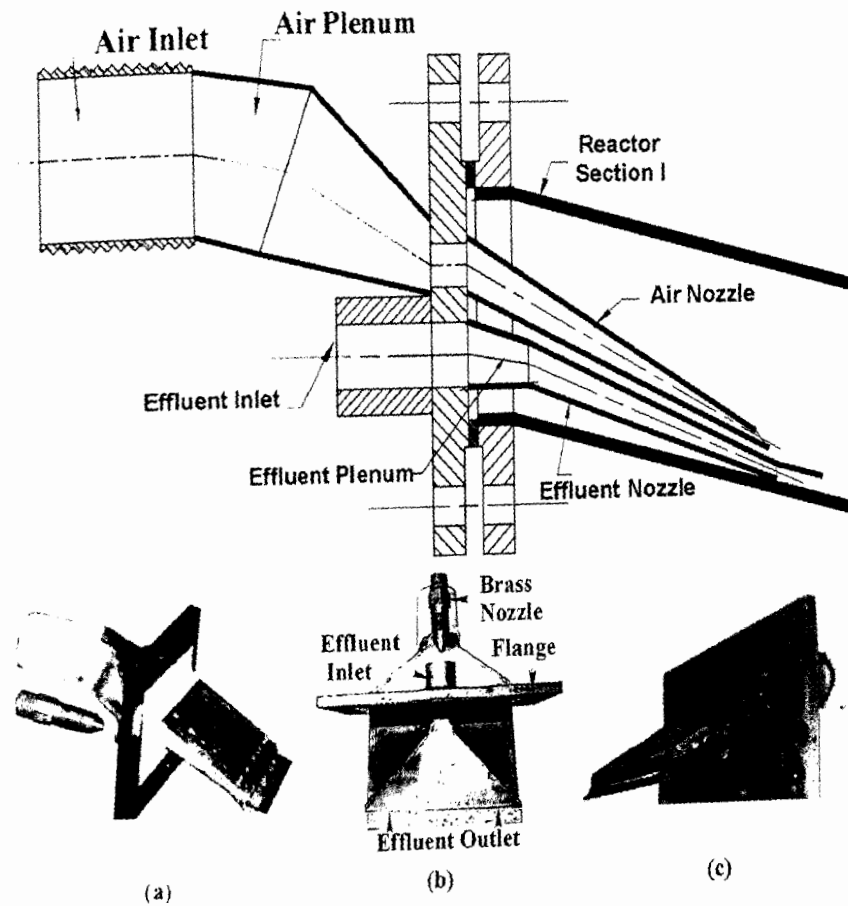


Figure A5.8: Sectional side view and three photographic views of film injector.

A5.1.4.1. Film Injector

The initial experiments using 60 % solids effluent were performed using film injector, which injected effluent and evenly flows over the cold reactor plate surface temperature much below Leidenfrost point (below which effluent does not float over its vapour film but liquid forms a film. In the case of water, this point is at $T_w \sim 373 \text{ K} - 473 \text{ K}$ above water saturation temperature) under gravity, as shown in Fig 5.9. The air and effluent inlets and outlets, welded to a flange are shown in the figure. The inclination of the lower plate on which effluent was injected is 47° to the horizontal line and the slope helped effluent film to penetrate deep into the hot zone downstream. To assist this, effluent combustion air was

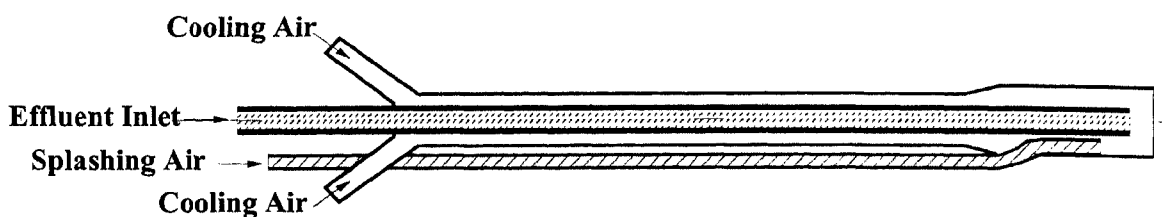


Figure A5.9: Schematic view of Splash Injector

injected with laterally uniform velocity ranging from 15 to 25 m/s in the direction of effluent flow from the outlet located above the diverging effluent outlet as shown in the figure. The effluent inlet received hot liquid effluent from a brass nozzle with 5 mm diameter hole, at a fixed flow rate from the effluent feed system from where it enters a square plenum. The other end of the plenum diverged width wise and converged height wise to form effluent outlet of rectangular cross section (160 mm long x 3mm height) with area equal to that of plenum area. The height was limited to 3 mm in order to ensure smooth flow of effluent. In the case of any blockage in the outlet, the feed line could be flushed with high-pressure air. The air and effluent outlets were separated by a thin sheet extended from the topside of effluent nozzle. This arrangement prevented the air jet disturbing effluent film and assisted effluent flow under ejection effect a little downstream. This whole arrangement was assembled to the first section of the reactor and was tested under cold condition by making visual observation of the effluent flow and effect of air velocity on the mass distribution by allowing effluent and air to flow over the inclined lower plate of this section. This injector was used for effluent with solid content below 73 %.

A5.1.4.2. Splash Injector

A5.9 depicts schematic view of splash injector. The primary aim was to obtain effluent distribution over a length of the bed as well as the side and the top walls of the reactor and prevent liquid accumulation. Using this injector, effluent could be directly injected into the hot zone (bed temperature, $T_w = 973 - 1173$ K) of the inclined reactor, either from its upstream end or fixed directly on the reactor top wall as shown in the schematic (Fig. A5.7). The bed temperature is above Leidenfrost point and therefore, the droplets would float on the layer of its own vapor which is maintained by the intense evaporation from droplet-vapour interface, due to heat conduction and radiation from the hot bed. Once the water and other volatiles are lost, the droplets become immobile. Hence distribution over wider

surface would prevent excess accumulation of partly devolatilized effluent or its char and is further pushed downstream of the reactor under major influence of drag force exerted by the flow of high velocity gases. The effluent tube was air cooled by the effluent combustion air supplied by the blower to avoid charring. The splashing air also helped cool the injector tip.

A motor driven, quick return, slider arm mechanism was devised for lateral traverse of injector. The laterally moving injector splashed effluent at different locations during its traverse cycle. This gave effluent film or droplet enough time to overcome its immobile phase prior to getting dragged downstream after which fresh effluent was injected on the same location. The injector was introduced from the back end of the reactor and the mechanism was fitted on to the same flange where film injector was fixed. Care was taken to avoid direct exposure of mechanism components to high temperature radiating walls of the reactor. Combustion air (or part of total gasification air) was allowed through the rear plate of the mechanism and maintained low temperature. Since the injector was in motion, flexible tubes capable of withstanding high temperature (in excess of 400 K) and high stresses were used to convey hot effluent and air (high pressure air for splashing and blower air for cooling) to the injector.

A5.1.4.3. Effluent Atomizer

In the third set experiments, effluent with solids in the range of 70 – 75 % was used. Splashing effluent did not give adequate effluent distribution due to higher mass density of concentrated effluent. Moreover, effluent would get into transition immobile phase soon after its injection due to low water content and therefore more effective distribution may be required. Effluent atomization was carried out for the purpose of effective distribution on bed as well as on the top and side walls of the reactor. Very fine atomization was not essentially required since the primary aim was distribution on confined walls. Air blast atomizer was used as described in Appendix A4; however, the effluent nozzle internal diameter was 5 mm with low swirl (swirl number $\sim 0.6 - 1$) atomization air. A fraction of combustion air was introduced as cooling air and passed through annular space as shown in Fig. A5.10.

A5.1.5. Effluent Feed system

The heating of the effluent in the initial first set of experiments was carried out by circulating effluent through heat exchanger tube fixed at the bottom of the reactor. Later electrical heating was adopted in order to simplify the operational aspects of already

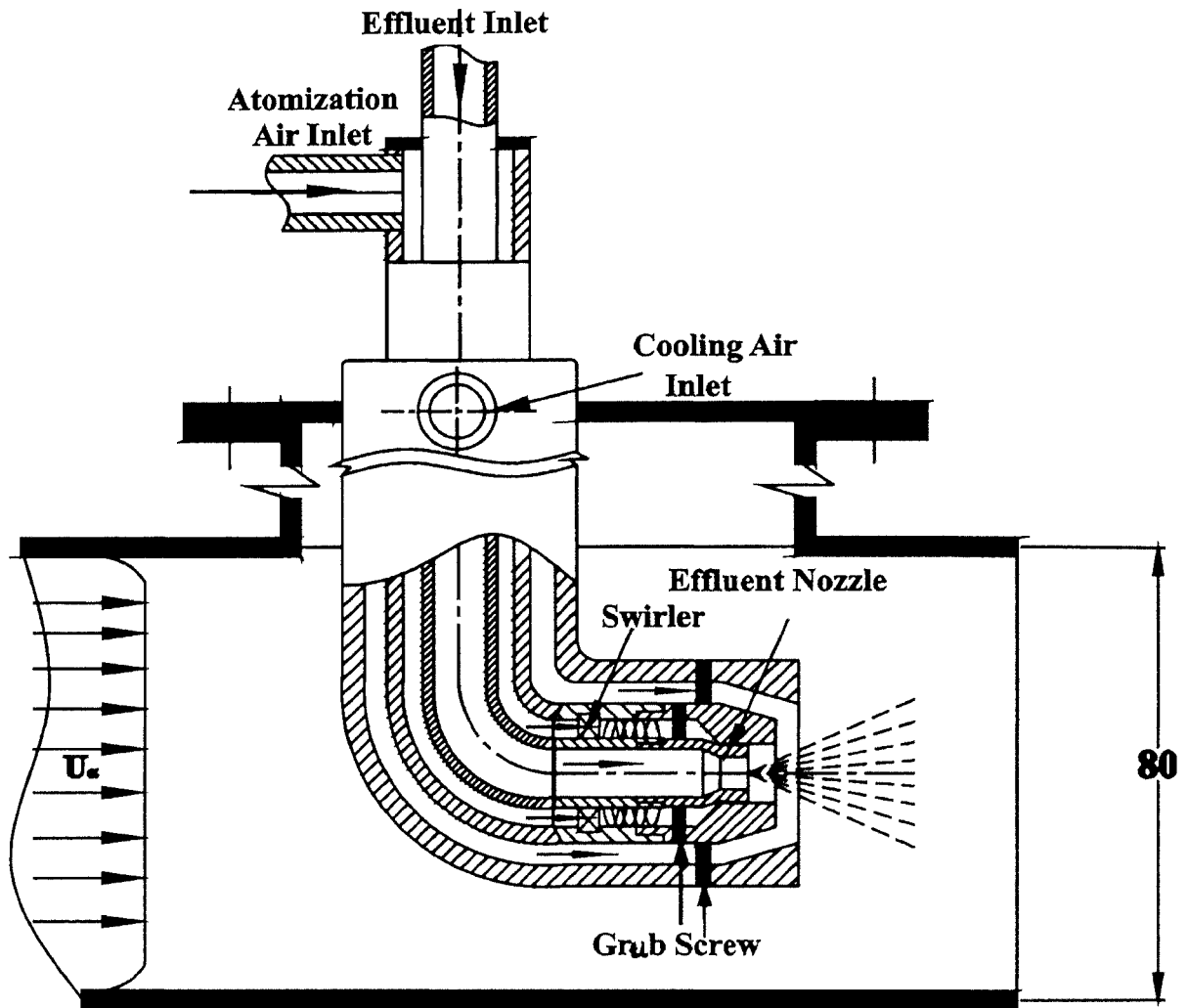


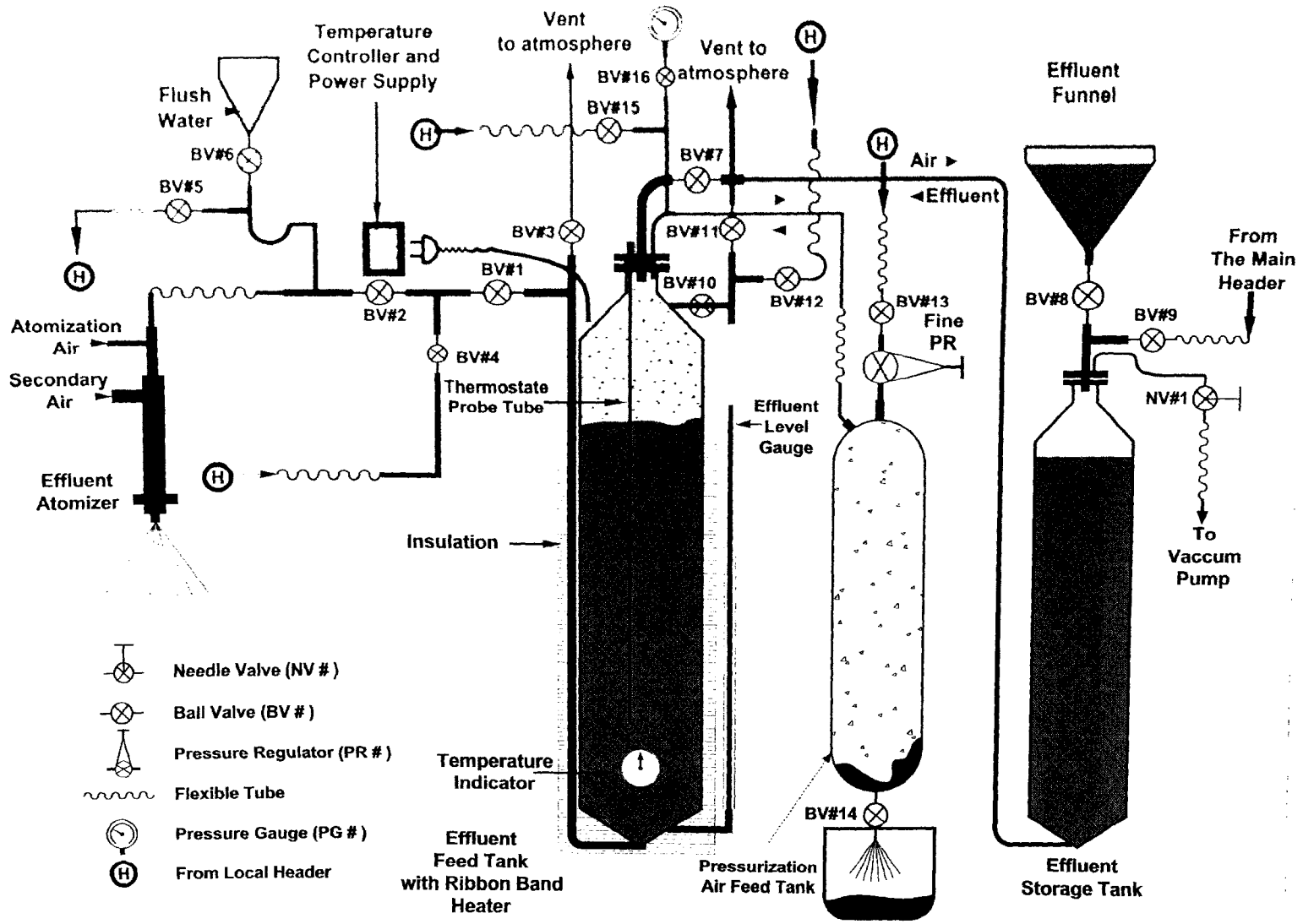
Figure A5.10: Effluent Atomizer

complex system. The injectors (film injector, splashing nozzle and atomizer) used in the present experiments were located in both the cold and hot zones (Fig A5.7) and effluent injected consisted of 60 % solids as well as 73 % solids. The use of higher solids effluent in the later part of experiments and its direct injection into the hot zone made the feed system more complex since it required elaborate air and water flush line arrangement to evacuate and clean feed lines with residual effluent prior to injecting effluent or after stopping injection during experiment in order to ensure consistent effluent flow. The aspects of agitating and mixing effluent, of applying feed pressure, selection of tubing material, all remained same. Figure A5.11 depicts the schematic view of the feed system.

A5.1.6. Air Feed System

The air feed system for the present experiment remains the same as was used in earlier experiment and is discussed in Appendix A4.1.7 The only difference is that the effluent feed

Figure AS.11: Effluent feed system.



system required additional high-pressure air purge lines and this was taken care of by providing an additional air header from where these lines were drawn to their utility points.

A5.1.7. Instrumentation

The instrumentation for pressure, flow and temperature measurement remains the same as was used in the previous experiments described in section 4.4.1. Computer aided data logging system was used to record temperature, pressure and selected gas fraction data. For measuring bed temperature thermocouples are welded to the lower part of the bed as depicted in Fig. A5.4.

The fraction analysis of CO, CO₂, H₂, CH₄, H₂S and O₂ was carried out on the dry basis at room temperature in this experiment using on-line gas analyzers and gas chromatograph.

A5.2. Experimental Procedure

This section explains the set up procedure of all the elements and the startup procedures. This section is divided in two parts: 1) initial setup procedure includes preparations to the setting up of the feed systems and 2) experiment startup procedure (results and discussions are described in the next section). The procedure remains same for all the experiments performed.

A5.2.1. Initial setup procedure

A5.2.1.1. Effluent preparation

The experiments were performed using effluent with 60% and 73 % solids. The procedures for feed line preparations are the same as in Appendix A4.2.1.1. except that in the present experiment, the effluent was heated using waste heat from the reactor or with an electric ribbon heater. *Continuous effluent flow, under applied feed pressure, through the heat exchanger tube was necessary to avoid getting effluent charred and immobile resulting in effluent blockage.* The range of flow rate used was 5 – 12 g/s. The initial level in the gauge was determined only after allowing effluent to fill the feed line under a fixed pressure. The effluent feed tank should contain at least 40 kg of hot effluent prior to heat-up phase. All the effluent and air feed lines are thoroughly cleaned prior to heatup phase in order to rule out any possibility of blockage caused by the charred effluent of accumulated during the first phase.

A5.2.1.2. Kerosene Feed System

For each experiment the kerosene consumption was recorded as 5 – 8 litre of which 4 litre will be consumed during Phase I (reactor heat up). The per-experimental preparation of the kerosene feed line and atomizer remained same as was earlier described earlier in Appendix A5. In the present experiment, two atomizers were used in the same burner. Atomizer 1 with nozzle diameter of 0.65 mm was used during heat-up phase during which burner power level was maintained in the range of 100 – 150 kW. While number 2 atomizer with nozzle diameter of 0.4 mm was operated during Phase II operation (effluent injection) at lower power range between 10 – 50 kW.

A5.2.1.3. Air Feed system

The air feed system remained same as described in 4 and therefore the per-experimental preparation of the air feed system are the same.

A5.2.1.4. Reactor

Residue of previous experiment collected at the dump is removed. The sight glasses are cleaned and are replaced along with new gaskets. Leak test is necessarily carried out particularly at the joints involving high temperature. The reactor experiences high thermal stresses during the operation and hence the deformation in the lower bed is checked prior to all the experiments. Scrubbing water is changed.

A5.2.1.5. Instrumentation

The thermocouples are directly welded on the lower surface of the bed which may deform and damage thermocouple. Therefore, the hot and cold thermocouple junctions and wiring were critically inspected for any discontinuity in the circuits as an essential step of the startup procedure. Electrical grounding of the reactor is necessary in order to ensure correct temperature recording.

The composition analysis of CO, CO₂, H₂, CH₄, H₂S and O₂ was carried out on the dry basis at room temperature in this experiment. The sample lines are cleaned. The pre-experimental preparation procedure remained the same for conditioning gas and calibrating instruments as in Appendix A4 for experiments described in chapter 4.

A5.2.2. Experimental startup

The reactor inclination angle was fixed at 30° . The experiments consisted of two phases: Phase I was reactor heat up and Phase II was effluent injection phase. During the first phase, the reactor was heated to temperature in excess of 1173 K using kerosene burner operating at power level of 80 - 90 kW. Once the bed attained 1173 K, kerosene burner power level was brought down to level lower than 30 kW. The effluent (363 K) was injected as thin film in cold zone using film injector or injected using splash injector or atomizer into hot zone of the reactor. Steady effluent injection and pre-ignition processes are critical for getting into gasification part of phase II. These phases are timed and are in sequence. They are carried out only after initial startup procedure is completed and continuous kerosene, effluent and air supply, flow of scrubbing water is ensured.

A5.2.2.1. Phase I: Reactor heat up phase

Water sprays in the scrubber and ejector primary air (30 g/s) are switched on first. A 2 kW LPG pilot burner is ignited in the initially phase of the experiment. Gas sampling pump is also switched on to determine O_2 , CO_2 and CO concentration. The startup procedure for the kerosene burner remains the same as described in Appendix A4 since the same burner was used in the present experiment. The burner is operated at constant power level in the range of 80 – 90 kW. The stoichiometric air quantity is divided into atomization air (3 – 4 %), combustion air (70 – 80 %) and effluent injector cooling air (16 – 27 %). The effluent injector is fixed protruding in the reactor and therefore to prevent it getting over heated and thermally damaged during this phase, a fraction of total combustion air is introduced as cooling air through the injector. This fraction of air gets thoroughly mixed with the spray reaction zone at the burner exit.

The ejector primary air flow rate is adjusted initially so that the reactor operating pressure is 10 – 15 mm of water below atmospheric. Figure A5.12 depicts the reactor pressure at various burner operating power levels for a fixed primary ejector nozzle air flow rate.

A5.2.2.2. Phase II: Effluent injection

Film Injection

Since airflow rate was continuous throughout the first phase the bed temperature at the end of heatup is found to be 623 – 673 K. The nozzle temperature kept below 383 K (much below Leidenfrost point). Therefore, water is injected through the nozzle prior to injecting

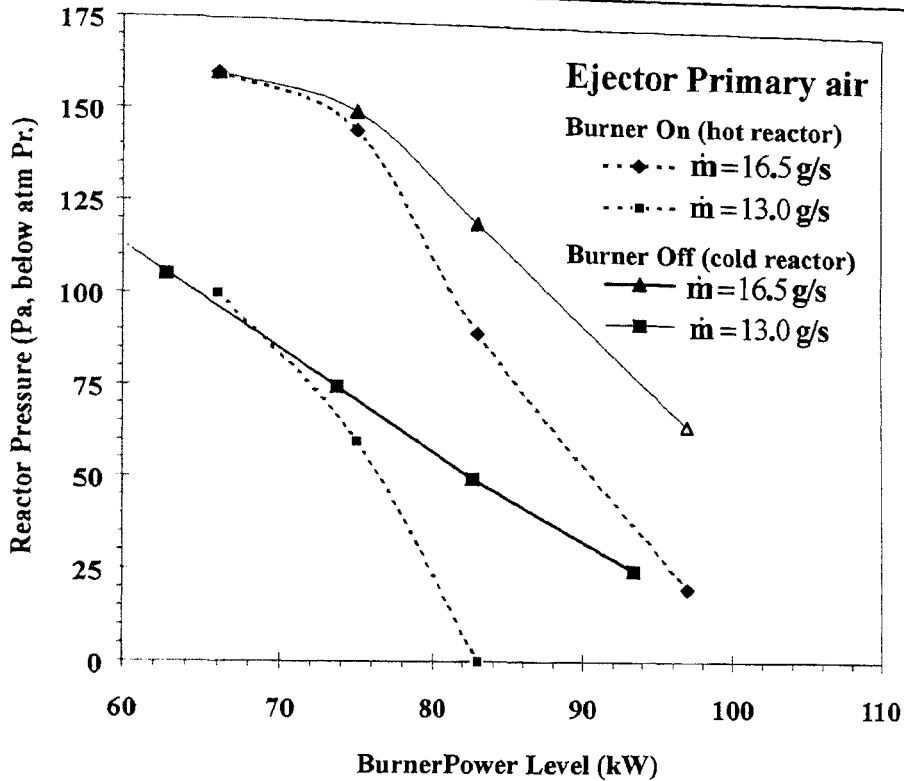


Figure A5.12: Reactor pressure vs. kerosene burner power level operated at equivalence ratio = 1 or air mass flow rate if burner is off.

the effluent. During this phase the kerosene flow rate is gradually reduced in the range of 0.3 to 0.5 g/s and stoichiometric air allowed through the kerosene burner. The required air for effluent combustion or gasification is injected through the effluent injector prior to effluent injection. Depending on the airflow rate, the velocity at the rectangular exit plane would range from 10 – 20 m/s. This is expected to assist in effluent film formation as well draw it to the hot zone.

The aerodynamic scrapper nozzles are flushed with water prior to heat-up phase. Determination of effluent flow rate, re-ignition of the burner during this phase is discussed in section A4.4.2

Injection in the hot zone

As was experimentally determined, injector protruding in the hot zone got heated to temperature in excess of 773 K in spite of the cooling air. Therefore, prior to injecting effluent, the injector was cooled by injecting water. This was repeated even with air blast atomizer.

Appendix A6

Gasification in Vertical Reactor: The Experimental Setup and Procedure

A6.1. The Experimental Setup

A6.1.1. The Reactor

The spray experiments were carried out in a reactor with relatively higher thermal inertia ensuring averaging of small time fluctuations in composition and temperature. Also the cross sectional area was chosen to accommodate a 20° spray. It was decided to use the shells of the vertical reactor that were earlier used in the spray injection experiment with modification. Appendix A4 (related to chapter 4) contains the description of the shells used in the present reactor assembly. The spray was injected from the top of the reactor and the auxiliary fuel burner was fixed tangential as shown in Fig. A6.1. A fixed grate capable of mechanical actuation was fixed to the bottom shell as shown in the figure. The solid residue can be transferred to the dump by lifting the grate using lever arrangement shown in Fig. A6.1, which depicts the direction of the flow of the product gases. From under the grate, the gas reverses the flow direction by 180° and passes through the outer annular shell prior to entering the series of wet scrubber. The flow reversal causes most entrained residue to fall back and facilitates its transfer to the dump. This arrangement also helps in regenerative heating of the material on the bed. The gases were burnt in the flare.

A6.1.2. Gas Scrubber, Ejector and Gas Flare

The condensable, odoriferous, water-soluble and other particulate matter from producer gas stream were water scrubbed as shown in the figure. The scrubber was the same as described in Appendix A5, section A5.1.2.

Aerodynamic ejectors maintain reactor pressure sub-atmospheric at all experimental flow rates. These facilities were same as in the previous experiments.

A6.1.3. Effluent Feed system

The use of higher solids effluent in the experiments (Expt. No. I-12 and I-13) and its direct injection into the hot zone made the feed system more complex since it required elaborate

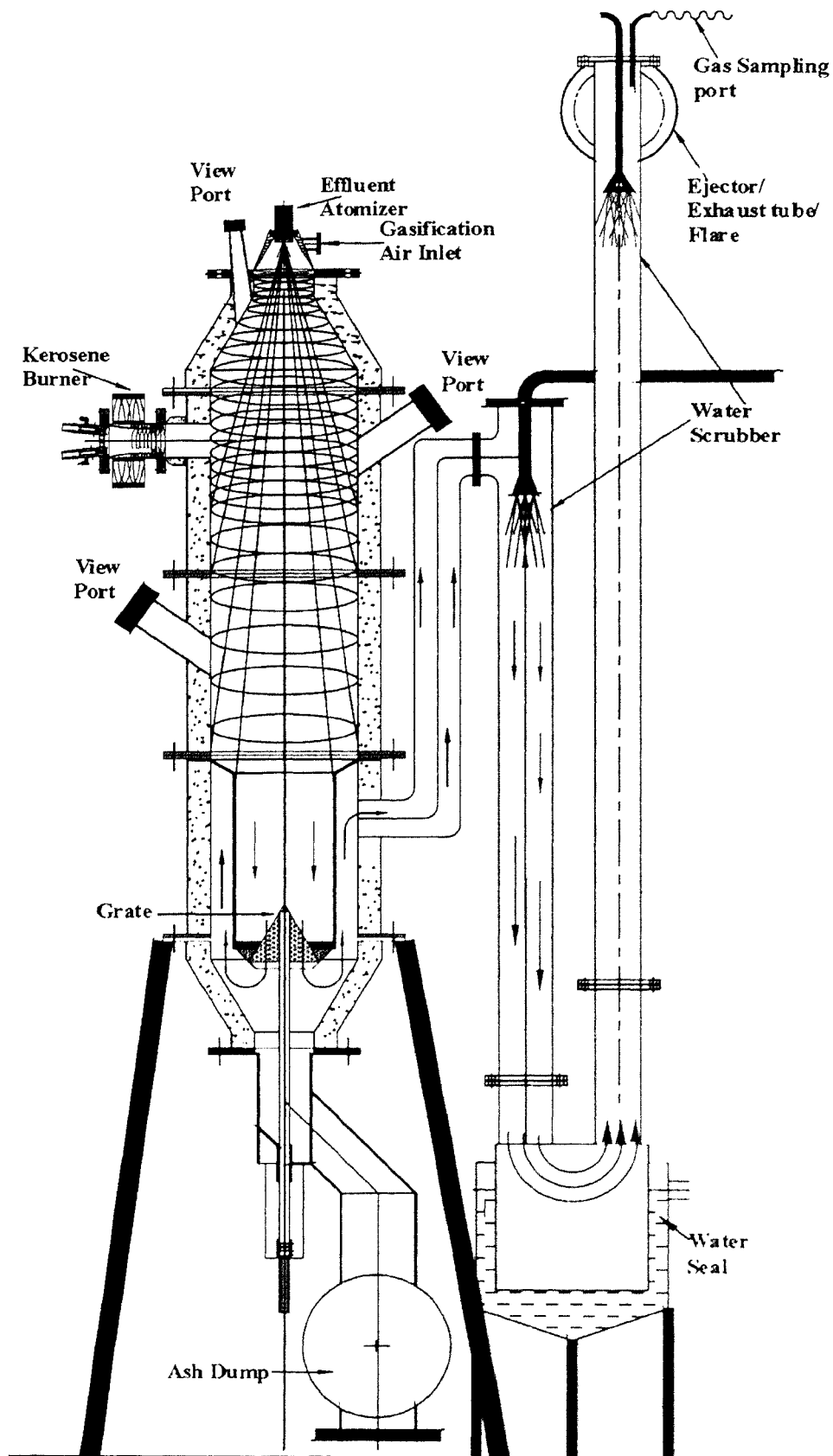


Figure A6.1: Modified vertical reactor

air and water flush line arrangements to evacuate and clean the feed lines with residual effluent prior to injecting effluent or after stopping injection during experiment in order to ensure consistent effluent flow. Same effluent feed system used during experiments conducted in inclined sheet reactor (I – 11 to I – 13) was used. The schematic view of the feed system is given in Fig. A5.11 (p. 193)

A6.1.4. Air Feed System

The air feed system for the present experiment remains the same as was used in earlier experiment and is discussed in Appendix A4.1.7. The only difference was that the effluent feed system required additional high-pressure air purge lines and this was taken care of by providing an additional air header from where these lines were drawn to their utility points.

A6.1.5. Effluent Atomizer

The schematic of the air blast atomizer is shown in the Fig A6.2. This atomizer consists of: effluent inlet to the core and annular passages for air, three orifices, and swirlers in the annular air passages. The atomizer was mounted on an annular conical nozzle through which tangential tertiary air was introduced into the reactor from the exit plane located 100 mm downstream of atomizer. All the parts of the atomizers were connected using BSP threads. The coaxiality of the orifices was necessary to maintain the spray symmetry. Three grab screws were used in both the annular passages to set the concentricity of the orifice. The air in the inner passage (atomization air) was compressed air while the outer passage (secondary air) and annular cones (tertiary air) were provided by a blower. The flow rates were measured by calibrated venturi meters.

The swirling motion of air was generated by passing it through guide vanes or passage at a helix angle. The air passages adopted for the experiments were (i) multiple rectangular helical passages with 5° helix angle and (ii) multiple circular holes drilled at 17° helix angle and both these geometries gave compact atomizer design. However, for generating low swirl intensity flow, circular holes were more suitable. The swirlers were modular and can be easily changed either to remove or to increase swirl intensity. Figure.A6.3 depicts the mass distribution of effluent spray obtained at two swirl intensities ($S \sim 0.9$ and 0.3) of atomization air. The mass distribution improves with increase in swirl intensity. An estimate of droplet size was obtained by capturing the spray droplets and it was found that at higher swirl ($S > 0.5$) the droplet size increases. Therefore, the swirl intensity of atomization air

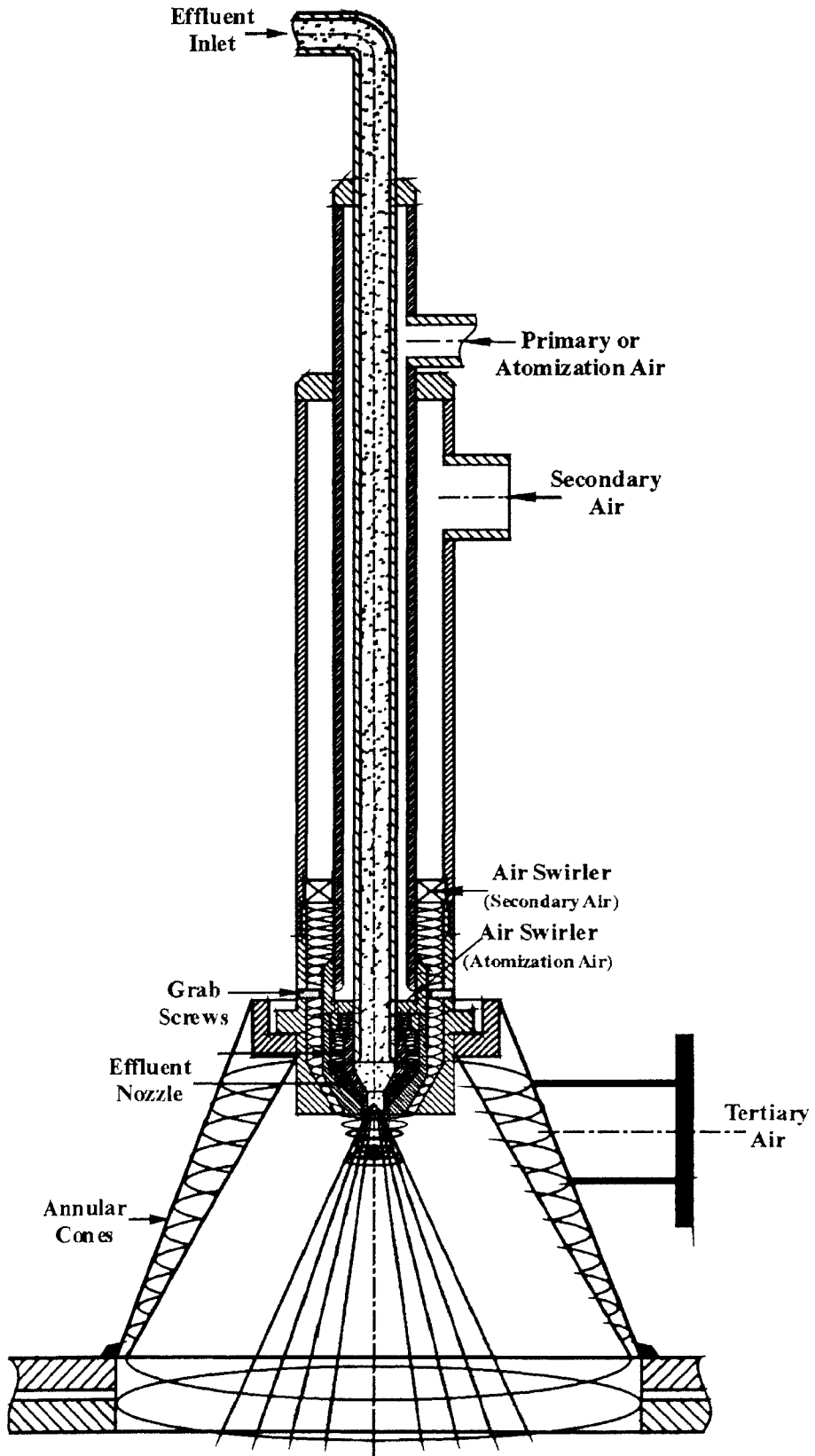


Figure A6.2: Effluent Atomizer

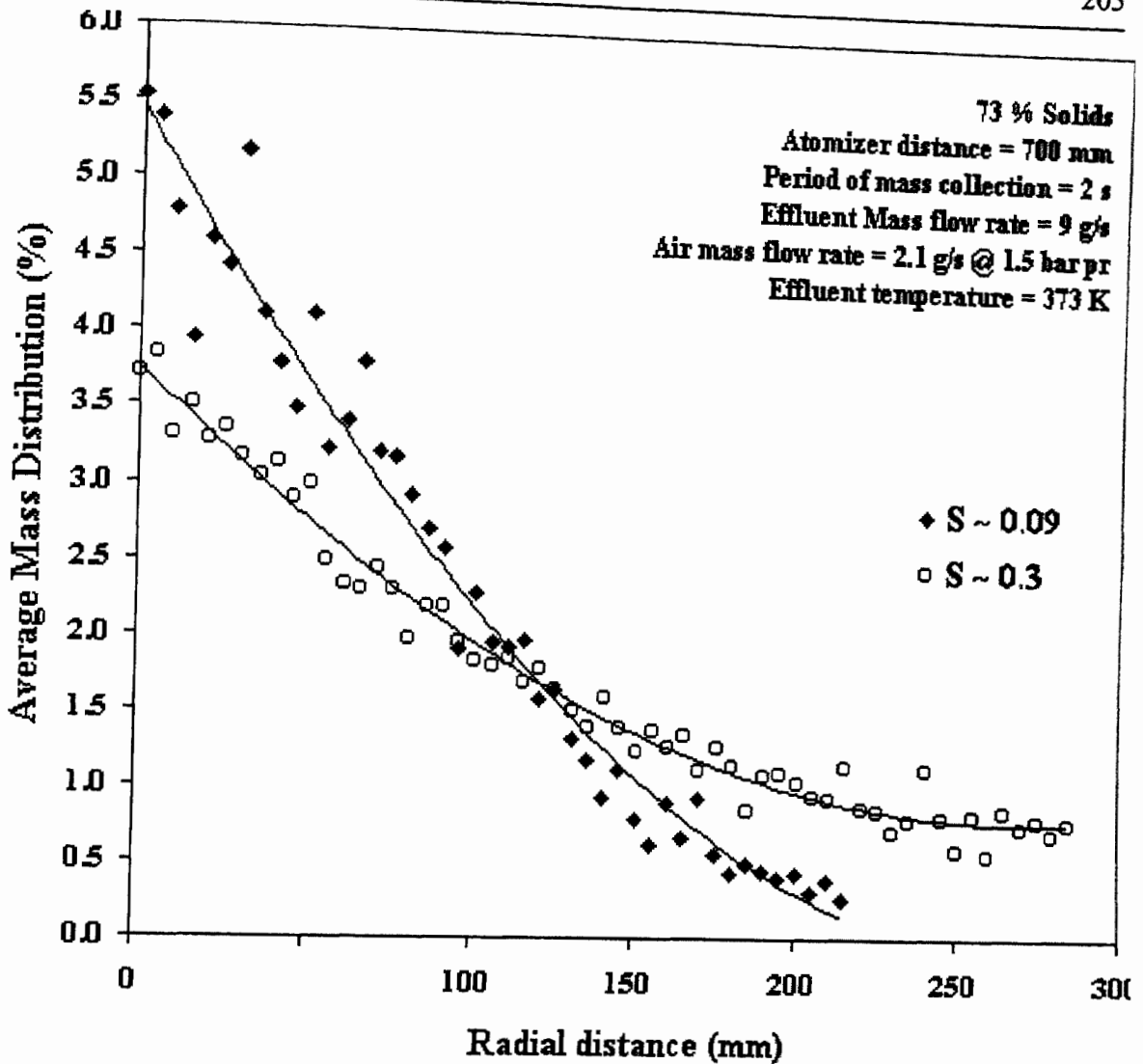


Figure A6.3: Average mass distribution of effluent spray vs radial distance (R = 0 at center)

was kept low (swirl number, $S \sim 0.14$) in order to have higher axial momentum flux necessary for fine atomization.

The swirl intensity of secondary air was fixed at 0.42 and the passage was convergent. This improved air interaction with the spray and improved mass distribution by centrifuging large size droplets. The air mass flow rate through this passage varied from 0 – 8 g/s. and this helped in keeping the atomizer cool and thus prevented the effluent tube getting blocked. The tertiary air mass flow rate was in the range of 0 – 14 g/s. The swirling air interacted with spray, pushed the droplets towards the hot walls of the reactor, and decreased velocity of droplet in the spray core.

A6.1.6. Instrumentations

Instrumentations used in the experiments were same and are discussed earlier (chapter 4, section 4.4.1 and A5.1.7).

A6.2. Experimental Procedure

This section is divided in two parts: 1) initial setup procedure includes preparation to the setting up of the feed systems and 2) experiment startup procedure. The procedure remains same for all the experiments performed.

A6.2.1. Initial setup procedure

This includes preparation of effluent, kerosene, and air feed system, the reactor, and instrumentation. The procedure remains same and is given in section A5.2.1

A6.2.2. Experimental startup

The experiments consisted of two phases: Phase I was reactor heat up and Phase II was effluent injection.

A6.2.2.1. Phase I: Reactor heat up phase

This phase takes about 50 - 55 minutes to heat up the reactor shells to temperature in excess of 1073 K. using kerosene burner power of 85 – 90 kW [kerosene flow rate: 2 - 2.1 g/s, air flow rate 35 g/s, O₂ = 0.5 %, CO₂ = 16%, CO = 0.1 % (dry basis)]. Burner exit gas temperature = 1500 K and gas velocity was about 30 to 32 m/s.

Water sprays in the scrubber and ejector primary air (30 g/s) were switched on first. A 2 kW LPG pilot burner was ignited in the initial phase of the experiment. Gas sampling pump was also switched on to determine O₂, CO₂ and CO concentration. The startup procedure for the kerosene burner remains the same as described in Appendix A4 since the same burner was used in the present experiment. The effluent atomizer remains in retracted position during this phase. Hence, all the stoichiometric air was allowed through the burner.

The ejector primary air flow rate was adjusted initially so that the reactor operating pressure was 10 – 15 mm of water below atmospheric.

A6.2.2.2. Phase II: Effluent injection

Fine spray of hot effluent was injected in the pre-heated reactor. The gasification air was introduced from secondary and tertiary air inlets as shown in Fig. A6.2. Secondary air was

swirl air, which serves the purpose of cooling the atomizer from radiant heat and providing air in the core of the spray in addition to the atomization air. This helped in achieving better interaction of effluent droplets with air. The remaining fraction of gasification air was introduced as tertiary air through tangential inlet shown fixed to annular conical space as shown in the figure. This arrangement provides air into the outer periphery of the spray. Mass flow rate of primary, secondary and tertiary air were controlled such that the droplets in the core could be distributed through the cross section of the reactor and could also be pushed close to the hot reactor wall. The kerosene burner operated during phases II with stoichiometric air.

Determination of effluent flow rate, re-ignition of the burner during this phase is discussed in section A4.4.2

Continuous effluent atomization throughout the experiment was preferred; however, if the flow was discontinued, the effluent lines need to be flushed with water after discontinuing the flow in order to prevent effluent charring in the feed line and prior to starting the flow. However, it was found from experience that retracting the atomizer was a better alternative.

References

1. Adams, T. N., and Frederick, W. J. (1988), Kraft recovery boiler physical and chemical processes, *American Paper Institute*, New York, pp. 86 – 91.
2. Andersen, B. K. (1977), Thermodynamic properties of $O_2 - O_2^- - O_2^{2-} - O^{2-}$ system in molten alkali carbonates, *Acta Chemica Scandinavica. (Copenhagen)*, A31, 242 – 245.
3. Annamalai, K., and Ryan, W. (1993), Interactive processes in gasification and combustion –II, Isolated carbon, coal and porous char particles, *Prog. Energy Combustion. Science*, Vol. 19, pp. 383 – 446.
4. Annamalai, K., and Durbetaki, P. (1977), A theory on transition of ignition phase of coal particle, *Combustion and Flame*, Vol. 29, pp. 193 – 208.
5. Arcoumanis, C., Khezzar, L., Whitelaw, D. S., and Warren, B. C. H. (1994), Breakup of Newtonian and non-Newtonian fluids in air flow, *Expts. In Fluids*, Vol. 13, pp. 423 – 428.
6. Blackwood, J. D., and Mcgrory, F. (1958), Carbon–steam reaction at high pressure, *Aust. J. Chem.*, Vol. 11, pp. 16 – 23.
7. Blackwood, J. D., and Ingeme, A. J. (1960), The reaction of carbon with carbon dioxide at high pressure, *Aust. J. Chem.*, Vol. 11, pp. 16 – 23.
8. Boukara, R., Gadiou, R., Gilot, P., Delfosse, L., and Prado, G. (1992), Study of the ignition of single coal and char particles in a drop tube furnace by a probability method, *Twenty-Fourth Symposium (International) on Combustion*, The Combustion Institute, Pittsburgh, pp. 1127 – 1133.
9. Bousfield, D. W., Stockel, I. H., and Nanivadekar, C. K. (1990), Breakup of viscous jets with large velocity modulations, *J. Fluid Mech.* Vol. 218, pp. 601 – 618.
10. Burgess, A. R., and Ghaffari, R. (1988), Pre-ignition phenomena and their effects on overall combustion rates of coal slurry droplets, *Twenty-Second Symposium (International) on Combustion*, The Combustion Institute, Pittsburgh, pp. 2009 – 2017.
11. Cameron, J. H. (1987), A kinetic Study of carbon oxidation in an alkali carbonate melt, *Ind. Eng. Chem. Res.* 26, pp. 1573 – 1578.
12. Cameron, J. H., and Grace, T. M. (1985), Kinetic study of sulfate reduction with kraft black liquor char, *Ind. Eng. Chem. Fundam.* 24, pp. 443 – 449.

13. Chakrabarty, R. N. (1964), Potash recovery – a method of disposal of distillery waste and saving foreign exchange, *Chemical Age of India*, Vol. 15, No. 1, pp. 93 – 96.
14. Clay, D. T., Grace, T. M., and Kapheim, R. J. (1984), *Fume formation from synthetic sodium salt melts and commercial kraft smelts*, AIChE Symposium Series No. 239, Vol. 80, pp. 99 – 106.
15. Clay, D. T., Lien, S. J., Grace, T. M., Macek, A., Semerjian, H. G., and Chargundla, S. R. (1987), US Dept. of Energy, Rep. No. DE880057756, Jan 1987.
16. Consonni, S., Larson, E. D., and Berglin, N. (1997), *Tran of ASME*.
17. Cortez, L. A. B., and Perez, B. (1997), Experience on vinasse disposal Part III: Combustion of vinasse-#6 fuel oil emulsions, *Brazilian J. of Chem. Engg.*, Vol. 14, No. 1, pp. 9 – 18.
18. Cortez, L. A. B., Freire, W. J., and Calle, F. R. (1998), Biodigestion of vinasse in Brazil, *Int. Sugar J.*, Vol. 100, No. 1196, pp. 403 – 413.
19. Dasappa, S., Sridhar, H. V., Paul, P. J., Mukunda, H. S., and Shrinivasa, U. (1994), On the combustion of wood-char spheres in O₂/N₂ mixture-experiment and analysis, *Twenty-Fifth Symposium (International) on combustion*, The Combustion Institute, Pittsburgh, pp. 569 – 576.
20. Davies, J. G. (1946), Methods of dunder disposal, *The International Sugar Journal*, pp. 266 – 269.
21. Dayton, D. C., and Frederick, W. J. (1996), Direct observation of alkali vapor release during biomass combustion and gasification. 2. Black liquor combustion at 1100° C, *Energy & Fuels*, Vol. 10, pp. 284 – 292.
22. Dunks, G. B., Stelman, D., and Yosim, S. J. (1982), Graphite oxidation sodium carbonate/sodium sulfate melts, *Inorg. Chem.*, Vol. 21, pp. 108 – 114.
23. Dutta, S. and Wen, C. (1977), Reactivity of coal and char 2. in oxygen-nitrogen atmosphere. *Ind. Eng. Chem.*, Process Des. Dev. No. 16-1, pp. 31 – 37.
24. Elvers, B., Hawkins, S. and Russey, W. (1990), *Ullman's Encyclopedia of Industrial Chemistry*, Vol. A25, pp. 403 – 405.
25. Empie, H. J., Lien, S., and Samuels, B. (1997), Distribution of mass flows in black liquor sprays, *AIChE Symp. Series* No. 315, Vol. 93, pp. 58 – 66.
26. Essenhigh, R. H., and Thring, M. W. (1958), Proceedings of the conference on science in the use of coal, Institute of fuel, London, pp. D21 – D27.

27. Essenhigh, R. H., and Howard, J. B. (1966), Toward a unified combustion theory, *I & EC*, Vol. 58, pp. 14 – 23.
28. Frederick, W. J., Hupa, M., Stenberg, J., and Hernberg, R. (1994), Optical pyrometric measurements of surface temperatures during black liquor char burning and gasification, *Fuel*, Vol. 73, pp. 1889 – 1983.
29. Frederick, W. J., and Hupa, M. (1994), The effect of temperature and gas composition on swelling of black liquor droplet during devolatilization, *J. Pulp and Paper Science*, Vol. 20, No. 10, pp. 274 – 280.
30. Groeneveld, M. J. (1980), The concurrent moving bed gasifier, Ph. D thesis, Twente University of Technology, Netherlands.
31. Howard, J. B. (1967), Combustion of carbon with oxygen, Technical report, MIT press.
32. Hupa, M., Solin, P., and Hyoty, P. (1987), *J. Pulp Paper Science*, 13(2), pp. j67 – j72.
33. Huttinger, K. J., and Minges, R. (1985), Mixture of potassium sulphate and iron sulphate as catalysts for water vapor gasification of carbon, *Fuel*, Vol. 64, pp. 364 – 367.
34. Ivin, P. C., and Doyle, C. D. (1987), Chloride ion concentration in mill process streams with relation to corrosion of stainless steel, *Proc. Conf. Aust. Doc. Sugar Cane Tech.*, pp. 267 – 273.
35. Jackson, C. J. (1956), Whisky and industrial alcohol distillery wastes, *Inst. Swage Purif. J. Proc.*, 204-14-A.
36. Joshi, H. C. (1999), Bio-energy Potential of Distillery Effluent. *Bio-Energy News*, Vol. 3, No. 3, pp. 10 – 15.
37. Kumagai, S., Sakai, T., and Okajima, S. (1972), Combustion of free fuel droplets in a freely falling chamber, *Thirteenth Symposium (International) on combustion*, The Combustion Institute, Pittsburgh, pp. 779 – 785.
38. Kane, R. D. (1999), Pick the right materials for wet oxidation, *Chem. Eng. Prog.*, March 1999, pp. 51 – 58.
39. Kanuary, A. M. (1982), *Introduction to combustion phenomena*, Gordon and Breach Science Publishers, New York.
40. Kapteijn, F., Abbel G., and Moulijn, J. A. (1984), CO₂ gasification of carbon catalyzed by alkali metals, *Fuel*, Vol. 63, pp. 1036 – 1042.
41. Kikuchi, E., Adachi, H., Momoki, T., Hirose, M., and Morita, Y. (1983), Supported alkali catalysts for steam gasification of carbonaceous residues from petroleum. *Fuel*, Vol. 62, pp. 226 – 230.

42. Kobayashi, H., Howard, J. B., and Sarofim, A. F. (1976), Coal devolatilization at high temperature, *Sixteenth Symposium (International) on Combustion*, The Combustion Institute, pp. 411 – 425.
43. Kujala, P., Hull R., Engstrom, F., and Jackman, E. (1976), Alcohol from molasses as a possible fuel and the economics of distillery effluent treatment, *Sugar y Azucar*, March 1996, pp. 28 – 39.
44. Kuwata, M., Stumbar, J.P., and Essenhigh, R.H. (1969), Combustion behavior of suspended paper spheres, *Twelfth Symposium (International) on Combustion*, The Combustion Institute, pp. 663 – 675.
45. Larson E. D., Consonni, S., Berglin, N., and Kreutz, T. (1996), Advanced technologies for biomass–energy utilization in the pulp and paper industry, First-year progress report to the U.S. Dept. of Energy, Dec. 1996.
46. Lee, J. (1996), Trade environment database / Rum trade (case No. 384) Mandala Projects, American University, Washington DC.
47. Lele, S. S., Shirgaonkar, I. Z., and Joshi, J. B. (1990), Effluent treatment for an alcohol distillery: thermal pretreatment with energy recovery followed by wet-air-oxidation, *Indian Chemical Engineer*, Vol. 32, No. 1, pp.36 – 43.
48. Li, J., and van Heiningen, A. R. P. (1990), Kinetics of CO₂ gasification of fast pyrolysis black liquor char, *Ind. Eng. Chem. Res.*, Vol. 29, No. 9, pp. 1776 - 1785.
49. Littlewood, K. (1977), Gasification: theory and application, *Prog. Energy Combust. Sci.*, Vol.3, pp. 35 – 71.
50. Liu, G. E., and Yao, Shi C. (1983), Behavior of suspended coal-water slurry droplets in combustion environment, *Combustion and Flame*, Vol. 51, pp. 335 – 345.
51. Liu, G. E., and Law, C. K. (1986), Combustion of coal - water slurry droplets, *Fuel*, Vol. 65, pp. 171 – 176.
52. Marcano, N., Pourkashanian, M., and Williams, A. (1991), The combustion of bitumen-in-water emulsion, *Fuel*, Vol. 70, pp. 917 – 923.
53. Macek, A. (1999), Research on combustion of black -liquor drops, *Prog. Energy Combust. Sci.*, Vol. 25, pp. 275 – 304.
54. McKeough, P. J., Kurkela, M., Arpiainen, V., Mikkanen, P., Kauppinen, E., and Jokiniemi, J. (1995), The release of carbon, sodium and sulphur during rapid pyrolysis of black liquor, *International Chemical Recovery Conference*, pp. A217 – A225.

55. Michale, E. T., Scheffee, R. S., and Rossmeissl, N. P. (1982), Combustion of coal/water slurry, *Combustion and Flame*, Vol. 45, pp. 121 – 135.
56. Mueller, C., Kilpinen, P., and Hupa, M. (1998), Influence of HCl on the homogeneous Reactions of CO and NO in postcombustion conditions—A kinetic modeling study, *Combustion and Flame*, Vol. 113, pp. 579 – 588..
57. Mukunda, H.S., Paul, P.J., Srinivasa, U., and Rajan, N.K.S. (1984), Combustion of wooden spheres – experiments and model analysis, *Twentieth Symposium (International) on Combustion*, The Combustion Institute, Pittsburgh, pp. 1619 – 1628.
58. Mullen, J. F. (1992), Consider fluid-bed incineration for hazardous waste destruction, *Che. Eng. Prog.*, June 1992. pp. 50 – 58.
59. Murdoch, P. L., Pourkashanian, M., and Williams, A. (1984), The mechanism of combustion of coal-water slurry, *Twentieth Symposium (International) on Combustion*, The Combustion Institute, Pittsburgh, pp. 1409 – 1418.
60. NETL (2000), http://www.fetc.doe.gov/publications/press/2000/tl_blackliq.html#top
61. Outassourt, T., Garo, A., Delfosse, L., and Prado, G. (1984), Combustion of a droplet of coal-water mixture heated by laser beam, *Twentieth Symposium (International) on Combustion*, The Combustion Institute Pittsburgh, pp. 1401 – 1407.
62. Patel, N. M., Paul, P. J., Mukunda, H. S., and Dasappa, S. (1996), Combustion studies on concentrated distillery effluents, *Twenty-Sixth Symposium (International) on Combustion*, The Combustion Institute, Pittsburgh, pp. 1401 – 1407.
63. Patel, N. M., Paul, P. J., and Mukunda, H. S. (1995), Droplet combustion studies on dried concentrated distillery effluents, XIV National conference on IC engines and Combustion, Pune, pp. 389 – 394.
64. Pellet, H. (1909), Bull. Assoc., *Chim. Sucr. Dist.*, 27, pp. 215 – 217.
65. Petarca, L., Vitolo, S., and Bresci, B. (1997), *CPL Press*, UK., pp. 374 – 381.
66. Polack, J. A., Day, D. F., and Cho, Y. K. (1981), Gasohol from sugarcane-stillage disposition, Audubon Sugar Institute, Louisiana State University, pp. 47 – 53.
67. Popov, V. D., Garyazha, V. T., and Yatsenko, E. A., Turdy, Kiev. Tekhnol. Ist. Pishch. Proin (1960), Vol. 22, pp. 43 – 47.
68. Regland, K. W., and Weiss, C. A. (1979), Combustion of single coal particle in a jet, *Energy* (U.K), Vol. 4, pp. 314 – 348.
69. Reich, G. T. (1929), *Chem. And Met. Engg.*, Vol. 36, No. 44, (1937); and U.S. Patents, 1930861 (1933) and 2010929 (1935).

70. Reich, G. T. (1945), Molasses stillage, *Ind. Engg. Chem.*, Vol.37, No. 5, pp. 534 – 538.
71. Roberts, O. C., and Smith, I.W. (1973), Measured and calculated burning histories of large carbon sphere in oxygen, *Combustion and Flame*, Vol. 21, pp. 123 – 127.
72. Saastamoinen, J., and Richard, J. (1996), Simultaneous drying and pyrolysis of solid fuel particles, *Combustion and Flame*, Vol. 106, pp. 288 – 300.
73. Sattler, L., and Zerban, F. W. (1949), *Ind. Eng. Chem.*, Vol. 41, No. 10, pp. 1401 – 1405.
74. Sakai, T., and Saito, M. (1983), Single-droplet combustion of coal slurry fuel, *Combustion and Flame*, Vol. 51, pp. 141 – 154.
75. Sharan, H., Buhler, R., Giordano, P., Hasler, P., and Salzmann, R. (1996), Adaptation of the IISc-Dasag gasifier for an application in Switzerland, Final Report, pp. 18 – 19.
76. Smoot, L., and Pratt, D. T. (1979), Pulverized coal combustion and gasification, Plenum Press, New York.
77. Spiro, C. L., McKee, D. W., Kosky, P. G., Edward, J. L., and Maylotte, D. H. (1983), Significant parameters in the catalyzed CO₂ gasification of coal char, *Fuel*, Vol. 62, pp. 323 – 330.
78. Spruytenburg, G. P. (1982), Vinasse pollution elimination and energy recovery, *The International Sugar Journal*, pp. 72 – 74.
79. Stellman, D., Darnell, A. J., Christie, J. R., and Yosim, S. J. (1976), *Molten Salts*, The electrochemical society, Princeton, pp. 299 – 314
80. Takei, M., Tsukamoto, T., and Nioka, T. (1993), Ignition of blended-fuel droplet in high-temperature atmosphere, *Combustion and Flame*, Vol. 93, pp. 149 – 156.
81. Takeno, K., Tokuda, K., and Ichinose, T. (1996), Fundamental experiment on the combustion of coal-water mixture and modeling of the process, *Twenty-Sixth Symposium (International) on Combustion*, The Combustion Institute Pittsburg, pp. 3223 – 3230.
82. Underkofler, L. A., and Hickey, R. J. (1954), *Industrial Fermentation Vol. I*, Chemical Publishing Company, New York, pp 273 – 346.
83. Verrill, C. L., and Dickinson, J. A. (1998), Development and Evaluation of a Low-Temperature Gasification Process for Chemical Recovery from Kraft Black Liquor, *International Chemical Recovery Conference, June 1 – 4*.
84. Verrill, C. L., and Nichols, K. M. (1994), Inorganic aerosol formation during black liquor drop combustion, *AIChE Symposium Series*, No. 302, Vol. 90, pp. 55 – 72.

85. Walsh, P. M., Zhang M., Farmayan, W. F., and Beer, J. M. (1984), Ignition and combustion of coal-water slurry in a confined turbulent diffusion flame, *Twentieth Symposium (International) on Combustion*, The Combustion Institute, Pittsburgh, pp. 1401 – 1407.
86. Yao, S. C., and Liu, L. (1983), Behavior of suspended coal-water-slurry droplets in a combustion environment, *Combustion and Flame*, Vol. 51, pp. 335 – 345.
87. Yavuz, R., Kucukbayrak, S., and Williams, A. (1998), Combustion characteristics of lignite-water slurries, *Fuel*, Vol. 77, pp. 1229 – 1235.
88. Zhao, H. (1988), Stable and intensified combustion of coal-water slurry utilizing multiannular opposing distributing jets, *Coal Combustion: Science and Technology Industrial and Utility Applications*, pp. 673 – 677.
89. Zaman, A. A., and Fricke, A. L. (1995), Effect of pulping conditions and black liquor composition on heat of combustion of slash pine black liquor, *AIChE Symposium Series*, Vol. 91, No. 307, pp. 154 – 161.
90. Zaman, A. A., and Fricke, A. L. (1995), Kraft black liquor rheological behavior with respect to solids concentration, temperature and shear rate, *AIChE Symposium Series*, Vol. 91, No. 307, pp. 162 – 171.

G-15879